DISSERTATION

INVESTIGATING THE ROLES PRION-LIKE DOMAINS PLAY IN CELLULAR STRESS RESPONSES

Submitted by

Jenifer Elizabeth Shattuck

Department of Biochemistry and Molecular Biology

In partial fulfillment of the requirements

For the Degree of Doctor of Philosophy

Colorado State University

Fort Collins, Colorado

Summer 2018

Doctoral Committee:

Advisor: Eric Ross

Olve Peersen
Santiago Di Pietro
Glenn Telling

ABSTRACT

INVESTIGATING THE ROLES PRION-LIKE DOMAINS PLAY IN CELLULAR STRESS RESPONSES

Prion-like domains are involved in the formation of either functional or pathogenic protein aggregates. These aggregates play an important role in regulating a broad-range of cellular functions.

In the budding yeast *Saccharomyces cerevisiae*, at least 10 proteins have been identified that form self-propagating amyloid-based prions. Most known yeast prion proteins contain a low-complexity, intrinsically-disordered prion-forming domain that is converted into stable, detergent-insoluble aggregates, necessary for prion activity. These prion-forming domains tend to be glutamine/asparagine (Q/N) rich, and relatively lacking in charged and hydrophobic amino acids. To better understand the amino acid sequence features that promote prion activity, we used the prediction algorithm PAPA to identify predicted aggregation-prone prion-like domains (PrLD). While from this study we did not identify new yeast prion proteins, we identified several PrLDs with aggregation activity. Therefore, in follow up studies we investigated the role these PrLDs play in other protein assemblies involved in cellular stress responses.

First, we investigated how a prion-like protein kinase, Sky1, plays a role in regulating stress granules. Stress granules are cytoplasmic assemblies that form when translation initiation is limiting, including under a variety of stress conditions. Because these cytoplasmic granules are important regulatory machinery for cellular homeostasis,

mutations that increase stress granule formation or decrease clearance have been linked to various neurodegenerative diseases. We provided evidence that Sky1 is recruited to stress granules through its aggregation-prone PrLD, and it phosphorylates an RNA-binding protein to efficiently disassemble stress granules. Additionally, we showed when Sky1 is overexpressed it can compensate for defects in other disassembly pathways. These findings contribute to understanding the regulation of stress granules, and provides a possible mechanism to mitigate persistent stress granules in neurodegenerative diseases.

Next, we investigated how PrLDs are used to assemble and activate a vacuole-signaling complex. Many cellular processes are regulated primarily through the production of phosphoinositides. Specifically, synthesis and turnover of phosphatidylinositol 3,5 bisphosphate (PtdIns(3,5)P_2) is regulated by a vacuole-signaling complex, containing prion-like proteins Fab1, Vac7, and Vac14. Interestingly, during hyperosmotic stress, there is a rapid and dramatic rise in PtdIns(3,5)P_2, which leads to vacuole remodeling, critical for cellular survival. We used aggregation-altering mutations to characterize the role of Fab1's PrLD in response to osmotic stress. Overall, these studies provided evidence that Fab1's activation requires its aggregation prone PrLD for recruitment and efficient activation for cellular adaptation to stress.

Collectively, the studies described below provide insights into the diverse roles PrLDs play in regulating cellular stress responses. Moreover, these studies have contributed to the field of aggregation-mediated cellular regulation by identifying new proteins involved, new proposed mechanisms, and new insights into the cellular consequences that arise from perturbations in regulation of these processes.

ACKNOWLEDGEMENTS

In the pursuit of my Ph.D. at Colorado State University I have been inspired and supported by several people who I would like to thank for my success.

First, I thank the extremely supportive Department of Biochemistry and Molecular Biology. Our department prospers a collaborative environment that has allowed me to interact and work with several labs over the years. I thank all those who have given me reagents and shared their technical expertise with me.

Second, I thank the entire Ross Lab for contributing helpful criticisms and alternative perspectives on my research over the years, which has aided in my success as student and scientist. In addition, I thank Kacy Paul, my fellow office mate, for our many great personal and scientific discussions as well as all your contributions to my projects over the years. Also, I thank my mentor, Dr. Eric Ross, for his consistent support, patience and training throughout my entire graduate career. In the beginning he worked closely with me to teach me the skills needed for me to eventually prosper as an independent scientist, which will be critical for my future career.

Lastly, I thank all my friends and family, near and far, for their support and love throughout this extremely challenging time in my life. I especially want to thank Brian Chapman for always being there for me when I needed you the most, and thank you for believing in me when I didn't believe in myself. Finally, I feel so lucky to have developed so many great friendships in this graduate program and I am confident that they will last a lifetime. Specifically, I thank Amanda, Sarah, Ali and Melissa for always being there to talk about science or anything, which helped keep me balanced throughout the years.

TABLE OF CONTENTS

CHAPTER 1: INTRODUCTION

Characteristics of prions and amyloid proteins

Mammalian prion biology

In 1982, Dr. Stanley Prusiner discovered the causative agent of a set of neurodegenerative diseases that plague mammals, described as prions (1). Prions are infectious proteins that have been the central cause of many disease epidemics throughout the last century. One example, Bovine Spongiform Encephalopathy (BSE), commonly known as mad cow disease, was a prion disease that transferred from cows to humans in the late 20th century (2). The prion protein was transmitted through the meat from cows, and resulted in a neurodegenerative prion disease, variant Creutzfeldt-Jacobs Disease (vCJD), in human. vCJD took many lives and could possibly take more in the future, as the epidemic may not be over (2).

The UV resistance of the prion agent suggested there was not an essential nucleic acid component, which led to the “protein-only” hypothesis. All known mammalian prion diseases are caused by misfolding of the mammalian protein PrP. When PrP misfolds, it self-assembles into a β-sheet rich amyloid structure that recruits and structurally converts soluble PrP. The amyloid fibers are then transferred to other cells; this transfer is the hallmark of prion formation (reviewed in (3)). The prion molecules continue to self-propagate, which leads to widespread infection, first affecting the brain followed by propagation throughout the central nervous system. Importantly, the prion molecules can be transferred from organism to organism, albeit differing in transmission efficiency (2, 4). While PrP is the only known mammalian prion protein, a

variety of other proteins form prion-like molecules that can spread from cell to cell and are associated with various neurodegenerative diseases, including Amyotrophic Lateral Sclerosis (ALS), Alzheimer's, and Parkinson's.

Yeast prion biology

The first yeast prion phenotype was first described by Brian Cox in 1965; however, it was until several decades later that Reed Wickner determined that the phenotype was due to a prion and shared similar characteristics to the mammalian prion protein (5, 6). The groundbreaking discovery of yeast prions introduced an entirely new field for research that prospered for several decades; continuing efforts will unravel the complex biology underlying prion biology. The information gained from studying yeast prion formation can be applicable to other higher eukaryotic systems including human neurodegenerative diseases mechanisms. Fortunately, yeast is an ideal model system to study the nucleation, aggregation and propagation steps in the formation of a prion fiber.

In *Saccharomyces cerevisiae*, budding yeast, several proteins form self-propagating and heritable aggregates *de novo* (reviewed by (7–9). There have been at least ten yeast prion proteins identified, all of which are involved in unique cellular functions (9): [URE3] is a prion of Ure2p, a regulator of nitrogen catabolism (6); [PSI+] is a prion of Sup35, a translation terminator regulator (6); [PIN+] or [RNQ+] is a prion of Rnq1, a protein of unknown function (10, 11); [SWI+] is a prion of Swi1, a component of a chromatin remodeling complex (12); [OCT+] is a prion of Cyc8, a component of a transcription repressor (13); [ISP+] is a prion of Sfp1, a transcription regulator (14); [MOT3] is a prion of Mot3, a transcription factor (15). In fact, [MOT3] was the first prion,

to suggest prion formation promotes a beneficial response in yeast during environmental stress instead of causing disease. Additionally, [MOD5] the prion form of Mod5, a yeast tRNA modifying enzyme (16) and [NUP100+] the prion form of Nup100, a component of the nuclear pore complex (17) have been identified.

Despite various functions in the cell, the yeast prion proteins share several prion characteristics, including adopting an amyloid structure *de novo* (7). Prion conversion is a rare event; however, the frequency of conversion can be increased by overexpressing the soluble protein or a prion domain (18) (Figure 1.1). Following this nucleation step, the prion "seed" can further fibrilize by recruiting and transforming soluble monomers into the growing fiber. Importantly, the fibers must be severed during cell division to transfer its trait to its progeny. The major cellular component responsible for the propagation of prion fibrils through generations is the yeast chaperone, Hsp104 ((7, 8, 19), see *Molecular Chaperones* for further discussion).

In addition to similar formation mechanisms, most known yeast prion proteins have a distinct modular domain, often referred to as a prion-forming domain (11, 20). Moreover, a prion forming domain acts independently and can be removed from its native context and retain its prion-forming ability (21). Yeast prion-forming domains are also enriched in glutamine and asparagine residues, possibly promoting initial polar interactions for the nucleation step in prion formation (22).

Experimentally, yeast prions have diverse phenotypes, but share many similar characteristics when tested among well-developed assays. Figure 1.2 represents some of innovations in the field that changed the way we study amyloid proteins. Furthermore, I highlighted the phenotypes observed when a protein has activity of a prion protein.

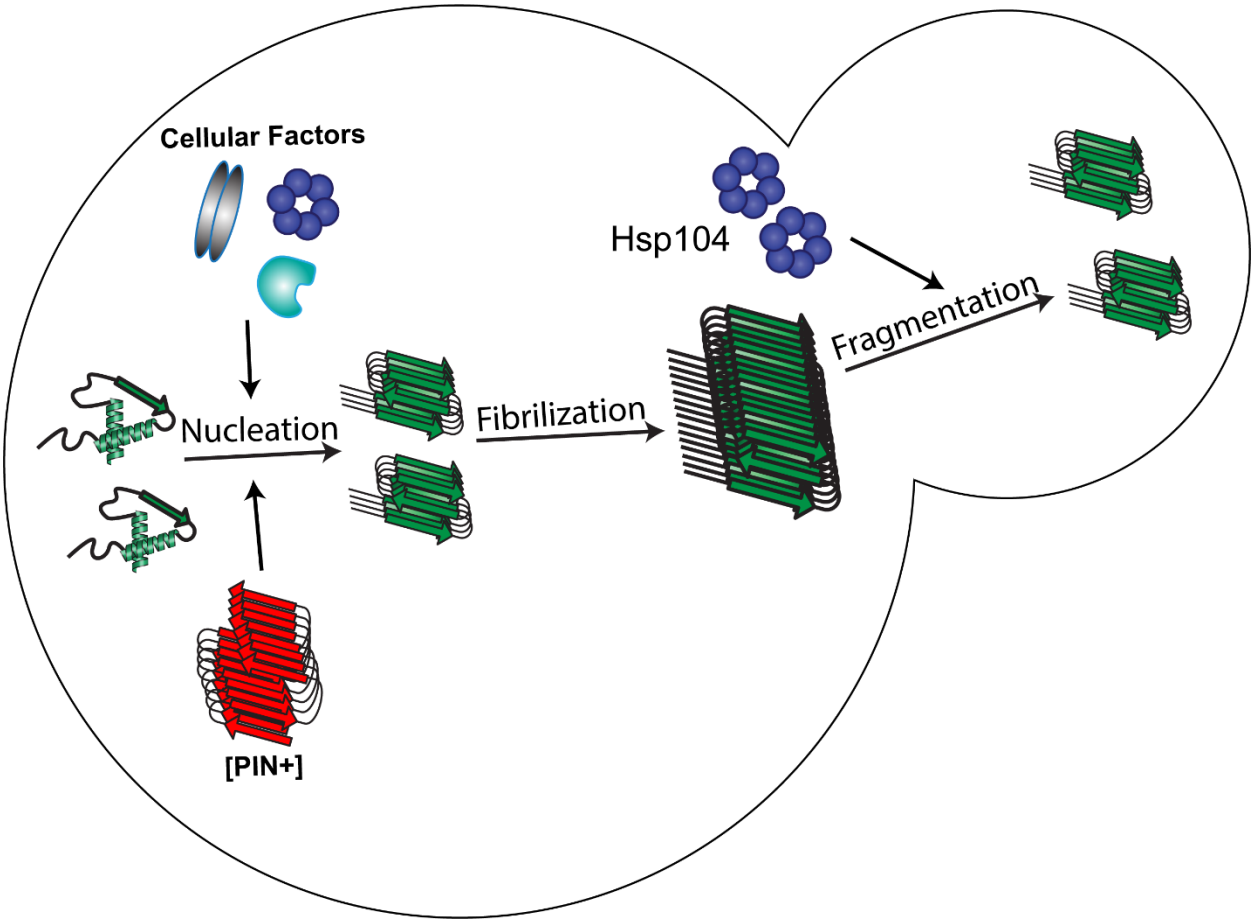

Figure 1.1: Steps in Yeast Prion Formation
Soluble protein undergoes a conformational change, exposing an intrinsically disordered prion domain that self-assembles into β-sheet rich prion “seeds”. Cellular factors and a known yeast prion, [PIN+] influence the appearance of yeast prions. Soluble protein continues to be recruited, converted and added to a growing prion fiber. Prion fibers are severed by Hsp104 into prion “seeds” and transferred to daughter cells for continued propagation

When the prion-forming domain is fused to GFP and transiently overexpressed, distinct foci are observed *in vivo* using confocal microscopy (20). Also, prion proteins form highly ordered, β-sheet rich aggregates *in vivo* (23). These highly ordered aggregates can be resolved from monomers by using a technique termed Semi-Denaturing Detergent-Agarose Gel Electrophoresis (SDD-AGE) (24). In addition to forming highly ordered, β-sheet rich aggregates *in vivo*, prion formation can also be monitored *in vitro* by using Thioflavin T dye fluorescence detection (25).

Overall, the common features that known yeast prions share are important to note when attempting to uncover new yeast prion candidates. As the field continues to discover more yeast prions, we will understand more about the necessary parameters for prion formation and unveil how prion formation contributes to yeast physiology.

Prion Prediction Algorithms

Recently, there have been several algorithms created to attempt to predict the propensity of proteins to form amyloid fibrils (reviewed by (26)). Among these is a structure-based model, ZipperDB created by (27), to analyze proteins with amyloid-like aggregation. This algorithm was developed based on the crystal structure of a short, 6 amino-acid peptide (NNQQNY) from Sup35 that forms fibrils. Using a six amino acid window, the algorithm threads other proteins of interest into the structure and evaluates the energetic fits (27–29). This algorithm was successful at determining areas of proteins that would form fibrils but failed to distinguish proteins that would not form fibrils, and thus may not be an optimal algorithm to predict yeast prions (30).

Another algorithm, based on composition similarity to known yeast prions, was first described in a study that investigated the entire yeast proteome for novel yeast

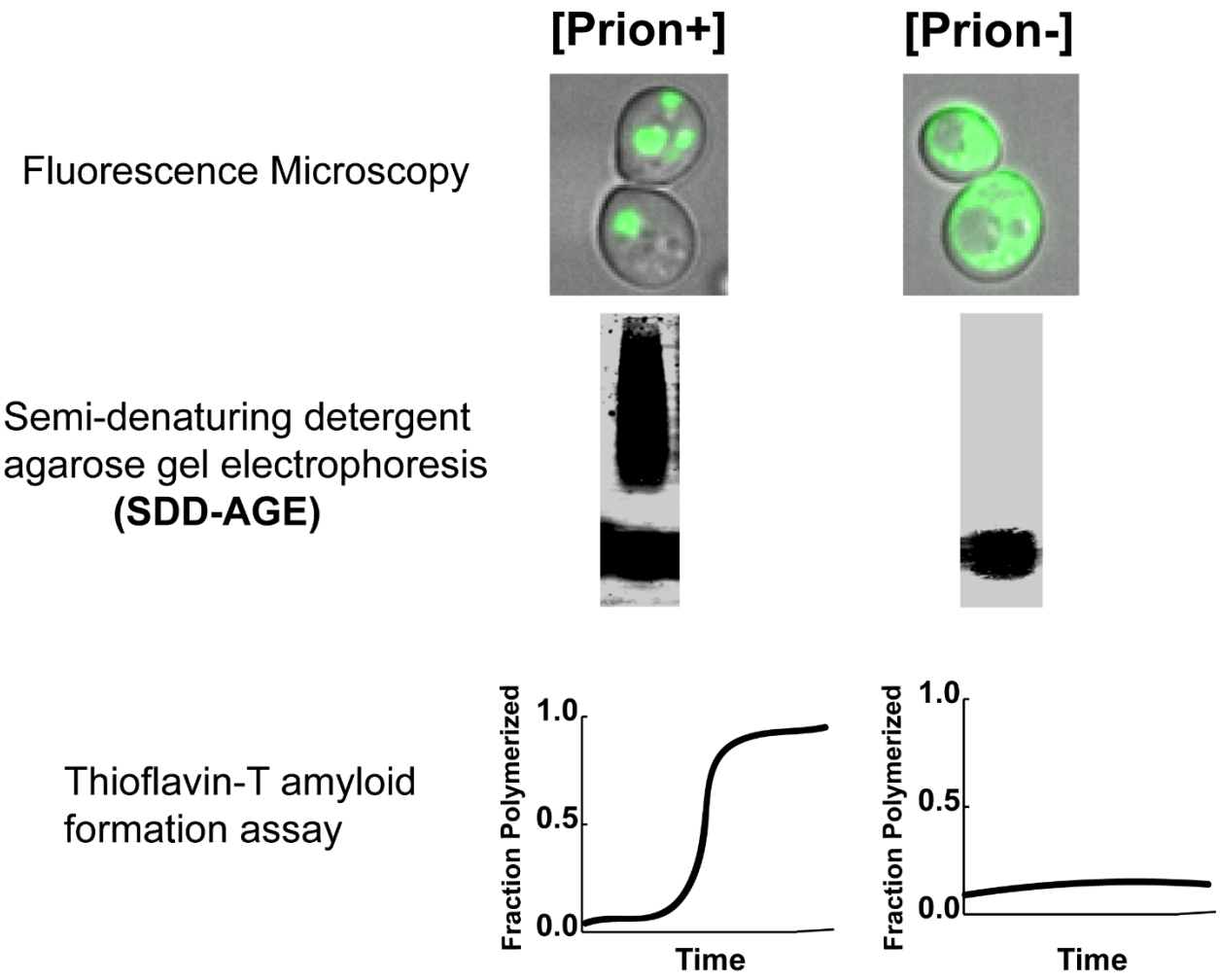

Figure 1.2: Biochemical assays to detect prion formation
(A) Proteins are GFP tagged, overexpressed and visualized using fluorescence microscopy. Proteins capable of aggregation are visualized as distinct foci within the cytoplasm. GFP signal is completely diffuse if proteins are not capable of aggregation. (B) Cell lysate is treated with low concentrations of SDS at room temperature and run out on an agarose gel, transferred to a membrane and blotted for the protein of interest. Prion formation is visualized as high molecular weight aggregates, while soluble protein run as a monomer through the gel. (C) Purified prion proteins are diluted into ThT assembly buffers and a change in fluorescence is monitored over time. ThT binds amyloid proteins after a lag phase, while ThT does not bind amorphous aggregates or soluble protein.

prion proteins (15, 31). Based on a Hidden Markov model, this algorithm was used to scan through the yeast proteome and select the top 100 yeast protein domain candidates that were predicted to form amyloid aggregates. The candidate proteins were tested in four prion activity assays. The results yielded 18 protein domains that displayed prion activity in all four assays, suggesting this algorithm was successful in predicting new prion candidates. However, the predicted prion propensity of these domains had little correlation to the experimentally determined prion activity, indicating some disconnects between predicted and observed prion propensity.

In recent years, our laboratory developed another prion propensity algorithm, termed Prion Aggregation Prediction Algorithm (PAPA) (30, 32). It was based on experimentally determined prion propensity scores for each amino acid (32). This is important because if a protein sequence deviates from a known prion protein sequence, we can evaluate how prion formation would be affected. Experimentally, an eight-amino acid window was randomly mutated in a scrambled version of the nucleation domain of Sup35 to build a library of clones, enabling the comparison of the amino acid composition of prion forming clones to a naive library. The results provided insight into how each amino acid affects prion propensity. Also, all known yeast prion forming domains are considered intrinsically disordered; therefore, PAPA also takes into account FoldIndex prediction and prion propensity of each individual amino acid (32). The balance between disorder propensity and prion propensity was validated by successfully designing synthetic prion forming domains based on PAPA (30).

In addition, PAPA was also validated by rescoring the Alberti *et al.,2009* data set. This validation is illustrated in Toombs *et al.,*2010. The prion propensity score of each

domain was then graphed against their activity in prion assays, which revealed a modest correlation. This validated that our algorithm is better able to properly predict proteins that show prion activity and distinguish them from compositionally similar proteins that show no prion activity.

Importantly, we have utilized PAPA to further investigate the parameters necessary for prion formation, including using PAPA to successfully predict disease associated mutations in human prion-like proteins (33); identify that hydrophobic amino acid insertions promote prion formation (34); and to fine-tune prion propensity in yeast proteins (35).

However, PAPA is not perfect. All validation of PAPA was performed on preselected and compositionally homogenous datasets, primarily of Q/N-rich proteins. Therefore, it was unclear whether PAPA would perform well on a more diverse dataset, more specifically the yeast proteome. Also, it was necessary to evaluate how glutamine and asparagine-rich amyloid proteins play a role is prion formation. Q/N-rich domains are not only prevalent within yeast prion proteins, but also proteins implicated in human diseases (36, 37). By uncovering more knowledge about the parameters necessary for prion formation and propagation in yeast, we would be able to translate this information to higher eukaryotic systems.

Therefore, in Chapter 2 we set out to address PAPA's limitations, as well as identify potential new yeast prion candidates (38). Briefly, we used PAPA to identify aggregation-prone domains, with diverse compositions, in the yeast proteome. Those domains were then tested for prion activity using well-characterized prion assays as described above. Although, from this study, we identified several exciting protein

candidates, we did not identify any *bona fide* yeast prions. For the protein candidates that showed prion-like activity (other studies discussed in Chapters 3-5), we identified their role in reversible protein aggregation assemblies that regulate cellular functions; this concept will be discussed later (see Reversible protein assemblies). Ultimately, from this study we gained a deeper understanding of the composition dependencies for aggregation propensity.

Cellular factors important for prion formation

Molecular Chaperones

Prion proteins require specific cellular factors for efficient formation and propagation (review by (8), Figure 1.1). The molecular chaperone that plays a central role in this process is Hsp104, a homohexameric AAA ATPase (19). Hsp104, proposed as a protein disaggregase, promotes the fragmentation of prion proteins into oligomers that are then passed to daughter cells, at which point they can initiate new rounds of prion propagation (39). This process is critical for prion propagation, because in the absence of Hsp104 all prions, with the exception of [ISP+], are eliminated ((40). Interestingly, the overexpression of Hsp104 eliminates [PSI+] (19, 39). The most plausible explanation is Hsp104 disaggregates Sup35 prion into protein monomers, and the elimination of the infectious material leads to the loss of [PSI+] (41). Remarkably, excess Hsp104 does not eliminate other yeast prions. The reason we observe differences in Hsp104 overexpression sensitivity is unclear. One study proposed that Sup35 contains a binding site for Hsp104 (42); however, based on preliminary results, I found the proposed site was not sufficient to cure [PSI+] (data not shown). Other yeast chaperones, Hsp70 and Hsp40, also play a crucial role in prion propagation (40).

Similar to the effects seen with altered Hsp104 levels, alterations in the expression of co-chaperones can also affect the efficient propagation of yeast prions (8, 40). Altogether, the balanced expression of Hsp104, and its co-chaperones, are important, and clearly any perturbations affect efficient propagation of [PSI+], and other prion proteins.

Yeast prion-prion interactions

Prion proteins have diverse normal functions and besides being Q/N-rich, prion proteins have little primary sequence similarities. However, prion aggregates share common structural aspects, i.e. β-sheet amyloid cores (8). The structure similarities that all prion proteins share suggest the presence of one prion protein may serve as a template for the fibrilization of other prion proteins. The most dramatic and well-characterized example is that the formation of [PSI+] is strongly promoted by the presence of [PIN+] (10). In fact, [PIN+] was first identified as a non-Mendelian factor that enhanced the appearance of [PSI+] (43). This observation led to two proposed models to explain how the presence of one prion can affect the appearance of another (Figure 1.3). First, there is evidence to suggest a cross-seeding model. This model proposes [PIN+] directly interacts with Sup35 to “seed”, assisting in Sup35 initial assembly, and conversion to a prion fiber (44, 45). This is primarily supported by a study *in vitro*, in which the presence of purified and preformed [PIN+] seeds dramatically enhances the fibrillization of Sup35 (44). On the other hand, the titration model provides an alternative indirect model. This model proposes the presence of [PIN+] may sequester or titrate away an inhibitor of prion formation, allowing sufficient formation of Sup35 oligomers, and prion formation prevails. This is supported by studies *in vitro* that

showed Sup35 sufficiently forms amyloid fibers, in the absence of cellular factors (23). However, the inhibitor that prevents Sup35 fibrillization in [pin-] cells has never been identified, yet it is plausible that [PIN+] aggregates are titrating away molecular chaperones that would otherwise disaggregate and prevent the early seeds of Sup35 from growing into a prion fiber (45, 46). While there is sufficient evidence for both models, neither model explains all the experimental data to date. Therefore, the models may not be mutually exclusive, and possibly both are correct. Furthermore, the presence of an amyloid template can serve both proposed functions, as a template for initial assembly and a site to sequester prion inhibitors.

[PIN+] is not the only cellular factor that enhances [PSI+] formation. In fact, overexpression of Q/N-rich proteins can compensate for the loss of [PIN+], when its protein determinant, Rnq1p is deleted (10, 38, 44, 47). Additionally, non-Q/N cellular components, including the actin cytoskeleton, have been shown to enhance [PSI+] formation (48). While [PIN+] has the most dramatic effect on the appearance of [PSI+], it shows modest effects on the appearance of other yeast prions. Interestingly, [PIN+] or the overexpression of Q/N-rich proteins enhances the appearance of Htt103Q aggregation in a yeast Huntington disease model (49–51).

Overall, prion-prion interactions are not completely understood and future studies will aid in deciphering this phenomenon that contributes to the complexity of prion biology. In Chapter 2, we investigated if these cellular components, Hsp104 and Rnq1, are required for Q/N-rich proteins to form SDS-resistant aggregates.

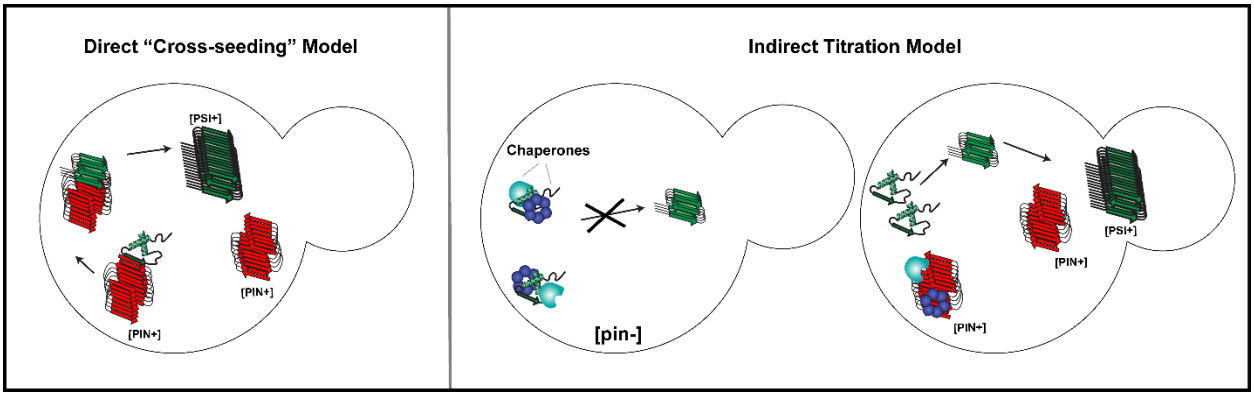

Figure 1.3: Possible mechanisms for the appearance of yeast prions
The direct “cross-seeding” model suggests [PIN+] (Red) aggregates are used as a site of initial Sup35 aggregation and conversion into [PSI+] (Green). The indirect titration model suggests in [pin-] cells, cellular factors keep Sup35 from aggregating and converting into [PSI+] (Left). In the presence of [PIN+], cellular factors are titrated away by binding [PIN+], allowing Sup35 to aggregate and convert into [PSI+] (Right).

Yeast prion formation: disease or beneficial assemblies?

One of the biggest controversies in yeast prion biology is whether yeast prions confer a disease state in yeast or serve a beneficial function (see (52) for a full discussion). There is sufficient evidence for both, therefore I feel some yeast prions are diseases, while others are beneficial, functioning as conformational switches in response to environmental fluctuations.

The controversy began from an early study showing that [PSI+] and [URE3] are not observed in nature, supporting the theory that prions are not beneficial (53). However, several years later 700 wild yeast strains were tested and many strains were found to contain [PSI+] (54), providing contradictory evidence to whether [PSI+] is naturally occurring. Additionally, another study provided evidence for both cases as well. When yeast cells were challenged with several different environmental stresses, [PSI+] was found to be detrimental to yeast viability, 75% of the time. In contrast, 25% percent of the time it was found to be beneficial and increase cellular viability during specific cellular stresses (55). It is hard to explain why prion domains, specifically Sup35's, are dispensable for their protein's normal function if the prion state of the protein is indeed beneficial (56). Therefore, for these reasons and many more, [PSI+] is most likely a protein-misfolding disease in yeast (56, 57).

However, there are several yeast prions that serve an important biological role in the cell, acting as environmental responsive factors. One example is Mot3, a transcription factor that forms the prion, [MOT3]. Under nutrient deprivation, [MOT3] activates the expression of FLO11 genes that promote multicellularity (58). Additionally, the fibrillization of Mod5 into [MOD5] provides cellular resistance to antifungal drugs

(16). Both studies provide evidence that the aggregated state of a protein is involved in yeast cellular adaptation to environmental fluctuations. Recently, this paradigm was expanded to include non-amyloid proteins, showing they stably form protein-based elements that were maintained for generations (59). This study suggests protein-based inheritance provides a mechanism for yeast to environmentally induce new traits as an adaptive response.

Yeast prions are often referred to as “bet-hedging” devices. In general, they exploit their propensity to aggregate, providing a structure that alters the protein’s function, which leads to increased yeast viability in a specific environment.

Reversible protein assemblies

Functional amyloid-like mechanisms in yeast

Classically, protein aggregation has been linked to being detrimental to cellular viability (60). However, there is an emerging concept suggesting protein aggregation can provide an advantageous function for the cell. Reversible protein assemblies form during environmental fluctuations but when conditions return to normal, the protein assemblies are reversible by dissolution or degradation. These reversible protein assemblies involve proteins that have similar sequence characteristics to known yeast prions, termed prion-like proteins. Prion-like proteins are often defined as proteins that contains an intrinsically disordered domain with low complexity of amino acid composition (LCDs), specifically enriched in uncharged polar amino acids, such as glutamine and asparagine residues (Q/N). These domains, which are modular, have specific biochemical and biophysical properties, similar to yeast prions, in which they have the propensity to self-assemble and form amyloid aggregates. While this draws

similarities to *bona fide* prion formation, it is fundamentally different because these protein aggregates are reversible and not inherited.

Yeast have several examples of reversible amyloid formation serving a beneficial role in the cell. Among these include a RNA-binding protein, Rim4, which forms amyloid-like aggregates that regulate gametogenesis (61, 62). Moreover, upon the initiation of sporulation in yeast, Rim4 monomers are converted to amyloid aggregates that actively repress translation of specific genes required in gametogenesis. However, upon the onset of meiosis II, the amyloid aggregates are degraded and translation resumes. Similarly, “kog1 bodies” play a role in cellular adaptation during suboptimal cellular conditions. Upon glucose deprivation, disassembly of the TORC1 complex is triggered and Kog1/Raptor, a component of TORC1 complex, is phosphorylated, which triggers formation of aggregates, called kog1 bodies. The aggregation creates a memory in the TORC1 pathway which maintains cellular quiescence during stress (63). In addition, the amyloid-like aggregation of Whi3, an RNA-binding protein, allows the cell to permanently escape pheromone-induced cell cycle arrest (64). Another example, Nab3, an essential RNA-binding protein, is required for transcription termination of short, non-coding transcripts. Specifically, amyloid formation of Nab3, via the PrLD, is essential for viability (65, 66).

Altogether, the cell exploits prion-like domains because they have a propensity to form amyloid structures, acting as environmental switches and aggregating in response to specific environmental cues. The aggregated form of the protein then serves temporary function or memory for the cell, the aggregate reverses when the environmental cue dissipates, which is crucial to maintaining cellular homeostasis.

Transient protein assemblies: Stress granules

In eukaryotic cells, there are several non-membranous compartments that contain RNA and protein complexes, termed ribonulceoproteins (RNP granules). Examples include nuclear bodies (Cajal bodies, paraspeckles, etc.) and cytoplasmic bodies (processing-bodies and stress granules), both serving diverse functions for the cell (67). Despite their diverse functions in the cell, their biophysical properties are similar. They form dynamic and reversible protein assemblies to concentrate specific cellular components to serve their function.

Stress granules and processing bodies are two types of cytoplasmic bodies that both play important yet distinct roles in RNA metabolism (reviewed by (68–70). Processing bodies, termed P-bodies, are primarily composed of proteins associated with mRNA decay, because mRNAs within P-bodies are typically targeted for degradation (71, 72). P-bodies are always present in the cell and increase in number and size during stress conditions, unlike stress granules which only form during stress conditions. Stress granules are primarily composed of mRNAs stalled in translation initiation; thus, they contain initiation factors along with a variety of RNA-binding proteins (68, 73). However, the diverse proteome of stress granules truly depends on the type of stress the cell is exposed to (74).

Under steady-state conditions, mRNA is exported from the nucleus where it assembles with protein translation machinery. Alternatively, during stress conditions, mRNAs bound by RNA-binding proteins are recruited to stress granules. This process is accompanied by inhibition of translation, specifically, the translation of “housekeeping” proteins, whereas the translation of mRNAs encoding molecular chaperones is

promoted (75). Also, stress granules are dynamic compartments; they interact and exchange protein components with P-bodies and the cytoplasm and are reversible upon stress relief (68, 76). Any perturbations in the regulation of stress granules could lead to aberrant stress granules, which are associated with many neurodegenerative diseases (77, 78).

Molecular Interactions Involved in Stress Granule Assembly

There are several important interactions that influence stress granule assembly, including protein-RNA interactions, protein-protein interactions and post-translational modifications (see Figure 1.4).

Stress granule formation is promoted by the accumulation of many weak non-covalent interactions (reviewed by (69)). For example, multiple mRNA-binding proteins can crosslink multiple mRNAs which can provide a scaffold for other multivalent interactions. These interactions lead to an elaborate network of many weak non-covalent interactions, which creates a dynamic and metastable stress granule. Multivalent interactions in stress granules are not defined; therefore, they can vary and are constantly rearranging, contributing to their dynamic nature. Historically, multivalent interactions have been described by interactions between RNA-binding proteins and RNA but recently, RNA alone has been shown to self-assemble and promote the formation of stress granules (79–81). Interestingly, repeat expansions in mRNA transcripts are associated with several neurodegenerative diseases including amyotrophic lateral sclerosis, Huntington disease, among others (reviewed by (82)). The hallmark of these diseases arises from the accumulation of repeat expanded transcripts in nuclear granules. In fact, a study found RNA containing repeat expansions

were able to make multivalent-basing pairing interactions that drove aggregation of RNA alone *in vitro* (80).

Another non-covalent interaction that contributes to the assembly of stress granules is protein-protein interactions. It appears the presence of specific proteins in stress granules can affect the localization and recruitment of other stress granule proteins. Specifically, when Pab1, a stress granule protein found in several different type of stress granules, is depleted from cells there is a reduction in the presence of stress granules (83).

In addition, many proteins, specifically RNA-binding proteins, found in stress granules contain intrinsically disordered regions (IDRs). IDRs are defined by lacking protein secondary structure and thereby are highly flexible, allowing them to adopt different conformations (84, 85). Also, they participate in promiscuous multivalent interactions, both homotypically and heterotypically, with other IDRs and RNA (86–88). The structural flexibility of IDRs provides several advantages, such as the propensity to aggregate rapidly and reversibly. Cells exploit these domains for cellular adaptation and survival, but these proteins are on the brink of aggregation; therefore, the assembly of these domains must be tightly regulated. In fact, dysregulation could lead to aberrant aggregation and pathological consequences, found in several neurodegenerative diseases.

IDRs are frequently low complexity domains (LCDs). LCDs are defined as a region of a protein with a strong amino acid bias. One specific type of low complexity domain is a prion-like domain, defined by having compositional similarity to yeast prion proteins and having the tendency to self-assemble and forming aggregates (15, 38).

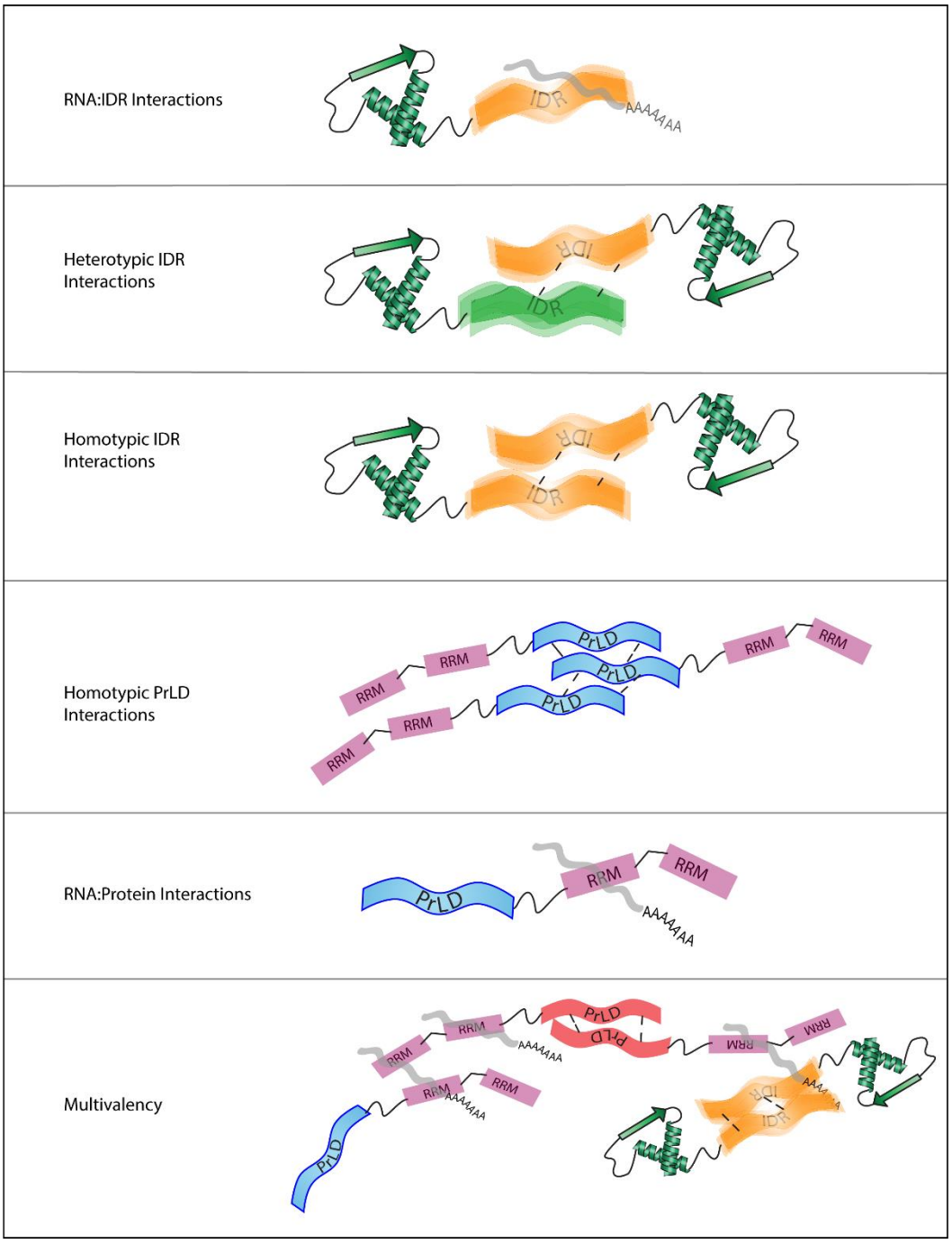

Figure 1.4: Molecular interactions involved in stress granule formation

PrLDs are prevalent in stress granule proteins, and mutations within the domains can promote amyloid formation. Amyloid formation reduces the dynamic nature of a stress granule, thereby leading to pathological consequences associated with neurodegenerative diseases (33, 37, 88–90).

PrLDs' nature to self-assemble and form aggregates is beneficial for the cell to respond to fluctuations in the environment. Moreover, they provide a conformational flexibility and participate in weak non-covalent multivalent interactions.

mRNA-binding proteins contain RNA recognition motifs and therefore have the propensity to bind RNA. Interestingly, there is an enrichment of the mRNA-binding proteins containing PrLDs in the human proteome (37). This provides mRNA-binding proteins the ability to participate in both protein-protein and protein-RNA interactions. It is well-characterized that PrLDs have the propensity to self-assemble; however, it remains unclear whether PrLDs have the propensity to participate in heterotypic interactions, as has been observed for some other IDRs. There has been an enormous effort to understand the biophysical properties of PrLDs, in general IDRs, *in vitro* (reviewed by (91)). Surprisingly, the conditions that drive protein aggregation *in vitro* (low temperatures, low salt and low pH) are contradictory to the conditions that drive aggregation *in vivo* (high temperatures, high salt and high pH) suggesting we have begun to uncover the biophysical properties of reversible protein assemblies *in vitro*, but it remains to be elucidated in a cellular environment.

Several investigations have found PrLDs are necessary for stress granule assembly. Interestingly, specific PrLDs are not necessary but require the presence of a

PrLD in general. This was illustrated by the swapping of PrLDs from other proteins to sufficiently regain the protein's ability to be recruited to stress granules (92, 93).

In Chapters 3 and 4 we set out to investigate the amino acid composition requirements of PrLDs to be recruited to heat-induced granules. In Chapter 3, we determined that the PrLD of a novel stress granule protein, Sky1, is necessary for its efficient recruitment to stress granules. Also, we showed the recruitment was primarily driven by PrLD interactions because PrLDs from other stress granule and prion proteins were sufficient for recruitment to stress granules, but non-aggregation prone PrLDs were not. In chapter 4, we screened a large dataset of PrLDs and determined if they were recruited to heat-induced stress granules. This screen was performed to better understand the compositional requirements for PrLDs' recruitment to stress granules.

Overall, IDRs, LCDs and PrLDs have together shed light on the assembly requirements for stress granule formation. They provide the structural flexibility to create the elaborate network of interactions that are critical to maintain the dynamic compartment, and that can adopt diverse structures depending on the environment.

Lastly, post-translational modifications, such as methylation and phosphorylation, contribute to stress granule assembly, most likely through altering protein-protein interactions. For example, arginine methylation of RGG domains, motifs found in many stress granule proteins, promote stress granule assembly (94, 95). In addition, protein phosphorylation is an important modification for stress granule assembly. In mammalian cells, stress granule assembly represses translation initiation via the phosphorylation of eIF2α, a hallmark of mammalian stress granules. However, yeast do not require this phosphorylation event to repress translation (96, 97). How post-translational

modifications modulate stress granules is described mostly in mammalian cells; therefore, future studies investigating the presence of these modifications in yeast will provide insights into interactions important for yeast stress granule assembly as well as identify important regulators of stress granules (see Chapter 6:Conclusions).

Stress granule assembly model

When cells are faced with fluctuations in their environment, they rapidly adapt by reorganizing their cellular processes and functions accordingly. Stress granules rapidly form in response to stress, but the mechanism of formation is still being uncovered. The current model suggests RNP granules are liquid-liquid phase separations (LLPS). This process is driven primarily by weak multivalent interactions made between mRNA and protein, which accumulate and lead to RNP granules concentrating into a separate phase within the cytoplasm (98). This creates a microenvironment, like oil in water, where the concentration of RNPs is high, thereby allowing them to find each other and facilitate rearrangement and regulation within the granule. Notably one study, using super-resolution microscopy, provided sufficient evidence to suggest a model for stress granule assembly (99, 100). Briefly, stress granules contain a subset of proteins that form a solid-like core that is surrounded by a more diverse proteome, including stress granule modulators, to form a dynamic shell, suggesting LLPS is restricted to the outer layer (Figure 1.5).

There is strong evidence supporting LLPS as a mechanism for stress granule assembly. First, at high concentrations, PrLDs and IDRs from known stress granule proteins, are sufficient to phase separate *in vitro* (87, 88, 101). Also, stress granules have liquid-like behavior in cells, visualized as being highly dramatic structures by

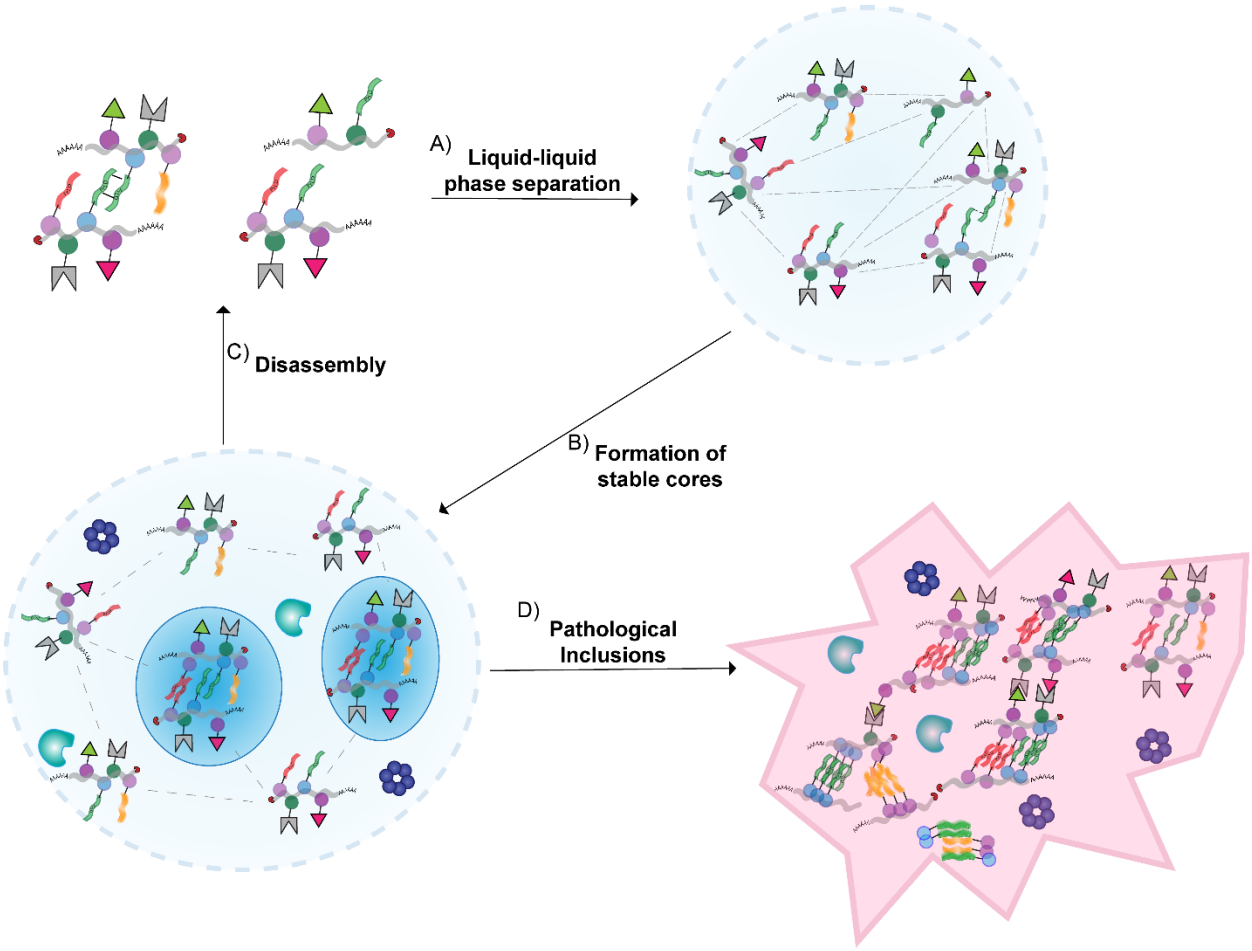

Figure 1.5: Model of stress granule formation
Stalled translation initiation complexes accumulate during stress. (A) High local concentrations of PrLDs triggers liquid-liquid phase separation. (B) Non-covalent interactions are made and rearranged to form the “solid”-like core (dark blue circles). mRNPs surround the core and form a dynamic shell of interactions. Regulators of stress granules are proposed to transiently associate with mRNPs within the dynamic shell. (C) Upon stress relief, the dissolution of stress granules occurs, and proteins return to their soluble state. (D) Mutation or dysregulation of stress granule proteins promote amyloid formation, and thereby leading to pathological inclusions.

fluorescence recovery after photobleaching (FRAP) (reviewed by (68, 95). Several studies, performed in higher eukaryotic organisms, have shown how phase transition compartmentalizes cellular factors and regulates various cellular processes (reviewed by (102)). Briefly, P-granules, a type of RNP, of the *C. elegans* germline exhibit liquid-like behavior, such as droplet fusion, and the formation of these dynamic P-granules is important for the development of *C. elegans* (103). Also, the size and shape of the nucleoli of *Xenopus laevis* is governed by dynamic RNP granules (104).

Stress granule disassembly

To elucidate the mechanism of how stress granules form and rapidly disassemble after the stress is relieved, identifying the diversity of proteins present in stress granules will aid in understanding the cellular pathways involved. Several studies have investigated the composition of stress granules in a variety of different stresses in yeast (99, 105–108) and mammalian cells (99, 109, 110). In summary, the client protein diversity of stress granules was confirmed by these studies but more importantly new insights into assembly and disassembly mechanisms were revealed.

The Wallace *et al.,* 2015 study used heat stress and identified a variety of RNA-binding proteins and RNA helicases, but their dataset was mostly absent of molecular chaperones. Molecular chaperones, specifically Hsp104, Ydj1 and Sis1, have been implicated in disassembly of stress granules (111, 112). This finding suggests a fundamental distinction between protein aggregation in stress granules and the recruitment of proteins to stress granules (107). Notably, they determined undamaged protein aggregates were completely dissolved and returned to normal function after cells were allowed to recover from heat stress. This is in contrast to previous studies

suggesting stress granules are degraded or cleared by autophagy (71, 111). Therefore, this study suggested heat-induced protein aggregation is an adaptive and autoregulatory process that aids in cellular adaptation.

The Jain *et al.,* 2016 study used NaN_3 stress and isolated several novel yeast stress granule proteins unique to NaN_3 stress. In addition, they showed distinct steps in stress granule formation and dissolution are modulated by ATP and ATP-dependent protein and nucleic acid remodeling complexes. The chaperonin-containing T complex (CCT), inhibited stress granule formation, while the mini-chromosome maintenance (MCM) and RuvB-like (RVB) complexes inhibited stress granule disassembly (99). Overall, this study provided insights into mechanisms underlying stress granule formation and regulation. The process requires modulators to actively regulate the proper organization of RNPs and dysregulation could lead to detrimental consequences for the cell.

Molecular chaperones are important cellular factors for efficient stress granule disassembly. Hsp104 is molecular chaperone important for thermotolerance and protein disaggregation in yeast (113, 114). The absence of Hsp104 has no effect on heat-induced stress granule assembly, but during recovery, cells are severely defective in resolubilizing stress granule proteins (111). In addition, Hsp40 molecular chaperones play important roles in the reorganization of cellular processes during recovery from cellular stresses (112). Specifically, Ydj1 promotes disassembly of stress granules by promoting translation during stress recovery. Sis1 has a different role in the disassembly during stress recovery, by targeting stress granules to the autophagy pathway. Altogether, this suggests the importance of molecular chaperones in the

concerted regulation of stress granule disassembly and in ensuring proteins regain normal function once the stress is no longer present (reviewed by (115).

As post-translation modifications play an important role in the assembly of stress granules, they also play a role in disassembly, by likely affecting protein-protein interactions. For example, Grb7, a protein translation repressor is an integral stress granule protein that aggregates during stress. Upon during stress recovery, Grb7 is hyper-phosphorylated, losing important interactions required for stress granule formation, and thereby promoting the disassembly of stress granules (116). Similarly, as a response to stress, Cdc19 aggregates, stalling the cell cycle. During stress recovery, Cdc19 is phosphorylated within its LCD which promotes stress granule dissolution, thereby allowing cells re-enter the cell cycle (117). Additionally, in Chapter 3, we identified a novel stress granule regulator, protein kinase Sky1. Sky1 was found to differentially phosphorylate a RNA-binding protein, Npl3, during stress recovery. The phosphorylation state of Npl3 modulated efficient stress granule disassembly. Also, we characterized the Sky1-mediated regulation pathway as an alternative and compensating pathway for stress granule disassembly.

Stress granules are fascinating. Cells utilize rapid and reversible protein aggregation into stress granules as a protective response to stress. However, any perturbation in these concerted pathways lead to disease (Figure 1.3B). The field has just begun to unravel the complexity of stress granules in eukaryotic cells. Clearly the important interactions involved in stress granule assembly have been identified, but clarifying the biophysical properties of stress granules in a cellular environment and identifying the important regulators in stress granules are important avenues for future

studies. The list of neurodegenerative diseases associated with aberrant stress granules continues to grow. Better understanding of the regulation of stress granules will provide potential therapeutic targets to combat these diseases (118).

Concluding remarks

The following chapters illustrate our findings about the role PrLDs play in the regulation of cellular processes, mostly stress induced responses. First in Chapter 2, we investigated the yeast proteome for aggregation-prone proteins. From this study, we identified several protein domains with aggregation propensity. In the follow-up studies, we set out to investigate the role the PrLDs contribute to the normal function of the full-length protein. In Chapter 3, we uncovered a novel stress granule regulator and its recruitment requires the presence of a PrLD. In Chapter 5, we propose the aggregation of several vacuolar proteins, primarily through the interactions of their PrLDs, mediates the activation of a vacuolar-signaling complex. Additionally, in chapter 4 we determined the extent of which PrLDs are recruited to stress granules, mostly to determine if the recruitment to stress granules is compositionally biased or driven by non-specific interactions.

REFERENCES

1. Bolton DC, McKinley MP, Prusiner SB (1982) Identification of a protein that purifies with the scrapie prion. *Science (New York, NY)* 218(4579):1309–11.
2. Aguzzi A, Polymenidou M (2004) Mammalian Prion Biology: One Century of Evolving Concepts. *Cell* 116(2):313–327.
3. Prusiner SB (1998) Prions. *Proceedings of the National Academy of Sciences of the United States of America* 95(23):13363–83.
4. Igel-Egalon A, Béringue V, Rezaei H, Sibille P (2018) Prion Strains and Transmission Barrier Phenomena. *Pathogens* 7(1):5.
5. Cox BS (1965) Ψ, A cytoplasmic suppressor of super-suppressor in yeast. *Heredity* 20(4):505–521.
6. Wickner RB (1994) [URE3] as an altered URE2 protein: evidence for a prion analog in Saccharomyces cerevisiae. *Science (New York, NY)* 264(5158):566–9.
7. Tuite MF, Marchante R, Kushnirov V (2011) Fungal prions: structure, function and propagation. *Topics in current chemistry* 305:257–98.
8. Liebman SW, Chernoff YO (2012) Prions in yeast. *Genetics* 191(4):1041–72.
9. Chernova TA, Wilkinson KD, Chernoff YO (2014) Physiological and environmental control of yeast prions. *FEMS microbiology reviews* 38(2):326–44.
10. Derkatch IL, Bradley ME, Hong JY, Liebman SW (2001) Prions affect the appearance of other prions: the story of [PIN(+)]. *Cell* 106(2):171–82.
11. Sondheimer N, Lindquist S (2000) Rnq1: an epigenetic modifier of protein function in yeast. *Molecular cell* 5(1):163–72.
12. Du Z, Park K-W, Yu H, Fan Q, Li L (2008) Newly identified prion linked to the chromatin-remodeling factor Swi1 in Saccharomyces cerevisiae. *Nature genetics* 40(4):460–5.
13. Patel BK, Gavin-Smyth J, Liebman SW (2009) The yeast global transcriptional co-repressor protein Cyc8 can propagate as a prion. *Nature cell biology* 11(3):344–9.
14. Rogoza T, et al. (2010) Non-Mendelian determinant [ISP+] in yeast is a nuclear-residing prion form of the global transcriptional regulator Sfp1. *Proceedings of the National Academy of Sciences of the United States of America* 107(23):10573–7.
15. Alberti S, Halfmann R, King O, Kapila A, Lindquist S (2009) A Systematic Survey Identifies Prions and Illuminates Sequence Features of Prionogenic Proteins. *Cell* 137(1):146–158.
16. Suzuki G, Shimazu N, Tanaka M (2012) A yeast prion, Mod5, promotes acquired drug resistance and cell survival under environmental stress. *Science (New York, NY)* 336(6079):355–9.
17. Halfmann R, Wright JR, Alberti S, Lindquist S, Rexach M (2012) Prion formation by a yeast GLFG nucleoporin. *Prion* 6(4):391–9.
18. Chernoff YO, Derkach IL, Inge-Vechtomov SG (1993) Multicopy SUP35 gene induces de-novo appearance of psi-like factors in the yeast Saccharomyces cerevisiae. *Current genetics* 24(3):268–70.
19. Chernoff YO, Lindquist SL, Ono B, Inge-Vechtomov SG, Liebman SW (1995) Role of the chaperone protein Hsp104 in propagation of the yeast prion-like factor

[psi+]. *Science (New York, NY)* 268(5212):880–4.
20. Edskes HK, Gray VT, Wickner RB (1999) The [URE3] prion is an aggregated form of Ure2p that can be cured by overexpression of Ure2p fragments. *Proceedings of the National Academy of Sciences of the United States of America* 96(4):1498–503.
21. Li L, Lindquist S (2000) Creating a protein-based element of inheritance. *Science (New York, NY)* 287(5453):661–4.
22. Perutz MF, Pope BJ, Owen D, Wanker EE, Scherzinger E (2002) Aggregation of proteins with expanded glutamine and alanine repeats of the glutamine-rich and asparagine-rich domains of Sup35 and of the amyloid beta-peptide of amyloid plaques. *Proceedings of the National Academy of Sciences of the United States of America* 99(8):5596–600.
23. Glover JR, et al. (1997) Self-seeded fibers formed by Sup35, the protein determinant of [PSI+], a heritable prion-like factor of S. cerevisiae. *Cell* 89(5):811–9.
24. Halfmann R, Lindquist S (2008) Screening for amyloid aggregation by Semi-Denaturing Detergent-Agarose Gel Electrophoresis. *Journal of visualized experiments : JoVE* (17). doi:10.3791/838.
25. LeVine H (1993) Thioflavine T interaction with synthetic Alzheimer's disease beta-amyloid peptides: detection of amyloid aggregation in solution. *Protein science : a publication of the Protein Society* 2(3):404–10.
26. Cascarina SM, Ross ED (2014) Yeast prions and human prion-like proteins: sequence features and prediction methods. *Cellular and molecular life sciences : CMLS* 71(11):2047–63.
27. Thompson MJ, et al. (2006) The 3D profile method for identifying fibril-forming segments of proteins. *Proceedings of the National Academy of Sciences of the United States of America* 103(11):4074–8.
28. Goldschmidt L, Teng PK, Riek R, Eisenberg D (2010) Identifying the amylome, proteins capable of forming amyloid-like fibrils. *Proceedings of the National Academy of Sciences of the United States of America* 107(8):3487–92.
29. Nelson R, Eisenberg D (2006) Recent atomic models of amyloid fibril structure. *Current Opinion in Structural Biology* 16(2):260–265.
30. Toombs JA, et al. (2012) De novo design of synthetic prion domains. *Proceedings of the National Academy of Sciences of the United States of America* 109(17):6519–24.
31. Lancaster AK, Nutter-Upham A, Lindquist S, King OD (2014) PLAAC: a web and command-line application to identify proteins with prion-like amino acid composition. *Bioinformatics (Oxford, England)* 30(17):2501–2.
32. Toombs JA, McCarty BR, Ross ED (2010) Compositional determinants of prion formation in yeast. *Molecular and cellular biology* 30(1):319–32.
33. Kim HJ, et al. (2013) Mutations in prion-like domains in hnRNPA2B1 and hnRNPA1 cause multisystem proteinopathy and ALS. *Nature* 495(7442):467–73.
34. Gonzalez Nelson AC, et al. (2014) Increasing prion propensity by hydrophobic insertion. *PloS one* 9(2):e89286.
35. Paul KR, Hendrich CG, Waechter A, Harman MR, Ross ED (2015) Generating new prions by targeted mutation or segment duplication. *Proceedings of the*

National Academy of Sciences of the United States of America 112(28):8584–9.
36. Michelitsch MD, Weissman JS (2000) A census of glutamine/asparagine-rich regions: implications for their conserved function and the prediction of novel prions. *Proceedings of the National Academy of Sciences of the United States of America* 97(22):11910–5.
37. King OD, Gitler AD, Shorter J (2012) The tip of the iceberg: RNA-binding proteins with prion-like domains in neurodegenerative disease. *Brain Research* 1462:61–80.
38. Shattuck JE, Waechter AC, Ross ED (2017) The effects of glutamine/asparagine content on aggregation and heterologous prion induction by yeast prion-like domains. *Prion* 11(4):249–264.
39. Shorter J, Lindquist S (2004) Hsp104 catalyzes formation and elimination of self-replicating Sup35 prion conformers. *Science (New York, NY)* 304(5678):1793–7.
40. Reidy M, Masison DC (2011) Modulation and elimination of yeast prions by protein chaperones and co-chaperones. *Prion* 5(4):245–249.
41. Kushnirov V V, Ter-Avanesyan MD (1998) Structure and replication of yeast prions. *Cell* 94(1):13–6.
42. Helsen CW, Glover JR (2012) Insight into molecular basis of curing of [PSI+] prion by overexpression of 104-kDa heat shock protein (Hsp104). *The Journal of biological chemistry* 287(1):542–56.
43. Derkatch IL, Bradley ME, Zhou P, Chernoff YO, Liebman SW (1997) Genetic and environmental factors affecting the de novo appearance of the [PSI+] prion in Saccharomyces cerevisiae. *Genetics* 147(2):507–19.
44. Derkatch IL, et al. (2004) Effects of Q/N-rich, polyQ, and non-polyQ amyloids on the de novo formation of the [PSI+] prion in yeast and aggregation of Sup35 in vitro. *Proceedings of the National Academy of Sciences of the United States of America* 101(35):12934–9.
45. Derkatch IL, Liebman SW (2007) Prion-prion interactions. *Prion* 1(3):161–9.
46. Osherovich LZ, Weissman JS (2002) The utility of prions. *Developmental cell* 2(2):143–51.
47. Yang Z, et al. (2013) Heterologous Gln/Asn-Rich Proteins Impede the Propagation of Yeast Prions by Altering Chaperone Availability. *PLoS Genetics* 9(1):e1003236.
48. Ganusova EE, et al. (2006) Modulation of prion formation, aggregation, and toxicity by the actin cytoskeleton in yeast. *Molecular and cellular biology* 26(2):617–29.
49. Kantcheva RB, Mason R, Giorgini F (2014) Aggregation-prone proteins modulate huntingtin inclusion body formation in yeast. *PLoS currents* 6. doi:10.1371/currents.hd.501008f3051342c9a5c0cd0f3a5bf3a4.
50. Duennwald ML, Jagadish S, Giorgini F, Muchowski PJ, Lindquist S (2006) A network of protein interactions determines polyglutamine toxicity.
51. Meriin AB, et al. (2002) Huntington toxicity in yeast model depends on polyglutamine aggregation mediated by a prion-like protein Rnq1. *The Journal of cell biology* 157(6):997–1004.
52. Halfmann R, Alberti S, Lindquist S (2010) Prions, protein homeostasis, and phenotypic diversity. *Trends in cell biology* 20(3):125–33.

53. Nakayashiki T, Kurtzman CP, Edskes HK, Wickner RB (2005) Yeast prions [URE3] and [PSI+] are diseases. *Proceedings of the National Academy of Sciences of the United States of America* 102(30):10575–80.
54. Halfmann R, et al. (2012) Prions are a common mechanism for phenotypic inheritance in wild yeasts. *Nature* 482(7385):363–368.
55. Tyedmers J, Madariaga ML, Lindquist S (2008) Prion switching in response to environmental stress. *PLoS biology* 6(11):e294.
56. Wickner RB, Edskes HK, Shewmaker F, Nakayashiki T (2007) Prions of fungi: inherited structures and biological roles. *Nature Reviews Microbiology* 5(8):611–618.
57. Edskes HK, McCann LM, Hebert AM, Wickner RB (2009) Prion Variants and Species Barriers Among Saccharomyces Ure2 Proteins. *Genetics* 181(3):1159–1167.
58. Holmes DL, Lancaster AK, Lindquist S, Halfmann R (2013) Heritable remodeling of yeast multicellularity by an environmentally responsive prion. *Cell* 153(1):153–65.
59. Chakrabortee S, et al. (2016) Intrinsically Disordered Proteins Drive Emergence and Inheritance of Biological Traits. *Cell* 167(2):369–381.e12.
60. Newby GA, Lindquist S (2013) Blessings in disguise: biological benefits of prion-like mechanisms. *Trends in cell biology* 23(6):251–9.
61. Berchowitz LE, et al. (2015) Regulated Formation of an Amyloid-like Translational Repressor Governs Gametogenesis. *Cell* 163(2):406–18.
62. Ford AF, Shorter J (2015) Fleeting Amyloid-like Forms of Rim4 Ensure Meiotic Fidelity. *Cell* 163(2):275–6.
63. Hughes Hallett JE, Luo X, Capaldi AP (2015) Snf1/AMPK promotes the formation of Kog1/Raptor-bodies to increase the activation threshold of TORC1 in budding yeast. *eLife* 4. doi:10.7554/eLife.09181.
64. Caudron F, Barral Y (2013) A super-assembly of Whi3 encodes memory of deceptive encounters by single cells during yeast courtship. *Cell* 155(6):1244–57.
65. Loya TJ, O'Rourke TW, Reines D (2017) The hnRNP-like Nab3 termination factor can employ heterologous prion-like domains in place of its own essential low complexity domain. *PLOS ONE* 12(10):e0186187.
66. O'Rourke TW, Loya TJ, Head PE, Horton JR, Reines D (2015) Amyloid-like assembly of the low complexity domain of yeast Nab3. *Prion* 9(1):34–47.
67. Spector DL (2006) SnapShot: Cellular Bodies. *Cell* 127(5):1071.e1-1071.e2.
68. Buchan JR, Parker R (2009) Eukaryotic stress granules: the ins and outs of translation. *Molecular cell* 36(6):932–41.
69. Protter DSW, Parker R (2016) Principles and Properties of Stress Granules. *Trends in Cell Biology* 26(9):668–679.
70. Kedersha N, Anderson P (2007) Mammalian Stress Granules and Processing Bodies. *Methods in Enzymology*, pp 61–81.
71. Buchan JR, Kolaitis R-M, Taylor JP, Parker R (2013) Eukaryotic Stress Granules Are Cleared by Autophagy and Cdc48/VCP Function. *Cell* 153(7):1461–1474.
72. Parker R, Sheth U (2007) P bodies and the control of mRNA translation and degradation. *Molecular cell* 25(5):635–46.
73. Hoyle NP, Castelli LM, Campbell SG, Holmes LEA, Ashe MP (2007) Stress-

dependent relocalization of translationally primed mRNPs to cytoplasmic granules that are kinetically and spatially distinct from P-bodies. *The Journal of cell biology* 179(1):65–74.
74. Buchan JR, Yoon J-H, Parker R (2011) Stress-specific composition, assembly and kinetics of stress granules in Saccharomyces cerevisiae. *Journal of cell science* 124(Pt 2):228–39.
75. Anderson P, Kedersha N (2002) Stressful initiations. *Journal of cell science* 115(Pt 16):3227–34.
76. Buchan JR, Muhlrad D, Parker R (2008) P bodies promote stress granule assembly in Saccharomyces cerevisiae. *The Journal of cell biology* 183(3):441–55.
77. Ramaswami M, Taylor JP, Parker R (2013) Altered ribostasis: RNA-protein granules in degenerative disorders. *Cell* 154(4):727–36.
78. Li YR, King OD, Shorter J, Gitler AD (2013) Stress granules as crucibles of ALS pathogenesis. *The Journal of cell biology* 201(3):361–72.
79. Van Treeck B, et al. (2018) RNA self-assembly contributes to stress granule formation and defining the stress granule transcriptome. *Proceedings of the National Academy of Sciences of the United States of America*:201800038.
80. Jain A, Vale RD (2017) RNA phase transitions in repeat expansion disorders. *Nature* 546(7657):243–247.
81. Schwartz JC, Wang X, Podell ER, Cech TR (2013) RNA seeds higher-order assembly of FUS protein. *Cell reports* 5(4):918–25.
82. La Spada AR, Taylor JP (2010) Repeat expansion disease: progress and puzzles in disease pathogenesis. *Nature reviews Genetics* 11(4):247–58.
83. Swisher KD, Parker R (2010) Localization to, and Effects of Pbp1, Pbp4, Lsm12, Dhh1, and Pab1 on Stress Granules in Saccharomyces cerevisiae. *PLoS ONE* 5(4):e10006.
84. Malinovska L, Kroschwald S, Alberti S (2013) Protein disorder, prion propensities, and self-organizing macromolecular collectives. *Biochimica et biophysica acta* 1834(5):918–31.
85. Wright PE, Dyson HJ (2015) Intrinsically disordered proteins in cellular signalling and regulation. *Nature Reviews Molecular Cell Biology* 16(1):18–29.
86. Protter DSW, et al. (2018) Intrinsically Disordered Regions Can Contribute Promiscuous Interactions to RNP Granule Assembly. *Cell reports* 22(6):1401–1412.
87. Lin Y, Protter DSW, Rosen MK, Parker R (2015) Formation and Maturation of Phase-Separated Liquid Droplets by RNA-Binding Proteins. *Molecular cell* 60(2):208–19.
88. Molliex A, et al. (2015) Phase Separation by Low Complexity Domains Promotes Stress Granule Assembly and Drives Pathological Fibrillization Article Phase Separation by Low Complexity Domains Promotes Stress Granule Assembly and Drives Pathological Fibrillization. *Cell* 163(1):123–133.
89. Murakami T, et al. (2015) ALS/FTD Mutation-Induced Phase Transition of FUS Liquid Droplets and Reversible Hydrogels into Irreversible Hydrogels Impairs RNP Granule Function. *Neuron* 88(4):678–90.
90. Patel A, et al. (2015) A Liquid-to-Solid Phase Transition of the ALS Protein FUS

Accelerated by Disease Mutation. *Cell* 162(5):1066–1077.
91. Boeynaems S, et al. (2018) Protein Phase Separation: A New Phase in Cell Biology. *Trends in Cell Biology*. doi:10.1016/j.tcb.2018.02.004.
92. Decker CJ, Teixeira D, Parker R (2007) Edc3p and a glutamine/asparagine-rich domain of Lsm4p function in processing body assembly in *Saccharomyces cerevisiae*. *The Journal of Cell Biology* 179(3):437–449.
93. Gilks N, et al. (2004) Stress granule assembly is mediated by prion-like aggregation of TIA-1. *Molecular biology of the cell* 15(12):5383–98.
94. Nott TJ, et al. (2015) Phase transition of a disordered nuage protein generates environmentally responsive membraneless organelles. *Molecular cell* 57(5):936–47.
95. Poornima G, Shah S, Vignesh V, Parker R, Rajyaguru PI (2016) Arginine methylation promotes translation repression activity of eIF4G-binding protein, Scd6. *Nucleic Acids Research* 44(19):9358–9368.
96. Kedersha NL, Gupta M, Li W, Miller I, Anderson P (1999) RNA-binding proteins TIA-1 and TIAR link the phosphorylation of eIF-2 alpha to the assembly of mammalian stress granules. *The Journal of cell biology* 147(7):1431–42.
97. Grousl T, et al. (2009) Robust heat shock induces eIF2alpha-phosphorylation-independent assembly of stress granules containing eIF3 and 40S ribosomal subunits in budding yeast, Saccharomyces cerevisiae. *Journal of cell science* 122(Pt 12):2078–88.
98. Weber SC, Brangwynne CP (2012) Getting RNA and Protein in Phase. *Cell* 149(6):1188–1191.
99. Jain S, et al. (2016) ATPase-Modulated Stress Granules Contain a Diverse Proteome and Substructure. *Cell* 164(3):487–98.
100. Wheeler JR, Matheny T, Jain S, Abrisch R, Parker R (2016) Distinct stages in stress granule assembly and disassembly. *eLife* 5. doi:10.7554/eLife.18413.
101. Guo L, Shorter J (2015) It's Raining Liquids: RNA Tunes Viscoelasticity and Dynamics of Membraneless Organelles. *Molecular Cell* 60(2):189–192.
102. Aguzzi A, Altmeyer M (2016) Phase Separation: Linking Cellular Compartmentalization to Disease. *Trends in cell biology* 26(7):547–558.
103. Brangwynne CP, et al. (2009) Germline P Granules Are Liquid Droplets That Localize by Controlled Dissolution/Condensation. *Science* 324(5935):1729–1732.
104. Brangwynne CP, Mitchison TJ, Hyman AA (2011) Active liquid-like behavior of nucleoli determines their size and shape in Xenopus laevis oocytes. *Proceedings of the National Academy of Sciences* 108(11):4334–4339.
105. Cherkasov V, et al. (2015) Systemic control of protein synthesis through sequestration of translation and ribosome biogenesis factors during severe heat stress. *FEBS Letters* 589(23):3654–3664.
106. Narayanaswamy R, et al. (2009) Widespread reorganization of metabolic enzymes into reversible assemblies upon nutrient starvation. *Proceedings of the National Academy of Sciences* 106(25):10147–10152.
107. Wallace EWJ, et al. (2015) Reversible, Specific, Active Aggregates of Endogenous Proteins Assemble upon Heat Stress. *Cell* 162(6):1286–1298.
108. Cary GA, Vinh DBN, May P, Kuestner R, Dudley AM (2015) Proteomic Analysis of Dhh1 Complexes Reveals a Role for Hsp40 Chaperone Ydj1 in Yeast P-Body

Assembly. *G3: Genes|Genomes|Genetics* 5(11):2497–2511.
109. Markmiller S, et al. (2018) Context-Dependent and Disease-Specific Diversity in Protein Interactions within Stress Granules. *Cell* 172(3):590–604.e13.
110. Youn J-Y, et al. (2018) High-Density Proximity Mapping Reveals the Subcellular Organization of mRNA-Associated Granules and Bodies. *Molecular Cell* 69(3):517–532.e11.
111. Cherkasov V, et al. (2013) Coordination of Translational Control and Protein Homeostasis during Severe Heat Stress. *Current Biology* 23(24):2452–2462.
112. Walters RW, Muhlrad D, Garcia J, Parker R (2015) Differential effects of Ydj1 and Sis1 on Hsp70-mediated clearance of stress granules in Saccharomyces cerevisiae. *RNA (New York, NY)* 21(9):1660–71.
113. Lindquist S, Kim G (1996) Heat-shock protein 104 expression is sufficient for thermotolerance in yeast. *Proceedings of the National Academy of Sciences of the United States of America* 93(11):5301–6.
114. Parsell DA, Kowal AS, Singer MA, Lindquist S (1994) Protein disaggregation mediated by heat-shock protein Hspl04. *Nature* 372(6505):475–478.
115. Walters RW, Parker R (2015) Coupling of Ribostasis and Proteostasis: Hsp70 Proteins in mRNA Metabolism. *Trends in Biochemical Sciences* 40(10):552–559.
116. Tsai N-P, Ho P-C, Wei L-N (2008) Regulation of stress granule dynamics by Grb7 and FAK signalling pathway. *The EMBO Journal* 27(5):715–726.
117. Saad S, et al. (2017) Reversible protein aggregation is a protective mechanism to ensure cell cycle restart after stress. *Nature cell biology* 19(10):1202–1213.
118. Maziuk B, Ballance HI, Wolozin B (2017) Dysregulation of RNA Binding Protein Aggregation in Neurodegenerative Disorders. *Frontiers in Molecular Neuroscience* 10:89.

CHAPTER 2:THE EFFECTS OF GLUTAMINE/ASPARAGINE CONTENT ON AGGREGATION AND HETEROLOGOUS PRION INDUCTION BY YEAST PRION-LIKE DOMAINS[1]

Introduction

In the budding yeast *Saccharomyces cerevisiae*, at least nine proteins have been identified that form self-propagating amyloid-based prions (1). Simple phenotypic assays have been developed to monitor prion activity, making the yeast prions useful model systems to study aggregation and prion activity. Most known yeast prion proteins contain a low-complexity, intrinsically-disordered prion-forming domain that is necessary for prion activity (2, 3). These prion-forming domains tend to be glutamine/asparagine (Q/N) rich, and relatively lacking in charged and hydrophobic amino acids (4). Scrambling the sequence of Q/N-rich prion domains does not eliminate prion activity, suggesting that amino acid composition is the primary determinant of prion propensity (5–7).

A variety of computational algorithms have been designed to identify proteins that are compositionally similar to known yeast prion proteins (8–10). Hundreds of proteins in the human genome contain such prion-like domains (PrLDs) (11, 12). Recently, mutations in a number of these PrLDs have been linked to degenerative disorders, including ALS (13, 14). Emerging evidence suggests that these PrLDs may be designed to form dynamic, functional aggregates, and that disease-associated mutations can drive the proteins to form stable, detergent-insoluble amyloid-like

[1] This chapter is adapted from Shattuck, J.E., Waechter, A.C., and Ross, E.D. (2017). The effects of glutamine/asparagine content on aggregation and heterologous prion induction by yeast prion-like domains. Prion *11*, 249–264. Aubrey C Waechter built a subset of PrLDs tested in this study under my supervision

aggregates (15–18). For example, stress granules are dynamic RNA-protein assemblies that form when translation is inhibited (19, 20). Many RNA binding proteins found in stress granules contain PrLDs, and weak dynamic interactions between these PrLDs are thought to drive liquid-liquid phase separation, promoting granule formation (21, 22). Disease-associated mutations in some of these PrLDs appear to drive conversion of the PrLDs into more stable amyloid-like aggregates, thereby disrupting stress granule dynamics (15–18).

Therefore, there has been growing interest in understanding how amino acid sequence affects both PrLD aggregation propensity and the stability of these aggregates. As a first step towards addressing this question, we experimentally determined the prion propensity of each amino acid in the context of a yeast prion domain, and used these values to develop the prediction algorithm PAPA (23, 24). PAPA scans proteins for regions of intrinsic disorder, and scores the prion propensities of these regions (25). PAPA has proven effective at predicting the prion-like activity of Q/N-rich PrLDs (10); designing mutations to modulate the aggregation activity of PrLDs (26–28); designing synthetic prion-forming domains (24); and predicting the effects of some disease-associated mutations in human PrLDs (29).

However, PAPA still has substantial limitations. First, all of these previous validations of PAPA have been done on compositional homogenous datasets of Q/N-rich proteins. Therefore, it is less clear whether PAPA would be effective at identifying aggregation-prone PrLDs from a more compositionally diverse dataset such as a whole proteome. In particular, it is surprising that Q/N residues dominate yeast prion domains, yet have relatively neutral prion propensities according to PAPA (4, 11). Intrinsic

disorder may provide a partial explanation for this discrepancy. The structural flexibility of yeast prion domains appears to be important for prion formation, likely because it increases accessibility of prion-nucleating regions (30). Q and N may therefore be over-represented in part because they balance intrinsic disorder and prion propensity.

However, this theory does not explain why the yeast prion domains tend to be specifically enriched in Q and N, and not amino acids like serine, threonine and glycine, which also promote intrinsic disorder and have similar aggregation propensities (23, 31). This bias may in part be an artifact of how yeast prion proteins have been discovered. The first two prion proteins identified, Ure2 and Sup35, are both Q/N rich. Many of the subsequent prion proteins were identified either because they share similar sequence features to Ure2 and Sup35 (3, 10, 32), or because they are able to promote prion formation by Sup35 (33–35). Both methods may be biased towards Q/N residues.

Alternatively, the low predicted prion propensities of Q and N may be an artifact of the experiments used to develop PAPA. Prion propensity scores were derived by randomly mutagenizing a small portion of a Q/N-rich prion domain and examining the compositional biases of mutants that retained the ability to form prions. These experiments therefore report how small compositional changes affect prion propensity. In the context of a highly Q/N-rich domain, it appears that subtle changes in Q/N content have little effect on prion propensity. However, it remains possible that a threshold number of Q/N residues is required for some prion-promoting activity. For example, it has been proposed that, when present at high enough density, Q/N residues can promote the formation of polar zippers (36).

A second major limitation of PAPA (and likely all available prion prediction algorithms) is that prion activity is a complex process, requiring a series of discrete steps, each of which may have distinct compositional requirement, yet PAPA does not separately assess the effects of amino acid composition on each of these steps. Specifically, for a protein to act as a prion in yeast, it needs to not only form prion aggregates, but also propagate these aggregates to daughter cells during cell division. We previously developed a method to separate the effects of composition on prion formation versus prion propagation, and found that PAPA predominantly measures prion formation propensity (37). Thus, PAPA could be more accurately characterized as an aggregation predictor for PrLDs, rather than a prion predictor. However, it is still not clear whether PAPA simply predicts aggregation propensity, or whether it specifically predicts the ability to form amyloid aggregates. This distinction is important in understanding how mutations affect the dynamics of PrLD-associated aggregates.

To begin to address both of these limitations of PAPA, we used PAPA to identify predicted aggregation-prone PrLDs with a range of compositions. Each domain was then tested for the ability to aggregate, and the ability to form stable, detergent insoluble aggregates. As a control, we identified Q/N-rich segments with low predicted aggregation propensity. Almost all of the predicted PrLDs formed foci when fused to GFP, while almost none of the control domains did; however, the ability to form the detergent-insoluble aggregates that characterize yeast prions was highly dependent on Q/N content. This suggests that high Q/N content has little effect on aggregation propensity, but promotes conversion of aggregates to an amyloid state. In most cases, the formation of detergent-insoluble aggregates was independent of [*PIN*$^+$], a prion that

is required for prion formation by the yeast prion protein Sup35 (3, 33). Strikingly, almost every protein from our dataset that formed detergent-insoluble aggregates was also able to substitute for [*PIN*$^+$] in stimulating prion formation by Sup35, highlighting the highly promiscuous nature of these interactions. Together these data aid in unraveling the complex biology and structural characteristics for a protein to form a prion in yeast.

Results

PAPA predicts the ability of PrLDs to form foci

Yeast prion domains are generally modular, meaning that they maintain aggregation and prion activity when transferred to other proteins (38). Alberti *et al.* previously scanned the yeast genome for domains that compositionally resembled known yeast prion domains, and taking advantage of this modularity, tested the top 100 PrLDs for aggregation and prion-like activity in a series of assays (10). PAPA was quite effective at predicting the ability of these PrLDs both to form foci when expressed as PrLD-GFP fusions, and to form SDS-insoluble aggregates (Figure 2.1). For these PrLDs, there was only a modest correlation between aggregation activity and Q/N content (10); in both assays, Q content showed a slight negative correlation with aggregation activity, while N content showed a slight positive correlation, consistent with subsequent studies showing that N has a higher amyloid aggregation propensity (39).

However, because the PrLDs were all identified based on compositional similarity to known yeast prion domains, this dataset was reasonably compositionally homogenous. For example, all of the PrLDs that were tested in the full set of assays were at least 22% Q/N. By contrast, many of the PrLDs predicted to be aggregation prone by PAPA have far lower Q/N-content. Therefore, while PAPA was accurate at

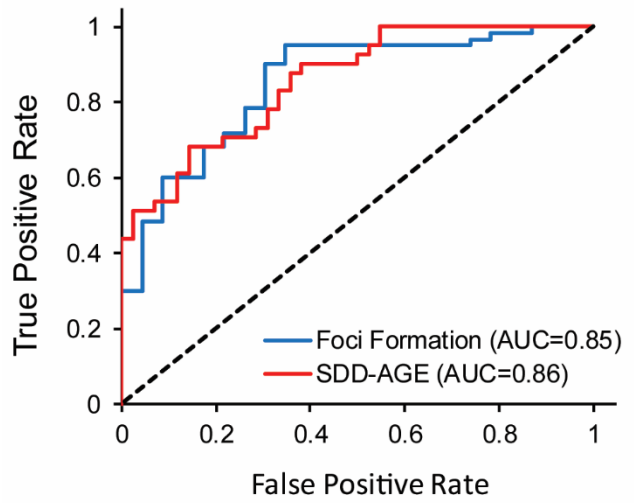

Figure 2.1. PAPA shows comparable accuracy in predicting foci formation and the formation of SDS-insoluble aggregates by Q/N-rich PrLDs.
Alberti *et al.* tested 100 yeast PrLDs for the ability to form foci when fused to GFP, and the ability to form SDS-insoluble aggregates by SDD-AGE. Shown are ROC (receiver operator characteristic) plot assessing PAPA's effectiveness at distinguishing between positive and negative examples from these two data sets. The area under the curve (AUC) for each plot is indicated. The dotted line reflects the prediction accuracy which would be expected by random chance.

predicting aggregation propensity for the Alberti dataset, and while there was only a weak correlation between Q/N content and aggregation activity, it is unclear whether these trends would remain for a more compositionally diverse dataset.

To address these questions, we searched the yeast proteome for PrLDs predicted by PAPA to be aggregation-prone. We identified 151 candidate PrLDs (PAPA score ≥0.05)(24). We excluded any PrLDs that overlapped with the Alberti dataset, and then selected 30 candidate PrLDs with a range of Q/N content (from 6-35% Q/N; Table 2.1). As a negative control, we additionally selected 10 Q/N-rich protein domains that scored well below PAPA's threshold.

To test for the ability to form foci, we generated PrLD-GFP fusions under control of the *GAL1* promoter. Although there was some variability in efficiency of expression among the fusions, most of the fusions showed efficient expression upon growth in galactose-containing medium (Figure 2.2). Likewise, while a few of the fusions showed some degradation, in most cases the predominant band corresponded to the approximate expected size of the fusion (Figure 2.2). Almost all of the candidate PrLDs formed distinct cytoplasmic foci (Figure 2.3, Table 2.1), regardless of Q/N content. This result suggests that high Q/N content is not critical for PrLD aggregation, and that PAPA is effective at identifying aggregation-prone domains, regardless of Q/N content. Additionally, all but one of the negative control PrLDs showed diffuse cytoplasmic signal (Figure 2.3, Table 2.1), confirming PAPA's ability to distinguish between aggregation-prone and non-aggregation-prone Q/N-rich domains.

Table 2.1: Summary of Results							
Protein Name	**PrLD Position**	**PAPA Score**	**%QN**	**%N**	**GFP Foci (%)**	**SDS-Insoluble Aggregates**	**[*PIN*$^+$] proteins**
Candidate prion-like domains							
Swi4	177-380	0.09	35.3	25.5	100	+	++++
Rpi1	192-306	0.05	33.0	27.8	96	+[c]	+
Var1[e]	191-349	0.20	31.0	30.4	100	+	++
Mfg1	1-96	0.07	29.2	11.5	0	-	-
Pam1	617-756	0.06	27.9	17.9	21	+	+
Dat1	102-236	0.09	27.4	12.6	100	+	+++
YML053C[d]	34-148	0.05	26.5	25.7	97	+[c]	++
Rna15	39-169	0.08	26.0	18.3	100	-	-
Cdc39[d]	966-1092	0.08	26.0	5.5	99	-	-
Slf1	183-311	0.11	25.6	16.3	100	-	-
Sky1	353-491	0.12	24.5	23.7	79	+	+++
Pin4	169-492	0.11	23.8	14.2	97	+	+++
Gis1	454-584	0.08	23.7	21.4	18	+	-
Cln2	362-503	0.09	23.2	15.5	47.9	+[c]	-
Fab1[d]	427-552	0.06	23.0	22.2	97	+	+++
Mex67	1-95	0.14	21.1	14.7	0	+	-
Q0255[e]	341-472	0.07	20.6	19.8	100	-	-
Tda7	513-636	0.10	20.2	12.9	42	-	-
YGL036W	270-478	0.15	20.1	15.8	100	-	+++
Bph1	1113-1243	0.10	19.1	14.5	100	-	-
Ssn2	1025-1211	0.09	18.2	8.0	100	-	-
Al3[e]	228-387	0.17	17.6	15.7	100	-	-
Lee1	151-301	0.12	17.2	11.3	19	-	-
Vac14	690-818	0.09	17.1	8.5	97	-	-
Cdc73	253-378	0.07	15.9	9.5	100	-	-
Mdm1	745-864	0.10	14.2	8.3	89	-	-
Pgs1	158-277	0.07	12.5	8.3	92	-	-
Nte1	1-169	0.12	12.4	8.3	0	-	-
Cos111	336-465	0.10	8.5	6.9	0	-	-
Izh3	176-492	0.13	6.0	3.8	100	-	-
Negative control Q/N-rich domains							
Dal81	4-168	-0.06	35.2	20.0	3	-	+
Yck2	369-533	-0.15	35.2	9.7	0	-	-
Hrk1	483-647	-0.12	30.3	15.8	0	-	-
Grr1	3-167	-0.02	29.7	21.2	3	+	+++
Apg13	250-414	-0.02	29.1	6.7	100	-	-
Siz1	390-554	-0.10	28.5	24.2	0	-	-
Crz1	15-179	-0.11	28.5	10.3	0	-	-
Vac7	377-541	-0.05	27.9	18.8	0	+	-
Tbs1	898-1062	-0.14	25.5	23.6	3	-	-
Vid22	641-806	-0.04	23.0	18.2	0	-	-

[a]Percentage of cells with GFP foci. At least 50 cells were counted for each strain.
[b]Cells were assessed for the ability to substitute for [*PIN*$^+$] in supporting [*PSI*$^+$] formation. +, ++, +++, and ++++ correspond to the number of spots in the dilution series with at least 10 colonies.
[c]SDS-insoluble aggregates forming after 48hrs
[d]Sequence polymorphism; see Methods
[e]Synthetically built; see Methods

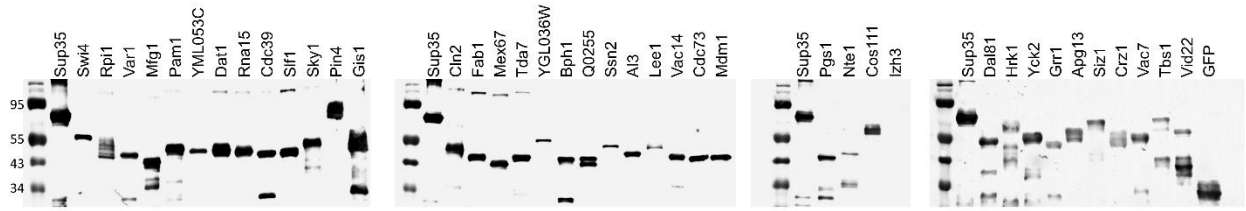

Figure 2.2: Western blot analysis of PrLD-GFP fusions

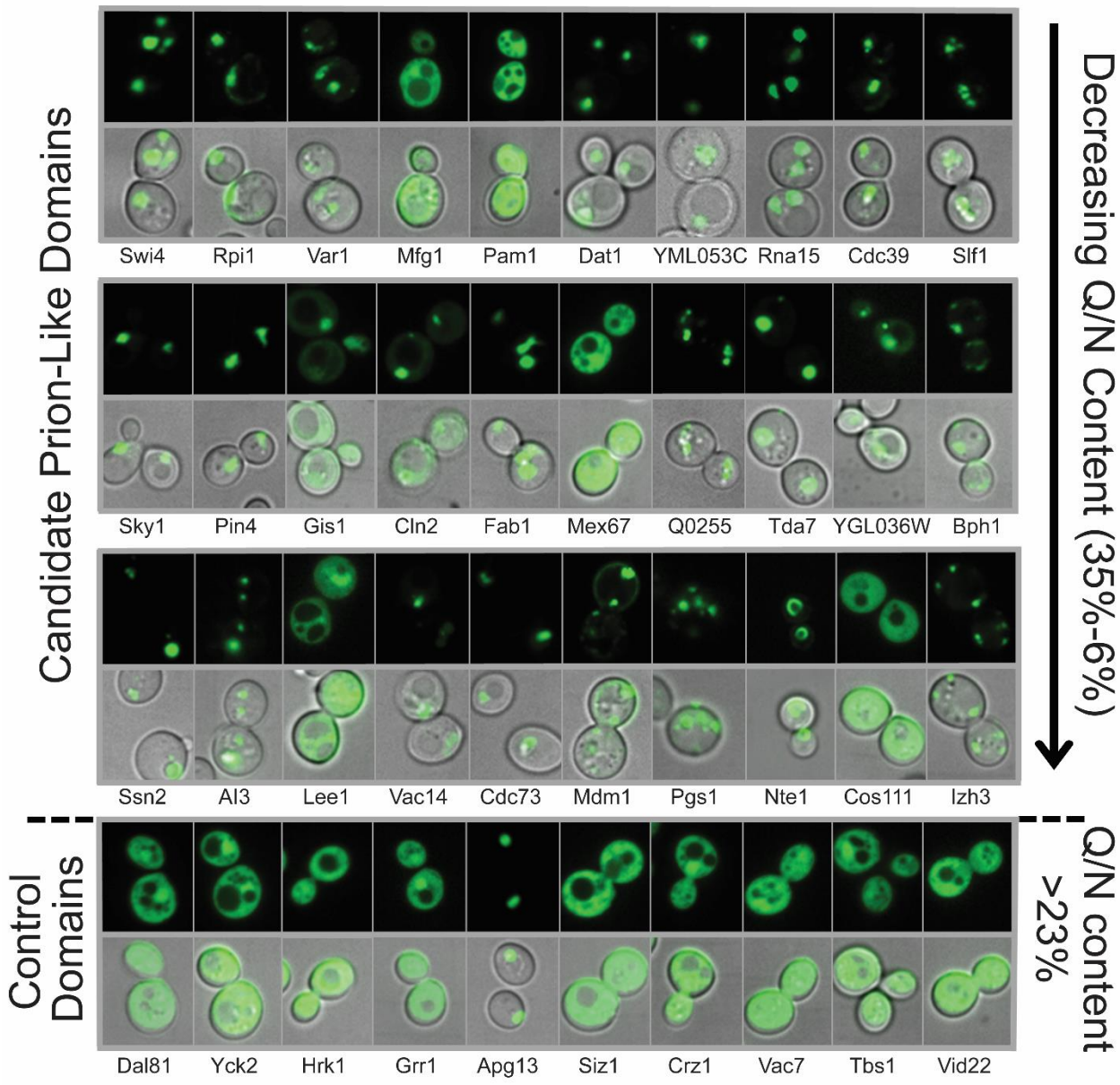

Figure 2.3: Prion-Like Domains form distinct foci in the cytoplasm.
The [*PIN*$^+$] strain yER632 was transformed with plasmids expressing PrLD-GFP fusions under control of the *GAL1* promoter. Cells were grown in galactose/raffinose dropout medium for 24 h, and then visualized by fluorescence microscopy and differential interference contrast (DIC). The first three rows contain PrLDs that are predicted by PAPA to be aggregation prone (PAPA score >0.05), ordered by Q/N content. The bottom row contains Q/N-rich domains predicted by PAPA not to be aggregation-prone. Representative images are shown. See Table 2.1 for quantification.

Prion-Like Domains Form SDS-Insoluble Aggregates

Foci formation, while common to the yeast prion proteins, is also seen with many non-prion proteins. Protein aggregates can range from amorphous aggregates to the highly ordered, detergent-insoluble amyloid aggregates that characterize yeast prions. Therefore, we used semi-denaturing detergent-agarose gel electrophoresis (SDD-AGE)(40) as a more stringent approach to determine if the PrLDs had the propensity to form SDS-insoluble aggregates *in vivo*.

HA-tagged PrLDs were transiently expressed from the *GAL1* promoter for 24 or 48 hours. Cells were then harvested, and cell lysates were examined by SDD-AGE. Many of the PrLDs formed high molecular weight SDS-insoluble aggregates after 24 hours of expression (Figure 2.4A). It should be noted that Figure 2.4A is overexposed to allow for detection of inefficient oligomer formation, and that for some of the PrLDs that formed SDS-insoluble aggregates (Swi4, Pin4 and Gis1), the majority of the protein was monomeric on SDD-AGE.

For all PrLDs that formed SDS-insoluble aggregates at 24 hours, aggregates were still observed at 48 hours; additionally, new SDS-insoluble aggregates for Cln2, YML053C and Rpi1 appeared, suggesting a longer lag phase (Figure 2.4B).

Strikingly, among the PrLDs with greater than 21% Q/N content, over 75% formed SDS-insoluble aggregates, while all of the PrLDs with less than 21% Q/N content failed to form SDS-insoluble aggregates. Additionally, only two of the negative control Q/N-rich domains formed SDS-insoluble aggregates. Thus, as was seen for the Alberti dataset (Figure 2.1), if our dataset is limited to Q/N-rich proteins, PAPA is reasonably effective at predicting which PrLDs will form detergent-insoluble aggregates

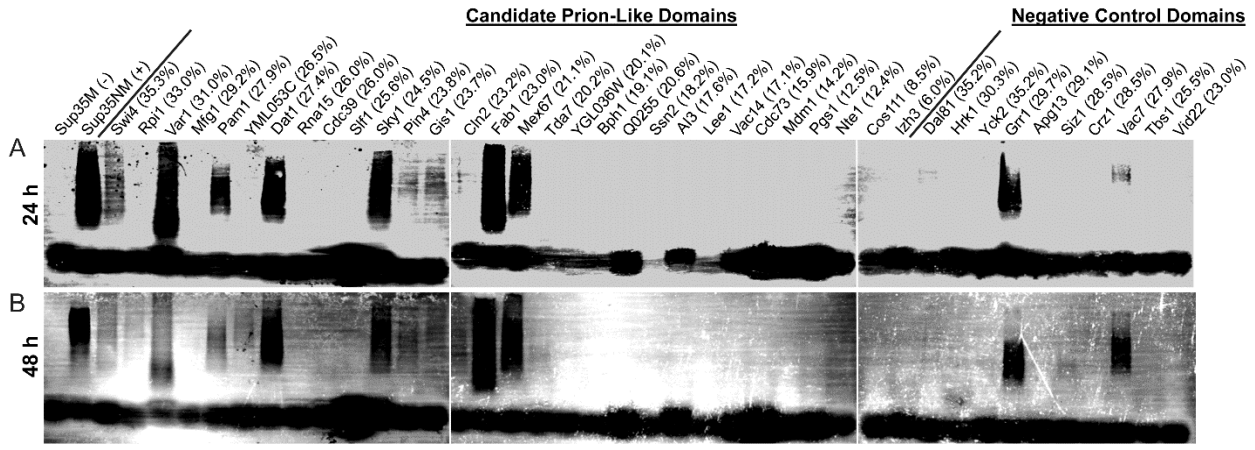

Figure 2.4: Q/N-rich PrLDs More Likely to Form SDS-Insoluble Aggregates.
The [PIN+] strain yER632 was transformed with plasmids expressing PrLD-GFP fusions under control of the GAL1 promoter. Cells were grown in galactose/raffinose dropout medium for 24 h (A) or 48 h (B) and analyzed by SDD-AGE. Q/N-content for each PrLD is indicated.

(Figure 2.5A); however, PAPA is not effective for domains with lower Q/N content (Figure 2.5A). By contrast, PAPA was equally effective at predicting foci formation for the full dataset and for the Q/N-rich subset (Figure 2.5B).

These data suggest that high Q/N content promotes the formation of SDS insoluble aggregates. In particular, formation of SDS-insoluble aggregates was correlated with N content, consistent with previous results suggesting that N more efficiently promotes conversion to an amyloid state (39). Among the predicted aggregation-prone PrLDs with >21% Q/N content, four failed to form SDS-insoluble aggregates: Mfg1, Rna15, Cdc39, and Slf1. Two of these (Mfg1 and Cdc39) had the lowest ratio of N:Q, and lowest N content of the PrLDs with >21% Q/N (Table 2.1). It is less clear why Rna15 and Slf1 failed to form SDS-insoluble aggregates.

Most PrLDs are Rnq1 independent, but Hsp104 dependent

[*PIN*$^+$] and [*PSI*$^+$] are the prion forms of the yeast prion proteins Rnq1 and Sup35, respectively. [*PIN*$^+$] is required for *de novo* [*PSI*$^+$] formation, and for formation of SDS-insoluble aggregates by Sup35 (3, 33, 41). [*PIN*$^+$] is thought to act as a template to cross-seed amyloid formation by Sup35 (42), although it remains possible that [*PIN*$^+$] may promote [*PSI*$^+$] formation by an indirect mechanism, such as titrating away an inhibitor of [*PSI*$^+$] formation. [*PIN*$^+$] also promotes, but is not required for, prion formation by the prion protein Ure2 (43). If [*PIN*$^+$] specifically promotes amyloid formation by Q/N-rich proteins, it could explain why the Q/N-rich proteins in our dataset were more likely

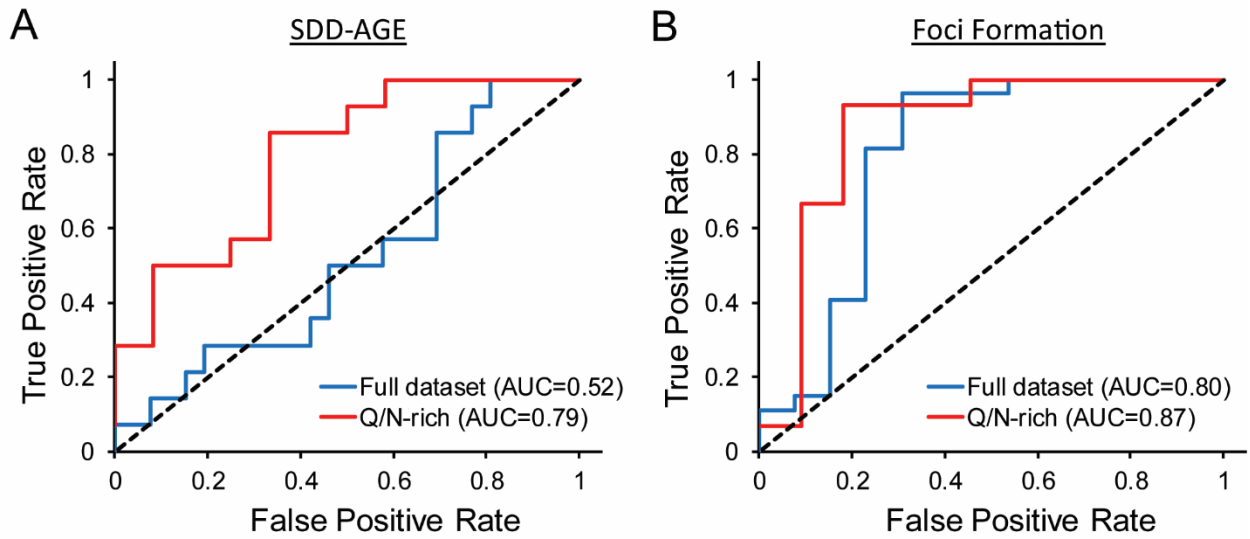

to form SDS-insoluble aggregates. However, most of the PrLDs that efficiently formed

SDS-insoluble aggregates still formed SDS-insoluble aggregates in the absence of

Figure 2.5: PAPA accuracy for the tested proteins.
A) ROC plot examining the ability of PAPA to predict formation of SDS-insoluble aggregates. Among the full dataset, PAPA shows almost no ability to distinguish between positive and negative examples (AUC=0.52), but among the subset of domains with greater than 21% Q/N content, PAPA shows reasonably accurate predictions (AUC=0.79). B) ROC plot examining the ability of PAPA to predict foci formation. For foci formation, PAPA shows roughly equivalent ability to distinguish between positive and negative examples among the full dataset and for the Q/N-rich subset.

Rnq1 (Figure 2.6A). Thus, [*PIN*$^+$] is not responsible for the observed bias towards Q/N-rich proteins among the PrLDs that formed detergent-insoluble aggregates.

By contrast, most of the PrLDs were dependent on Hsp104 for efficient formation of SDS-insoluble aggregates (Figure 2.6A). Hsp104 is a chaperone required for the maintenance of almost all yeast prions (1, 44). Hsp104 is a homohexameric AAA+ ATPase that fragments prion fibers, creating new prion seeds to offset dilution by cell division (45). Additionally, Hsp104 promotes *de novo* aggregation by Sup35; by contrast, Hsp104 is not required for *de novo* aggregation of the prion-like protein Pin4, one of the proteins in our dataset (46). Hsp104 deletion eliminated or substantially diminished formation of SDS insoluble aggregates for all of the PrLDs except Pin4's and Var1's. While Hsp104 deletion results in loss of [*PIN*$^+$], the fact that the PrLDs all formed SDS-insoluble aggregates in the absence of [*PIN*$^+$] suggests that Hsp104 promotes formation of SDS-insoluble aggregates by a mechanism independent of [*PIN*$^+$].

Interestingly, for the Fab1, Swi4, Sky1, and Grr1 PrLDs, Hsp104 deletion substantially reduced or eliminated formation of SDS-insoluble aggregates, but did not prevent the formation of foci, suggesting that Hsp104 may specifically promote conversion to a stable amyloid-like state (Figure 2.6B). The nature of these non-amyloid foci is unclear. None of the respective full-length proteins has been reported for form foci; in a large-scale screen of GFP fusions expressed at endogenous levels, Fab1 localized to the vacuolar membrane, Sky1 showed diffuse cytoplasmic localization, and Swi4 was diffusely localized to the cytoplasm and nucleus (Grr1 was not visualized in this screen) (47). Nevertheless, foci formation could reflect localization of the PrLD to a subcellular compartment rather than aggregation *per se*.

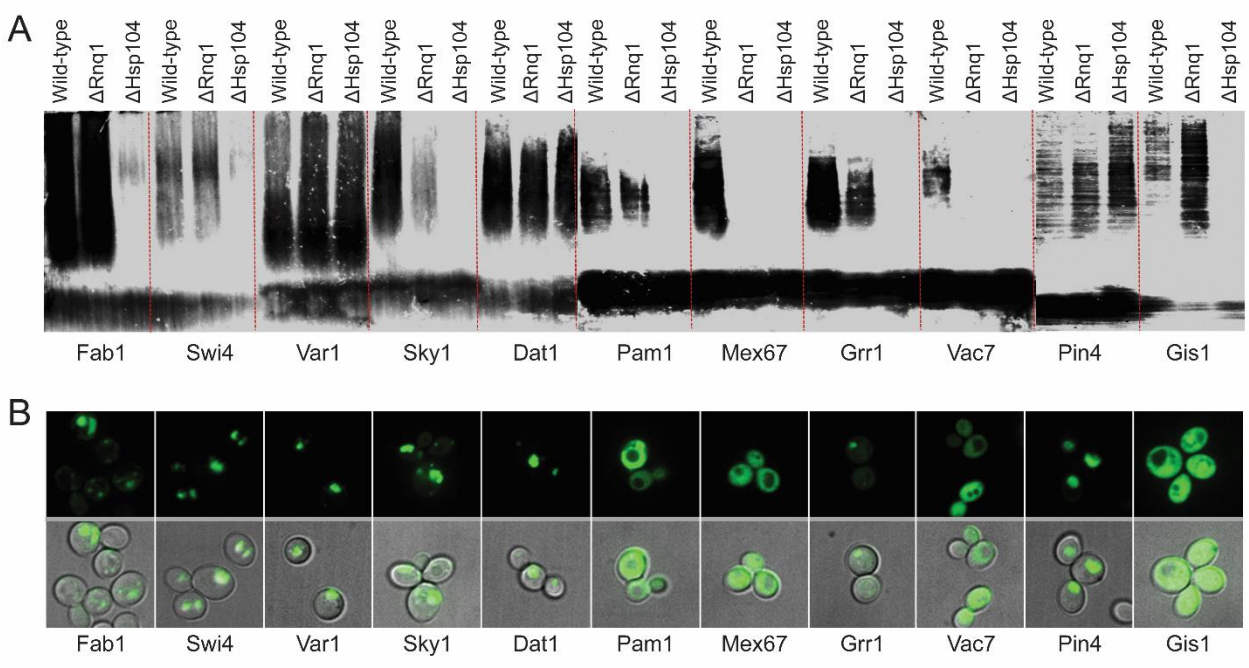

Figure 2.6: Effect of [PIN+] and Hsp104 on PrLD aggregation.
A) Plasmids expressing PrLD-HA fusions that formed SDS-insoluble aggregates were transformed into yER1017 (rnq1Δ) and yER1018 (hsp104Δ). Cells were grown for 24 h in galactose/raffinose dropout medium, and analyzed by SDD-AGE. B) Plasmids expressing PrLD-GFP fusions were transformed into the hsp104Δ strain yER1615. Cells were grown for 24 h in galactose/raffinose dropout medium, and visualized by fluorescence microscopy and differential interference contrast.

Pin⁺ activity of Q/N-rich prion-like domains

Although [*PIN*⁺] is generally required for prion formation by Sup35, overexpression of either poly-Q or various Q/N-rich PrLDs can substitute for [*PIN*⁺] in promoting [*PSI*⁺] formation (33, 42). However, it is not known whether every aggregation-prone Q/N-rich domain has Pin⁺ activity (i.e., can substitute for [*PIN*⁺] in promoting *de novo* [*PSI*⁺] formation), or whether this property is unique to only a subset of Q/N-rich aggregation-prone domains. Because many of the tested PrLDs were able to form SDS-insoluble aggregates independent of Rnq1, we examined whether these PrLDs could substitute for [*PIN*⁺] in promoting [*PSI*⁺] formation.

[*PSI*⁺] formation was detected by monitoring nonsense suppression of the *ade2-1* allele (48). Sup35 is a GTP binding protein that interacts with Sup45 to form the release factor that recognizes in-frame stop codons in mRNAs (49). [*PSI*⁺] formation reduces the pool of active Sup35, increasing stop codon read-through, and allowing *ade2-1* cells to grow in the absence of adenine. In a strain lacking *RNQ1,* we monitored the formation of Ade⁺ colonies when each PrLD was co-overexpressed with Sup35NM (Figure 2.7A and data not shown). Interestingly, almost all of the PrLDs that formed SDS-insoluble aggregates in the absence of Rnq1 were able to substitute [*PIN*⁺] in promoting Ade⁺ colony formation by Sup35, highlighting the lack of sequence specificity for this activity. By contrast, only two PrLDs that failed to form SDS-insoluble aggregates were able to promote Ade⁺ colony formation by Sup35 (YGL036W and Dal81). In all cases, formation of Ade⁺ colonies was associated with [*PIN*⁺]-independent foci formation by the PrLDs (Figure 2.7B).

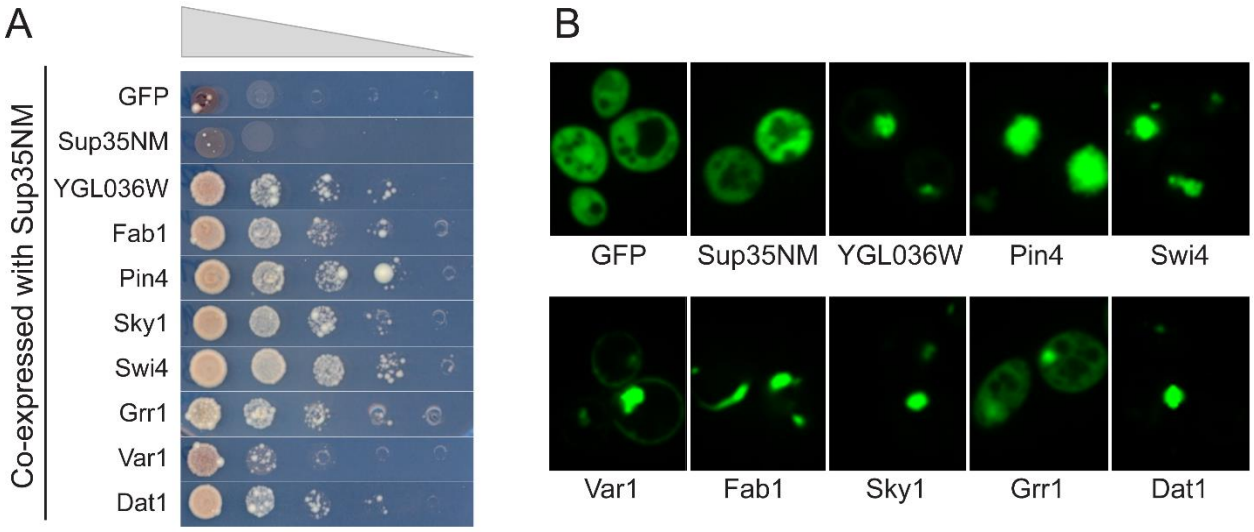

Figure 2.7: Q/N rich prion-like domains have the ability to act like [PIN+]. Yeast strain yER1019 (rnq1Δ) expressing Sup35NM from the GAL1 promoter was transformed with plasmids expressing PrLD-GFP fusions from the GAL1 promoter. A) Cells were grown for 72 h in galactose/raffinose dropout medium, and then 10-fold serial dilutions were plated onto medium lacking adenine to select for [PSI+] formation. B) Cells were grown for 24 h in galactose/raffinose dropout medium, and visualized by microscopy to test for [PIN+]-independent foci formation.

The ability to promote Ade$^+$ colony formation was not limited to naturally-occurring yeast PrLDs. We previously used PAPA to design two synthetic Q/N-rich prion domains (24). Both formed foci when expressed as PrLD-GFP fusions (Figure 2.8A), and formed SDS-insoluble aggregates (Figure 2.8B). By contrast, synthetic Q/N-rich PrLDs designed to have low aggregation activity remained soluble (Figure 2.8A,B). Consistent with what was observed for naturally-occurring yeast PrLDs, both of the synthetic PrLDs were able to promote [*PSI*$^+$] formation, while the negative control Q/N-rich domains were not (Figure 2.8C).

Discussion

There appears to be distinct classes of amyloid-forming proteins. For many amyloid-forming proteins, amyloid formation is thought to be driven by short, generally hydrophobic segments (31, 50). This class of amyloid proteins includes amyloid β and the human prion protein PrP. By contrast, other amyloid-forming proteins, including many yeast prion proteins, lack these short, highly amyloidogenic segments (51). Instead, amyloid propensity is more diffusely spread across a long, intrinsically disordered low-complexity domain. For example, the entire prion domain of both Ure2 and Sup35 can be scrambled without disrupting prion formation (5, 6), and no single segment of these scrambled prion domains is required for prion formation (6, 23). This second class of amyloid-forming proteins includes proteins that are mutated in ALS and FTLD (11, 52). Here, we are specifically examining the sequence features that promote amyloid formation by this second class of proteins.

While it is clear that PrLDs are important both in normal biology and in pathology, the exact definition of what constitutes a PrLD has never been rigorously defined.

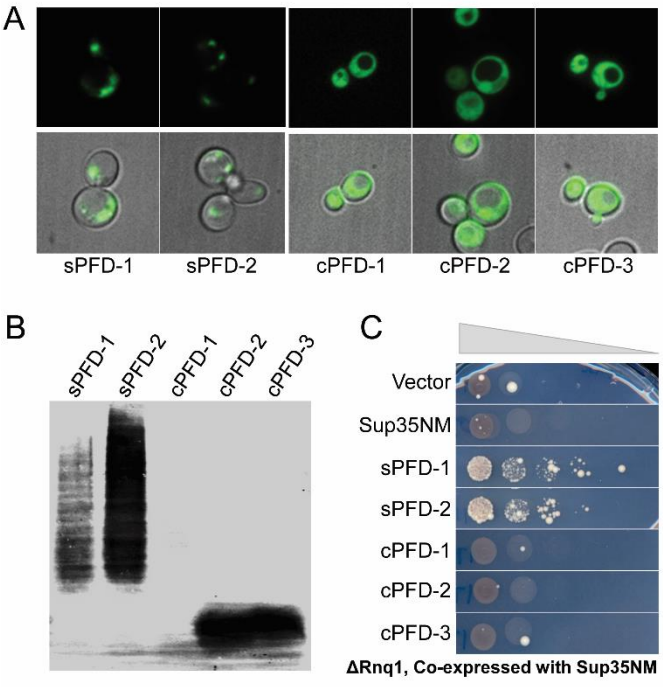

Figure 2.8: Q/N-rich synthetic PrLDs have the ability to act as [PIN+].
A) Plasmids expressing synthetic PrLDs (sPFD) and negative control Q/N-rich domains (cPFD) fused to GFP were transformed into the [PIN+] strain yER632. Cells were grown 24 h in galactose/raffinose dropout medium and visualized by microscopy. B) SDD-AGE of sPFD-HA and cPFD-HA fusions in [PIN+] strain yER632. C) sPFDs can substitute for [PIN+]. Plasmids expressing PrLD-GFP and Sup35NM were transformed into the rnq1Δ strain yER1019. Cells were grown for 72 h in galactose/raffinose dropout medium and plated onto medium lacking adenine to select for [PSI+] formation.

Almost all yeast prion proteins contain a Q/N-rich prion domain. Various studies suggest that glutamine and asparagine residues have relatively low aggregation propensities, so the importance of Q/N content is unclear (31, 53). Yeast prion domains are also intrinsically disordered, so we previously hypothesized that Q/N content is common simply because Q and N balance aggregation propensity and intrinsic disorder. However, other polar residues (serine, glycine, and threonine) have similar characteristics (23), making it unclear why aggregation-prone PrLDs tend to be specifically enriched in Q and N.

Our current results suggest an answer. Q/N content does not appear to be important for PrLD aggregation, as there was little correlation between Q/N content and foci formation among the tested PrLDs (Figure 2.3). However high Q/N content, particularly N content, was highly correlated with formation of SDS-insoluble aggregates (Table 2.1). This result suggests a challenge in predicting PrLD aggregation propensity: the effect of a given mutation will be dependent on context. For example, we previously showed that small changes in Q/N content have little effect on the aggregation propensity of highly Q/N-rich yeast prion proteins (23). However, our current results showed a threshold effect at about 20% Q/N content, where above this level PrLDs were much more likely to form SDS-resistant aggregates. This suggests that near this threshold, small changes in Q/N content could significantly affect formation of the SDS-insoluble aggregates that characterize both the yeast prions and the disease-associated PrLD aggregates. This finding is important, because many of the disease-associated human PrLDs have Q/N content near this threshold (11).

Our results also suggest an additional challenge for PrLD prediction: that the prediction method needs to be optimized for the desired task. We have shown PAPA is sufficient if the goal is to identify aggregation-prone low complexity domains. However, for identifying proteins that form SDS-insoluble aggregates, PAPA needs to be coupled with a pre-selection for Q/N content. To identify bona fide prions, sequence features that promote chaperone-dependent cleavage need to be accounted for. These factors have not been rigorously defined, but aromatic residues seem to promote this process (37, 54).

Our results also provide insight into the requirements for Pin$^+$ activity. Previous studies have shown that various Q/N-rich domains can substitute for [*PIN*$^+$] in promoting [*PSI*$^+$] formation, but it was unclear whether this was a universal feature of aggregation-prone Q/N-rich domains. We found that almost every PrLD that formed [*PIN*$^+$]-independent SDS-insoluble aggregates was able to substitute for [*PIN*$^+$] in supporting [*PSI*$^+$] formation. These results highlight the lack of sequence specificity of this activity, and suggest that a diverse array of proteins may influence [*PSI*$^+$] formation. However, it should be noted that the mechanistic basis for this effect remains unclear. It is not known why Sup35, which efficiently forms amyloid in vitro, requires [*PIN*$^+$] for prion formation in vivo. Additionally, although a variety of evidence suggests that [*PIN*$^+$] promotes [*PSI*$^+$] formation at least in part through direct cross-seeding (1), it remains possible that proteins with Pin$^+$ activity may support [*PSI*$^+$] formation by an indirect mechanism, such as titration of an inhibitor of [*PSI*$^+$] formation (1, 46).

Although our current study addresses the sequence features that support PrLD aggregation and formation of SDS-insoluble aggregates, and provides insights into the

promiscuity of Q/N-rich proteins, whether the identified PrLDs can support formation of bona fide prions is still unclear. We performed preliminary tests using the well characterized Sup35 fusion assay (38), but it proved inconclusive (data not shown). In this assay, potential prion domains are inserted in the place of the Sup35 prion domain; cells expressing the fusion protein are then tested for prion formation using the *ade2*-1 reporter described above. Unfortunately, most of our PrLD-Sup35 fusions had a constitutive Ade^+ phenotype (data not shown). This suggests that these fusion proteins were non-functional, either because the PrLDs interfered with Sup35 activity, or because the fusion proteins aggregated so rapidly that they lacked a stable soluble state. Because of the substantial limitations of this assay, we opted not to pursue it further. Specifically, the Sup35 fusion assay is prone to both false positives and false negatives. The majority of the PrLDs that show prion activity in this assay have not been demonstrated to support prion activity in their native context, and the prion domains from two known yeast prion proteins, Cyc8 and Mot3, are unable to form prions in this assay (10, 35, 55). Because of these limitations, we are instead focusing on developing assays to test interesting PrLDs in their native context.

It is also worth noting that many PrLDs form biologically-relevant aggregates that are not prions. In mammalian cells, a segment of a melanosome protein, Pmel17 forms amyloid fibers in order for proper melanin production (56). In addition, yeast also have several examples of amyloid formation serving a beneficial role to the cell. Among these include a RNA-binding protein, Rim4, which forms amyloid-like aggregates that regulate gametogenesis (57, 58). Likewise, the amyloid-like aggregation of Whi3, an RNA-binding protein, allows the cell to permanently escape pheromone-induced cell cycle

arrest (59). Furthermore, as previously discussed, many PrLDs are thought to support formation of non-amyloid aggregates, such as the dynamic liquid-liquid phase separation that is seen with stress granules. Overall, cells exploit PrLDs because they have a propensity to form various types of protein aggregates, providing an increase in concentration of the prion-like protein, as well as its binding partners, at sites of interest. These interactions can be regulated based on environmental cues like stress, changing salt or ion concentration, etc. Therefore, our results revealed several promising candidates for PrLDs that may form functional amyloid or non-amyloid aggregates.

Materials and Methods:

Predicting Prion-Like Domains in S. cerevisiae

The *S. cerevisiae* proteome was scanned using PAPA (23). PAPA effectively uses an 81-aa window, but weights each amino acid inverse proportion to its distance from the center of the window. The predicted prion propensities of all 81-aa windows across the proteome were calculated. PrLDs were excluded if they had been previously tested for prion-like activity (10). Each PrLD contains the core 81 amino acids predicted by PAPA; the PrLDs were extended to include all flanking amino acids that were scored positive (>0) by PAPA. If two high scoring PrLD were separated by a small region (less than the length of an average prion domain) that scored below 0, the entire region was included. Specifically, the PrLD of Pin4 contains three high scoring segments, separated by 66 and 51 amino acid low scoring segments, so the entire region was included. PrLDs of Var1 and Swi4 contains two high scoring segments separated by 10 and 31 amino acid low scoring segments, respectively, so the entire segment was included. The average length of the PAPA positive PrLD was 165 amino acids.

Therefore, PAPA negative domains were chosen by identifying 165 amino acid Q/N-rich segments with low PAPA scores.

Plasmid construction

To generate the PrLD-GFP fusions, the PrLDs were amplified from strain yER632 (26), adding BamHI and XhoI restriction sites, as well as a start codon at the beginning of the PrLD and a flexible linker at the end of the PrLD (see Tables 2.2 and 2.3 for primer sequences and plasmid names, respectively). PCR products were digested with BamHI and XhoI and ligated into pER760, a *TRP1* 2µm plasmid containing GFP under control of the *GAL1* promoter (26). To generate PrLD-HA fusions for SDD-AGE, PrLDs were amplified from the respective GFP plasmids, using the same sense primer as for construction of the GFP plasmids, paired with a common antisense primer that added a C-terminal HA tag, a stop codon, and a SalI restriction site for cloning into pER687 (a *TRP1* 2µm plasmid containing the *GAL1* promoter and *ADH1* terminator) (26). All sequences were confirmed by DNA sequencing. Three PrLD sequences (from YML053C, Cdc39, and Fab1) contained minor polymorphisms that altered the amino acid sequence from the reference strains in the *Saccharomyces* Genome Database; see Table 2.4 for protein sequences.

Mitochondria use different codons; therefore, the mitochondrial PrLDs (from Var1, Q0255, AI3) were built synthetically using overlapping primers, followed by primers to add the restriction sites for cloning. We omitted single cysteine residues that were present in each mitochondria PrLD to prevent disulfide bond formation; see Table 2.4 for protein sequences.

Yeast Strains and Media

Standard yeast media and methods were used as previously described (60). In all experiments, yeast were grown at 30ºC. See Table 2.5 for a list of strains used in this study.

Foci formation

Foci formation assays were performed as previously described (27). Briefly, yeast strains yER632, yER1019, and yER1615 were transformed with *TRP1* plasmids expressing each PrLD-GFP from the *GAL1* promoter. Strains were grown in galactose/raffinose dropout medium lacking tryptophan for 24 hours, and then imaged by confocal microscopy.

To examine the ability of PrLDs to promote Sup35N foci formation in an *rnq1Δ* strain, yER1019 was transformed with both a *TRP1* plasmid expressing PrLD-GFP fusion from the *GAL1* promoter and a *LEU2* plasmid expressing Sup35N from the *GAL1* promoter. Cells were grown in galactose/raffinose dropout medium lacking leucine and tryptophan for 24 hours.

Semi-Denaturing Detergent-Agarose Gel Electrophoresis (SDD-AGE)

For SDD-AGE, yER632, yER1017 and yER1018 were transformed with *TRP1* plasmids expressing each PrLD-HA from the *GAL1* promoter. Strains were grown for 24 or 48 hours in galactose/raffinose dropout medium lacking tryptophan. Cells were harvested and lysed as previously reported (61). 80ug of total protein lysate was incubated in 2% SDS loading buffer for 7 minutes at room temperature prior to loading onto a 1.5% agarose gel containing 0.1% SDS and 1 x TAE. The gel was run in running buffer (1 x TAE, 0.1% SDS) at 60 volts for 3 hours. Protein was transferred to a PVDF

membrane by capillary transfer for 24 hours using 1 x PBS at room to temperature. The membrane was probed with an anti-HA primary antibody (HA.11 16B12, Covance), and Alexa Fluor IR800 goat anti-mouse secondary antibody (Rockland).

[PIN$^+$] assays

To examine the ability of PrLDs to substitute for [*PIN*$^+$] in promoting [*PSI*$^+$] formation, yER1019 was transformed with both a *TRP1* plasmid expressing PrLD-GFP fusion from the *GAL1* promoter and a *LEU2* plasmid expressing Sup35N from the *GAL1* promoter. Cells were grown in galactose/raffinose dropout medium lacking leucine and tryptophan for 72 hours, and 10-fold serial dilutions were plated on medium lacking adenine.

Table 2.2: Primers to Construct GFP fusions		
Protein	**Sense Primer**	**Antisense Primer**
Swi4	GAGCTACTGGATCCACAATGTCTAAGAACAGTAGTTCATCAACATCGGCTAC	GTCGATGCTACTCGAGCCAGATTGATTCAGCTTTTTCCTCCTTTTTTTACTATTGC
Rpi1	GAGCTACTGGATCCACAATGTCTTTATCTAGAATGCAGTATTTGCTAGTGCAG	GTCGATGCTACTCGAGCCTTGAGCCGGGCTAATGAAGG
Var1	GAGCTACTGGATCCACAATGTCTTTGAATATTTTGTCTTATTATTATAAAAAAAAAGTTACCATCGAGCCAATCAAGTTGTCCTAC	GTCGATGCTACTCGAGCCATTCAACAAATTAGTAGTAGAAGTTCTACCATTATTATTAGACAATCTACCTTTAAACTTGATGGACCAACCGACCAGATAC
Mfg1	GAGCTACTGGATCCACAATGTCTATGTACCAAGGCCCACCG	GTCGATGCTACTCGAGCCGCTGCCAGGGCCC
Pam1	GAGCTACTGGATCCACAATGTCTCCAACGAGTAGAAAAAACAGAAGTAGTG	GTCGATGCTACTCGAGCCTGAGGTACCGTTTTGAGATAGAGAC
YML053C	GAGCTACTGGATCCACAATGTCTACGATCATGAATAAAAGAAAAAATGACCATTTCGAG	GTCGATGCTACTCGAGCCCTCTTCTGTTTCAGAATAAAATTCAGATTCGTTC
Dat1	GAGCTACTGGATCCACAATGTCTGATTATACCCATCAGTCATTCATGGATC	GTCGATGCTACTCGAGCCAGTGATATGTGCTGCCGGCGATG
Rna15	GAGCTACTGGATCCACAATGTCTAGTAATGTTGGGCCCGTGATCAATTTG	GTCGATGCTACTCGAGCCTAGTTCGCTCGATATCATCATAGCAGG
Cdc39	GAGCTACTGGATCCACAATGTCTACTTTCGAAGTTGAGGTTTTATTAAAATCTTTTAATTTGACCAC	GTCGATGCTACTCGAGCCAAATACCCTCTTCAAGTCAGGGTGG
Slf1	GAGCTACTGGATCCACAATGTCTAGAAATTATCAAAACAGGAATGGCAAAACAAGATACAAC	GTCGATGCTACTCGAGCCTATCAAACTCATGGGGATAAATCCGTCATTG
Sky1	GAGCTACTGGATCCACAATGTCTAGTATGCCCTGCGGCTCAAG	GTCGATGCTACTCGAGCCCATTATGTCCTCGTTATTATTGTTGTTACTGTTG
Pin4	GAGCTACTGGATCCACAATGTCTAGAGAAAGAATCGAGAGGGAGAAGAG	GTCGATGCTACTCGAGCCTTGCTGTGTTTGTGGTTGAGGTTGTTG
Gis1	GAGCTACTGGATCCACAATGTCTTTAACTCCGCAATTACCGCAGATG	GTCGATGCTACTCGAGCCCGTCAATCTTGGTGACGCAG
Cln2	GAGCTACTGGATCCACAATGTCTCAAAGAAAACTGCAAATTGCATCCAACTTG	GTCGATGCTACTCGAGCCCCCATTGAGGTAATGCGCCG

Fab1	GAGCTACTGGATCCACAATGTCTGACAACCCCGGTCGCCATCATC	GTCGATGCTACTCGAGCCGTAATTTCTATGAGCATAATTCCCGATAATACGATTGGCAGGCTCCAGTATGGAAGAAGACTGTGC
Mex67	GAGCTACTGGATCCACAATGTCTATGAGCGGATTTCACAATGTTGGAAATATCAATATG	GTCGATGCTAGTCGACCCCCCATTGTTATCTAAAAGTTCGAACTTTAAATTACTGC
Tda7	GAGCTACTGGATCCACAATGTCTGAGGCGTCACTTCAAGCTCAAG	GTCGATGCTACTCGAGCCTATAATTTCCCTCAAGAACCCTTGTGAATTGTTC
YGL036W	GAGCTACTGGATCCACAATGTCTAATGGTGGTGGTGAGAACTCCAG	GTCGATGCTACTCGAGCCCAAACAGCGTAATACATCATTTACAATCATAATTGAATCC
Bph1	GAGCTACTGGATCCACAATGTCTGCAGTCTTCAATTGTATGAAAGTGATCATTAAGAAC	GTCGATGCTACTCGAGCCTGATATGGACTTTTTGATTTTAAAATCTAAGGATGTGTTGTC
Q0255	GAGCTACTGGATCCACAATGTCTGAAATTTATATGAAAGGTTTGCATAATACTACTAAAGGTTCCAACTTGCTGAAGCTGATC	GTCGATGCTACTCGAGCCATCCAACAAAATATTTTTCAAAATATATTTATTCATGAACACGTTGCCGTTCTTGATGTACTTGGCGATCTCATGCTTGCTG
Ssn2	GAGCTACTGGATCCACAATGTCTAACGTGCCACCAATATTAATAATTTTACCCTTG	GTCGATGCTACTCGAGCCTCCGAATTTTTTAGACGCTAAATTTAGGGC
AI3	GAGCTACTGGATCCACAATGTCTAACATTAAAATTAAACCATTGGATACTTCTGATATTGGTTCTAATGCATGGTTGGCAGGTATGACTGATGCAGATGG	GTCGATGCTACTCGAGCCTAACTCCCAAGAACCATTAGTTTTCATAGATTGACCTTCATTATTAATCAAGATGACCAGCTTAGACCAATCC
Lee1	GAGCTACTGGATCCACAATGTCTAACAGTAAAGAACCTATTGACATCACTCCC	GTCGATGCTACTCGAGCCTTCATGACAGTATCTGGAATTGAAATTGTGAATAAG
Vac14	GAGCTACTGGATCCACAATGTCTGTGCAGTTGGATATTTTGATTCAGTTGTTC	GTCGATGCTACTCGAGCCTTTATTGTTAGCACCATGGTCAAGCC
Cdc73	GAGCTACTGGATCCACAATGTCTGCAAATATAAAACAGTTCCTGCTGGAG	GTCGATGCTACTCGAGCCATAACGCACGACTTCCACATCC
Mdm1	GAGCTACTGGATCCACAATGTCTTTGAAAATTTTAAAAAAGTCACAAAGAACCCTATTAAAGGAACTAG	GTCGATGCTACTCGAGCCTTTTGTAACATGATATTTCAATGACATTTTCACTTTTGACGG
Pgs1	GAGCTACTGGATCCACAATGTCTAAGACGCCTGCTTATCATGGTTG	GTCGATGCTACTCGAGCCAAAGCCATCTAGTAATTGAGATGCTTCC

Nte1	GAGCTACTGGATCCACAATGTCTATGCGTTCAATGAATTGCACTACGAACAAC	GTCGATGCTACTCGAGCCACCTATGGCGGGTGGCG
Cos111	GAGCTACTGGATCCACAATGTCTGACTTGGCATTAGCTGGTTGGAG	GTCGATGCTACTCGAGCCTGACGTAATGTCAGATATAGGTTTTGCTTTCTG
Izh3	GAGCTACTGGATCCACAATGTCTAAATCCATGGTAAAGACGGAAATCCTCATTG	GTCGATGCTACTCGAGCCACTGCATTTGGAATGGGCTGTTGG
Dal81	GAGCTACTGGATCCACAATGTCTCACCAATCACCAGCTGATAATGCC	GTCGATGCTACTCGAGCCGTTGCCTAGGTCGGGAAAATAGTTG
Hrk1	GAGCTACTGGATCCACAATGTCTTCAAACTTGAAAACAGTTCAAAATCAAGTTCCAAATACTC	GTCGATGCTACTCGAGCCTTGTTGTTGTTGTTGTTGTTGTTGTTGTTGTTG
Yck2	GAGCTACTGGATCCACAATGTCTGATTTGTCGATAAACAAAAAGCCGAACTTACATG	GTCGATGCTACTCGAGCCGTTACTATTTCTATCTTGCGCTGCGTTTTTAG
Grr1	GAGCTACTGGATCCACAATGTCTCAGGATAACAACAACCACAATGACAGC	GTCGATGCTACTCGAGCCTTGGATTTTTTTGCCCACTATTAGCTTGAATTCG
Apg13	GAGCTACTGGATCCACAATGTCTGGACTCTTAAGAGTCTCGGTATCATAC	GTCGATGCTACTCGAGCCATTCATTTGTGGCCCGTAGTTGGAG
Siz1	GAGCTACTGGATCCACAATGTCTCACTCCCAACTACAAATTCCTACGTG	GTCGATGCTACTCGAGCCATTATTACTATTGGAGTCGTTGTTCTCGATGCTG
Crz1	GAGCTACTGGATCCACAATGTCTAGTAATGGAGAGGAGCAAAGTATAAACAACAAAAAC	GTCGATGCTACTCGAGCCATTAGATCTTGGAGATAAAAACTGGTTTGTGAGG
Vac7	GAGCTACTGGATCCACAATGTCTAACAACAACGGCAATAACAGTAATAGTGCATC	GTCGATGCTACTCGAGCCATTGTTCTGCATCACATTAGAATTCAAGTTCGG
Tbs1	GAGCTACTGGATCCACAATGTCTAATATTTTCAATGAAATAACAATCCAGGATTTGAACTTCTTGC	GTCGATGCTACTCGAGCCTTGTTCATTCTCATCTCTATAATCATTCGCCG
Vid22	GAGCTACTGGATCCACAATGTCTATAGGCAACGTTAACAACAGTCATAATACTTCC	GTCGATGCTACTCGAGCCGTTCATTGGTTGTTCTAGCTCTCCAATAATAG

Table 2.3: Plasmid List		
Protein	**GFP Plasmid**	**HA**
Swi4	pER875	pER1163
Rpi1	pER1182	pER1274
Var1	pER879	pER1165
Mfg1	pER878	pER1204
Pam1	pER1181	pER1272
YML053C	pER1188	pER1273
Dat1	pER1184	pER1276
Rna15	pER876	pER1225
Cdc39	pER877	pER1203
Slf1	pER874	pER1205
Sky1	pER994	pER1168
Pin4	pER873	pER1226
Gis1	pER1179	pER1270
Cln2	pER1180	pER1271
Fab1	pER881	pER1164
Mex67	pER973	pER1210
Tda7	pER959	pER1212
YGL036W	pER872	pER1202
Bph1	pER962	pER1237
Q0255	pER880	pER1206
Ssn2	pER1187	pER1269
AI3	pER995	pER1207
Lee1	pER963	pER1211
Vac14	pER1183	pER1275
Cdc73	pER1185	pER1277
Mdm1	pER964	pER1214
Pgs1	pER1186	pER1278
Nte1	pER961	pER1166
Cos111	pER960	pER1213
Izh3	pER996	pER1295
Dal81	pER981	pER1221
Hrk1	pER1191	pER1174
Yck2	pER977	pER1167
Grr1	pER980	pER1220
Apg13	pER982	pER1222
Siz1	pER976	pER1208
Crz1	pER983	pER1223
Vac7	pER979	pER1169
Tbs1	pER978	pER1215
Vid22	pER975	pER1219
sPFD-1	pER1713	pER1746
sPFD-2	pER1714	pER1747
cPFD-1	pER1715	pER1748
cPFD-2	pER1716	pER1749
cPFD-3	pER1717	pER1750

Table 2.4: PrLD Sequences	
Protein Name	**Sequence**
Swi4	KNSSSSTSATTTAANKKGKKNASINQPNPSPLQNLVFQTPQQFQVNS SMNIMNNNDNHTTMNFNNDTRHNLINNISNNSNQSTIIQQQKSIHENSF NNNYSATQKPLQFFPIPTNLQNKNVALNNPNNNDSNSYSHNIDNVINS SNNNNNGNNNNLIIVPDGPMQSQQQQQHHHEYLTNNFNHSMMDSIT NGNSKKRRKKLNQS
Rpi1	LSRMQYLLVQLQNTFSFVNGNIILKSQKTLKPNKNGTNDNINNHYYNN CNNNNNNINNSNNSNNNNSNNINRNSNHSTNVFSTPEHIQSSINLDKL ESLPALDTKGEPSFISPAQ
Var1	LNILSYYYKKKVTIEPIKLSYIYLNSDIFSKYISLNDMDKYNNGILTNYQR MLNNIMPKLNDHNISMNYINNINNINNNKYNNMINLLNNNNNINNNNNY NNNNNNYIGNINNIYNNMTIDNIPMDILMYKYLVGWSIKFKGRLSNNNG RTSTTNLLN
Mfg1	MYQGPPQPPPQAVPMPYIVNNNTPPYPNGNINFPPTAQQNIPPTVYP QQVPFPGQPQGGQFPQPSSEQQVFNQLPQVTQTFHNSAQNTNATG GPGS
Pam1	PTSRKNRSSVMPNIGYVPGLTNNEYGRKFNGNGMNGTQSRLNSLSN QSTFRSQQGPPITQQKSFQNNGGSMRTNRIPSANYNISNQQSGFVNS ISSPNLSNLENRNTVQNSRNADSAPCVNQLNSDSPPQLQSLSQNGTS
Dat1	DYTHQSFMDQQQQQQQQQQQLLQQQRVDVVPPKPFITHKILLSST GNSGGHVNSNYNADHSINHNSNHNLNSNVNVNMNFTINGSNQDPSS SFLMGPYNYLQRPFIVKPYLDLSTSTAASNQPRTQPSPAAHIT
YML053C	TIMNKRKNDHFEFDTHTFYQRSKRTKRDSVSTKFSVGSGCANLNNNN NIIINNNNNNNNNNNHNHNNSNNTATYNNIHYKKNIEICPLKPVSMHHT MNSRLLNESEFYSETEE
Rna15	SNVGPVINLKMMFDPQTGRSKGYAFIEFRDLESSASAVRNLNGYQLG SRFLKCGYSSNSDISGVSQQQQQQYNNINGNNNNNGNNNNNSNGPD FQNSGNANFLSQKFPELPSGIDVNINMTTPAMMISSEL
Cdc39	TFEVEVLLKSFNLTTKSLKPSNFINTPEVIETLSGALGSITLEQQQTEQQ RQIILMQQHQQQMLIYQQRQQQQQQRQQQQQHHISANTIADQQAAF GGESSISHDNPFNNLLGSTIFVTHPDLKRVF
Slf1	RNYQNRNGKTRYNNNSRHSQAANNAISFPNNYQARPEYIPNASHWL NNNSRNSYKQLSYFRQQQYYNNINYQQQLQTPYYYSMEPIFKSIESIK NQIEFYFSEENLKTDEFLRSKFKKANDGFIPMSLI
Sky1	SMPCGSSSNSKSRSIEKDLSKRCFRRPRRHTIITGSQPLPSPISSSNFF EMRAHFCGSSHNSFSSVSGNRNIPSSINNNSINNGIGIKNSNNSFLNSV PHSVTRMFINEDSNDNNNNDNSKNKNNNNNNSNNNNNEDIM
Pin4	RERIEREKREKRGQLEEQHRSSSNLSLDSLSKMSGSGNNNTSNNQLF STLMNGINANSMMNSPMNNTINNNSSNNNNSGNIILNQPSLSAQHTSS SLYQTNVNNQAQMSTERFYAPLPSTSTLPLPPQQLDFNDPDTLEIYSQ LLLFKDREKYYYELAYPMGISASHKRIINVLCSYLGLVEVYDPRFIIIRRKI LDHANLQSHLQQQGQMTSAHPLQPNSTGGSMNRSQSYTSLLQAHAA AAANSISNQAVNNSSNSNTINSNNGNGNNVIINNNSASSTPKISSQGQF SMQPTLTSPKMNIHHSSQYNSADQPQQPQPQTQQ

Gis1	LTPQLPQMNIPSNSSNFGTPSLTNTNSLLSNITATSTNPSTTTNGSQNH NNVNANGINTSAAASINNNISSTNNSANNSSSNNNVSTVPSSMMHSST LNGTSGLGGDNDDNMLALSLATLANSATASPRLT
Cln2	QRKLQIASNLNISRKLTISTPSCSFENSNSTSIPSPASSSQSHTPMRNM SSLSDNSVFSRNMEQSSPITPSMYQFGQQQSNSICGSTVSVNSLVNT NNKQRIYEQITGPNSNNATNDYIDLLNLNESNKENQNPATAHYLNG
Fab1	DNPGRHHHLDSVPTRYTIRDMDNISHYDTNSNSTLRPHYNTNNSTITIN NLNNTTSNNSNYNNTNSNSNINNPAHSLRRSIFHYVSSNSVNKDSNNS SATPASSAQSSSILEPANRIIGNYAHRNY
Mex67	MSGFHNVGNINMMAQQQMQQNRIKISVRNWQNATMNDLINFISRNAR VAVYDAHVEGPLVIGYVNSKAEAESLMKWNGVRFAGSNLKFELLDNN G
Q0255	EIYMKGLHNTTKGSNLLKLINNNINKKRYYSNYNISKNIIDDVLNMNTIYN YKLPYRMNSDIQRLNSMNNNNTKFINVGVFVYDLNNTLIMTFTGYRPA ATYFNSKHEIAKYIKNGNVFMNKYILKNILLD
Tda7	EASLQAQDSGSQQRNTETASANNPFSNEFNFKARGNPPPVPPPRNV TAMNGSFQNMRSNFMDQENRFSYGSSFTYSSLGSSTQGGFSTLSSN SIRLGRGLDNDISHDERNTVQNNSQGFLREII
YGL036W	NGGGENSSDKIDPTDLSFHLQVLMEVIDHPELNYLQENRLILLLDIALNY LILVPTHCLHSNFGELGSTQSLASTLNIIQFLLSKFLINMGSISQLINQYN RKCITTNNINNNNINNNGVINGSTNTTSTTTTTITNNNNNSNNSSISNNN RKIDWTQSYQTRYQIPYWFEDSILPPIPPISKSLFTFDKNLDHESDSIMI VNDVLRCL
Bph1	AVFNCMKVIIKNKERKLKEVACFFDPANKSEVLEGLSNILSCNNSETMN LITEQYPFFFNNTQQVRFINIVTNILFKNNNFSPISVRQIKNQVYEWKNA RSEYVTQNNKKCLILFRKDNTSLDFKIKKSIS
Ssn2	NVPPILIILPLDNATLTELVDKANIFQVIKNEVCAKMPNIELYLKVIPMDFI RNVLVTVDQYVNVAISIYNMLPPKSVKFTHIAHTLPEKVNFRTMQQQQ MQQQQQQQQQQNNSTGSSSIIYYDSYIHLAYSRSVDKEWVFAALSD SYGQGSMTKTWYVGNSRGKFDDACNQIWNIALNLASKKFG
Al3	NIKIKPLDTSDIGSNAWLAGMTDADGNFSINLMNGKNRSSRAMPYYLE LRQNYQKNSNNNNINFSYFYIMSAIATYFNVNLYSRERNLNLLVSTNNT YKTYYSYKVMVANTYKNIKVMEYFNKYSLLSSKHLDFLDWSKLVILINN EGQSMKTNGSWEL
Lee1	NSKEPIDITPPSQNNYLSHARSASFSTYTSPPLSAQTEFSHSASNANYF SSQYLMYSPQKSPEALYTEFFSPPSSSSSYINYSYNNSNINAYSPVSS SSSNIWQEQGQTTLSNPSVNQNLRYRTGPAIQEESDNEIEDLLIHNFN SRYCHE
Vac14	VQLDILIQLFESPVFTRMRLQLLEQQKHPFLHKCLFGILMIIPQSKAFETL NRRLNSLNIWTSQSYVMNNYIRQRENSNFCDSNSDISQRSVSQSKLH FQELINHFKAVSEEDEYSSDMIRLDHGANNK
Cdc73	ANIKQFLLESKYVNPRNLPSVPNGLVNIEKNFERISRPIRFIIVDNTRMFT KPEYWDRVVAIFTTGHTWQFNNYQWNSPQELFQRCKGYYFHFAGDS VPQHVQQWNVEKVELDKNKRFKDVEVVRY

Mdm1	LKILKKSQRTLLKELEMKELLKQQYMVQENGNSLFRKTKIYIRSYFSEN SSNGLKEITYYIINIHHFNNGQVSSWDMARRYNEFFELNTYLKKNFRDL MRQLQDLFPSKVKMSLKYHVTK
Pgs1	KTPAYHGWKKVLVPKRFNEGLGLQHMKIYGFDNEVILSGANLSNDYFT NRQDRYYLFKSRNFSNYYFKLHQLISSFSYQIIKPMVDGSINIIWPDSNP TVEPTKNKRLFLREASQLLDGF
Nte1	MRSMNCTTNNTNNTGQNTKNSLGSSFNSSNYTSYRFQTCLTDQIISE AQTWSLSSLFNFSWVVSYFVMGASRMIFRYGWYLATLSLLRIPKWIFF KLHHVQFTLSFWLILFALAVIVFVTYTIMKERILSQYKRLTPEFLPLENTG KSGSSANINAASTQSANAPPAIG
Cos111	DLALAGWRDWRYRNEPLYSSPLLNSFKLKKVVSRSSSITSTSSGNST GVHSTRRQRSNSSVASITTSIMSSIYNTSHVSLSSTTSNTSNGNISSGS NLSRVSTAGSLKKASAKSTRSSPQKAKPISDITS
Izh3	KSMVKTEILIEEPLNPTTDIKSFINSYNHGKAYSLGETQHLHYYQLPFP WRENRYIIHGYRFYNTHSKSLLSIFNWYGWHNETSNIWSHLLGAIYIIYL AIYDFPQSEVWRNSQVPPQARWIVFMFLAAALKCMLSSVFWHTFNGT SFLKLRSKFACVDYSGITILITASILTTEFVTMYSCYWAMYTYMSISLAL GVFGVFMNWSPRFDRPEARPLRIRFFILLATMGVLSFLHLIFLTDLHYA ATLFSPVTYKSVVWYLVGVVFYGSFIPERFRSDVQVDKTIPTNYELSTD LEIITKQREIHFREVPTAHSKCS
Dal81	HQSPADNAASPTKSVKATTKNSSTNNNVNSNNSNNNSNHDILNFNDN YTTILQHLANDHPNILREKGGSQQQQHQQQQQQQQQQQQQQQQQQS LDTLLHHYQSLLSKSDNAIAFDDNVSNSADHNGSNSNNNNNNNDISSP GNLMGSCNQCRLKKTKCNYFPDLGN
Hrk1	SNLKTVQNQVPNTPASIQGKSDNKPDIVEEETEENKEDDSNNDKESTP DNDKESTIDIKISKNENKSTVVSANPKKVDADADADCDANGDSNGRVD CKANSDCNDKTDCNANNDCSNESDCNAKVDTNVNTAANANPDMVPQ NNPQQQQQQQQQQQQQQQQQQQ
Yck2	DLSINKKPNLHGYGHPNPPNEKSKRHRSKNHQYSSPDHHHHYNQQQ QQQQAQAQAQAQAQAKVQQQQLQQAQAQQQANRYQLQPDDSHYD EEREASKLDPTSYEAYQQQTQQKYAQQQQKQMQQKSKQFANTGAN GQTNKYPYNAQPTANDEQNAKNAAQDRNSN
Grr1	QDNNNHNDSNRLHPPDIHPNLGPQLWLNSSGDFDDNNNNNNNNNNN NSTRPQMPSRTRETATSERNASEVRDATLNNIFRFDSIQRETLLPTNN GQPLNQNFSLTFQPQQQTNALNGIDINTVNTNLMNGVNVQIDQLNRLL PNLPEEERKQIHEFKLIVGKKIQ
Apg13	GLLRVSVSYRRDWKFEINNTNDELFSARHASVSHNSQGPQNQPEQE GQSDQDIGKRQPQFQQQQQPQQQQQQQQQQQRQHQVQTQQQRQI PDRRSLSLSPCTRANSFEPQSWQKKVYPISRPVQPFKVGSIGSQSAS RNPSNSSFFNQPPVHRPSMSSNYGPQMN
Siz1	HSQLQIPTWQCPVCQIDIALENLAISEFVDDILQNCQKNVEQVELTSDG KWTAILEDDDDSDSDSNDGSRSPEKGTSVSDHHCSSSHPSEPIIINLD SDDDEPNGNNPHVTNNHDDSNRHSNDNNNNSIKNNDSHNKNNNNN NNNNNNNNDNNNSIENNDSNSNN
Crz1	SNGEEQSINNKNDIDDNSAYRRNNFRNSSNSGSHTFQLSDLDLDVDM RMDSANSSEKISKNLSSGIPDSFDSNVNSLLSPSSGSYSADLNYQSLY

	KPDLPQQQLQQQQLQQQQQQQQQQQQQQKQTPTLKVEQSDTFQ WDDILTPADNQHRPSLTNQFLSPRSN
Vac7	NNNGNNSNSASNKTNADIKNSNADLSASTSNNNAINDDSHESNSEKP TKADFFAARLATAVGENEISDSEETFVYESAANSTKNLIFPDSSSQQQ QQQQQPPKQQQQQQNHGITSKISAPLLNNNKKLLSRLKNSRHISTGAI LNNTIATISTNPNLNSNVMQNN
Tbs1	NIFNEITIQDLNFLQFSSIPKLWENKTLEPGEEYHHSNGTNTDNNETTG ADDTDDNNNNNNNNNKNGNNSSSTINNNNNNYSNSNNNDNDNNIND DDDDDDDDDDDDDDDDDDDDNDDDYSNNGADDDEEDDDYDRSLFP TGLASLLDASYPERTANDYRDENEQ
Vid22	IGNVNNSHNTSNHSNMNIHTDNQTNNINNRSGNNSDNNDNEHDNDN DNHSNSNTPASRIDIDPTGGENSVLPEQQPQNSNNNLSFGSLSDTHH LSDSTISKEIDSIFLQIIQEDLYDYLSTVNSIVPISYRSYCEQSNFIRDSGR FKKRIITEDSIIGELEQPMN
sPFD-1	MSQQYNQNNLYQQGQQQNNGEQSFWYQQNNNLQQQGNYQQYNY TNGNNNQTSQISQGQQNGGNQNQNNRQQNQNQNTAPNSTSTSTNG YGASGHGRSTTSYGVQDHSGARIESAAGFQPQSQ
sPFD-2	MSNQYNNNVNWQIDQLQQNQNGYYNNQNQIQQAQQNTQNNSSNNS MQHQNTNFQYQRNQNTQNQSQQANLNQPQYNANNQNQSGEHMTS HFHGELASRHSHMTGSETGSTYTATAGFQPQSQ
cPFD-1	MSQAASTKQSTETQNGALNQTQDQNHHQTPVGRNNQNGTQNPYNS EQPNQNNWNTRNQSNNSAQNQQPQQDNQNNTRGNQQQEPQQAS GTSLAMNQHTKLNNENNSQDFLQQMWAGFQPQSQG
cPFD-2	MSTSQTMPMQEQLPEQDLQNNNGAHQQLNMSNNNASNMQNKHQIQ QKNQQMNKRYNKKYSSNHTQQTSNHNWPPGANNFLQQDNKQNNQ GTKLDQQNQGTDQNPSQNHNQIQNNAGFQPQSQG
cPFD-3	MSDQHKTNSQQRQVNSPQHQKQKVGQHEQNSDNRQNNEQFNNKQ KTNKRSQQNIPNQRNQNYHQNPSAGQALQHQNHKRYENNQAWEQQ AQGHYSQKQQAGTKTNNSQQTQNQQAGFQPQSQG

Table 2.5: Strain List	
Strain	**Genotype**
yER632	*MAT*α *kar1-1 SUQ5 ade2-1 his3 leu2 trp1 ura3 sup35*::KanMx [*psi*$^-$] [*PIN*$^+$] pJ533(*URA3*) [a]
yER1017	*MAT*α *kar1-1 SUQ5 ade2-1 his3 leu2 trp1 ura3 sup35*::KanMx [*psi*$^-$] *rnq1*::*HIS3* pJ533(*URA3*)
yER1018	*MAT*α *kar1-1 SUQ5 ade2-1 his3 leu2 trp1 ura3 sup35*::KanMx *hsp104*::*HIS3* pJ533(URA3)
yER1019	*MAT*α *kar1 SUQ5 ade2-1 his3 leu2 trp1 ura3 rnq1*::KanMx [*psi*$^-$]
yER1615	*MAT*α *kar1 SUQ5 ade2-1 his3 leu2 trp1 ura3 hsp104*::KanMX

[a] pJ533 is a cen plasmid expressing Sup35 from the *SUP35* promoter (26).

REFERENCES

1. Liebman SW, Chernoff YO (2012) Prions in yeast. *Genetics* 191(4):1041–72.
2. Edskes HK, Gray VT, Wickner RB (1999) The [URE3] prion is an aggregated form of Ure2p that can be cured by overexpression of Ure2p fragments. *Proceedings of the National Academy of Sciences of the United States of America* 96(4):1498–503.
3. Sondheimer N, Lindquist S (2000) Rnq1: an epigenetic modifier of protein function in yeast. *Molecular cell* 5(1):163–72.
4. Du Z (2011) The complexity and implications of yeast prion domains. *Prion* 5(4):311–316.
5. Ross ED, Baxa U, Wickner RB (2004) Scrambled prion domains form prions and amyloid. *Molecular and cellular biology* 24(16):7206–13.
6. Ross ED, Edskes HK, Terry MJ, Wickner RB (2005) Primary sequence independence for prion formation. *Proceedings of the National Academy of Sciences of the United States of America* 102(36):12825–30.
7. Afsar Minhas F ul A, Ross ED, Ben-Hur A (2017) Amino acid composition predicts prion activity. *PLOS Computational Biology* 13(4):e1005465.
8. Michelitsch MD, Weissman JS (2000) A census of glutamine/asparagine-rich regions: implications for their conserved function and the prediction of novel prions. *Proceedings of the National Academy of Sciences of the United States of America* 97(22):11910–5.
9. Harrison PM, Gerstein M (2003) A method to assess compositional bias in biological sequences and its application to prion-like glutamine/asparagine-rich domains in eukaryotic proteomes. *Genome biology* 4(6):R40.
10. Alberti S, Halfmann R, King O, Kapila A, Lindquist S (2009) A Systematic Survey Identifies Prions and Illuminates Sequence Features of Prionogenic Proteins. *Cell* 137(1):146–158.
11. Cascarina SM, Ross ED (2014) Yeast prions and human prion-like proteins: sequence features and prediction methods. *Cellular and molecular life sciences : CMLS* 71(11):2047–63.
12. March ZM, King OD, Shorter J (2016) Prion-like domains as epigenetic regulators, scaffolds for subcellular organization, and drivers of neurodegenerative disease. *Brain Research* 1647:9–18.
13. King OD, Gitler AD, Shorter J (2012) The tip of the iceberg: RNA-binding proteins with prion-like domains in neurodegenerative disease. *Brain Research* 1462:61–80.
14. Li YR, King OD, Shorter J, Gitler AD (2013) Stress granules as crucibles of ALS pathogenesis. *The Journal of cell biology* 201(3):361–72.
15. Molliex A, et al. (2015) Phase Separation by Low Complexity Domains Promotes Stress Granule Assembly and Drives Pathological Fibrillization. *Cell* 163(1):123–133.
16. Murakami T, et al. (2015) ALS/FTD Mutation-Induced Phase Transition of FUS Liquid Droplets and Reversible Hydrogels into Irreversible Hydrogels Impairs RNP

Granule Function. *Neuron* 88(4):678–90.
17. Lin Y, Protter DSW, Rosen MK, Parker R (2015) Formation and Maturation of Phase-Separated Liquid Droplets by RNA-Binding Proteins. *Molecular cell* 60(2):208–19.
18. Patel A, et al. (2015) A Liquid-to-Solid Phase Transition of the ALS Protein FUS Accelerated by Disease Mutation. *Cell* 162(5):1066–1077.
19. Parker R, Sheth U (2007) P bodies and the control of mRNA translation and degradation. *Molecular cell* 25(5):635–46.
20. Anderson P, Kedersha N (2009) RNA granules: post-transcriptional and epigenetic modulators of gene expression. *Nature reviews Molecular cell biology* 10(6):430–6.
21. Kato M, et al. (2012) Cell-free formation of RNA granules: low complexity sequence domains form dynamic fibers within hydrogels. *Cell* 149(4):753–67.
22. Kroschwald S, et al. (2015) Promiscuous interactions and protein disaggregases determine the material state of stress-inducible RNP granules. *eLife* 4:e06807.
23. Toombs JA, McCarty BR, Ross ED (2010) Compositional determinants of prion formation in yeast. *Molecular and cellular biology* 30(1):319–32.
24. Toombs JA, et al. (2012) De novo design of synthetic prion domains. *Proceedings of the National Academy of Sciences of the United States of America* 109(17):6519–24.
25. Ross ED, MacLea KS, Anderson C, Ben-Hur A (2013) A Bioinformatics Method for Identifying Q/N-Rich Prion-Like Domains in Proteins. *Methods in Molecular Biology (Clifton, N.J.)*, pp 219–228.
26. Gonzalez Nelson AC, et al. (2014) Increasing prion propensity by hydrophobic insertion. *PloS one* 9(2):e89286.
27. Paul KR, Hendrich CG, Waechter A, Harman MR, Ross ED (2015) Generating new prions by targeted mutation or segment duplication. *Proceedings of the National Academy of Sciences of the United States of America* 112(28):8584–9.
28. Paul KR, et al. (2017) The effects of mutations on the aggregation propensity of the human prion-like protein hnRNPA2B1. *Molecular and Cellular Biology*:MCB.00652-16.
29. Kim HJ, et al. (2013) Mutations in prion-like domains in hnRNPA2B1 and hnRNPA1 cause multisystem proteinopathy and ALS. *Nature* 495(7442):467–73.
30. Scheibel T, Lindquist SL (2001) The role of conformational flexibility in prion propagation and maintenance for Sup35p. *Nature structural biology* 8(11):958–62.
31. Pawar AP, et al. (2005) Prediction of “Aggregation-prone” and “Aggregation-susceptible” Regions in Proteins Associated with Neurodegenerative Diseases. *Journal of Molecular Biology* 350(2):379–392.
32. Halfmann R, Wright JR, Alberti S, Lindquist S, Rexach M (2012) Prion formation by a yeast GLFG nucleoporin. *Prion* 6(4):391–9.
33. Derkatch IL, Bradley ME, Hong JY, Liebman SW (2001) Prions affect the appearance of other prions: the story of [PIN(+)]. *Cell* 106(2):171–82.
34. Du Z, Park K-W, Yu H, Fan Q, Li L (2008) Newly identified prion linked to the chromatin-remodeling factor Swi1 in Saccharomyces cerevisiae. *Nature genetics* 40(4):460–5.
35. Patel BK, Gavin-Smyth J, Liebman SW (2009) The yeast global transcriptional co-

repressor protein Cyc8 can propagate as a prion. *Nature cell biology* 11(3):344–9.
36. Perutz MF, Pope BJ, Owen D, Wanker EE, Scherzinger E (2002) Aggregation of proteins with expanded glutamine and alanine repeats of the glutamine-rich and asparagine-rich domains of Sup35 and of the amyloid beta-peptide of amyloid plaques. *Proceedings of the National Academy of Sciences of the United States of America* 99(8):5596–600.
37. MacLea KS, et al. (2015) Distinct amino acid compositional requirements for formation and maintenance of the [PSI$^+$] prion in yeast. *Molecular and cellular biology* 35(5):899–911.
38. Li L, Lindquist S (2000) Creating a protein-based element of inheritance. *Science (New York, NY)* 287(5453):661–4.
39. Halfmann R, et al. (2011) Opposing Effects of Glutamine and Asparagine Govern Prion Formation by Intrinsically Disordered Proteins. *Molecular Cell* 43(1):72–84.
40. Bagriantsev SN, Kushnirov V V, Liebman SW (2006) Analysis of amyloid aggregates using agarose gel electrophoresis. *Methods in enzymology* 412:33–48.
41. Derkatch IL, Bradley ME, Zhou P, Chernoff YO, Liebman SW (1997) Genetic and environmental factors affecting the de novo appearance of the [PSI+] prion in Saccharomyces cerevisiae. *Genetics* 147(2):507–19.
42. Derkatch IL, et al. (2004) Effects of Q/N-rich, polyQ, and non-polyQ amyloids on the de novo formation of the [PSI+] prion in yeast and aggregation of Sup35 in vitro. *Proceedings of the National Academy of Sciences of the United States of America* 101(35):12934–9.
43. Bradley ME, Edskes HK, Hong JY, Wickner RB, Liebman SW (2002) Interactions among prions and prion "strains" in yeast. *Proceedings of the National Academy of Sciences of the United States of America* 99 Suppl 4:16392–9.
44. Chernoff YO, Lindquist SL, Ono B, Inge-Vechtomov SG, Liebman SW (1995) Role of the chaperone protein Hsp104 in propagation of the yeast prion-like factor [psi+]. *Science (New York, NY)* 268(5212):880–4.
45. Wegrzyn RD, Bapat K, Newnam GP, Zink AD, Chernoff YO (2001) Mechanism of prion loss after Hsp104 inactivation in yeast. *Molecular and cellular biology* 21(14):4656–69.
46. Arslan F, Hong JY, Kanneganti V, Park S-K, Liebman SW (2015) Heterologous aggregates promote de novo prion appearance via more than one mechanism. *PLoS genetics* 11(1):e1004814.
47. Huh W-K, et al. (2003) Global analysis of protein localization in budding yeast. *Nature* 425(6959):686–691.
48. Cox BS (1965) Ψ, A cytoplasmic suppressor of super-suppressor in yeast. *Heredity* 20(4):505–521.
49. Tuite MF, Marchante R, Kushnirov V (2011) Fungal prions: structure, function and propagation. *Topics in current chemistry* 305:257–98.
50. Esteras-Chopo A, Serrano L, de la Paz ML (2005) The amyloid stretch hypothesis: Recruiting proteins toward the dark side. *Proceedings of the National Academy of Sciences* 102(46):16672–16677.
51. Ross ED, Toombs JA The effects of amino acid composition on yeast prion formation and prion domain interactions. *Prion* 4(2):60–5.

52. Ramaswami M, Taylor JP, Parker R (2013) Altered ribostasis: RNA-protein granules in degenerative disorders. *Cell* 154(4):727–36.
53. Chiti F, Stefani M, Taddei N, Ramponi G, Dobson CM (2003) Rationalization of the effects of mutations on peptide and protein aggregation rates. *Nature* 424(6950):805–8.
54. Alexandrov AI, Polyanskaya AB, Serpionov G V., Ter-Avanesyan MD, Kushnirov V V. (2012) The Effects of Amino Acid Composition of Glutamine-Rich Domains on Amyloid Formation and Fragmentation. *PLoS ONE* 7(10):e46458.
55. Holmes DL, Lancaster AK, Lindquist S, Halfmann R (2013) Heritable remodeling of yeast multicellularity by an environmentally responsive prion. *Cell* 153(1):153–65.
56. Berson JF, et al. (2003) Proprotein convertase cleavage liberates a fibrillogenic fragment of a resident glycoprotein to initiate melanosome biogenesis. *The Journal of cell biology* 161(3):521–33.
57. Berchowitz LE, et al. (2015) Regulated Formation of an Amyloid-like Translational Repressor Governs Gametogenesis. *Cell* 163(2):406–18.
58. Ford AF, Shorter J (2015) Fleeting Amyloid-like Forms of Rim4 Ensure Meiotic Fidelity. *Cell* 163(2):275–6.
59. Caudron F, Barral Y (2013) A super-assembly of Whi3 encodes memory of deceptive encounters by single cells during yeast courtship. *Cell* 155(6):1244–57.
60. Sherman F (1991) Getting started with yeast. *Methods in enzymology* 194:3–21.
61. Halfmann R, Lindquist S (2008) Screening for amyloid aggregation by Semi-Denaturing Detergent-Agarose Gel Electrophoresis. *Journal of visualized experiments : JoVE* (17). doi:10.3791/838.

CHAPTER 3: THE PRION-LIKE PROTEIN KINASE, SKY1, IS REQUIRED FOR EFFICIENT STRESS GRANULE DISASSEMBLY[2]

Introduction

Stress granules form in the cytoplasm when translation initiation is limiting, including under a variety of stress conditions (1). Stress granules are composed of mRNAs and protein, and contain mRNPs stalled in translation initiation. These cytoplasmic granules are important for cellular homeostasis, and mutations that increase stress granule formation or decrease clearance have been linked to various neurodegenerative diseases, as well as some cancers (2, 3). Stress granules are part of a growing class of non-membranous organelles that includes processing bodies, nuclear speckles and nucleoli (4). While all of these assemblies are dynamic and reversible protein-RNA complexes, they differ in their composition and function.

Stress granules show liquid-like properties, and are thought to form at least in part by liquid-liquid phase separation (LLPS) (1). Many of the RNA-binding proteins found in stress granules contain intrinsically disordered low-complexity domains; some of these low-complexity domains are prion-like domains (PrLDs), defined as protein domains that compositionally resemble yeast prion domains (5). *In vitro*, many of these PrLDs can undergo LLPS. Recent studies suggest that stress granule assembly is a multistep process, in which untranslated mRNPs assemble into a core structure, concentrating low-complexity domains; these low-complexity domains create a liquid shell, thereby recruiting other low-complexity domains by LLPS (6). Thus, it has been

[2] This chapter is adapted from a manuscript in preparation for publication. Kacy R Paul built PrLD swaps (Figure 3.5).

proposed that stress granules contain two phases: a less dynamic core, stabilized by stronger interactions; and a dynamic shell composed of a diverse proteome that is continually exchanging with its surroundings (6, 7).

While it is known that stress granules are highly dynamic and reversible, the mechanisms of regulation of granule resolution are not fully understood. Stress granules can be degraded by autophagy (8). Additionally, a variety of mechanisms for dissolution have been proposed. A variety of evidence indicates that protein quality control system play a role in disassembly (9, 10). RNA/DNA helicases have been proposed promote disassembly by utilizing ATP hydrolysis to disrupt RNA-protein interactions (11, 12). Post-translational modifications including methylation and phosphorylation have also been shown to influence stress granule assembly by altering protein-protein interactions (13–16), so similar modifications may likewise influence granule dissolution. These mechanisms are not mutually exclusive, and since different stresses result in granules with different protein compositions (17, 18), the mechanisms of dissolution may vary depending on the type of stress present.

Here we provide evidence that the PrLD-containing yeast protein kinase Sky1 acts as a novel regulator of stress granule dissolution. Sky1 phosphorylates various proteins that have been identified as components of heat-induced stress granules (19–21). Therefore, we hypothesized that it might act as a stress granule regulator. Although Sky1 had previously not been characterized as a component of stress granules, we found that it indeed localizes to stress granules, and that its PrLD plays an important role in this recruitment. Strikingly, Sky1's kinase activity was necessary for efficient disassembly of stress granules. Sky1 promotes granule dissolution at least in part

through phosphorylation of Npl3, an mRNA shuttling protein (22). Npl3's phosphorylation state is important for its dynamic shuttling behavior (21, 23); disrupting phosphorylation dynamics resulted in inefficient stress granule disassembly. Finally, when Sky1 was overexpressed it compensated for defects in other disassembly pathways. These findings contribute to understanding the regulation of stress granules and importantly provides a possible mechanism to mitigate persistent stress granules in neurodegenerative diseases, including ALS (3, 24, 25).

Results

Sky1 is a novel stress granule component

A recent mass spectrometry study characterized protein components of heat-induced stress granules in yeast (19). We noticed that multiple known or proposed targets of the protein kinase Sky1 were found in heat-induced granules (20, 21, 26). We therefore hypothesized that Sky1 might act as a novel regulator of stress granules. None of the previous studies characterizing protein components of yeast stress granules identified Sky1 as a component (7, 19, 27–29). However, each of these studies involved purification of stress granules from cells, so likely missed proteins that loosely associated with the dynamic outer shell. To test whether Sky1 is recruited into heat-induced stress granules, we subjected yeast cells to heat shock at 46^{o}C for 15 and 30 minutes, and tested for colocalization between Sky1 and known stress granule proteins. After both 15 and 30 minutes of heat shock, Sky1-GFP was found in foci that colocalized with mCherry-tagged versions of the stress granule proteins Pab1, Tif4631, Pub1, and Ded1 (Fig 3.1 and Fig 3.2A).

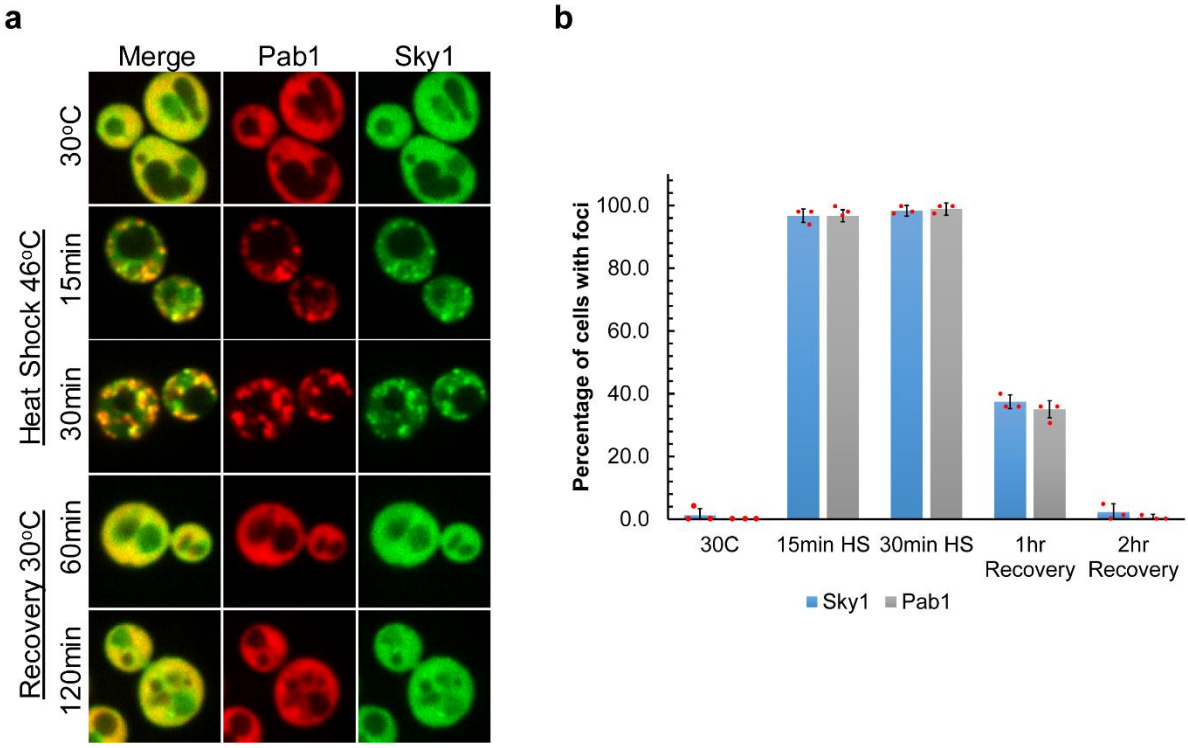

Figure 3.1: Sky1 is a novel stress granule protein
(a) Sky1 colocalizes with Pab1 foci during heat stress. Yeast expressing Sky1-GFP and Pab1-mCherry from the corresponding endogenous locus were grown at 30°C to mid-log, subjected to heat shock at 46°C, and allowed to recover at 30°C. Cells were visualized by fluorescence microscopy during heat shock and recovery. (b) Quantification of the percentage of cells with Pab1 or Sky1 foci. Data represent means ± SEM of n = 3 independent replicates.

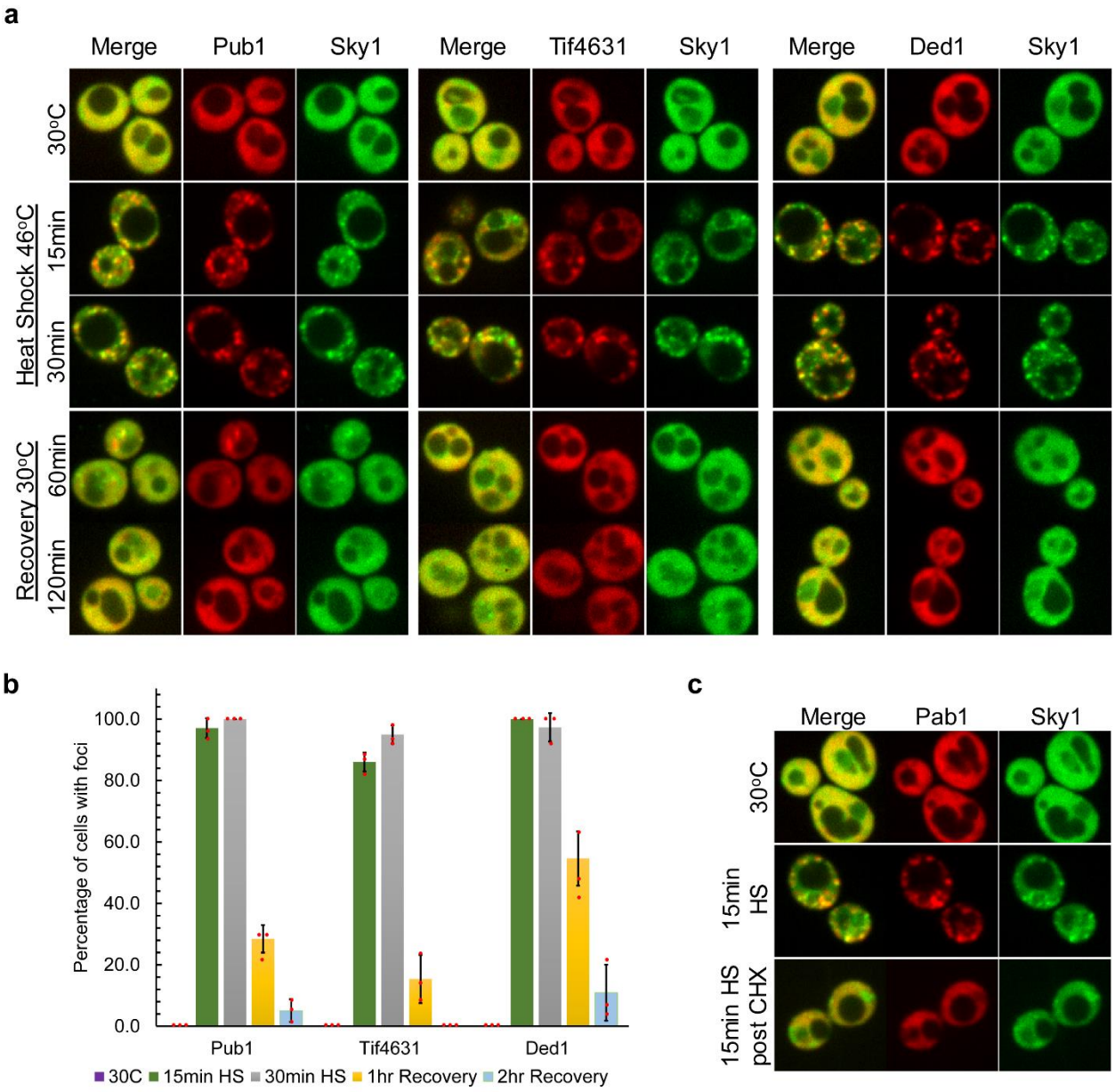

Figure 3.2: Sky1 is a novel stress granule protein
(a) Sky1 colocalizes with multiple stress granule markers during heat stress. Yeast strains expressing Sky1-GFP and the known stress granules proteins Pub1-mCherry, Tif4631-mCherry, or Ded1-mCherry, each from their corresponding endogenous locus were grown to mid log phase and visualized by fluorescence microscopy during heat stress and recovery. (b) Quantification of the percentage of cells with foci. Data represent means $\pm$ SEM of n = 3 independent replicates. (c) Pre-treatment of cells with cycloheximide reduces heat-induced foci formation by Sky1. Yeast expressing Sky1-GFP and Pab1-mCherry from their corresponding endogenous loci were grown to mid-log. Cells were then either subjected to heat shock for 15 minutes at 46°C, or pre-treated with 50ug/ml cycloheximide for 10 minutes prior to heat shock.

After 30 minutes of heat shock, cells were allowed to recover at 30ºC. After 1 h recovery, approximately 60% of the cells showed diffuse Sky1-GFP signal, while almost all cells showed diffuse signal after 2 h. Each of the stress granule markers showed slightly different rates of resolubilization during recovery, but each showed almost entirely diffuse signal by 2 h (Figure 3.1B, 3.2B)

Active protein translation is required for stress granule formation (30, 31). Stress granule formation is therefore inhibited by cycloheximide, a chemical that stalls ribosomes by blocking translation elongation (32). Addition of cycloheximide substantially reduced foci formation by Sky1-GFP and Pab1-mCherry (Figure 3.2C). Collectively, these data indicate that Sky1 is a novel component of stress granules.

Sky1's PrLD promotes recruitment to stress granules

PrLDs are prevalent in stress granule proteins (33), and are thought to promote recruitment to granules. We previously showed that Sky1 contains an aggregation-prone PrLD (34). When overexpressed, the PrLD forms SDS-insoluble cytoplasmic aggregates (34). Therefore, we tested whether the PrLD was sufficient for recruitment to stress granules. When expressed as a GFP fusion from a moderate-strength constitutive promoter, the PrLD was diffusely localized (Figure 3.3A). Upon heat shock, it formed foci that co-localized with Pab1-mCherry foci (Figure 3.3A). After 2 h recovery, the PrLD again showed almost entirely diffuse fluorescence (Figure 3.3A), indicating that the PrLD is sufficient for reversible recruitment into stress granules.

Next, we tested if the PrLD was necessary for Sky1 recruitment into stress granules. Deletion of the core PrLD did not entirely eliminate foci formation by Sky1-GFP, but did result in a statistically significant reduction in the fraction of Sky1 in foci

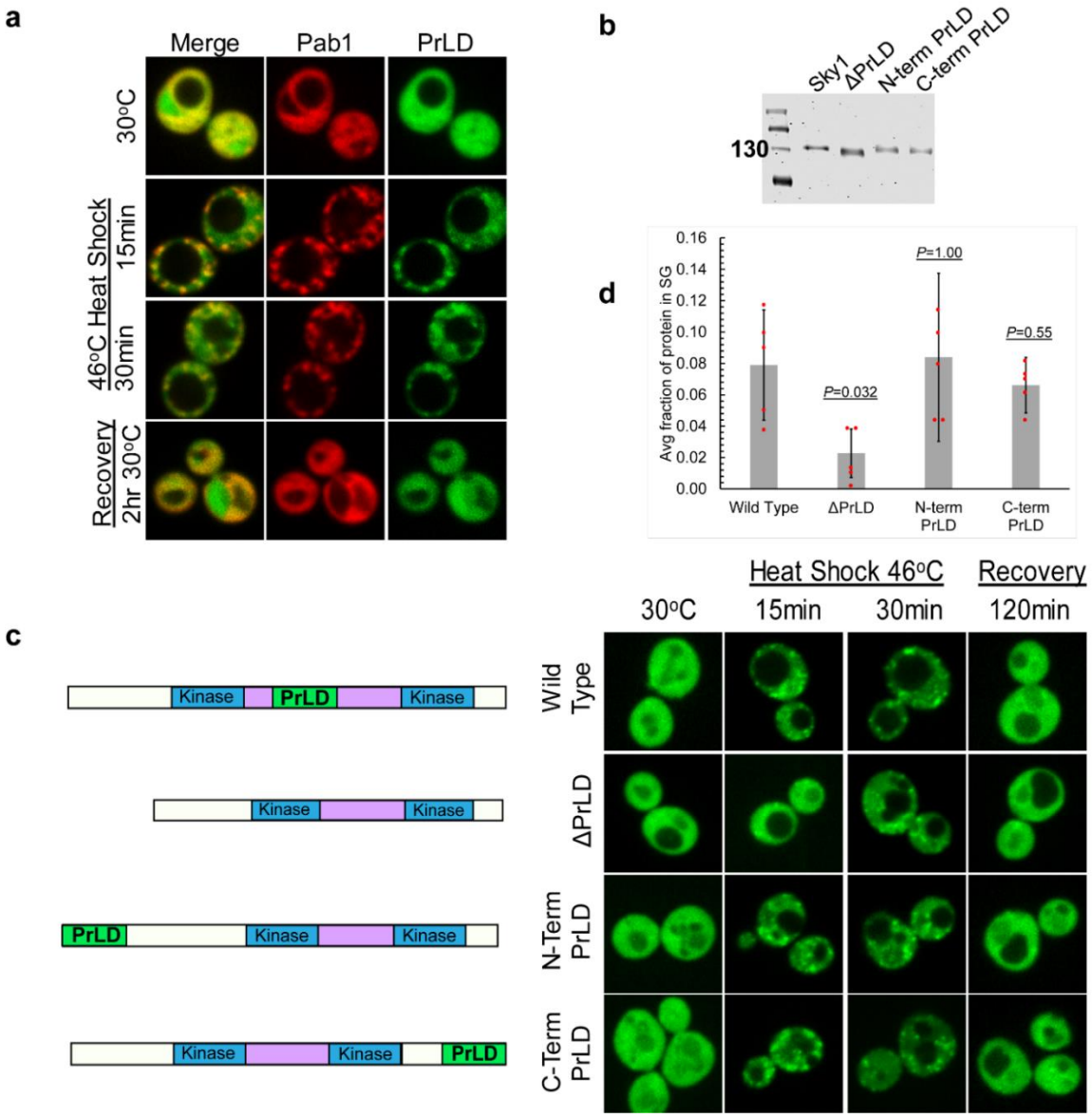

Figure 3.3: Sky1's PrLD is sufficient and necessary for stress granule formation
(a) The Sky1 PrLD is sufficient to associate with stress granules. Yeast expressing Pab1-mCherry from the endogenous locus were transformed with plasmids expressing the Sky1 PrLD fused to GFP, under control of the *SUP35* promoter. Cells were visualized by fluorescence microscopy during heat shock at 46°C and recovery at 30°C. (b-d) Analysis of yeast expressing from the endogenous *SKY1* locus GFP-tagged Sky1 mutants in which the core PrLD (amino acids 388-457) was deleted (ΔPrLD) or moved to the N-terminus (N-term PrLD) or C-terminus (C-term PrLD). Cells were grown to mid-log phase and either analyzed by western blot (B) or subject to heat shock and recovery (c). A schematic of each mutant is shown. (d) Quantification of the fraction of Sky1 in stress granules foci after 15 min of heat shock. Data represent mean ± SEM from of n = 5 independent replicates. *, $P < 0.05$ (Mann-Whitney test).

upon heat stress (Figure 3.3C,D). One possible explanation for the reduction in granule recruitment is that PrLD deletion could perturb the normal structure of Sky1. This seemed unlikely; the PrLD falls within a “spacer” region between the two kinases domains of Sky1 (35), and previous studies have shown that Sky1 is still functional and normally folded when the entire spacer domain is deleted (36). Consistent with normal folding, a $Sky^{\Delta PrLD}$ mutant showed similar protein levels to wild-type Sky1 (Figure 3.3B). Nevertheless, to confirm that the deletion did not compromise Sky1 activity, we monitored the localization of Npl3, a known phosphorylation target of Sky1. Npl3 is a mRNA shuttling protein that is phosphorylated by Sky1 in the cytoplasm to release its mRNA and return Npl3 to the nucleus (23). Under steady state conditions, Npl3 is predominantly in the nucleus, but when Sky1s inactivated, Npl3 shows significant cytoplasmic localization (Figure 3.4A). Deletion of the Sky1 PrLD did not alter Npl3’s nuclear localization (Figure 3.4A), indicating that PrLD deletion does not significantly affect Sky1’s kinase activity.

The aggregation activity of PrLDs is generally modular, meaning that PrLDs maintain aggregation activity when transferred to other proteins (37). The fact that the Sky1 PrLD maintains granule recruitment when fused to GFP suggests that it has similar modular activity. Therefore, if the PrLD promotes stress granule recruitment through a prion-like assembly mechanism, we hypothesized that this activity should be independent of the position of the PrLD within Sky1. Indeed, moving the PrLD to the N- or C-terminus did not significantly affect Sky1’s localization to granules (Figure 3.3C,D, 3.4B). These mutations also did not affect nuclear localization of Npl3 (Figure 3.4A), indicating that they did not perturb Sky1 function. These results clearly indicate that the

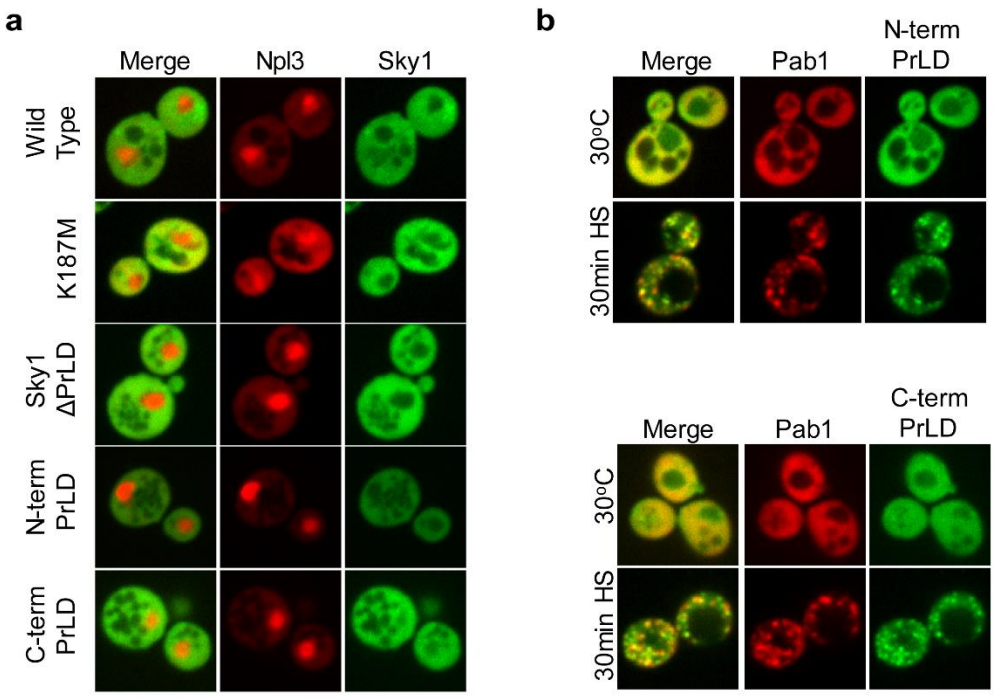

Figure 3.4: Sky1 PrLD mutant constructs are functional.
(a) Deleting or moving the Sky1 PrLD does not significantly alter Sky1-dependent localization of Npl3. Fluorescence microscopy during heat shock and recovery of yeast expressing from the corresponding endogenous loci Npl3-mCherry and GFP-tagged Sky1 mutants in which the core PrLD was deleted (ΔPrLD) or moved to the N-terminus (N-term PrLD) or C-terminus (C-term PrLD). (b) Sky1 mutant constructs localize to stress granules. Yeast expressing Sky1-GFP mutants and Pab1-mCherry were visualized by fluorescence microscopy during heat shock and recovery.

reduction in stress granule localization upon PrLD deletion is due to the loss of the PrLD *per se*, rather than conformational changes in the protein resulting from deletions in the spacer region

Prion-like activity of the Sky1 PrLD

Lsm4 and TIA-1 contain PrLDs that support recruitment to P bodies and stress granules, respectively (38, 39). In both cases, other prion domains can functionally replace these PrLDs in supporting granule recruitment, suggesting that these PrLDs act through prion-like assembly mechanisms. Therefore, we tested whether other PrLDs could similarly substitute for the Sky1 PrLD in supporting stress granule recruitment. We previously showed that Cdc39 contains a PrLD that has similar compositional characteristics to the Sky1 PrLD, and that it efficiently forms foci when overexpressed in yeast (34). Ded1 is a known stress granule protein, and contains a predicted PrLD (11, 40). Replacement of the Sky1 PrLD with the Cdc39 PrLD restored efficient stress-induced assembly, while replacement with the Ded1 PrLD partially restored assembly (Figure 3.5A,B), consistent with a prion-like assembly mechanism.

Like most yeast prion domains, the Sky1 PrLD is glutamine/asparagine-rich. We previously built three synthetic PrLDs designed to have high glutamine/asparagine content, but low aggregation activity (34, 40). When expressed as GFP-fusions, these cPFDs were not sufficient to support stress granule recruitment (Figure 3.6). When the Sky1 PrLD was replaced with each of these cPFDs, recruitment into granules was almost completely abolished (Figure 3.5A,B), consistent with the idea that the Sky1 PrLD supports stress granule recruitment by a prion-like assembly mechanism. The observed differences were not due to altered protein expression (Figure 3.5C).

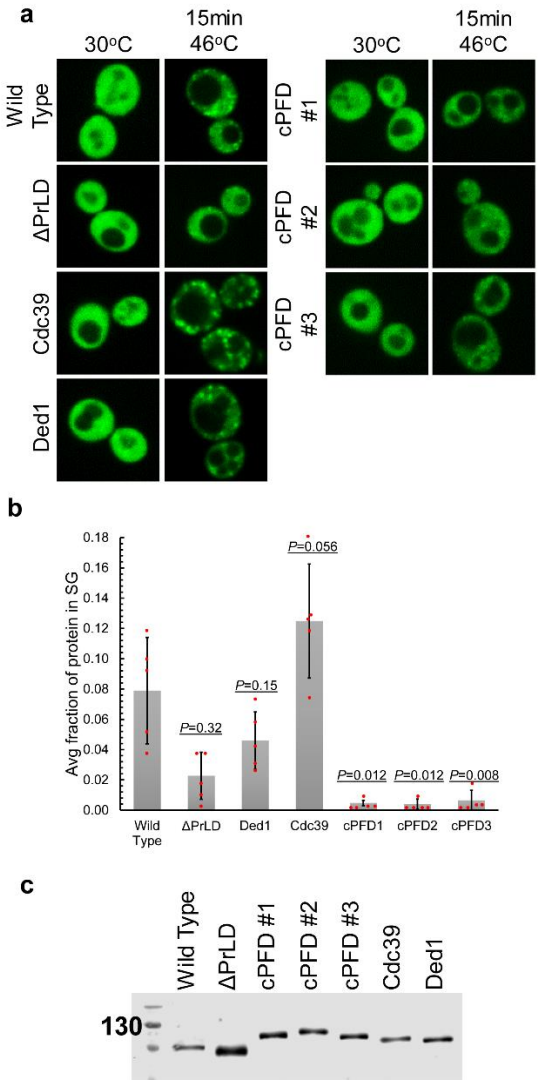

Figure 3.5: Sky1 is recruited to stress granules by a prion-like mechanism
(a) Yeast strains were generated expressing from the endogenous *SKY1* locus versions of Sky1-GFP in which the core PrLD was deleted (ΔPrLD), replaced with the PrLDs from Cdc39 or Ded1, or replaced with non-aggregation-prone PrLDs (cPFD#1, cPFD#2, cPFD#3). Cells were grown to mid-log, then subjected to heat shock at 46°C for 15 min. (b) Quantification of the fraction of Sky1 in stress granules foci after 15 min of heat shock. Data represent mean ± SEM of $n = 5$ independent replicates. *, $P < 0.05$; ** $P < 0.01$; n.s., not significant (Mann-Whitney test). (c) Western blot analysis of each mutant.

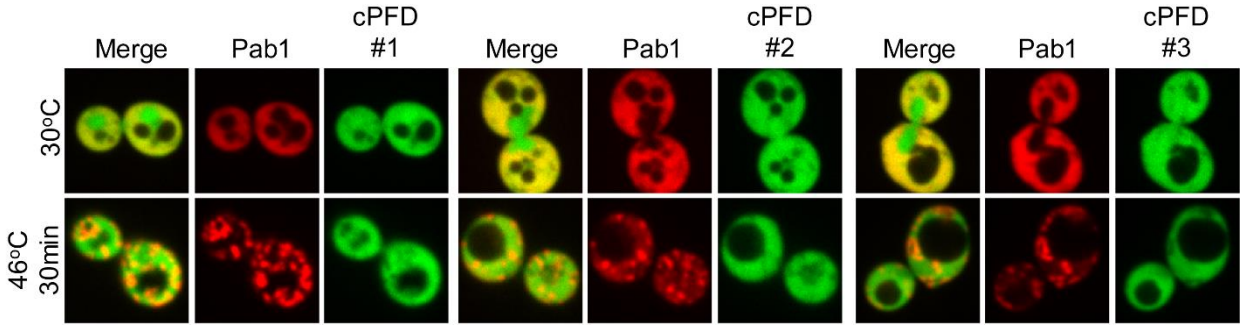

Figure 3.6: cPFDs are not sufficient to be recruited to stress granules
Yeast expressing Pab1-mCherry from its endogenous locus were transformed with plasmids expressing GFP-cPFD#1-3 fusions under control of the *SUP35* promoter. Cells were grown to mid-log and visualized by fluorescence microscopy during a heat shock.

Kinase activity dependent disassembly of stress granules

Sky1 is an SR protein kinase that is responsible for regulating the phosphorylation state of nuclear shuttling proteins involved in mRNA export (41). To test whether Sky1's kinase activity might be involved in the regulation of stress granule formation or disassembly, we replaced the *SKY1* open reading frame with either the GFP open reading frame or a GFP-tagged *sky1*^{K187M} allele; K187M is an ATP binding site mutation that inactivates Sky1's kinase activity (41). Neither deletion nor inactivation of Sky1 prevented stress granule assembly (Figure 3.7A-D and Figure 3.8), indicating that Sky1 activity is not required for efficient stress granule formation. However, in both *sky1*Δ and *sky1*^{K187M} strains, a significantly higher fraction of cells maintained Pab1-mCherry, Ded1-mCherry, and Pub1-mCherry foci after 1 hour of recovery than in wild-type *SKY1* cells (Figure 3.7A-D and Figure 3.8). These data indicate Sky1's kinase activity promotes efficient clearance of heat-induced stress granules.

A previous study showed cellular adaptation to stress is affected when Pab1's aggregation propensity is altered (42). Because Sky1 inactivation delays dissolution of Pab1-mCherry foci, we investigated whether Sky1 activity might similarly affect adaptation to chronic heat stress. Sky1 inactivation did not significantly affect growth at 30^{o}C, but almost completely eliminated growth at 40^{o}C, demonstrating that Sky1 activity is critical for adaptation to chronic stress (Figure 3.7E).

Npl3's phosphorylation state affects stress granules

We next examined the mechanism by which Sky1's kinase activity influences stress granule dynamics. Sky1 has two confirmed *in vivo* targets, Npl3 and Gbp2 (20, 21), as well as 40 additional potential targets identified by *in vitro* protein array

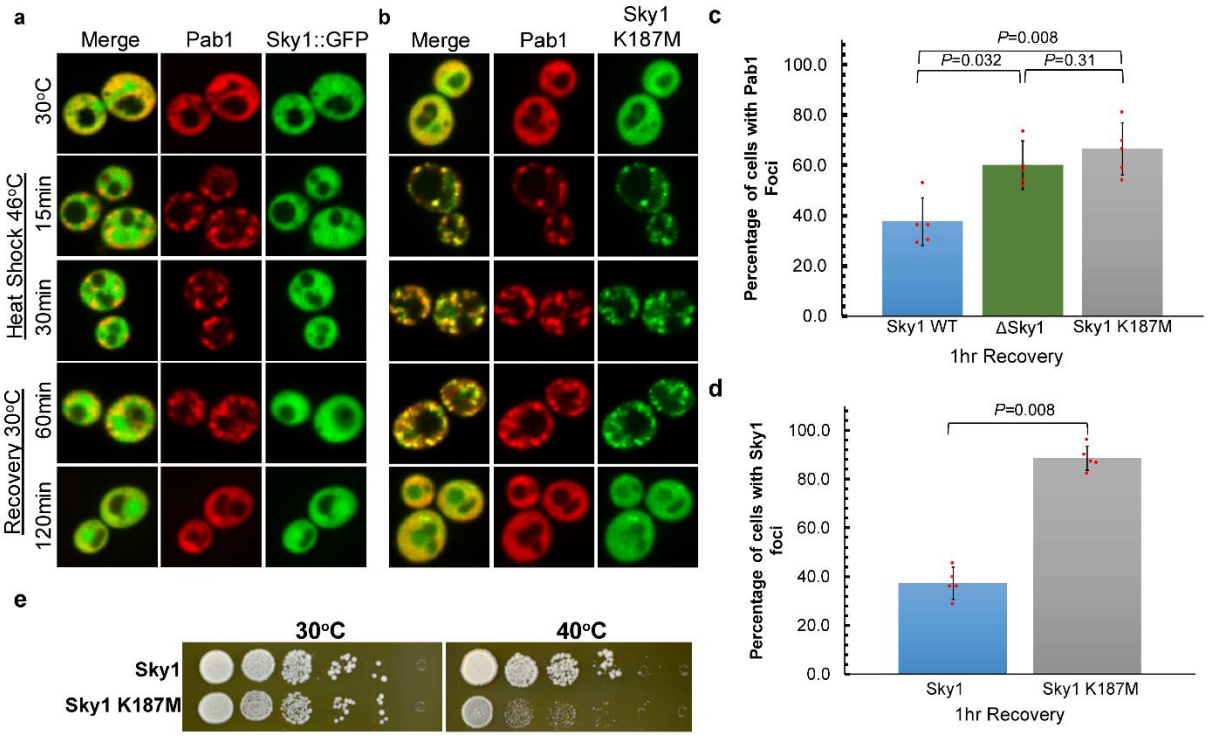

Figure 3.7: Sky1 and its kinase activity is required for efficient dissolution of Pab1 from stress granules

In yeast strains expressing Pab1-mCherry from the endogenous *PAB1* locus, the *SKY1* open reading frame was replaced with either the GFP open reading frame (a) or a catalytically inactive *sky1*^{K187M}-GFP allele (b). Cells were grown to mid-log and visualized by fluorescence microscopy during heat shock and recovery. (c,d) Quantification of the percentage of cells containing Pab1 foci (c) or Sky1 foci (d). Data represent means $\pm$ SEM of $n = 5$ independent replicates. *, $P < 0.05$; ** $P < 0.01$; *** $P < 0.001$ (Mann-Whitney test). (e) Yeast strains expressing Sky1-GFP and Sky1^{K187M}-GFP were grown to mid-log phase, and serial dilutions were plated on YPD plates. Cells were grown for either 2 days at 30°C or 4 days at 40°C to test for sensitivity to chronic heat stress.

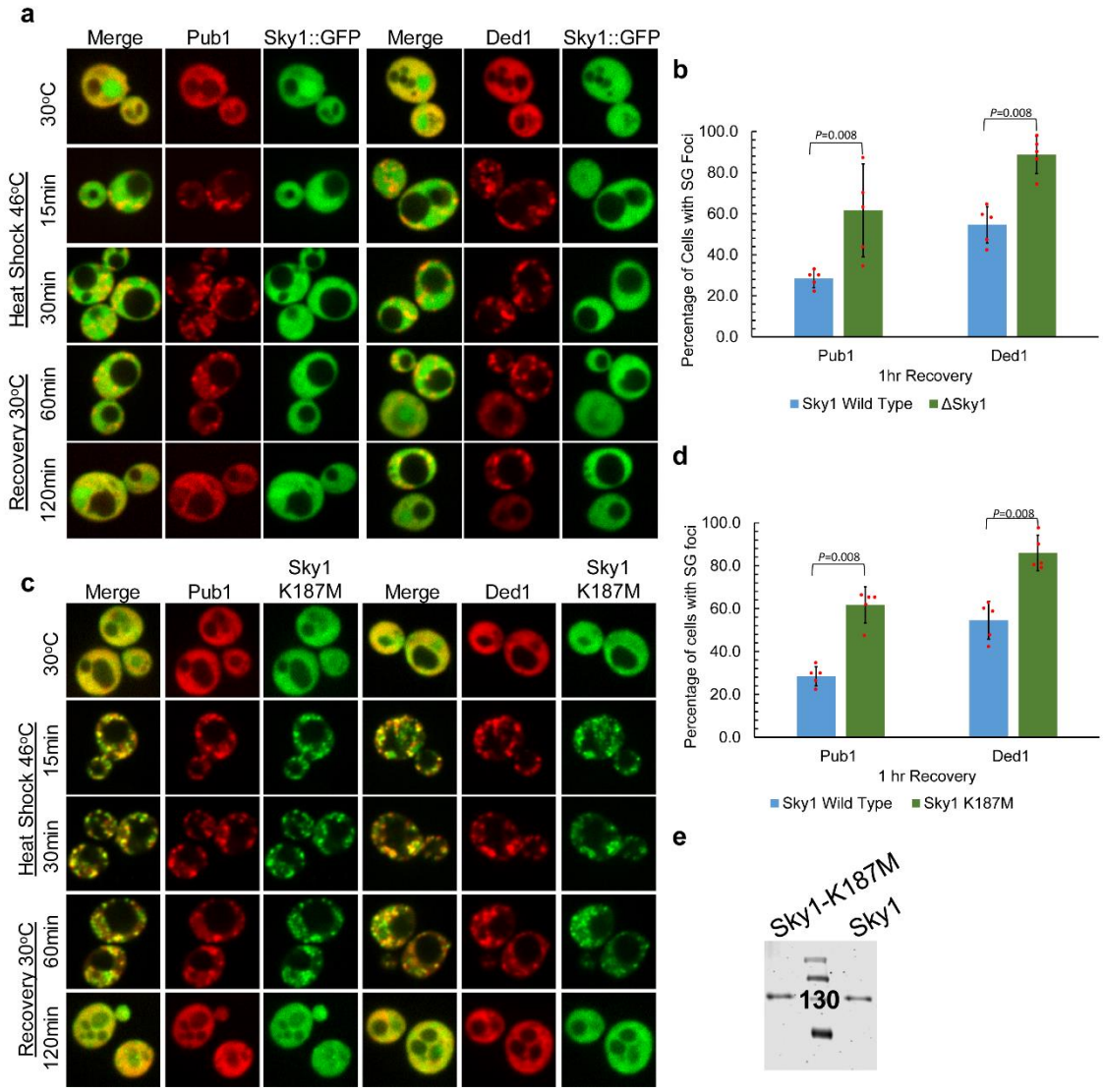

Figure 3.8: Sky1 and its kinase activity is required for efficient dissolution of stress granules

In yeast strains expressing mCherry-tagged granule proteins from the corresponding endogenous loci, the *SKY1* open reading frame was replaced with either the GFP open reading frame (a,b) or a catalytically inactive *sky1*^{K187M}-GFP allele (c,d). Cells were visualized by fluorescence microscopy during heat shock and recovery, and the percentage of cells containing foci was quantified. Data represent means ± SEM of n = 5 independent replicates. (e) Western blot analysis comparing expression of Sky1-GFP and Sky1^{K187M}-GFP.

experiments (26), Npl3 seemed like a particularly intriguing candidate. Npl3 is an mRNA shuttling protein (22), whose shuttling and mRNA dissociation is regulated by Sky1 (23). Upon heat stress, Npl3 shows increased cytoplasmic localization (43), and Npl3 has been isolated from several different types of stress granules (7, 19). Additionally, various core stress granule proteins, including Pab1 and Ded1, co-purify with TAP tagged Npl3 (44). Finally, prolonged association of Npl3 with mRNA inhibits translation (45).

Therefore, we characterized Npl3 protein localization during heat shock and recovery. As previously reported (22), Npl3-GFP was predominantly nuclear under non-stress conditions (Figure 3.9A). After 15 minutes of heat shock, Npl3-GFP was still predominantly nuclear, but showed a small increase in cytoplasmic localization (Figure 3.9A). However, by 30 minutes of heat shock, in most cells Npl3-GFP had relocalized into cytoplasmic foci that colocalized with Pab1-mCherry (Figure 3.9A). After one hour of recovery, Npl3-GFP returned to the nucleus. Thus, Npl3-GFP is recruited into stress granules, but exhibits slower recruitment and more rapid disassembly dynamics than core stress granule proteins. In a *sky1*^{K187M} strain, Npl3-GFP was still predominantly nuclear in the absence of stress, but showed increased cytoplasmic localization (Figure 3.9B). Upon heat stress, Npl3-GFP showed much faster relocalization to stress granules in the *sky1*^{K187M} strain, and these granules persisted much longer than in the *SKY1* strain (Figure 3.9A-D). Thus, Sky1 kinase activity regulates Npl3 localization during and after stress.

To confirm that Sky1 phosphorylates Npl3 during and after heat shock, we used phos-tag SDS-PAGE western blots to examine the phosphorylation profile of Npl3.

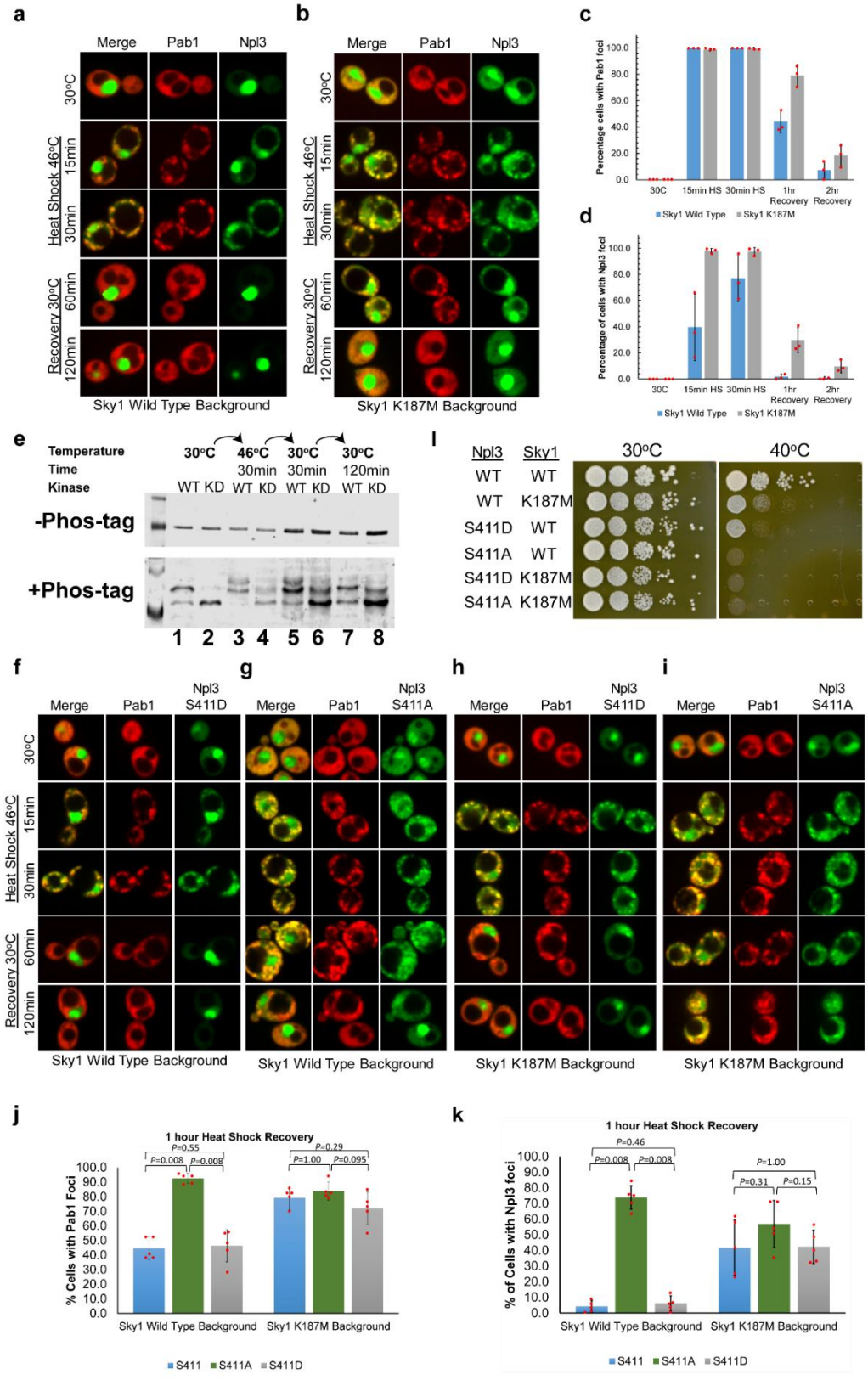
a
Merge
Pab1
Npl3
30°C
Heat Shock 46°C 15min
30min
Recovery 30°C 60min
120min
Sky1 Wild Type Background
b
Sky1 K187M Background
c
Percentage cells with Pab1 foci
30C
15min HS
30min HS
1hr Recovery
2hr Recovery
Sky1 Wild Type
Sky1 K187M
d
Percentage of cells with Npl3 foci
e
Temperature
Time
Kinase
30°C 46°C 30°C 30°C
30min 30min 120min
WT KD WT KD WT KD WT KD
-Phos-tag
+Phos-tag
1 2 3 4 5 6 7 8
l
Npl3 Sky1
WT WT
WT K187M
S411D WT
S411A WT
S411D K187M
S411A K187M
30°C
40°C
f
g
h
i
Npl3 S411D
Npl3 S411A
Sky1 Wild Type Background
Sky1 K187M Background
j
1 hour Heat Shock Recovery
% Cells with Pab1 Foci
P=0.55
P=0.008
P=0.008
P=0.29
P=1.00
P=0.095
S411
S411A
S411D
k
% of Cells with Npl3 foci
P=0.46
P=0.008
P=0.008
P=1.00
P=0.31
P=0.15

Figure 3.9: Npl3's phosphorylation by Sky1 is required for efficient stress granule dissolution

(a,b) Fluorescence microscopy during heat shock and recovery of yeast expressing Pab1-mCherry, Npl3-GFP, and either wild-type Sky1 (a) or Sky1^{K187M} (b), each from corresponding endogenous locus. (c,d) Quantification of the percentage of cells containing Pab1 foci (c) or Npl3 foci (d). Data represent means $\pm$ SEM of $n = 3$ independent replicates. (e) Yeast expressing Npl3-mCherry-Hisx8 and either wild-type Sky1 (WT, odd lanes) or Sky1^{K187M} (Kinase Dead (KD), even lanes) from the corresponding endogenous loci were grown to mid-log phase in YPD, and subjected to a heat shock and recovery. Cells were analyzed by western blotting with and without the addition of Phos-tag. (f-i) Fluorescence microscopy during heat shock and recovery of yeast expressing Pab1-mCherry; either Npl3^{S411D}-GFP (f,h) or Npl3^{S411A}-GFP (g,i); and either wild-type Sky1 (f,g) or Sky1^{K187M} (h,i) from the corresponding endogenous loci. (j,k) Quantification of the percentage of cells containing Pab1 foci (j) or Npl3 foci (k). Data represent means $\pm$ SEM of $n = 5$ independent replicates. ** $P < 0.01$; n.s., not significant (Mann-Whitney test). (l) Both *npl3^{S411D}* and *npl3^{S411A}* mutations inhibit growth under chronic heat stress.

Phos-tag is a compound that slows the electrophoretic migration of phosphorylated proteins (46). Npl3 from both *SKY1* and *sky1*^{K187M} strains harvested under steady state conditions migrated as a single band in the absence of phos-tag (Figure 3.9E). However, in the presence of phos-tag, Npl3 from the *SKY1* strain migrated as two bands; this second band was lost in the *sky1*^{K187M} strain (Figure 3.9E Lanes 1,2), confirming that Npl3 shows Sky1-dependent phosphorylation, as previously reported (41). The pattern was more complex during heat shock and recovery. Under both conditions, only a single band was observed by western blot in the absence of phos-tag for both the *SKY1* and *sky1*^{K187M} strains (Figure 3.9E). For the *SKY1* strain, addition of phos-tag resulted in the appearance of two slower-migrating bands, only one of which was lost in the *sky1*^{K187M} strain (Figure 3.9E, lanes 3-6). This indicates that during and after heat stress, Npl3 is subject to both Sky1-dependent and Sky1-independent phosphorylation. Sky1 is reported to phosphorylate Npl3 at a single site, S411 (23). To confirm that the Sky1-dependent changes observed on the phos-tag gel were a result of phosphorylation at this site, the experiment was repeated in an *npl3*^{S411A} strain. Under all conditions, Npl3^{S411A} showed similar migration on the phos-tag gel between the *SKY1* and *sky1*^{K187M}, confirming that Sky1 phosphorylates Npl3 before, during, and after heat shock (Figure 3.10).

To determine whether this Sky1-dependent phosphorylation of Npl3 is responsible for Sky1's effects on stress granule dynamics, we replace *NPL3* with alleles encoding either the non-phosphorylatable mutant Npl3^{S411A} or the phosphomimetic mutant Npl3^{S411D}. The *npl3*^{S411D} mutation had no significant effect on formation or dissolution of Pab1 foci (Figure 3.9F,J). By contrast, expression of Npl3^{S411A} mimicked

the effects of the *sky1*^{K187M} mutation; Npl3^{S411A} formed foci more rapidly than wild-type Npl3, and both Npl3 and Pab1 persisted in foci longer in the *npl3*^{S411A} strain than the *NPL3* strain (Figure 3.9G,J,K), suggesting that Sky1-dependent phosphorylation of Npl3 is required for efficient stress-granule dissolution. However, Sky1 also exerted an effect on granule dynamics that was independent of Npl3 phosphorylation at S411, as the *sky1*^{K187M} *npl3*^{S411D} double mutant showed more rapid formation of Pab1 foci and slower dissolution of these foci than the *npl3*^{S411D} strain (Figure 3.9H-K).

Next, we investigated whether the alterations in Npl3's phosphorylation state affects cellular adaptation to heat shock. The *npl3*^{S411D} and *npl3*^{S411A} mutations had no effect on growth at 30^{o}C. Interestingly, while only the *npl3*^{S411A} mutation significantly affected stress granule dynamics (Figure 3.9F), the both *npl3*^{S411D} and *npl3*^{S411A} mutations strongly inhibited growth at 40^{o}C, suggesting that Npl3's phosphorylation cycle is critical for cellular adaptation to stress (Figure 3.9L).

Sky1 activity can compensate for Hsp104 deficiencies

Various yeast chaperones, including Hsp104, Hsp70s, and Hsp40s are required for efficient stress granule clearance (9, 10). We therefore asked whether increasing Sky1 activity could compensate for loss of chaperones that are required for efficient stress granule disassembly. Plasmids expressing GFP, Sky1-GFP, and Sky1^{K187M}-GFP from the strong constitutive *GPD* promoter were introduced into either an *hsp104*Δ or *HSP104* strain containing the wild-type *SKY1* gene. In the presence of *HSP104*, overexpression of Sky1-GFP had little effect on formation or dissolution of Pab1-mCherry foci, while overexpression of Sky1^{K187M}-GFP exerted a dominant-negative effect, slowing dissolution of Pab1-mCherry foci even in the presence of an endogenous

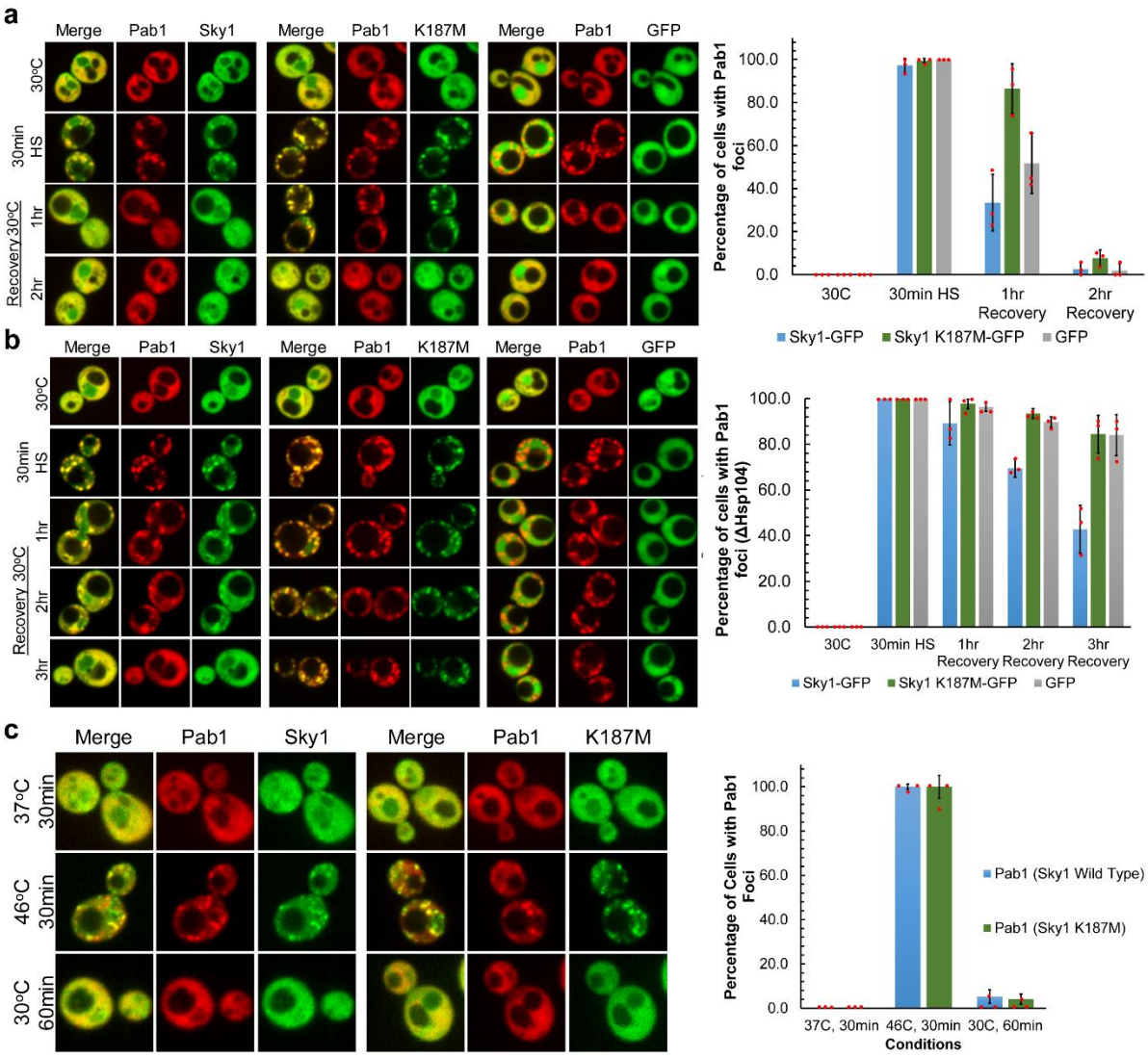

Figure 3.11: Sky1 and its kinase activity is an alternative and compensating pathway for efficient dissolution of stress granules

(a,b) Sky1 overexpression compensates for deficiencies in Hsp104. Either an *HSP104 (a) or hsp104*Δ (b) strain expressing Pab1-mCherry from its endogenous locus was transformed with plasmids expressing Sky1-GFP, Sky1^{K187M}-GFP, and GFP under control of the *GPD* promoter. Cells were visualized by fluorescence microscopy during a heat shock and recovery and the percentage of cells containing Pab1 foci was determined. Data represent means ± SEM of *n* = 3 independent replicates. (c) Pretreatment with mild heat stress to upregulate chaperone levels compensates for *sky1* deficiency. Yeast expressing Pab1-mCherry and either Sky1-GFP or Sky1^{K187M}-GFP from the corresponding endogenous loci were grown to mid-log phase, and then subjected to 37ºC for 30 minutes to upregulate chaperone levels.

copy of *SKY1* (Figure 3.11A). As expected, the *hsp104*Δ strain showed substantially slower dissolution of Pab1-mCherry foci. Overexpression of Sky1-GFP, but not Sky1^{K187M}-GFP significantly accelerated dissolution of foci (Figure 3.11B), indicating that elevated Sky1 kinase activity can partially reverse the effect of chaperone deficiencies.

We likewise asked whether elevated chaperone levels could compensate for deficiencies in Sky1 activity. Pretreatment of yeast cells at 37ºC elevates chaperone levels, and increases survival during heat shock at 46ºC (47). Pretreatment of both *SKY1* or *sky1^{K187M}* strains at 37ºC for 30 minutes prior to 46ºC heat shock substantially accelerated the dissolution of Pab1-Cherry foci during recovery for heat stress, with almost complete elimination of visible foci after 60 minutes of recovery (Figure 3.11C). These results highlight the extent to which multiple pathways contribute to stress granule dissolution, and demonstrate that activating one pathway can compensate for deficiencies in others.

Discussion

When cells are faced with fluctuating environments, they utilize elaborate mechanisms to spatiotemporally reorganize cellular processes for cellular adaptation and survival. Central to this cellular response is the rapid formation of stress granules, which are dynamic protein assemblies in the cytoplasm. Importantly, once the cellular stress is relieved, stress granules rapidly dissolve and the cell regains the normal cellular functions that were repressed during stress. The dysregulation of stress granules has detrimental consequences for the cell and can lead to neurodegenerative diseases (3), but the intricate mechanisms underlying the regulation of stress granules are not fully understood. Here, we identify and characterize a novel yeast prion-like

protein kinase that regulates stress granule dissolution. We demonstrated that the presence of functional Sky1 is required for efficient granule disassembly, and that this activity is mediated in part by phosphorylation of an RNA-binding protein, Npl3.

Prion-like protein Kinase, Sky1 as a novel stress granule protein

PrLDs are prevalent in stress granule proteins, and mutations in various PrLD-containing RNA-binding proteins have been linked to degenerative diseases (3, 48, 49). Disease-causing mutations are associated with the formation of cytoplasmic inclusions that share common components with stress granules (3, 48, 49). In vitro, many disease-associated mutations accelerate conversion to a stable amyloid state, or perturb LLPS dynamics (50–53). These results have led to the hypothesis that these PrLDs have evolved to mediate LLPS interactions that help localize proteins to granules, and that disease-associated mutations dysregulate granule formation and disassembly, or convert granules to more stable structures (3, 48, 49).

PrLDs' ability to self-assemble may help cells respond to fluctuations in the environment. Moreover, PrLDs provide conformational flexibility to participate in weak non-covalent multivalent interactions. Therefore, deleting the PrLDs would decrease the number of weak non-covalent interactions available, leading to a reduction in stress granule formation (38, 39). Consistent with the theory that the PrLD is involved in prion-like assembly within stress granules, efficient Sky1 recruitment to stress granules was rescued by either moving the PrLD to the termini or replacing the PrLD with known stress granule PrLDs, but not by replacing the PrLD with non-aggregation prone PrLDs (Figure 3.3 and Figure 3.5).

An obvious question is why Sky1 had not been previously identified as a stress granule component. A number of studies have attempted to characterize the diversity of yeast proteins sequestered in stress granules (7, 19, 27–29). However, other known regulators of stress granules, including Hsp104, Ydj1, Sis1, have not always been identified by these methods (19, 28), suggesting there may be a distinction between protein aggregation within stress granules and the recruitment to stress granules for regulation (19). Additionally, while Sky1 is enriched in granules, this enrichment is less dramatic than for other stress granule markers (Figure 3.1A and Figure 3.2A), potentially explaining why it may not have been detected. This failure to identify regulators may also reflect limitations of the methods used to characterize stress granule proteins. In most of these studies, stress granules were first isolated from cells, allowing for proteomic identification of the components. Components weakly associated with the outer shell of stress granules may be lost during the isolation of stress granules. Consistent with this explanation, recent studies using proximity labeling have identified Sky1's human homolog, SRPK1 (54), and Npl3's human homolog, SRSF1 (55), as being associated with stress granules.

Sky1-mediated disassembly pathway

Post-translational modifications, including protein phosphorylation, are postulated to broadly regulate aggregation-prone proteins found in stress granules (56), and several studies have shown that protein phosphorylation can regulate aggregation propensity *in vivo* and *in vitro* (57–59). However, the specific kinases and phosphatases involved in stress granule regulation, and the targets of these enzymes, have not been fully delineated.

While our results clearly suggest that Sky1-dependent phosphorylation of Npl3 affects stress granule dynamics, the observation that Sky1 inactivation delays granule dissolution even in an *npl3*^{S411D} strain suggests that other Sky1 may be acting on other targets to influence granule dissolution. The full range of Sky1 targets is not known. Sky1 is the only SR protein kinase in yeast. In mammals, SR kinases generally phosphorylate regions with multiple SR dipeptide repeats (41). However, the two confirmed *in vivo* targets of Sky1, Npl3 and Gbp2 (20, 21), lack extended SR repeats. Instead, Npl3 is phosphorylated at an isolated RS dipeptide, while Gbp2 is phosphorylated in a short stretch of three RS dipeptides (35). Thus, Sky1 may phosphorylate other proteins containing single SR dipeptides or short SR dipeptide motifs. In fact, protein mircoarray experiments have identified 40 proteins that can be phosphorylated by Sky1 *in vitro* (26).

Although Npl3 has previously been identified in yeast (7, 19) and mammalian cells (7, 55) as a component of stress granules, its phosphorylation state has not previously been implicated in regulating stress granules dynamics. During steady-state conditions, Npl3 binds mRNA in the nucleus to facilitate mRNA export. Phosphorylation by Sky1 in the cytoplasm reduces Npl3's binding affinity to mRNA (23), resulting in the release of RNA and rapid nuclear reimport of Npl3 (21). Interestingly, prolonged association of Npl3 with RNA inhibits translation (45), and Npl3 can directly interact with eIF4G to repress translation (60). Thus, phosphorylation of Npl3 may promote stress granule dissolution by releasing stalled translation complexes. Alternatively, phosphorylation may simply reduce the number of multivalent interactions available to Npl3 by reducing mRNA binding. It should be noted that while one previous study

suggests Npl3 is preferentially exported from the nucleus without RNA during stress, these experiments were performed under mild heat shock (42^{o}C) for 15 minutes (43). We showed Npl3 is not recruited to stress granules until severe stress (46^{o}C) for 30 minutes (Figure 3.9A, B). In addition, it is well-characterized mRNA is present in stress granules and plays a major role as a scaffolding factor to stabilize multivalent interactions within stress granules (31, 61–63).

Although Sky1 inactivation resulted in only a modest delay in stress granule dissolution, it showed a much more profound effect on survival during chronic mild heat stress. Interestingly, while *SKY1* strains expressing the phosphomimetic Npl3^{S411D} mutant showed similar stress granule dissolution rates to wild-type cells, both *npl3*^{S411A} and *npl3*^{S411D} strains showed diminished growth under chronic heat stress (Figure 3.9L). The exact mechanism for this effect is unclear, but it suggests that maintaining the ability to cycle between a phosphorylated and dephosphorylated state is important for surviving chronic heat stress. Wild type cells adapt to chronic heat stress (42, 57). Npl3 may contribute to this adaptation by maintaining the dynamic nature of stress granules formed under chronic heat stress, by maintaining normal mRNA shuttling during chronic heat stress, or by preventing the formation of persistent granules under chronic stress. Interestingly, nuclear-cytoplasmic shuttling mechanisms are closely linked to mammalian stress granule regulation, and defects have recently been linked to the progression of neurodegenerative disease in mammalian cells (64–66).

Conclusions

We propose that Sky1-mediated regulation provides a novel regulation pathway for dissolution of stress granules. During stress recovery, a concerted process between

molecular chaperones, RNA helicases, and Sky1 actively targets granules for efficient dissolution, allowing cellular components sequestered in stress granules during stress to regain normal function. Intriguingly, these pathways are clearly partially redundant, as Sky1 overexpression could partially compensate for *hsp104* deletion (Figure 3.11A), and stimulating chaperones by pretreatment with mild heat stress could partially compensate for Sky1 inactivation (Figure 3.11C). This result has significant potential health implications. If SRPK1 has a similar function in mammalian cells, targeted increase in SRPK1 may be able to compensate for disease-associated defects in the disassembly machinery.

Materials and Methods

Yeast Strains and Media

Standard yeast media and methods were used as previously described (67). In all experiments, yeast strains were grown at 30^{o}C. See Table 3.1 for strain descriptions, and Table 3.3 for primers used for strain construction.

A PCR-based homologous recombination protocol based on the methods of Longtine et al.1998 (68) was used to endogenously tag genes with mCherry, Briefly, an mCherry-URA3 cassette was PCR amplified from pER1372 (kind gift from Dr. Steven Markus), adding regions of homology to allow for in-frame fusion of the cherry tag with the target gene. These products were transformed into the Sky1-GFP strain from the GFP collection (69), selecting on SC-Ura. Genomic PCR and DNA sequencing were performed to confirm correct insertion.

A “flip in, flip out” scheme was used to generate endogenous Sky1 mutants, adapted from Riback *et al*. (42) First, a URA3 cassette was inserted into the target site

within *SKY1* using homologous recombination. Next, PCR products were generated containing the desired mutations; these PCR products were transformed into the *URA3* strain. Cells were plated on medium containing 5-FOA to select for loss of the URA3 cassette, and mutations were confirmed using genomic PCR and DNA sequencing.

To generate Npl3 (S411A/S411D)-GFP strains for microscopy, the HIS3 cassette from pFA6a-GFP(S65T)-HIS3MX6 (68) was PCR amplified, adding regions of homology to allow for in-frame fusion of the GFP tag, while changing the S411 codon. This fragment was inserted into Pab1-mCherry strains by homologous recombination.

To generate Npl3-mCherry-His_8 strains for phos-tag western blots, the KanMX cassette from pFA6a-GFP(S65T)-KanMX6(68) was PCR amplified, adding a His_8-tag at the 5'end. This fragment was inserted into Npl3-mCherry strains by homologous recombination. To generate the hsp104Δ strain, a HIS3 cassette was amplified from pRS313 (34), and inserted in place of the HSP104 open reading frame in strain yER1171 by homologous recombination. All transformants were confirmed by PCR and DNA sequencing. See Table 3.3 for primers used for strain construction.

Plasmid Construction

To generate the GFP-PrLD fusions, first GFP was cloned under control of the *SUP35* promoter by replacing the Sup35 open reading frame in pJ526 (70), adding a GSAGGS spacer, and BamHI and BglII sites, to generate plasmid pER843. Sky1's PrLD was amplified from the strain ATCC 201388 (69) and cPFD1-3 were amplified from previously described plasmids (34), adding BglII and BamHI restriction sites. PCR products were cut with BglII and BamHI and cloned into pER843 to generate GFP-PrLDs fusions expressed from the *SUP35* promoter.

To create Sky1-GFP fusions under control of the strong constitutive *GPD* promoter, Sky1-GFP, Sky1 K187M-GFP, and GFP open reading frames were amplified from yER1001 and yER1530, adding tails homologous to pER1440 for In-fusion cloning. See Table 3.2 for plasmid descriptions, and Table 3.4 for primers used for plasmid construction.

Microscopy

To monitor stress granule formation, yeast strains were grown to mid-log phase in YPD. 1ml of cell culture was harvested and washed in SC media prior to imaging by confocal microscopy using an Olympus IX81 Inverted Spinning Disk Microscope and a cascade II EMCCD camera. Heat shock and recovery were performed in 46^{o}C and 30^{o}C water baths, respectively. To upregulate chaperone levels, cells were incubated at 37^{o}C for 30 minutes prior to heat shock.

To monitor stress granule association by GFP-PrLD fusions, yeast strain yER1405 was transformed with *LEU2* plasmids expressing GFP-PrLD from the *SUP35* promoter. Cells were grown in dropout medium lacking leucine to mid-log phase, and analyzed as above.

Quantification of microscopy images

To determine the percentage of cells with foci, at least 30 cells from at least 3 independent experiments were counted. Mann-Whitney test was used to determine statistical significance at 1h recovery time points.

To determine the fraction of protein in stress granules, images of at least 30 cells from 5 independent experiments were analyzed. Quantification was performed using Slidebook (Intelligent Imaging Innovations, 3i). Region masks were applied to cells by

tracing the cell outline. Then, a 2D Lapacian filter was applied to the images and the average background fluorescence for all cells in each experiment was calculated. Regions within the cell with fluorescence 50% above background we considered granules; this filter was applied to each cell. For each cell, the fraction of protein in granules was calculated as:

$$\frac{\text{stress granule mask (mean intensity)} * \text{stress granule mask (microns}^2\text{)}}{\text{entire cell mask (mean intensity)} * \text{entire cell mask (microns}^2\text{)}}$$

A Mann-Whitney Test was used to determine statistical significance.

Western Blotting

To access protein expression levels, Sky1-GFP strains were grown to mid-log phase. Cells were harvested and lysed in 2M SUMEB lysis buffer (2M Urea, 10mM EDTA, 10mM MOPS). Samples were normalized based on total protein. The membrane was probed with an anti-GFP primary antibody (Santa Cruz, sc-9996), and Alexa Fluor IR800 goat anti-mouse secondary antibody (Rockland, 610-132-121).

To monitor protein phosphorylation, we supplemented SDS-PAGE gels with 50uM phos-tag™ (Wako). Yeast strains were grown to mid-log phase in YPD, then cell cultures were incubated in a 46°C water bath, followed by recovery at 30°C for indicated time. To halt all enzymatic activity, trichloroacetic acid (TCA) was directly added to cell cultures to a final 6%, and the mixture was incubated in an ice slurry bath for 10 minutes. Cells were harvested, lysed in 2M SUMEB lysis buffer, and normalized based on total protein. Normalized protein samples were TCA/acetone precipitated to remove contaminants and resuspended in 1x running buffer (15% glycerol, 80mM Tris Base, 3.5% SDS, bromophenol blue, BME). Samples were run on 7.5% acrylamide SDS-PAGE gels and 7.5% acrylamide SDS-PAGE gels with 50uM phos-tag and 100uM

$MnCl_2$. To remove the Mn^+ ions, the gel was incubated in 1x transfer buffer + 10mM EDTA for 20 minutes twice, followed by 1x transferred buffer for 10 minutes. Protein was transferred to PVDF membrane. The membrane was probed with an anti-His Tag primary antibody (Sigma, SAB1305538), and Alexa Fluor IR800 goat anti-mouse secondary antibody.

Cell Viability During Chronic Heat Stress

Cell viability during chronic heat stress was assayed as previously described.(42) Briefly, overnight yeast strains were diluted in YPD and grown to mid-log phase. Cell cultures were normalized based on OD_{600}, and serially diluted into fresh pre-warmed YPD. 5ul of each dilution was spotted onto YPD plates in duplicate. Plates were grown either at 30^{o}C for 2 days or at 40^{o}C for 4 days.

Table 3.1: Yeast strains

Strain Name	Genotype
yER1171	MAT**a** his3D1 leu2D0 met15D0 ura3D0 SKY1::SKY1-GFP-His3 PAB1::PAB1-mCherry-URA3
yER1405	MAT**a** his3D1 leu2D0 met15D0 ura3D0 PAB1::PAB1-mcherry-URA3
yER1001	MAT**a** his3D1 leu2D0 met15D0 ura3D0 SKY1::SKY1-GFP-His3
yER1752	MAT**a** his3D1 leu2D0 met15D0 ura3D0 SKY1::SKY1-dPrLD-(aa388-457)-GFP-His3
yER2166	MAT**a** his3D1 leu2D0 met15D0 ura3D0 SKY1::SKY1-N-term PrLD, dPrLD-GFP-His3 (PrLD aa388-457 inserted after G2, and deletion of PrLD in original location
yER2174	MAT**a** his3D1 leu2D0 met15D0 ura3D0 SKY1::SKY1-dPrLD-C-term PrLD-GFP-His3 (deletion of PrLD in original location aa388-457, PrLD inserted after H742
yER2144	MAT**a** his3D1 leu2D0 met15D0 ura3D0 SKY1::SKY1 PrLD (aa388-457)::Cdc39 PrLD (aa966-1092)-GFP-His3
yER2227	MAT**a** his3D1 leu2D0 met15D0 ura3D0 SKY1::SKY1 PrLD (aa388-457)::Ded1 PrLD (aa1-97)-GFP-His3
yER2204	MAT**a** his3D1 leu2D0 met15D0 ura3D0 SKY1::SKY1 PrLD (aa388-457)::cPFD#1 PrLD-GFP-His3
yER2205	MAT**a** his3D1 leu2D0 met15D0 ura3D0 SKY1::SKY1 PrLD (aa388-457)::cPFD#2 PrLD-GFP-His3
yER2206	MAT**a** his3D1 leu2D0 met15D0 ura3D0 SKY1::SKY1 PrLD (aa388-457)::cPFD#3 PrLD-GFP-His3
yER2095	MAT**a** his3D1 leu2D0 met15D0 ura3D0 SKY1::GFP-KanMx PAB1::PAB1-mcherry-Ura3
yER1551	MAT**a** his3D1 leu2D0 met15D0 ura3D0 SKY1::SKY1(K187M)-GFP-His3 PAB1::PAB1-mcherry-URA3
yER2118	MAT**a** his3D1 leu2D0 met15D0 ura3D0 NPL3::NPL3-GFP-His3 PAB::PAB1-mCherry-URA3
yER2160	MAT**a** his3D1 leu2D0 met15D0 ura3D0 SKY1::SKY1(K187M) NPL3::NPL3-GFP-His3 PAB::PAB1-mCherry-URA3
yER1746	MAT**a** his3D1 leu2D0 met15D0 ura3D0 SKY1::SKY1-GFP-His3 NPL3::NPL3-mCherry-Hisx8-KanMX
yER1747	MAT**a** his3D1 leu2D0 met15D0 ura3D0 SKY1::SKY1(K187M)-GFP-His3 NPL3::NPL3-mCherry-Hisx8-KanMX
yER1889	MATa his3D1 leu2D0 met15D0 ura3D0 NPL3::NPL3(S411D)-GFP-His3 PAB1::PAB1-mCherry-URA3
yER1894	MATa his3D1 leu2D0 met15D0 ura3D0 NPL3::NPL3(S411A)-GFP-His3 PAB1::PAB1-mCherry-URA3
yER2085	MATa his3D1 leu2D0 met15D0 ura3D0 SKY1::SKY1(K187M) NPL3::NPL3(S411D)-GFP-His3 PAB1::PAB1-mCherry-URA3
yER2086	MATa his3D1 leu2D0 met15D0 ura3D0 SKY1::SKY1(K187M) NPL3::NPL3(S411A)-GFP-His3 PAB1::PAB1-mCherry-URA3
yER2145	MAT**a** his3D1 leu2D0 met15D0 ura3D0 PAB1::PAB1-mcherry-URA3 HSP104::HIS3
yER1541	MAT**a** his3D1 leu2D0 met15D0 ura3D0 SKY1::SKY1-GFP-His3 PUB1::PUB1-mCherry-URA3

yER1507	MAT**a** his3D1 leu2D0 met15D0 ura3D0 SKY1::SKY1-GFP-His3 TIF4631::TIF4631-mCherry-URA3
yER1799	MAT**a** his3D1 leu2D0 met15D0 ura3D0 SKY1::SKY1-GFP-His3 DED1:DED1-mCherry-URA3
yER1461	MAT**a** his3D1 leu2D0 met15D0 ura3D0 SKY1::SKY1-GFP-HIS3 NPL3::NPL3-mCherry-URA
yER1553	MAT**a** his3D1 leu2D0 met15D0 ura3D0 SKY1::SKY1(K187M)-GFP-His3 NPL3::NPL3-mcherry-URA3
yER2147	MAT**a** his3D1 leu2D0 met15D0 ura3D0 SKY1::SKY1(dPrLD-core (aa388-457)-GFP-His3 NPL3::NPL3-mCherry-URA3
yER2203	MAT**a** his3D1 leu2D0 met15D0 ura3D0 SKY1::SKY1(N-Term PrLD,dPrLD-core (aa388-457)-GFP-His3 NPL3::NPL3-mCherry-URA3
yER2207	MAT**a** his3D1 leu2D0 met15D0 ura3D0 SKY1::SKY1-dPrLD(aa388-457)-C-term PrLD-GFP-His3 NPL3::NPL3-mCherry-URA3
yER2211	MAT**a** his3D1 leu2D0 met15D0 ura3D0 SKY1::SKY1(N-Term PrLD,dPrLD-core (aa388-457)-GFP-His3 PAB1::PAB1-mCherry-URA3
yER2202	MAT**a** his3D1 leu2D0 met15D0 ura3D0 SKY1::SKY1-dPrLD(aa388-457)-C-term PrLD-GFP-His3 PAB1::PAB1-mCherry-URA3
yER2096	MAT**a** his3D1 leu2D0 met15D0 ura3D0 SKY1::GFP-KanMx DED1::DED1-mcherry-Ura3
yER2124	MAT**a** his3D1 leu2D0 met15D0 ura3D0 SKY1::GFP-KanMx PUB1::PUB1-mcherry-Ura3
yER1550	MAT**a** his3D1 leu2D0 met15D0 ura3D0 SKY1::SKY1(K187M)-GFP-His3 PUB1::PUB1-mcherry-URA3
yER1801	MAT**a** his3D1 leu2D0 met15D0 ura3D0 SKY1::SKY1(K187M)-GFP-His3 DED1::DED1-mcherry-URA3
yER2161	MATa his3D1 leu2D0 met15D0 ura3D0 NPL3::NPL3(S411A)-mCherry-Hisx8-KanMx
yER2162	MATa his3D1 leu2D0 met15D0 ura3D0 Sky1::Sky1 (K187M) NPL3::NPL3(S411A)-mCherry-Hisx8-KanMx

Table 3.2: Plasmids

Plasmid Name	Description
pER1588	*LEU2*,cen, P_{SUS35}-GFP-Sky1 PrLD (aa 353-492)
pER1924	*LEU2*,cen, P_{GPD}-Sky1-GFP *K740Q mutation from GFP collection
pER1943	*LEU2*,cen, P_{GPD}-Sky1(K187M)-GFP *K740Q mutation from GFP collection
pER2050	*LEU2*,cen, P_{GPD}-GFP
pER1965	*LEU2*,cen, P_{SUP35}-GFP-cPFD#1
pER1947	*LEU2*,cen, P_{SUP35}-GFP-cPFD#2
pER1948	*LEU2*,cen, P_{SUP35}-GFP-cPFD#3

Table 3.3: Oligonucleotides used for strain construction

Oligo number	Used to in yERxxx construction	Oligo DNA Sequence
3018	1171,1405,1551, 2118, 2160, 2211, 2202,2095,1889, 1894,2085,2086, 2145	CTGCCTATGAGTCTTTCAAAAAGGAGCAAGAACAACA AACTGAGCAAGCTatggtgagcaagggcgagg
3036	1171,1405,1551, 2118, 2160, 2211, 2202,2095,1889, 1894,2085,2086, 2145	AAAAAGATGATAAGTTTGTTGAGTAGGGAAGTAGGTG ATTACATAGAGCAgtatcacgaggcccttcg
3605	1541,1550,2124	GAATGACCAACAACAACCGGTTATGTCTGAGCAACAA CAGCAACAGCAGCAACAGCAGCAACAACAAatggtgagc aagggcgagg
3606	1541,1550,2124	GCCTCTCTTTATTCTTTCTTTTTGTTTCATTCCACTTTT CTTCATAATATgtatcacgaggcccttcg
3603	1507,1552	CCGCAACAAATATGTTCAGTGCATTAATGGGAGAAAG TGATGACGAAGAGatggtgagcaagggcgagg
3604	1507,1552	CATCCTTGTATCCAAGTGACATTTTCGATACTTAACAT GATCTATTCATGgtatcacgaggcccttcg
3975	1799,1801,2096	AGTCTTCTGGCTGGGGTAACAGCGGTGGTTCAAACAA CTCTTCTTGGTGGatggtgagcaagggcgagg
3976	1799,1801,2096	AGACATGCTAGAGCAGAAAACGAAGAATCCTCACCCT AGTTTGTCTGAAAgtatcacgaggcccttcg
3566	1551,1550,1552, 1801	taagaaagctgggatggggccacttctccaccgtttggttggcaaaggatATG GTAAACAACACTCACGTTGCTATGATGATTGTTCGGG GCGACAAAGT
3567	1551,1550,1552, 1801	ccctcaacatctccaatctccatcaacacgttttctggtttaatatctgtGTGTAT AATACCACACCGCCTATG
4483	2095,2096,2124	ACCCCCTTTTGAGGTTGAAGAGATAGAGTAAAGAAGA AGTGTAGACATTAatgAGTAAAGGAGAAGAACTTTTCA CTGGAG
4484	2095,2096,2124	AAACAGAAAAAAAAGTAAAAGGCAAGGGCAAAATAAA GGTATAAAGGTAACAGTATAGCGACCAGCATTCAC
3560	1461,1553,2147, 2203,2207	GAGATGCATACAGAACCAGAGATGCTCCACGTGAAAG ATCACCAACCAGGatggtgagcaagggcgagg
3561	1461,1553,2147, 2203,2207	TCATATCTTTTGTTAATTTCTCCTTTTTTTTTCTCAACTA TATAAATGGCgtatcacgaggcccttcg
3800	1746,1746,2161, 2162,2164,2165	TTAAAACAATTCATATCTTTTGTTAATTTCTCCTTTTTTT TTCTCAACTATATAAATGGCttacagtatagcgaccagcattcac
3844	1746,1746,2161, 2162,2164,2165	GAACGCGCCGAGGGCCGCCACTCCACCGGCGGCAT GGACGAGCTGTACAAGCATCACCACCATCATCATCAC CATTAGGGCGCGCCACTTCTAAATAAG
3153	2118,2160,1746, 1747,1889,1894, 2085,2086	TCATATCTTTTGTTAATTTCTCCTTTTTTTTTCTCAACTA TATAAATGGCgaattcgagctcgtttaaactgg
4089	2161,2162,1894, 2086	GAGATGCATACAGAACCAGAGATGCTCCACGTGAAAG AGCTCCAACCAGGcggatccccgggttaattaacag

4090	1889,2085	GAGATGCATACAGAACCAGAGATGCTCCACGTGAAAG AGATCCAACCAGGcggatccccgggttaattaacag
2709	2145	ACAAAGAAAAAAGAAATCAACTACACGTACCATAAAAT ATACAGAATATcagattgtactgagagtgcacc
2710	2145	TATTATATTACTGATTCTTGTTCGAAAGTTTTTAAAAAT CACACTATATTAAActacataagaacacctttggtggag
3810	1752	TGTCAAAAAGATGCTTTAGAAGACCTAGACGTCATAC AATTATCACAGGGTTCATAAATGAAGACAGTAATGATA ACAACAATAATGATAATAGTAAAAA
3811	1752	TTTTTACTATTATCATTATTGTTGTTATCATTACTGTCTT CATTTATGAACCCTGTGATAATTGTATGACGTCTAGGT CTTCTAAAGCATCTTTTTGACA
4448	2166,2211	TTTTGAGGTTGAAGAGATAGAGTAAAGAAGAAGTGTA GACATTAATGGGTAGTATGCCCTGCGGCTC
4449	2166,2211	TCAGCCAAATGAGCGCTTTTAGTCACAAACCCAGGAT AGTTAATTGATGACATTATGTCCTCGTTATTATTGTTGT TACTGTTG
4452	2174,2202	GTTCCGATATCCCCGGATGGTTTGAAGAAGTCCGCGA TCATAAAAGACATAGTATGCCCTGCGGCTC
4453	2174,2202	actccagtgaaaagttcttctcctttactgttaattaacccggggatccgCATTA TGTCCTCGTTATTATTGTTGTTACTGTTG
4544	2144	TGTCAAAAAGATGCTTTAGAAGACCTAGACGTCATAC AATTATCACAGGGactttcgaagttgaggttttattaaaatcttttaatttga ccac
4545	2144	TTTTTACTATTATCATTATTGTTGTTATCATTACTGTCTT CATTTATGAAaaataccctcttcaagtcagggtgg
4567	2204	TGTCAAAAAGATGCTTTAGAAGACCTAGACGTCATAC AATTATCACAGGGATGTCTCAAGCAGCATCTACTAAA CAATC
4569	2205	TGTCAAAAAGATGCTTTAGAAGACCTAGACGTCATAC AATTATCACAGGGATGTCTACTTCTCAAACTATGCCAA TG
4570	2206	TGTCAAAAAGATGCTTTAGAAGACCTAGACGTCATAC AATTATCACAGGGATGTCTGATCAACATAAAACTAATT CTCAACAAAGAC
4568	2204,2205,2206	TTTTTACTATTATCATTATTGTTGTTATCATTACTGTCTT CATTTATGAAACCTTGAGACTGTGGTTGGAAAC
4563	2227	TGTCAAAAAGATGCTTTAGAAGACCTAGACGTCATAC AATTATCACAGGGatggctgaactgagcgaacaag
4564	2227	TTTTTACTATTATCATTATTGTTGTTATCATTACTGTCTT CATTTATGAATGGAGCTGGGACATGTTTGC

Table 3.4: Oligonucleotides used in plasmid construction

Oligo number	Used for pERxxx construction	Oligo DNA Sequence
3407	1588	GTCGATGCTAagatctccttaCATTATGTCCTCGTTATTATTGTTGTTACTGTTG
2289	1588	GAGCTACTGGATCCACAatgtctAGTATGCCCTGCGGCTCAAG
4231	1924,1943	ttcgacggattctagATGGGTTCATCAATTAACTATCCTGGG
4309	1924,1943,2050	aattacatgactcgagctatttgtatagttcatccatgccatgtgt
4591	2050	ttcgacggattctagaatgAGTAAAGGAGAAGAACTTTTCACTGG
4305	1965	ttctgctggtGGATCCATGTCTCAAGCAGCATCTACTAAACAATCTACTG
4307	1947	ttctgctggtGGATCCATGTCTACTTCTCAAACTATGCCAATGC
4308	1948	ttctgctggtGGATCCATGTCTGATCAACATAAAACTAATTCTCAACAAAGAC
4306	1965,1947,1948	tgcaagaaatAGATCTtcaACCTTGAGACTGTGGTTGGAAAC

REFERENCES

1. Protter DSW, Parker R (2016) Principles and Properties of Stress Granules. *Trends in Cell Biology* 26(9):668–679.
2. Anderson P, Kedersha N, Ivanov P (2015) Stress granules, P-bodies and cancer. *Biochimica et Biophysica Acta (BBA) - Gene Regulatory Mechanisms* 1849(7):861–870.
3. Ramaswami M, Taylor JP, Parker R (2013) Altered ribostasis: RNA-protein granules in degenerative disorders. *Cell* 154(4):727–36.
4. Spector DL (2006) SnapShot: Cellular Bodies. *Cell* 127(5):1071.e1-1071.e2.
5. Alberti S, Halfmann R, King O, Kapila A, Lindquist S (2009) A Systematic Survey Identifies Prions and Illuminates Sequence Features of Prionogenic Proteins. *Cell* 137(1):146–158.
6. Wheeler JR, Matheny T, Jain S, Abrisch R, Parker R (2016) Distinct stages in stress granule assembly and disassembly. *eLife* 5. doi:10.7554/eLife.18413.
7. Jain S, et al. (2016) ATPase-Modulated Stress Granules Contain a Diverse Proteome and Substructure. *Cell* 164(3):487–98.
8. Buchan JR, Kolaitis R-M, Taylor JP, Parker R (2013) Eukaryotic Stress Granules Are Cleared by Autophagy and Cdc48/VCP Function. *Cell* 153(7):1461–1474.
9. Cherkasov V, et al. (2013) Coordination of Translational Control and Protein Homeostasis during Severe Heat Stress. *Current Biology* 23(24):2452–2462.
10. Walters RW, Muhlrad D, Garcia J, Parker R (2015) Differential effects of Ydj1 and Sis1 on Hsp70-mediated clearance of stress granules in Saccharomyces cerevisiae. *RNA (New York, NY)* 21(9):1660–71.
11. Hilliker A, Gao Z, Jankowsky E, Parker R (2011) The DEAD-Box Protein Ded1 Modulates Translation by the Formation and Resolution of an eIF4F-mRNA Complex. *Molecular Cell* 43(6):962–972.
12. Chalupníková K, et al. (2008) Recruitment of the RNA helicase RHAU to stress granules via a unique RNA-binding domain. *The Journal of biological chemistry* 283(50):35186–98.
13. Poornima G, Shah S, Vignesh V, Parker R, Rajyaguru PI (2016) Arginine methylation promotes translation repression activity of eIF4G-binding protein, Scd6. *Nucleic Acids Research* 44(19):9358–9368.
14. Tsai W-C, et al. (2016) Arginine Demethylation of G3BP1 Promotes Stress Granule Assembly. *Journal of Biological Chemistry* 291(43):22671–22685.
15. Kedersha N, et al. (2002) Evidence That Ternary Complex (eIF2-GTP-tRNAiMet)-Deficient Preinitiation Complexes Are Core Constituents of Mammalian Stress Granules. *Molecular Biology of the Cell* 13(1):195–210.
16. Yoon J-H, Choi E-J, Parker R (2010) Dcp2 phosphorylation by Ste20 modulates stress granule assembly and mRNA decay in Saccharomyces cerevisiae. *The Journal of cell biology* 189(5):813–27.
17. Buchan JR, Parker R (2009) Eukaryotic stress granules: the ins and outs of translation. *Molecular cell* 36(6):932–41.
18. Buchan JR, Yoon J-H, Parker R (2011) Stress-specific composition, assembly

and kinetics of stress granules in Saccharomyces cerevisiae. *Journal of cell science* 124(Pt 2):228–39.
19. Wallace EWJ, et al. (2015) Reversible, Specific, Active Aggregates of Endogenous Proteins Assemble upon Heat Stress. *Cell* 162(6):1286–1298.
20. Windgassen M, Krebber H (2003) Identification of Gbp2 as a novel poly(A)+ RNA-binding protein involved in the cytoplasmic delivery of messenger RNAs in yeast. *EMBO Reports* 4(3):278–283.
21. Yun CY, Fu XD (2000) Conserved SR protein kinase functions in nuclear import and its action is counteracted by arginine methylation in Saccharomyces cerevisiae. *The Journal of cell biology* 150(4):707–18.
22. Lee MS, Henry M, Silver PA (1996) A protein that shuttles between the nucleus and the cytoplasm is an important mediator of RNA export. *Genes & development* 10(10):1233–46.
23. Gilbert W, Siebel CW, Guthrie C (2001) Phosphorylation by Sky1p promotes Npl3p shuttling and mRNA dissociation. *RNA (New York, NY)* 7(2):302–13.
24. Maziuk B, Ballance HI, Wolozin B (2017) Dysregulation of RNA Binding Protein Aggregation in Neurodegenerative Disorders. *Frontiers in Molecular Neuroscience* 10:89.
25. Li YR, King OD, Shorter J, Gitler AD (2013) Stress granules as crucibles of ALS pathogenesis. *The Journal of cell biology* 201(3):361–72.
26. Ptacek J, et al. (2005) Global analysis of protein phosphorylation in yeast. *Nature* 438(7068):679–684.
27. Cherkasov V, et al. (2015) Systemic control of protein synthesis through sequestration of translation and ribosome biogenesis factors during severe heat stress. *FEBS Letters* 589(23):3654–3664.
28. Narayanaswamy R, et al. (2009) Widespread reorganization of metabolic enzymes into reversible assemblies upon nutrient starvation. *Proceedings of the National Academy of Sciences* 106(25):10147–10152.
29. Cary GA, Vinh DBN, May P, Kuestner R, Dudley AM (2015) Proteomic Analysis of Dhh1 Complexes Reveals a Role for Hsp40 Chaperone Ydj1 in Yeast P-Body Assembly. *G3: Genes|Genomes|Genetics* 5(11):2497–2511.
30. Mokas S, et al. (2009) Uncoupling Stress Granule Assembly and Translation Initiation Inhibition. *Molecular Biology of the Cell* 20:2673–2683.
31. Mollet S, et al. (2008) Translationally repressed mRNA transiently cycles through stress granules during stress. *Molecular biology of the cell* 19(10):4469–79.
32. Kedersha N, Anderson P (2007) Mammalian Stress Granules and Processing Bodies. *Methods in Enzymology*, pp 61–81.
33. King OD, Gitler AD, Shorter J (2012) The tip of the iceberg: RNA-binding proteins with prion-like domains in neurodegenerative disease. *Brain Research* 1462:61–80.
34. Shattuck JE, Waechter AC, Ross ED (2017) The effects of glutamine/asparagine content on aggregation and heterologous prion induction by yeast prion-like domains. *Prion* 11(4):249–264.
35. Lukasiewicz R, et al. (2007) Structurally Unique Yeast and Mammalian Serine-Arginine Protein Kinases Catalyze Evolutionarily Conserved Phosphorylation Reactions. *Journal of Biological Chemistry* 282(32):23036–23043.

36. Nolen B, et al. (2001) The structure of Sky1p reveals a novel mechanism for constitutive activity. *Nature Structural Biology* 8(2):176–183.
37. Sondheimer N, Lindquist S (2000) Rnq1: an epigenetic modifier of protein function in yeast. *Molecular cell* 5(1):163–72.
38. Gilks N, et al. (2004) Stress granule assembly is mediated by prion-like aggregation of TIA-1. *Molecular biology of the cell* 15(12):5383–98.
39. Decker CJ, Teixeira D, Parker R (2007) Edc3p and a glutamine/asparagine-rich domain of Lsm4p function in processing body assembly in *Saccharomyces cerevisiae*. *The Journal of Cell Biology* 179(3):437–449.
40. Toombs JA, et al. (2012) De novo design of synthetic prion domains. *Proceedings of the National Academy of Sciences of the United States of America* 109(17):6519–24.
41. Siebel CW, Feng L, Guthrie C, Fu XD (1999) Conservation in budding yeast of a kinase specific for SR splicing factors. *Proceedings of the National Academy of Sciences of the United States of America* 96(10):5440–5.
42. Riback JA, et al. (2017) Stress-Triggered Phase Separation Is an Adaptive, Evolutionarily Tuned Response. *Cell* 168(6):1028–1040.e19.
43. Krebber H, Taura T, Lee MS, Silver PA (1999) Uncoupling of the hnRNP Npl3p from mRNAs during the stress-induced block in mRNA export. *Genes & development* 13(15):1994–2004.
44. Hurt E, Luo M-J, Röther S, Reed R, Strässer K (2004) Cotranscriptional recruitment of the serine-arginine-rich (SR)-like proteins Gbp2 and Hrb1 to nascent mRNA via the TREX complex. *Proceedings of the National Academy of Sciences of the United States of America* 101(7):1858–62.
45. Windgassen M, et al. (2004) Yeast Shuttling SR Proteins Npl3p, Gbp2p, and Hrb1p Are Part of the Translating mRNPs, and Npl3p Can Function as a Translational Repressor. *Molecular and Cellular Biology* 24(23):10479–10491.
46. Kinoshita E, Kinoshita-Kikuta E, Takiyama K, Koike T (2006) Phosphate-binding Tag, a New Tool to Visualize Phosphorylated Proteins. *Molecular & Cellular Proteomics* 5(4):749–757.
47. Lindquist S, Kim G (1996) Heat-shock protein 104 expression is sufficient for thermotolerance in yeast. *Proceedings of the National Academy of Sciences of the United States of America* 93(11):5301–6.
48. March ZM, King OD, Shorter J (2016) Prion-like domains as epigenetic regulators, scaffolds for subcellular organization, and drivers of neurodegenerative disease. *Brain Research* 1647:9–18.
49. Wolozin B (2012) Regulated protein aggregation: stress granules and neurodegeneration. *Molecular Neurodegeneration* 7(1):56.
50. Molliex A, et al. (2015) Phase Separation by Low Complexity Domains Promotes Stress Granule Assembly and Drives Pathological Fibrillization Article Phase Separation by Low Complexity Domains Promotes Stress Granule Assembly and Drives Pathological Fibrillization. *Cell* 163(1):123–133.
51. Patel A, et al. (2015) A Liquid-to-Solid Phase Transition of the ALS Protein FUS Accelerated by Disease Mutation. *Cell* 162(5):1066–1077.
52. Kim HJ, et al. (2013) Mutations in prion-like domains in hnRNPA2B1 and hnRNPA1 cause multisystem proteinopathy and ALS. *Nature* 495(7442):467–73.

53. Mackenzie IR, et al. (2017) TIA1 Mutations in Amyotrophic Lateral Sclerosis and Frontotemporal Dementia Promote Phase Separation and Alter Stress Granule Dynamics. *Neuron* 95(4):808–816.e9.
54. Youn J-Y, et al. (2018) High-Density Proximity Mapping Reveals the Subcellular Organization of mRNA-Associated Granules and Bodies. *Molecular Cell* 69(3):517–532.e11.
55. Markmiller S, et al. (2018) Context-Dependent and Disease-Specific Diversity in Protein Interactions within Stress Granules. *Cell* 172(3):590–604.e13.
56. Aguzzi A, Altmeyer M (2016) Phase Separation: Linking Cellular Compartmentalization to Disease. *Trends in cell biology* 26(7):547–558.
57. Saad S, et al. (2017) Reversible protein aggregation is a protective mechanism to ensure cell cycle restart after stress. *Nature cell biology* 19(10):1202–1213.
58. Rhoads S, Monahan Z, Yee D, Shewmaker F (2018) The Role of Post-Translational Modifications on Prion-Like Aggregation and Liquid-Phase Separation of FUS. *International Journal of Molecular Sciences* 19(3):886.
59. Monahan Z, et al. (2017) Phosphorylation of the FUS low-complexity domain disrupts phase separation, aggregation, and toxicity. *The EMBO Journal* 36(20):2951–2967.
60. Rajyaguru P, She M, Parker R (2012) Scd6 Targets eIF4G to Repress Translation: RGG Motif Proteins as a Class of eIF4G-Binding Proteins. *Molecular Cell* 45:244–254.
61. Zhang H, et al. (2015) RNA Controls PolyQ Protein Phase Transitions. *Molecular Cell* 60(2):220–230.
62. Van Treeck B, et al. (2018) RNA self-assembly contributes to stress granule formation and defining the stress granule transcriptome. *Proceedings of the National Academy of Sciences of the United States of America*:201800038.
63. Lin Y, Protter DSW, Rosen MK, Parker R (2015) Formation and Maturation of Phase-Separated Liquid Droplets by RNA-Binding Proteins. *Molecular cell* 60(2):208–19.
64. Hofweber M, et al. (2018) Phase Separation of FUS Is Suppressed by Its Nuclear Import Receptor and Arginine Methylation. *Cell* 173(3):706–719.e13.
65. Zhang K, et al. (2018) Stress Granule Assembly Disrupts Nucleocytoplasmic Transport. *Cell*. doi:10.1016/j.cell.2018.03.025.
66. Guo L, et al. (2018) Nuclear-Import Receptors Reverse Aberrant Phase Transitions of RNA-Binding Proteins with Prion-like Domains. *Cell* 173(3):677–692.e20.
67. Sherman F (1991) Getting started with yeast. *Methods in enzymology* 194:3–21.
68. Longtine MS, et al. (1998) Additional modules for versatile and economical PCR-based gene deletion and modification in Saccharomyces cerevisiae. *Yeast* 14(10):953–961.
69. Huh W-K, et al. (2003) Global analysis of protein localization in budding yeast. *Nature* 425(6959):686–691.
70. Ross ED, Edskes HK, Terry MJ, Wickner RB (2005) Primary sequence independence for prion formation. *Proceedings of the National Academy of Sciences of the United States of America* 102(36):12825–30.

CHAPTER 4: PRION-LIKE DOMAIN RECRUITMENT REQUIREMENTS INTO HEAT-INDUCED STRESS GRANULES[3]

Introduction

Eukaryotic cells have specialized mechanisms to reorganize cellular processes during environmental fluctuations. One mechanism is the formation of cytoplasmic RNA-protein assemblies, termed stress granules. Stress granules are non-membrane bound compartments in the cytoplasm, containing many RNA-binding proteins and translation initiation factors (1, 2). The formation of stress granules alter RNA metabolism and regulate gene expression (3). Stress granules are thought to be sites of repression that allow the cell to conserve energy by repressing the translation of “house-keeping” genes, while promoting the translation of molecular chaperones to aid in the stress response (4). Stress granules rapidly form under stress and dynamically exchange with its surroundings, but upon stress relief, they dissolve by disassembly or degradation (5, 6). Any perturbations in stress granule regulation may lead to aberrant stress granules. Aberrant stress granules have pathological consequences to the cells, highlighted by its prevalence in many neurodegenerative diseases (7, 8).

A number of studies have attempted to characterize the diversity of yeast proteins sequestered in stress granules (9–13). However, the protein composition in stress granules is dependent on the type of stress the cell is experiencing (2). While these studies highlight the diverse proteome associated with different types of stress granules, it remains undiscovered if recruitment to stress granules require specific protein sequence features.

[3] Kacy R Paul and Andrew Lamb (under my supervision) helped build GFP-PrLD fusions.

While the mechanism of stress granule assembly is still not understood, specific protein-RNA and protein-protein interactions appear to contribute. RNA-binding proteins are prevalent in stress granules. They contain RNA recognition motifs that bind RNA, an important interaction for the assembly of stress granules. Also, many of them contain prion-like domains, PrLDs (14). PrLDs are defined as regions within a protein with compositional similarity to yeast prion proteins (Alberti et al., 2009). Also, PrLDs are intrinsically disordered domains, providing structural flexibility for these domains to adopt several different conformational states, which can constantly rearrange (16). Altogether, the cell exploits PrLDs in stress granule assembly because they have the propensity to rapidly self-assemble into dynamic structures, providing metastable granules for controlled gene expression during stress.

PrLDs from known stress granule proteins have been shown to be sufficient for self-assembly *in vitro* (17, 18). Additionally, PrLDs appear to be necessary for stress granule formation *in vivo* (19). While there is strong evidence that PrLD interactions play an important role in stress granule assembly, it remains to be understood whether there are specific amino acid compositional requirements for a PrLD to participate in such interactions.

In this preliminary report, we evaluated several PrLDs ability to be recruited to heat-induced stress granules. Overall, we showed several PrLDs were recruited to stress granules, while a subset was not. By analyzing the amino acid composition of the PrLDs, we determined modest amino acid compositional biases. Interestingly, the PrLDs that were not sufficient to be recruited to stress granules correlated with amyloid propensity, suggesting there are distinct underlying mechanisms to limit amyloid-prone

PrLDs in stress granules. This preliminary study lays the foundation for interesting future experiments and contributes to our efforts to understand the complex nature of stress granule assembly.

Results and Discussion

PrLDs are sufficient to be recruited to stress granules

As mentioned above, several datasets have been published recently illustrating that stress granules contain a diverse proteome. One study investigated the proteins found in heat-induced stress granules (11). Using mass spectrometry, they identified about 170 proteins. Interestingly, we determined 19 of those proteins contained PrLDs based on prion prediction algorithms (15, 20, 21) (Table 4.1). To investigate if these PrLDs are sufficient to be recruited to stress granules, we N-terminally GFP tagged the PrLDs and expressed them from a weak constitutive promoter, *Sup35*. Upon heat shock at 46^{o}C, several PrLDs formed distinct puncta that colocalized with a known stress granule marker, Pab1 (Figure 4.1A, data not shown). Not all PrLDs identified from this study were sufficient to be recruited to stress granules (Figure 4.1B). These data support that PrLDs alone are sufficient for stress granule recruitment. For the PrLDs that failed to be recruited to stress granules, the full-length protein's recruitment to stress granules may be through other important interactions. For example, through its coordination with RNA or other protein factors that modulate stress granule assembly.

To approach the recruitment requirements from an alternative direction, we asked whether known aggregation-prone PrLDs, as a more general phenomenon, were sufficient to be recruited to stress granules. Moreover, are aggregation-prone PrLDs alone sufficient to be recruited to stress granules or do they require a stress granule

Table 4.1: Summary of Results

Protein	Amino Acid Range	PAPA score	Heat-Induced Foci	SDD-AGE (overexpressed)
Pub1	243-327	0.14	-	+
New1	1-118	0.14	-	+
Sup35	1-123	0.1	-	+
Ubp3	1-99	0.04	-	-
Ccr4	1-147	0.09	-/+	+
Myo2	417-497	0.04	+	-
Hrr25	395-494	NA	-	+[c]
Cdc39	966-1092	0.08	+	-
Mca1	1-104	0.06	-	+[c]
Nab3	559-802	0.05	-	+[c]
Ded1	1-97	0.05	+	-
Tif4631	1-131	0.03	-	+[c]
Prt1	193-273	0.01	+	-
Trm1	286-366	0.01	+	-
Npl3	276-414	0.01	-/+	-
Sro9	198-282	0.01	-	+[c]
Rsc8	232-312	0.01	+	-
Bem2	1800-1880	0.06	-/+[a]	-
Swi4	177-380	0.09	-	+
Rpi1	192-306	0.05	+	+[b]
Var1	191-349	0.20	-/+	+
Mfg1	1-96	0.07	-	-
Pam1	617-756	0.06	-	+
YML053C	34-148	0.05	-	+[b]
Dat1	102-236	0.09	-/+	+
Rna15	39-169	0.08	+	-
Slf1	183-311	0.11	-/+[a]	-
Sky1	353-491	0.12	+	+
Pin4	169-492	0.11	-	+
Gis1	454-584	0.08	-	+
Cln2	362-503	0.09	-/+	-
Fab1	427-552	0.06	-/+	+
Mex67	1-95	0.14	-	+
Tda7	513-636	0.10	-	-
YGL036W	270-478	0.15	-/+	-
Bph1	1113-1243	0.10	+	-
Q0255	341-472	0.07	NA	-

Ssn2	1025-1211	0.09	-/+	-
Al3	228-387	0.17	+	-
Lee1	151-301	0.12	-	-
Vac14	690-818	0.09	+	-
Cdc73	253-378	0.07	+	-
Mdm1	745-864	0.10	+	-
Pgs1	158-277	0.07	-/+[a]	-
Nte1	1-169	0.12	-	-
Cos111	336-465	0.10	+	-
Izh3	176-492	0.13	-/+	-
Dal81	4-168	-0.06	-/+	-
Hrk1[t]	483-647	-0.12	-	-
Yck2	369-533	-0.15	-	-
Grr1	3-167	-0.02	-/+	+
Apg13	250-414	-0.02	+	-
Siz1	390-554	-0.10	+	-
Crz1	15-179	-0.11	-	-
Vac7	377-541	-0.05	-	+
Tbs1	898-1062	-0.14	-/+	-
Vid22	641-806	-0.04	+	-

[a] No localization with Pab1
[b] SDS-insoluble aggregates forming after 48hr
[c] Low molecular weight aggregates

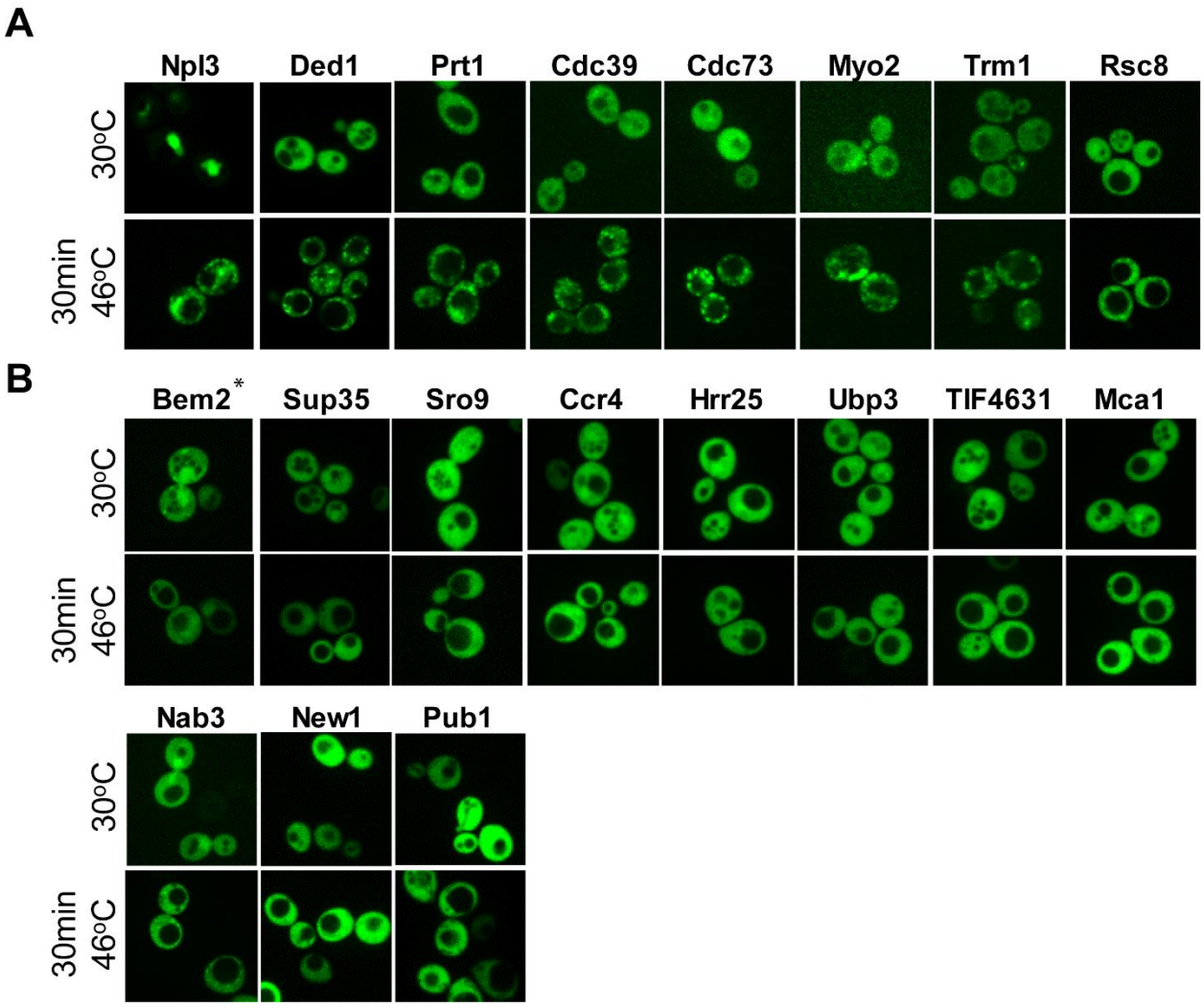

Figure 4.1: Heat-induced PrLDs are sufficiently recruited to stress granules
Yeast strain yER1405 (Pab1-mCherry) was transformed with plasmids expressing GFP-PrLD fusion under control of the *Sup35* promoter. Cells were grown to mid-log phase in glucose dropout media to mid-log phase and visualized by fluorescence microscopy during a heat shock time course. Representative images are shown for PrLDs sufficiently recruited to stress granules (A) and PrLDs not sufficiently recruited to stress granules (B). * represents PrLDs that aggregated during stress but did not co-localize with Pab1 (data not shown).

protein context? Therefore, we investigated 37 PrLDs from a recent proteome screen for PrLDs with prion-like activity (22). We visualized a subset of PrLDs sufficient to be recruited to stress granules, and a subset that were not sufficient (Figure 4.2A and B, respectively). These data suggest some PrLDs alone are sufficient to be recruited stress granules, however not in general. This raises the question what intrinsic properties do the subset of PrLDs sufficient to be recruited to stress granules, have in common?

Compositional Analysis of PrLDs

The amino acid composition of PrLDs found in proteins with prion-like activity is well-characterized (15, 20, 22–24). Briefly, yeast PrLDs contain long stretches of polar residues, specifically glutamine and asparagine residues, with hydrophobic amino acids interspersed to promote prion formation. However, stress granules are fundamentally different from yeast prions, mainly because the former are dynamic protein assemblies that are reversible, unlike the irreversible yeast prion amyloid structures. Therefore, one would assume the amino acid composition would likely differ to drive the formation of these different types of protein assemblies. To better understand the recruitment requirements of PrLDs to stress granules, we analyzed the amino acid composition. Overall, out of the 56 PrLDs tested we determined 18 PrLDs (+) were recruited to stress granules, 15 PrLDs had mixed phenotypes (-/+), classified by not co-localizing with Pab1 or less than 25% of cells formed stress granules, and 23 PrLDs had no localization to stress granules (-) (Table 4.1). Interestingly, the sufficient PrLDs had a significantly lower average percentage of Q/N residues versus the PrLDs that were not sufficient to be recruited to stress granules (Figure 4.3). Other notable differences

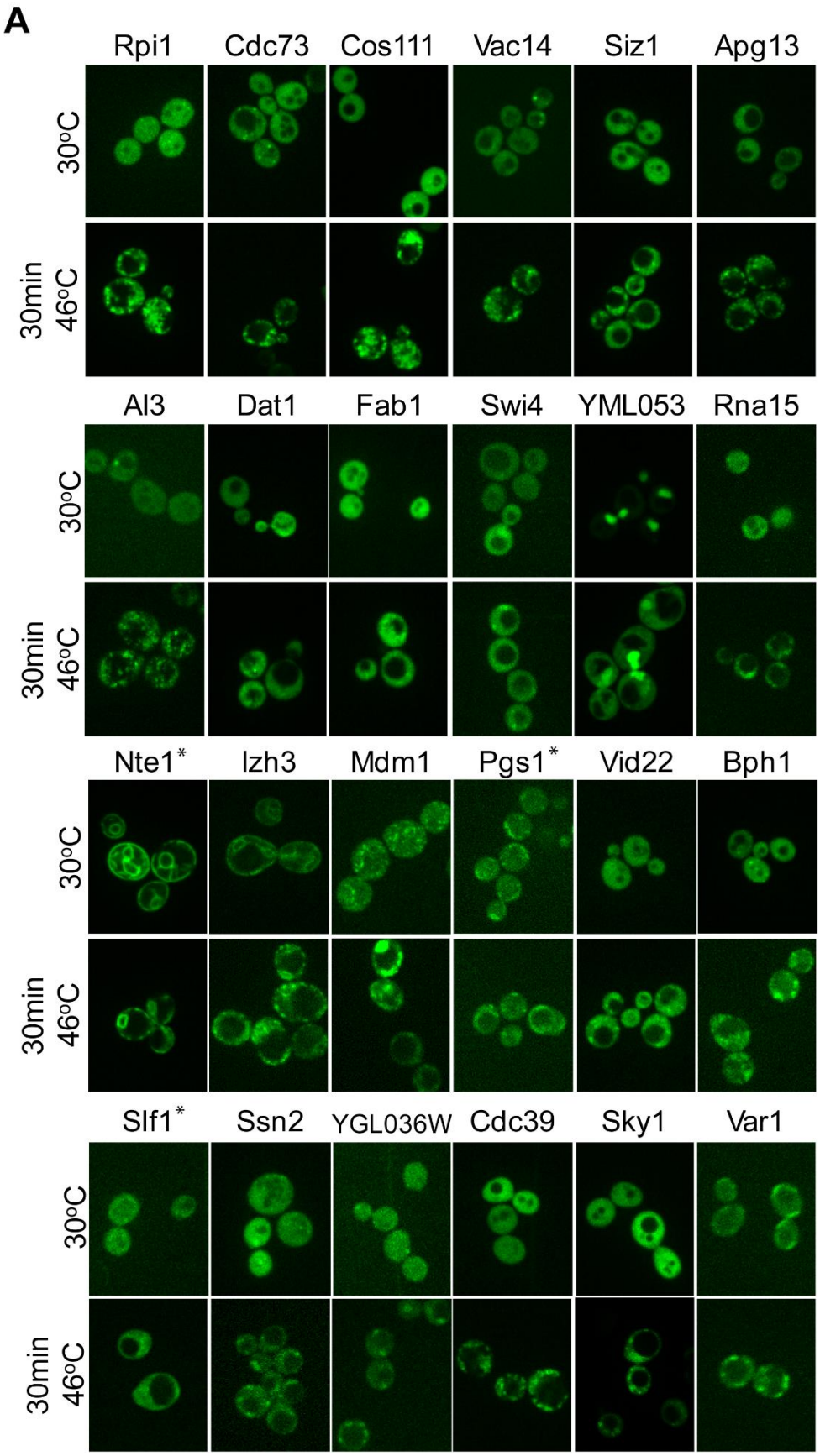
A
Rpi1
Cdc73
Cos111
Vac14
Siz1
Apg13
30°C
30min 46°C
Al3
Dat1
Fab1
Swi4
YML053
Rna15
30°C
30min 46°C
Nte1*
Izh3
Mdm1
Pgs1*
Vid22
Bph1
30°C
30min 46°C
Slf1*
Ssn2
YGL036W
Cdc39
Sky1
Var1
30°C
30min 46°C

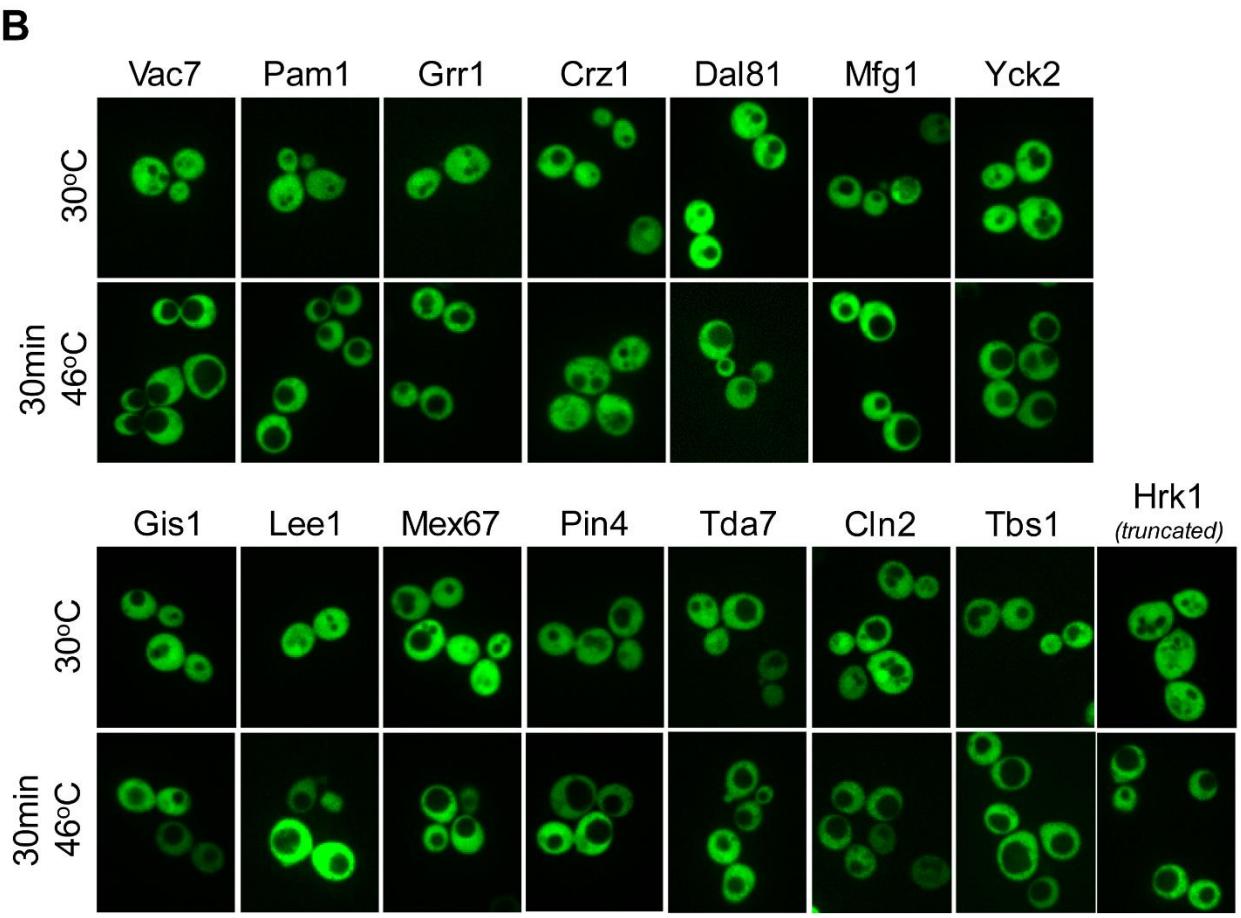

Figure 4.2: Aggregation prone PrLDs are sufficiently recruited to stress granules. Yeast strain yER1405 (Pab1-mCherry) was transformed with plasmids expressing GFP-PrLD fusion under control of the *Sup35* promoter. Cells were grown to mid-log phase in glucose dropout media to mid-log phase and visualized by fluorescence microscopy during a heat shock time course. (A) PrLDs sufficiently recruited to stress granules, (B) PrLDs not recruited to stress granules. Representative images are shown for PrLDs sufficiently recruited to stress granules. * represents PrLDs that aggregated during stress but did not co-localize with Pab1 (data not shown)

between the subset of PrLDs; the sufficient PrLDs had a higher median net charge; hydrophobic residues (FWY) tend to be more prevalent in sufficient PrLDs. These data support PrLDs found in stress granules are compositionally different than PrLDs found in yeast prion-like proteins. This is not surprising because stress granules utilize PrLDs for their conformational flexibility and not their propensity to form stable β-sheet rich structures. Furthermore, we previously showed Q/N residues promote the formation of SDS-insoluble aggregates (22), suggesting a reason why dynamic reversible aggregates may tend to have less Q/N content.

The propensity for PrLDs to form SDS-resistant assemblies does not correlate with stress granule recruitment

Mutations within PrLDs of known stress granule proteins have been shown to promote amyloid formation, leading to aberrant stress granules, and thereby causing pathological consequences (25, 26). To investigate the mechanisms underlying amyloid formation in stress granules, we investigated the PrLDs propensity to form SDS-insoluble aggregates, a hallmark of amyloid formation. We expressed PrLD-GFP fusions from a strong inducible promoter, *GAL1* and analyzed cell lysate using semi-denaturing detergent agarose gel electrophoresis, SDD-AGE (27). SDD-AGE is a technique that resolves amyloid-like formation from amorphous protein aggregation. In this report, we investigated only PrLDs identified in heat-induced aggregates, for the others have been characterized previously (22) (Table 4.1). Interestingly, the PrLDs that formed SDS-resistant aggregates mostly correlated with PrLDs that were not sufficient to be recruited to stress granules (Figure 4.4, see Table 4.1 for summary). These data support an interesting theory. It suggests that the ability for PrLDs to be recruited to

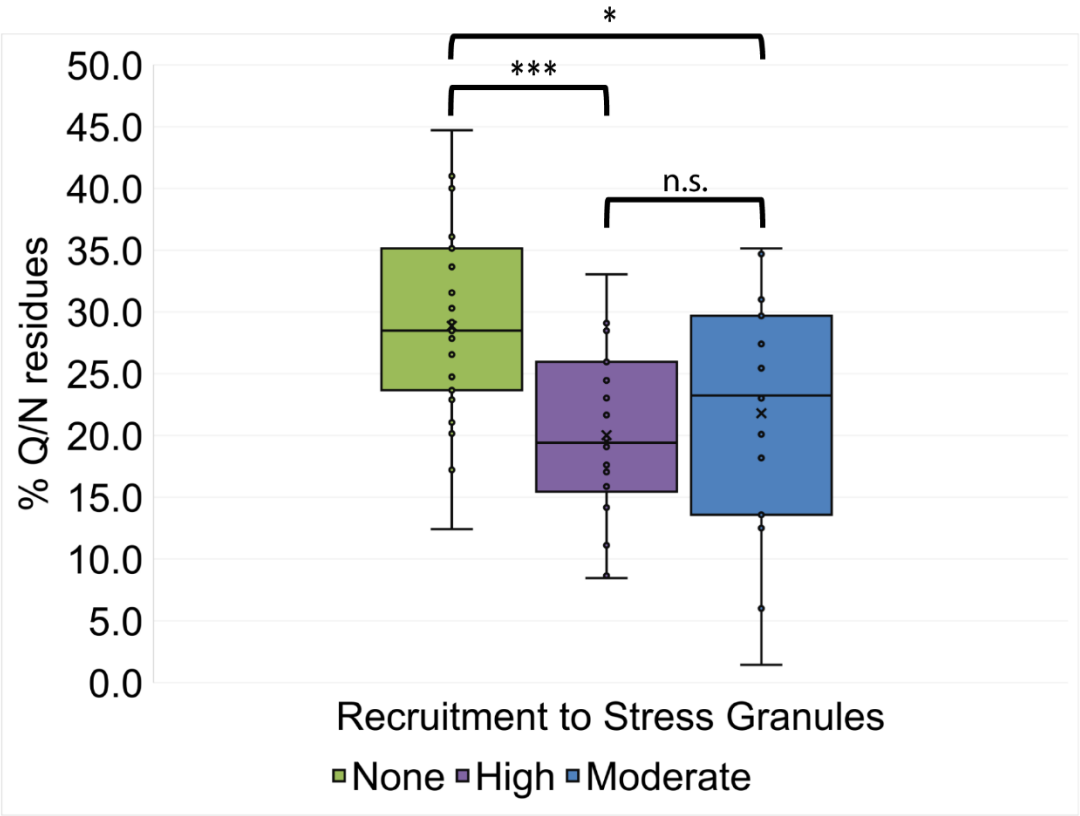

Figure 4.3: PrLDs enriched in Q/N residues are not recruited to stress granules. Median percentage of glutamine and asparagine residues within the PrLD was calculated. Data is represented as box and whisker plots. *, $P < 0.05$; ** $P < 0.01$; n.s., not significant (Mann-Whitney test).

stress granules is most likely through promiscuous amorphous interactions, and those that are not, may be more tightly regulated to limit the presence of amyloid formation within the stress granule, to maintain its dynamic nature.

Future Directions

The study described in this report provided a preliminary data set that lays the foundation for future experiments as we continue to unravel the complex assembly mechanism involved in stress granule formation. However, many outstanding questions still exist.

Are there compositional requirements for PrLDs to be recruited to stress granules?

The amino acid composition of PrLDs of known stress granule proteins have never been analyzed. We predicted that the amino acid composition of PrLDs of stress granule proteins would differ from the composition of PrLDs of prion-like proteins, because they are associated with fundamentally different protein assemblies. This hypothesis was supported here, showing there were moderate amino acid compositional biases (Figure 4.3). Interestingly, PrLDs not sufficient to be recruited to stress granules, were enriched in Q/N residues. To confirm these compositional biases, we will increase our dataset of heat-induced PrLDs. Also, we will utilize more sophisticated bioinformatic approaches to uncover other biases within these domains. Using these results, we will make mutations in non-sufficient PrLDs and determine if they can drive recruitment to stress granules and vice versa. These future studies will uncover the compositional requirements for stress granule assembly, which has never been investigated.

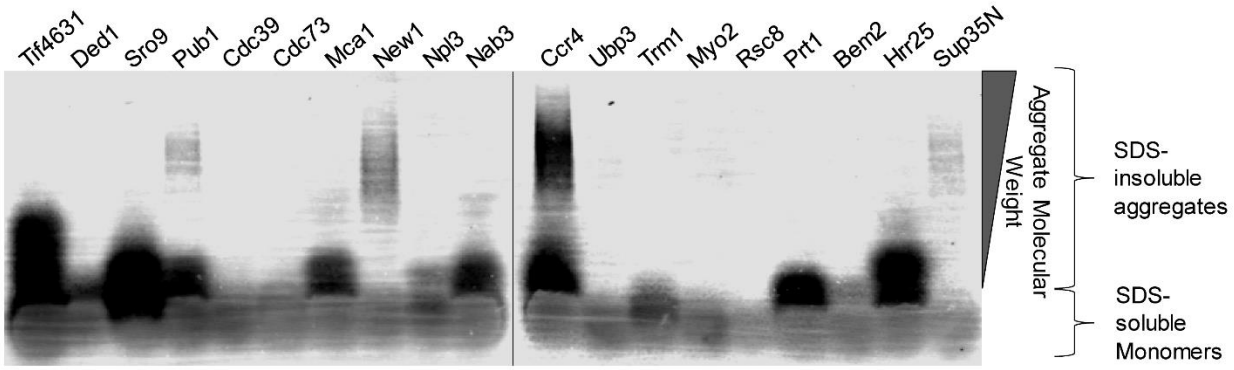

Figure 4.4: Non-sufficiently recruited PrLDs form SDS-insoluble aggregates. Yeast cells were transformed with plasmids expressing PrLD-GFP fusions under control of the GAL1 promoter. Cells were grown in galactose/raffinose dropout medium for 24 h, and then analyzed by SDD-AGE.

Is the recruitment to stress granules a regulated process?

These preliminary data showed some PrLDs are recruited to stress granules through promiscuous amorphous interactions. Moreover, the PrLDs not capable of forming SDS-insoluble aggregates *in vivo* were correlated with PrLDs that were recruited to stress granules. However, PrLDs with the propensity to form amyloid-like aggregates were not sufficient to be recruited to stress granules. These data suggest amyloid-prone PrLDs may be more tightly regulated, thereby limiting their recruitment to stress granules, and preventing the possibility of aberrant aggregation. To elucidate this, investigating the recruitment to stress granules proteins in the absence of stress granule assembly regulators may support this theory. Unfortunately, it remains unclear if there are cellular factors that actively regulate the assembly of stress granules.

Do different types of stress granules require different protein amino acid compositions for their recruitment to stress granules?

While the preliminary data was collected using heat as a cellular stress, it is unclear if PrLD recruitment is universal to all types of stress granules. Previous studies have demonstrated different types of stresses result in different proteins recruited to stress granules (2). Therefore, investigating the PrLDs recruitment under different stresses may uncover different amino acid composition requirements. These results will provide new insights into the stress-specific assembly mechanisms.

Overall, while there are several questions still unanswered, this preliminary study lays the foundation for future work to elucidate the mechanism underlying stress granule assembly. From this and future studies we hope to gain insight into the compositional

requirements of PrLDs recruitment to stress granules. Additionally, we will refine the fundamental differences between PrLDs involved in different protein assemblies.

Materials and Methods

Yeast Strains and Media

Standard yeast media and methods were used as previously described (28). In all experiments, yeast strains were grown at 30^{o}C.

A PCR-based homologous recombination protocol based on the methods of Longtine *et al.*1998 (29), to endogenously tag Pab1 with mCherry, Briefly, an mCherry-URA3 cassette was PCR amplified from pER1372 (kind gift from Dr. Steven Markus), adding regions of homology to allow for in-frame fusion of the mcherry tag with the target gene. These products were transformed into the parent strain from the GFP collection (30), selecting on SC-Ura. Genomic PCR and DNA sequencing were performed to confirm correct insertion.

Plasmid Construction

Prion-like domains were predicted by PAPA as previously described (22) or identified previously (Hrr25 and Ccr4 (15)). To generate the GFP-PrLD fusions, the PrLDs were amplified from the strain yER632/pJ533 (31), adding BamHI and XhoI/BglII restriction sites. PCR products were cut with BamHI and XhoI and cloned into pER842 to generate GFP-PrLDs fusions expressed from a strong inducible promoter, GAL1. PCR products were cut with BglII and BamHI and cloned into pER843 to generate GFP-PrLDs fusions expressed from a weak constitutive promoter, *Sup35* (Shattuck et al., 2018 in prep). All sequences were confirmed by DNA sequencing. Table 4.2 for plasmid numbers.

Microscopy

Foci formation assays were performed as previously described (Shattuck *et al.*, 2018, in preparation). Briefly, yeast strains yER1405 (endogenous Pab1-mCherry-URA3) were transformed with *LEU2* plasmids expressing each GFP-PrLD from the *Sup35* promoter. Strains were grown in glucose dropout medium lacking leucine to mid-log phase, and then imaged by confocal microscopy. To visualize heat-induced granules, cells were incubated in a water bath at 46^{o}C for 30 minutes prior to imaging.

Semi-Denaturing Detergent-Agarose Gel Electrophoresis (SDD-AGE)

For SDD-AGE, yER980 were transformed with *TRP1* plasmids expressing each GFP-PrLD from the *GAL1* promoter. Strains were grown for 24 hours in galactose/raffinose dropout medium lacking tryptophan. Cells were harvested and lysed as previously reported (22). The membrane was probed with an anti-GFP primary antibody (Santa Cruz), and Alexa Fluor IR800 goat anti-mouse secondary antibody (Rockland).

Table 4.2: List of Plasmids

Protein	Amino Acid Range	Plasmid # (*Sup35* Promoter)	Plasmid # (*GAL1* promoter)
Pub1	243-327	1612	1578
New1	1-118	1610	1582
Sup35	1-123	1636	1633
Ubp3	1-99	1585	1583
Ccr4	1-147	1855	1609
Myo2	417-497	1634	1629
Hrr25	395-494	1857	1632
Cdc39	966-1092	1604	1579
Mca1	1-104	1607	1581
Nab3 (Large)	559-802	1608	1616
Ded1	1-97	1584	1577
Tif4631	1-131	1603	1575
Prt1	193-273	1856	1631
Trm1	286-366	1639	1628
Npl3	276-414	1606	1587
Sro9	198-282	1575	1586
Rsc8	232-312	1658	1630
Bem2	1800-1880	1635	1638
Swi4	177-380	1838	(22)
Rpi1	192-307	1821	(22)
Var1	191-377	1885	(22)
Mfg1	1-96	1826	(22)
Pam1	617-757	1844	(22)
YML053C	34-148	1839	(22)
Dat1	102-237	1822	(22)
Rna15	39-169	1837	(22)
Slf1	183-311	1781	(22)
Sky1	353-492	1588	(22)
Pin4	169-492	1780	(22)
Gis1	454-585	1777	(22)
Cln2	362-504	1776	(22)
Fab1	427-552	1551	(22)
Mex67	1-95	1779	(22)
Tda7	513-649	1783	(22)
YGL036W	270-478	1784	(22)
Bph1	1113-1244	1775	(22)
Q0255	341-489	NA	(22)

Ssn2	1025-1211	1782	(22)
Al3	228-386	1845	(22)
Lee1	151-302	1778	(22)
Vac14	690-819	1550	(22)
Cdc73	253-379	1830	(22)
Mdm1	745-864	1834	(22)
Pgs1	158-273	1833	(22)
Nte1	1-169	1823	(22)
Cos111	336-465	1835	(22)
Izh3	175-492	1846	(22)
Dal81	4-169	1827	(22)
Hrk1[t]	483-648	1851	(22)
Yck2	369-534	1828	(22)
Grr1	3-168	1832	(22)
Apg13	250-415	1847	(22)
Siz1	390-555	1829	(22)
Crz1	15-180	1848	(22)
Vac7	377-542	1549	(22)
Tbs1	898-1063	1849	(22)
Vid22	641-806	1831	(22)

REFERENCES

1. Buchan JR, Parker R (2009) Eukaryotic stress granules: the ins and outs of translation. *Molecular cell* 36(6):932–41.
2. Buchan JR, Yoon J-H, Parker R (2011) Stress-specific composition, assembly and kinetics of stress granules in Saccharomyces cerevisiae. *Journal of cell science* 124(Pt 2):228–39.
3. Kedersha NL, Gupta M, Li W, Miller I, Anderson P (1999) RNA-binding proteins TIA-1 and TIAR link the phosphorylation of eIF-2 alpha to the assembly of mammalian stress granules. *The Journal of cell biology* 147(7):1431–42.
4. Anderson P, Kedersha N (2006) RNA granules. *The Journal of cell biology* 172(6):803–8.
5. Buchan JR, Kolaitis R-M, Taylor JP, Parker R (2013) Eukaryotic Stress Granules Are Cleared by Autophagy and Cdc48/VCP Function. *Cell* 153(7):1461–1474.
6. Protter DSW, Parker R (2016) Principles and Properties of Stress Granules. *Trends in Cell Biology* 26(9):668–679.
7. Ramaswami M, Taylor JP, Parker R (2013) Altered ribostasis: RNA-protein granules in degenerative disorders. *Cell* 154(4):727–36.
8. Maziuk B, Ballance HI, Wolozin B (2017) Dysregulation of RNA Binding Protein Aggregation in Neurodegenerative Disorders. *Frontiers in Molecular Neuroscience* 10:89.
9. Cary GA, Vinh DBN, May P, Kuestner R, Dudley AM (2015) Proteomic Analysis of Dhh1 Complexes Reveals a Role for Hsp40 Chaperone Ydj1 in Yeast P-Body Assembly. *G3: Genes|Genomes|Genetics* 5(11):2497–2511.
10. Jain S, et al. (2016) ATPase-Modulated Stress Granules Contain a Diverse Proteome and Substructure. *Cell* 164(3):487–98.
11. Wallace EWJ, et al. (2015) Reversible, Specific, Active Aggregates of Endogenous Proteins Assemble upon Heat Stress. *Cell* 162(6):1286–1298.
12. Cherkasov V, et al. (2015) Systemic control of protein synthesis through sequestration of translation and ribosome biogenesis factors during severe heat stress. *FEBS Letters* 589(23):3654–3664.
13. Narayanaswamy R, et al. (2009) Widespread reorganization of metabolic enzymes into reversible assemblies upon nutrient starvation. *Proceedings of the National Academy of Sciences* 106(25):10147–10152.
14. King OD, Gitler AD, Shorter J (2012) The tip of the iceberg: RNA-binding proteins with prion-like domains in neurodegenerative disease. *Brain Research* 1462:61–80.
15. Alberti S, Halfmann R, King O, Kapila A, Lindquist S (2009) A Systematic Survey Identifies Prions and Illuminates Sequence Features of Prionogenic Proteins. *Cell* 137(1):146–158.
16. Aguzzi A, Altmeyer M (2016) Phase Separation: Linking Cellular Compartmentalization to Disease. *Trends in cell biology* 26(7):547–558.
17. Riback JA, et al. (2017) Stress-Triggered Phase Separation Is an Adaptive, Evolutionarily Tuned Response. *Cell* 168(6):1028–1040.e19.

18. Patel A, et al. (2015) A Liquid-to-Solid Phase Transition of the ALS Protein FUS Accelerated by Disease Mutation. *Cell* 162(5):1066–1077.
19. Gilks N, et al. (2004) Stress granule assembly is mediated by prion-like aggregation of TIA-1. *Molecular biology of the cell* 15(12):5383–98.
20. Toombs JA, McCarty BR, Ross ED (2010) Compositional determinants of prion formation in yeast. *Molecular and cellular biology* 30(1):319–32.
21. Lancaster AK, Nutter-Upham A, Lindquist S, King OD (2014) PLAAC: a web and command-line application to identify proteins with prion-like amino acid composition. *Bioinformatics (Oxford, England)* 30(17):2501–2.
22. Shattuck JE, Waechter AC, Ross ED (2017) The effects of glutamine/asparagine content on aggregation and heterologous prion induction by yeast prion-like domains. *Prion* 11(4):249–264.
23. Michelitsch MD, Weissman JS (2000) A census of glutamine/asparagine-rich regions: implications for their conserved function and the prediction of novel prions. *Proceedings of the National Academy of Sciences of the United States of America* 97(22):11910–5.
24. Halfmann R, et al. (2011) Opposing Effects of Glutamine and Asparagine Govern Prion Formation by Intrinsically Disordered Proteins. *Molecular Cell* 43(1):72–84.
25. Kim HJ, et al. (2013) Mutations in prion-like domains in hnRNPA2B1 and hnRNPA1 cause multisystem proteinopathy and ALS. *Nature* 495(7442):467–73.
26. Murakami T, et al. (2015) ALS/FTD Mutation-Induced Phase Transition of FUS Liquid Droplets and Reversible Hydrogels into Irreversible Hydrogels Impairs RNP Granule Function. *Neuron* 88(4):678–90.
27. Halfmann R, Lindquist S (2008) Screening for amyloid aggregation by Semi-Denaturing Detergent-Agarose Gel Electrophoresis. *Journal of visualized experiments : JoVE* (17). doi:10.3791/838.
28. Sherman F (1991) Getting started with yeast. *Methods in enzymology* 194:3–21.
29. Longtine MS, et al. (1998) Additional modules for versatile and economical PCR-based gene deletion and modification in Saccharomyces cerevisiae. *Yeast* 14(10):953–961.
30. Huh W-K, et al. (2003) Global analysis of protein localization in budding yeast. *Nature* 425(6959):686–691.
31. Gonzalez Nelson AC, et al. (2014) Increasing prion propensity by hydrophobic insertion. *PloS one* 9(2):e89286.
32. Paul KR, Hendrich CG, Waechter A, Harman MR, Ross ED (2015) Generating new prions by targeted mutation or segment duplication. *Proceedings of the National Academy of Sciences of the United States of America* 112(28):8584–9.

CHAPTER 5: ALTERING THE AGGREGATION PROPENSITY OF FAB1'S PRION-LIKE DOMAIN CHANGES THE PHENOTYPIC RESPONSE TO OSMOTIC STRESS[4]

Introduction

Compartmentalization in eukaryotic cells is essential for the organization of cellular components and facilitation of cellular regulation. One intracellular compartment in *Saccharomyces cerevisiae* that is critical for cellular homeostasis is the vacuole. The yeast vacuole plays many roles including being the main storage compartment and site of macromolecule turnover. In addition, the vacuole regulates pH and osmolarity (1, 2). Moreover, when the cell encounters an environmental stress, the dynamic yeast vacuole rapidly changes its morphology (size, shape and number); these changes are critical for cellular adaptation and survival.

Cell growth and membrane trafficking are some cellular processes that are regulated primarily through the production of phosphoinositides (3). Specifically, regulated synthesis and turnover of phosphatidylinositol 3,5 bisphosphate (PtdIns(3,5)P_2) underlies many aspects of vacuole-related functions (2). The synthesis of PtdIns(3,5)P_2 is required for proper acidification of the vacuole as well as membrane protein sorting into the lumen of the vacuole (4, 5). While PtdIns(3,5)P_2 concentration is low during steady-state conditions, its synthesis increases when the cell undergoes hyperosmotic stress (6).

The production of PtdIns(3,5)P_2 requires several cellular components. Vps34, a protein kinase that produces the required phosphoinositol precursor, PtdIns(3)P for

[4] This chapter is adapted from a manuscript in preparation for publication. Aubrey C Waechter built mPrLD-GFP fusions under my supervision.

PtdIns(3,5)P_2 (7). Fab1 is the sole PtdIns(3)P-5-kinase responsible for production of PtdIns(3,5)P_2; and its deletion eliminates PtdIns(3,5)P_2 production and results in severe defects in cell viability (5). Additionally, there are several proteins that modulate Fab1's kinase activity. The cellular factors involved in regulating Fab1's activity include the positive regulators Vac14 and Vac7, and the negative regulators Fig4 and Atg18; all of these proteins are required for proper production of PtdIns(3,5)P_2 (8). In addition, Ivy1 inhibits Fab1 activity (9). Ivy1 directly binds PtdIns(3,5)P_2, and interacts with Fab1 kinase; therefore, proper separation of these proteins must occur for Fab1 activation. Many studies have investigated and confirmed direct interactions between Fab1 and its effectors (10–14), suggesting a multiprotein complex is required for proper Fab1 recruitment, activation and function. However, the mechanism of how these proteins are recruited to the vacuole membrane and transduce the signal to regulate the production of PtdIns(3,5)P_2 is still unclear.

Interestingly, PtdIns(3,5)P_2 is present in low concentrations and increases nearly 20-fold, reaching levels similar to other phosphoinositides, during hyperosmotic stress. The dramatic rise occurs within minutes, and by 60 minutes after the onset of hyperosmotic stress, the concentration returns to basal levels (6). This large and rapid change in levels suggest the dramatic change in PtdIns(3,5)P_2 may signal a protective response.

Recently, a number of reversible protein assemblies, including stress granules, have been shown to form by a process of liquid-liquid phase separation of RNA-binding proteins into stress granules (15–17). Stress granules are non-membraneous compartments that form in the cytoplasm as a response to stress. Many stress granules

proteins contain prion-like domains, defined as protein segments with compositional similarity to yeast prion domains. While there is strong evidence suggesting prion-like domains play an important role in the formation of stress granules, the mechanism is not well understood (15). Studies have indicated that prion-like domains provide a stress-sensor for the cell to utilize for cellular adaptation to stress (18, 19) Intriguingly, Fab1 and its positive effectors (Vac7 and Vac14) contain PrLDs that we previously showed to be aggregation prone (20). Therefore, we hypothesized that during hyperosmotic stress Fab1 and its complex components may aggregate via its PrLDs to activate and produce PtdIns(3,5)P_2. This aggregation could act as an osmolarity-sensor to transduce the signal for a cellular response to stress.

Here, we use rational aggregation-altering mutations to further characterize the role of Fab1's PrLD in response to osmotic stress. As predicted, these mutations altered Fab1 aggregation propensity *in vivo* and *in vitro*. Furthermore, these rational mutations affected Fab1's ability to remodel the vacuole during osmotic stress. Additionally, overexpression of the PrLDs from Fab1's complex partners is sufficient to fragment the vacuole, suggesting that PrLD interactions are critical for this process. These results propose a possible mode of action underlying the previously unclear mechanism of Fab1's activation to remodel the vacuole during osmotic stress. Overall, Fab1's activation requires its aggregation prone PrLD for recruitment and efficient activation for the cell to adapt to cellular stresses.

Results

PAPA accurately predicts aggregation propensity of Fab1's prion-like domain in vivo

Previously, we developed a prion prediction algorithm, PAPA, that uses the amino acid composition of a protein to predict the aggregation propensity of PrLDs. Recently, we used PAPA to investigate the yeast proteome for proteins that have prion-like activity (20). From this screen we identified that Fab1 contains a PrLD. Interestingly, when Fab1's PrLD is overexpressed the protein aggregates in the cytoplasm and forms SDS-insoluble aggregates. This led us to further investigate the amino acid compositional requirements for this aggregation activity.

We used PAPA to alter the aggregation propensity of Fab1's PrLD. Initially, we tested two segments of Fab1 for prion-like activity: the previously characterized oPrLD (aa427-552) and a larger segment rPrLD (aa427-606). When expressed as GFP fusions, both PrLDs formed aggregates in the cytoplasm, visualized by distinct puncta or lines (Figure 5.1A). To dial aggregation propensity up and down, we used PAPA to design mutant versions of Fab1's PrLD (mPrLD). We replaced predicted aggregation-promoting residues with proline residues (Proline PrLD), positively charged residues (K/R PrLD) or negatively charged residues (D/E PrLD). We visualized mPrLD-GFP chimeras to determine they showed diminished ability to form aggregates in the cytoplasm. Indeed, all three non-aggregation prone PrLDs showed diffuse cytoplasmic signal, suggesting these mutations eliminated the interactions required for self-assembly. In addition, we created a mutant PrLD that was predicted to be more aggregation prone than wild type by PAPA (aggPos PrLD). Consistent with our predictions, when we replaced non-aggregation prone amino acids with aggregation

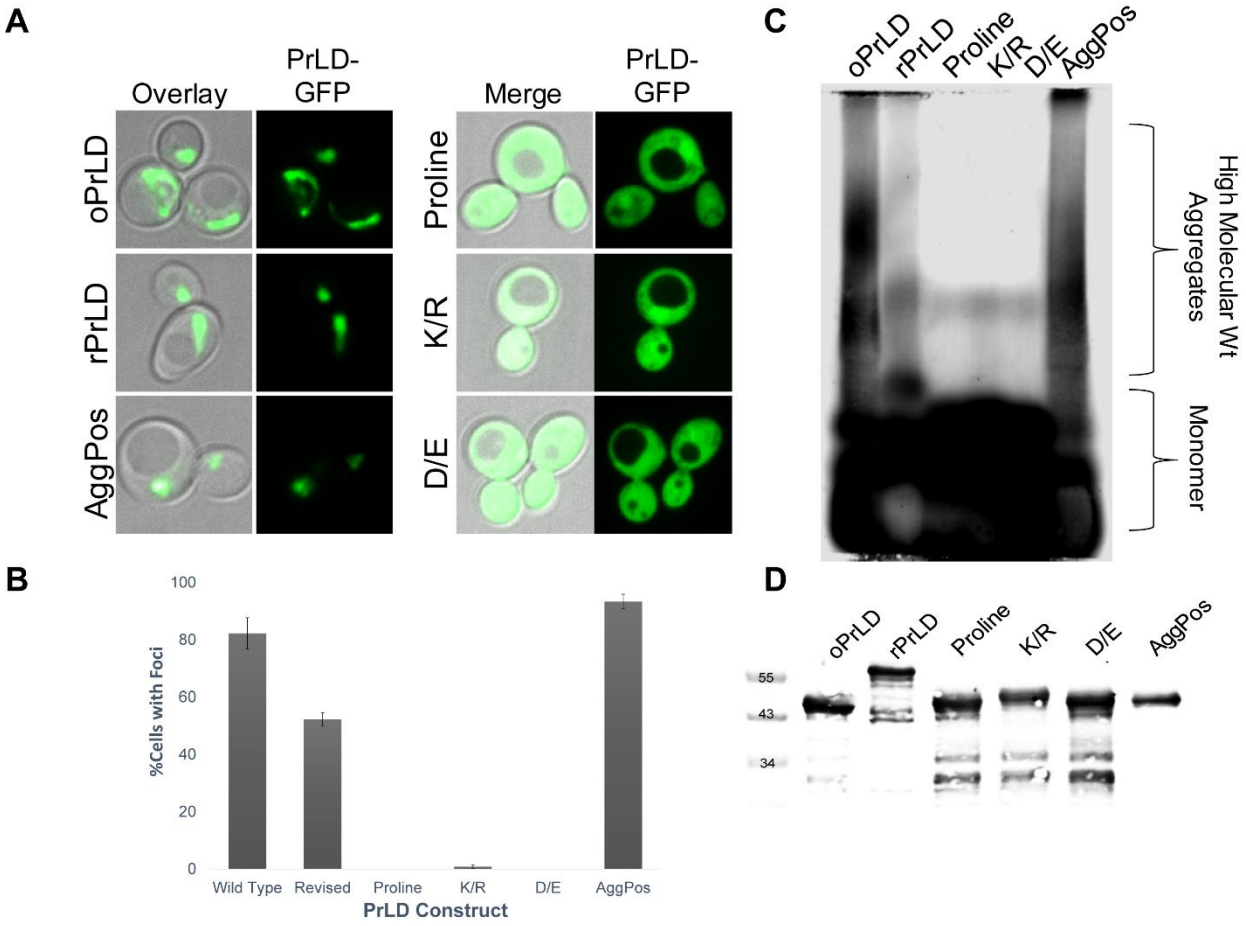

Figure 5.1: PAPA accurately predicts aggregation propensity of Fab1's prion-like domain in vivo.
Yeast cells were transformed with plasmids expressing PrLD-GFP fusions under control of the *GAL1* promoter. Cells were grown in galactose/raffinose dropout medium for 24h, and then (A) visualized by fluorescence microscopy and differential interference contrast (DIC). Representative images are shown from three independent experiments and (B) percentage of cells with foci for each mutant was calculated and represented as mean ± SEM. (C) analyzed by SDD-AGE, and (D) analyzed by western blot.

prone amino acids, the mutant formed distinct puncta formation in the cytoplasm in a higher percentage of cells than the wild-type PrLD (Figure 5.1A,B).

Proteins can form amorphous or ordered amyloid-like aggregates, which can be resolved using an assay called semi-denaturing agarose gel electrophoresis (SDD-AGE) (21). SDD-AGE exploits the properties of amyloid-like aggregates, which are resistant to SDS when treated at room temperature. Therefore, we investigated Fab1 mPrLD for SDS-insoluble aggregates. Consistent with our microscopy data, aggregation prone PrLDs (oPrLD, rPrLD and aggPos PrLD) all formed high molecular weight aggregates, while all non-aggregation prone PrLDs (Proline, K/R, D/E PrLDs) were visualized as monomers on the gel (Figure 5.1C). The observed differences between the mutants were not due to altered protein expression (Figure 5.1D). Altogether, these data suggest the aggregation of Fab1's PrLD requires aggregation-promoting residues as predicted by PAPA.

PAPA predicts amyloid formation of Fab1's prion-like domains in vitro

Thioflavin-T (ThT) dye shows increased fluorescence upon binding to amyloid and amyloid-like protein aggregates (22, 23). Therefore, we bacterial-expressed and purified Fab1 PrLDs, and then used ThT to monitor amyloid formation. Consistent with amyloid formation, oPrLD showed an increase in fluorescence (Figure 5.2). By contrast, SNAP-Proline PrLD, SNAP-K/R PrLD and SNAP-D/E PrLD, showed little increase in ThT signal. Interestingly, the aggPos PrLD showed substantially higher ThT signal than the wild type PrLD. While these results are consistent with decreased amyloid formation for the aggregation-inhibiting mutations, it is not clear whether absolute ThT fluorescence intensity is an accurate reporter of the degree of amyloid formation among

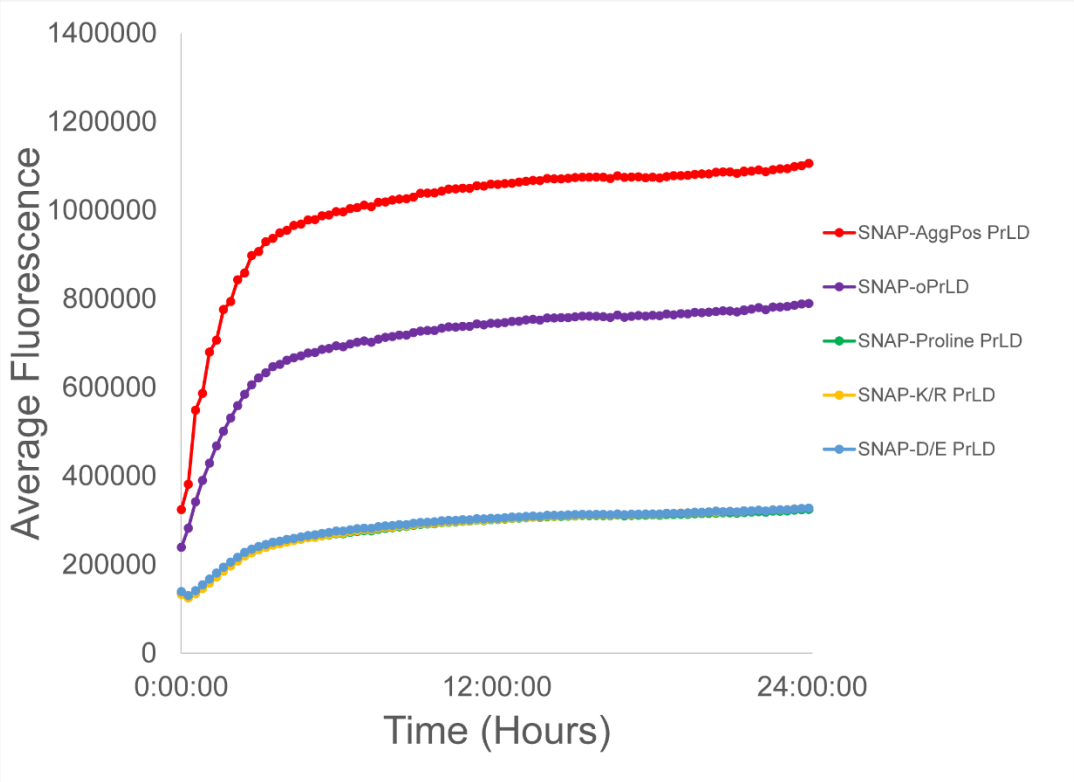

Figure 5.2: PAPA accurately predicts amyloid formation of Fab1 PrLDs in vitro. Aggregation of Fab1 PrLD and mutant PrLDs was monitored by Thioflavin-T fluorescence. Bacterially expressed and purified PrLDs were diluted into ThT reaction assembly buffers and incubated with intermittent shaking for 24 hours. Fluorescence readings were taken approximately every 90 minutes. Data represents the average fluorescence of two independent samples.

different mutants. To further resolve the properties of amyloid aggregates, we will use TEM to visual the aggregates after the assembly reaction is complete.

Recent studies suggest that amyloid-like protein assemblies, such as stress granules, form by a process referred to as liquid-liquid phase separation (LLPS) (24). This process is driven primarily by weak non-covalent interactions made between proteins (PrLDS), which accumulate and lead to concentration into a separate phase within the cytoplasm (25). This creates a microenvironment, like oil in water, where the protein concentration is high, thereby promoting interactions between these proteins. In addition, *in vitro* LLPS experiments have shown that cellular components exhibit dynamic kinetics that allow for rapid exchange of protein components within the environment (26, 27). Therefore, we will investigate LLPS properties of Fab1 PrLD and mutants. Also, we will determine if Fab1 and its complex proteins' PrLDs induce LLPS, as understanding the proteins involved in this process would provide insights into complex formation *in vivo*.

PrLDs are sufficient to aggregate upon osmotic stress

As a lipid kinase, Fab1 is a key regulator of the production of PtdIns(3,5)P_2 and vacuole fragmentation during hyperosmotic stress. However, Fab1 requires other protein effectors for proper production of PtdIns(3,5)P_2 including Vac7, Vac14 and Fig4 (reviewed by (8)). The results above, suggest Fab1 may utilize its PrLD for efficient recruitment to the vacuole and proper activation. Interestingly, Fab1's effectors also contain PrLDs, as predicted by PAPA. Vac7 and Vac14 have been previously characterized and both have prion-like activity (20). While Fig4 has not been previously characterized for prion-like activity, PAPA predicts Fig4 has a PrLD; therefore, we

investigated its aggregation propensity in this study. We determined if the PrLDs of Fab1 and its complex partners were sufficient to aggregate under hyperosmotic stress *in vivo.* GFP-PrLDs chimeras were expressed under a weak constitutive promoter, *Sup35*, and the cells were subjected to hyperosmotic stress (0.9M NaCl). Intriguingly, the PrLDs that are predicted to be aggregation prone (Fab1, Vac14 and Fig4 (poor expression, data not shown) formed aggregates in the cytoplasm upon hyperosmotic stress (Figure 5.3). While Vac7 was previously shown to form SDS-resistant aggregates when overexpressed, the PrLD is not predicted to be aggregation prone. The PrLD was not sufficient to aggregate after exposure to hyperosmotic stress conditions (Figure 5.3). These data suggest that some of these proteins may utilize their PrLDs for rapid aggregation and recruitment to the vacuole under hyperosmotic stress, possibly acting as an osmolarity-sensor.

Overexpressing mutant prion-like domains alters vacuole morphology

When cells are exposed to hyperosmotic stress, the vacuole fragments to adapt to the change in osmolarity in the vacuole. Again the key regulator of this process is Fab1 and its production of PtdIns(3,5)P_2. Previous studies have shown that the overexpression of Fab1's complex partners (Vac7, Vac14 and Fig4) results in fragmented vacuoles without cellular exposure of hyperosmotic stress, suggesting increased activity of Fab1 (5, 28). Therefore, we investigated if overexpression of the PrLDs alone was sufficient to fragment the vacuoles. PrLD-GFP chimeras were expressed from an inducible strong promoter, *GAL1*, in a yeast strain with Vph1-mCherry to visualize vacuoles. Fascinatingly, the aggregation prone PrLDs (Vac14, Fig4, Fab1), had more fragmented vacuoles than when we overexpressed GFP alone

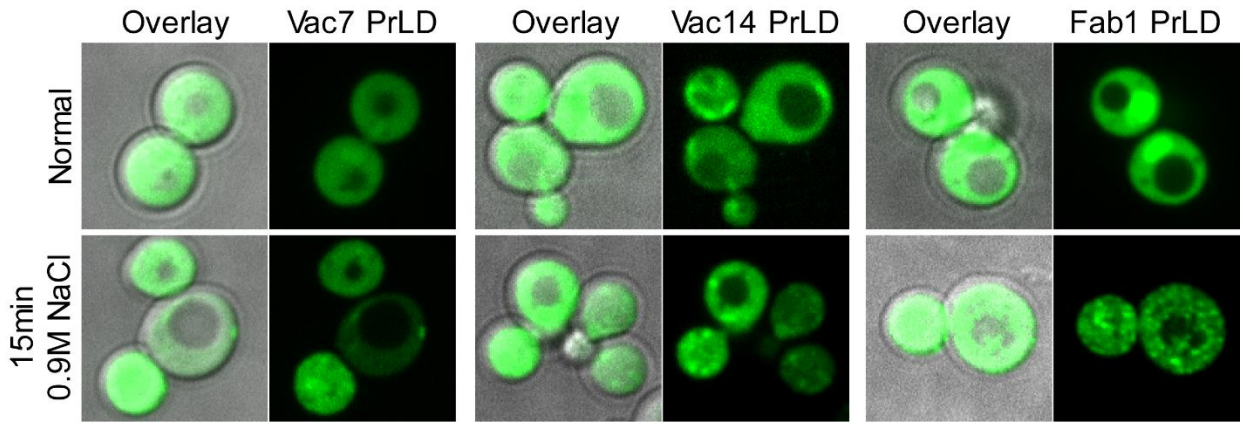

Figure 5.3: Fab1 and its known complex partners PrLDs are sufficient to aggregate upon osmotic stress.
Yeast cells were transformed with plasmids expressing GFP-PrLD fusions under control of the *Sup35* promoter. Cells were grown in glucose dropout medium to mid-log phase, and then visualized by fluorescence microscopy and differential interference contrast (DIC) during normal conditions and after 15min of 0.9M NaCl. Representative images are shown.

(Figure 5.4). These data suggest the activation of Fab1's kinase activity may be dependent on a prion-like mechanism.

Next, we investigated if the aggregation propensity of Fab1's PrLD affects vacuole fragmentation. Overexpression the non-aggregation prone PrLDs, we visualized no vacuole fragmentation, suggesting these mutants have a decreased propensity to aggregate and transduce the activation signal for Fab1. Intriguingly, the overexpression of full-length Fab1 does not lead to fragmented vacuoles (5); however, we visualized fragmented vacuoles when the aggregation prone PrLDs were overexpressed, suggesting Fab1's PrLD may serve as a scaffold to recruit other components of the complex, thereby, transducing a signal for Fab1's activation. Overall, these data suggest vacuole fragmentation can be induced by overexpressing the PrLDs of Fab1 and its complex partners alone and alterations in Fab1's PrLD aggregation propensity affects its ability to induce vacuole fragmentation.

Alterations in Fab1's aggregation propensity affects vacuole adaptation to osmotic stress

We investigated if Fab1 and its complex partner's PrLDs, expressed endogenously, play a role in vacuole fragmentation upon hyperosmotic stress. We observed vacuole morphology in a wild type strain and a strain with Fab1 deleted (ΔFab1) to determine vacuole morphology under normal and defective conditions. We visualized vacuole morphology at two different time points by staining the vacuole with FM4-64 as previously described (29). In a wild type strain, we visualized the vacuole as a single or double lobe (Figure 5.5B). On the other hand, in a ΔFab1 strain the vacuoles are grossly enlarged. After 5 minutes of hyperosmotic stress (0.9M NaCl), PtdIns(3,5)P_2

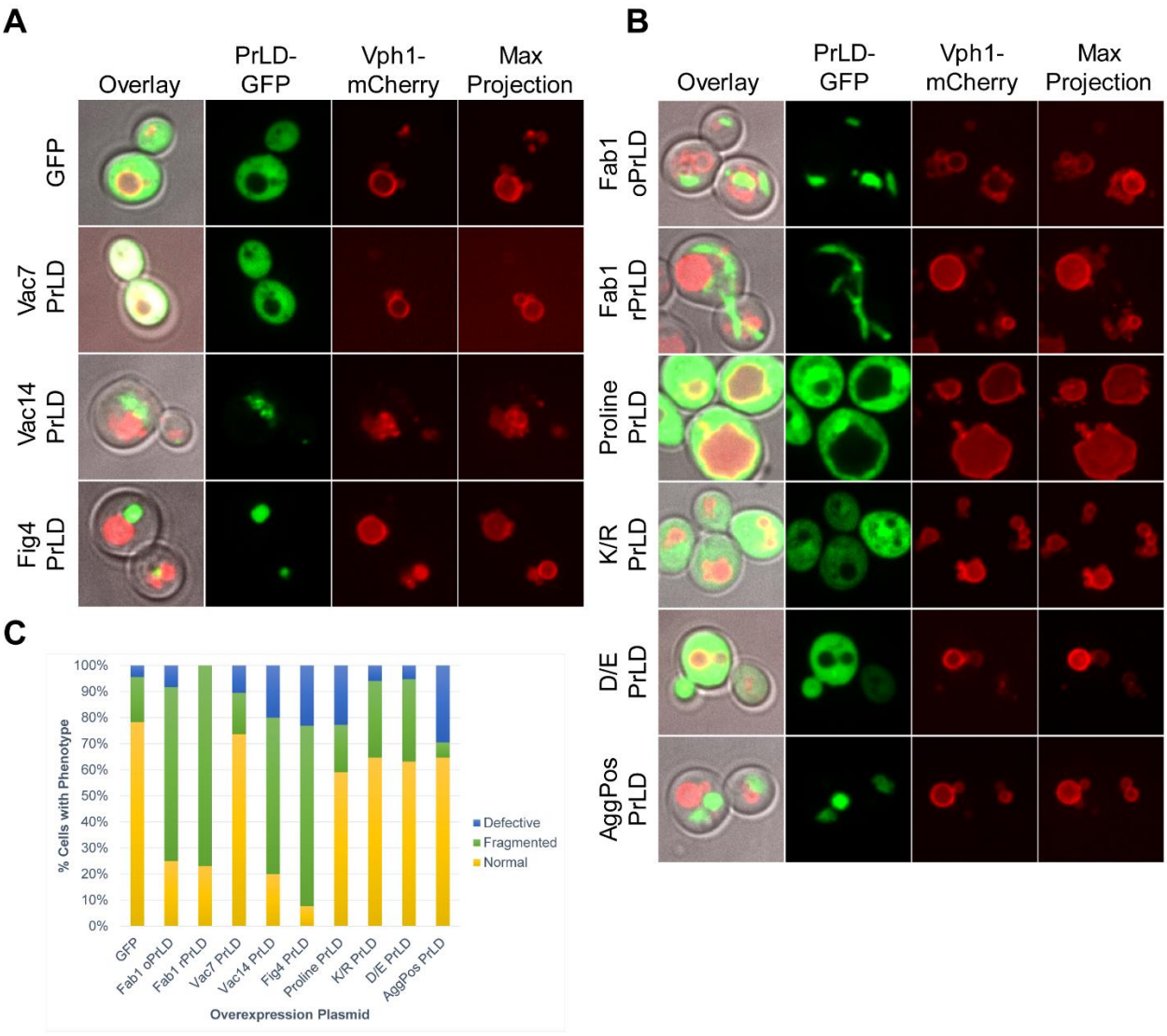

Figure 5.4: Overexpressing PrLDs alter vacuole morphology.
A yeast strain with Vph1 endogenously tagged with mCherry (yER1919) was transformed with plasmids expressing PrLD-GFP fusions under control of the *GAL1* promoter. Cells were grown in galactose/raffinose dropout medium for 24 h, and then (A) visualized by fluorescence microscopy and differential interference contrast (DIC). Representative images are shown and (B) percentage of cells with normal vacuoles (single/double lobed), defective (enlarged), and fragmented (>3 vacuoles) were calculated.

levels are the highest (6), wild type vacuoles fragment successfully, while in the ΔFab1 strain the vacuoles were visualized as enlarged and attempting to fragment, visualized by invaginations and blebbing of the vacuole membrane (Figure 5.5B). These data confirm that our staining protocol and strain background are consistent with previous studies.

The absence of Fab1 or any of its complex partners results in defective vacuole fragmentation upon osmotic stress (5, 10, 28, 30). Therefore, we investigated the role of Fab1's PrLD plays in vacuole fragmentation by endogenously deleting the PrLD from Fab1 and visualizing vacuole morphology. At steady-state conditions, we observed defects in vacuole morphology, suggesting PrLDs are required for normal vacuole morphology (Figure 5.5B). Intriguingly, after 5 minutes of hyperosmotic stress, we observed abnormal vacuole fragmentation, i.e. vacuole blebbing and enlarged vacuoles, suggesting a loss of protein-protein interactions.

Deleting a portion of Fab1 may affect its recruitment and/or function apart from eliminating protein-protein interactions. Therefore, to decipher these effects, we replaced the wild type PrLD with the mutant PrLDs characterized above (Figure 5.1). We replaced the endogenous PrLD with non-aggregation prone PrLD (Proline, K/R, and D/E PrLD). When all three mutants were expressed under steady-state conditions, we visualized similar results, i.e. slightly enlarged single lobed vacuoles (Figure 5.5B). However, upon hyperosmotic stress there were slight differences between mutants. The proline PrLD fragmented the vacuoles, albeit not as often as wild type, while the K/R and D/E PrLDs were defective in vacuole fragmentation. Next, we replaced Fab1's endogenous PrLD with an aggregation prone Fab1 domain, aggPos PrLD, and with

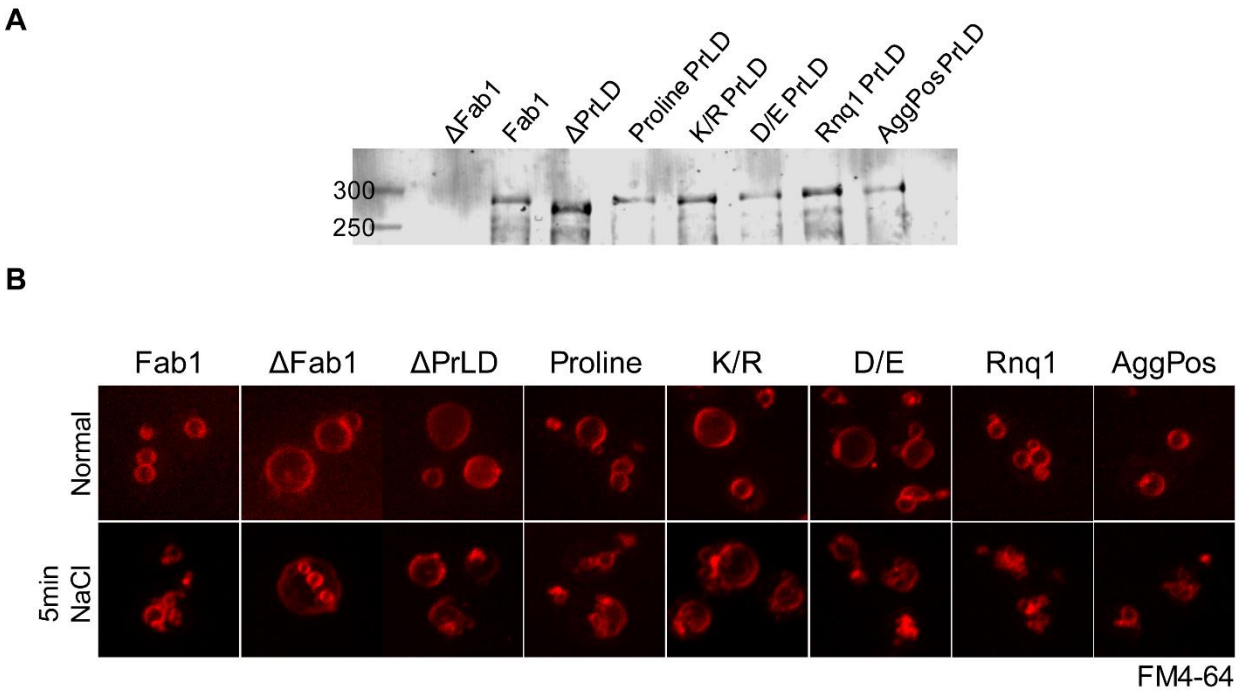

Figure 5.5: Alterations in Fab1's aggregation propensity affects vacuole adaptation to hyperosmotic stress.
Yeast strains, containing endogenous Fab1 PrLD mutants, were grown to mid log phase and (A) analyzed by western blot and (B) labeled with FM4-64 dye to visualize vacuole volume and number of vacuole lobes under steady-state conditions and after 5 minutes of hyperosmotic stress (0.9M NaCl).

known prion-forming domain, Rnq1 PFD (31). Under steady-state conditions, the expression of both mutants resulted in vacuole morphology similar to wild type in which the vacuoles were visualized as single and double lobed. As one would predict, upon 5 minutes of hyperosmotic stress, vacuoles fragmented normally (Figure 5.5B). The observed results were not due to altered protein expression for all mutants were expressed at similar levels (Figure 5.5A)

Altogether, these data contribute to an interesting conclusion. The aggregation of Fab1's PrLD is critical for proper recruitment, activation and production of PtdIns(3,5)P_2. Specific point mutations in the PrLD that decreased its aggregation propensity resulted defective adaptation to hyperosmotic stress, while mutations that increased Fab1's PrLD aggregation propensity had no defect. Furthermore, proper activation of Fab1 is likely explained by a prion-like mechanism because we were able to replace Fab1's PrLD with a known PFD and proper vacuole fragmentation was achieved. This phenomenon has been shown for other prion-like mechanisms in biology (32, 33).

Discussion

Within the yeast proteome there are several proteins that contain PrLDs, as predicted by our previously characterized algorithm, PAPA, and other prion prediction algorithms (20, 34, 35). This begs the question why do so many proteins contain these compositionally restricted domains if they do not serve a purpose in yeast biology? In this report, we set out to characterize the aggregation propensity of Fab1, and we propose protein aggregation as a mechanism for efficient recruitment and activation of a vacuole-signaling complex.

Using our previously described prion prediction algorithm, PAPA, we identified the proteins found in a vacuole-signaling complex to contain PrLDs (20, 36, 37). PAPA was previously developed by experimentally determining the amino acid composition that promoted prion formation. PAPA successfully predicted known prion proteins and proteins with prion-like activity (37). Additionally, PAPA was utilized to identify disease-associated mutations in RNA-binding proteins (38); rationally mutate yeast proteins to dial prion propensity up and down (39); and identify several new yeast proteins with prion-like activity, including Fab1 (20). Additionally, in this report we successfully used PAPA to make rational changes to Fab1's PrLD that either eliminated or increased its aggregation propensity in a predictive manner both *in vivo* and *in vitro*. Therefore, PAPA has proven to be a useful tool to identify and characterize proteins with aggregation propensity, and we now extend the use of PAPA for predicting proteins involved in reversible protein assemblies.

There are several examples of how cells exploit prion-like mechanisms to regulate reversible protein assemblies that play a role in cellular regulation. For example, in mammalian cells, a segment of a melanosome protein, Pmel17 forms amyloid fibers in order for proper melanin production (40). Yeast also have several examples of amyloid-formation that serves a beneficial role in the cell. Among these is a RNA-binding protein, Rim4, which forms amyloid-like aggregates that regulate gametogenesis (16, 41). Also, the amyloid-like aggregation of Whi3, an RNA-Binding protein, which allows the cell to permanently escape pheromone-induced cell cycle arrest (17). Similarly, stress granules are membrane-less compartments, which are involved in regulating cellular function during stress conditions. Most stress granules

proteins contain prion-like domains that rapidly assemble into highly dynamic and reversible aggregates in the cytoplasm (reviewed by (15)).

The cell exploits prion-like domains for several reasons. PrLDs have the propensity to form reversible amyloid-like structures, primarily through several weak non-covalent interactions between PrLDs. These interactions initiate an increase in local protein concentration of the prion-like proteins that recruits other proteins to sites of interest based on environmental cues like stress, changing salt or ion concentration, etc. The resulting protein assemblies play a role in cellular protection; Rim4 is sequestered so the cell can enter meiosis; stress granules sequester stalled translational machinery as a protective response for cellular stress response; potentially, Fab1 and its complex partners aggregate to transduce a signal required for a stress response. Importantly, once the fluctuations in cellular conditions is stabilized or relieved the protein assemblies dissolve by disassembly or degradation. In this report, we provided several pieces of evidence that Fab1 and its complex partners are participating in such interactions.

The activation of Fab1 for proper remodeling of the vacuole during hyperosmotic stress requires an elaborate network of proteins including Vac7, Vac14 and Fig4. Indeed, deletion of any of these proteins result in grossly enlarged vacuoles and virtually no increase in PtdIns(3,5)P_2 production during hyperosmotic stress. Several studies have attempted to define the interaction domains required for the proper activation of Fab1. The FYVE domain of Fab1 is important for localization to the vacuole, through binding to PtdIns(3)P; however, it is not required for PtdIns(3,5)P_2 production (11). This suggests that other parts of the protein are involved in activating

the Fab1's kinase activation. On the other hand, the CCT and CCR domains of Fab1, referred to as the GroL-like domain, is not required for vacuole targeting, but is suggested to stabilize Fab1 on the vacuole through the interaction with Vac14 and Fig4 (10–13, 42, 43). Furthermore, Vac14 and Fig4 have been found to interact first, and this complex is mutually dependent for its interaction with Fab1 (43). Also, this interaction network does not require Vac7, the positive regulator of Fab1 (13, 43). This is consistent with our findings; Vac7's PrLD is not sufficient to aggregate during hyperosmotic stress and overexpressing the PrLD does not alter vacuole morphology. Overall, the intricate protein interactions that are required to quickly activate Fab1 and elevate PtdIns(3,5)P_2 levels, during hyperosmotic stress, draws parallels to prion-like mechanisms. In this report, we observed several interesting parallels that suggest Fab1 and its complex partners are participating in a prion-like complex.

First, we showed the prion-like domains from the vacuolar Fab1 complex were sufficient to drive aggregation in the cytoplasm. These data show the potential for homologous interactions, and suggests the possibility that the PrLDs aggregate in the cytoplasm prior to recruitment to the vacuole that results in the activation of Fab1. Also, these data support the predictive power of PAPA because only the PrLDs that are predicted to be aggregation prone were shown to be sufficient to aggregate: Fab1, Vac14, Fig4 but not Vac7. However, Vac7 is also a transmembrane vacuolar protein; therefore, Vac7 PrLD may not aggregate because its full-length protein is unable to be used as a template (30). Future experiments are required to determine if the prion-like domains form heterologous interactions *in vivo*. A possible experiment to observe these interactions would be to tag all the PrLDs with mCherry and express PrLD combinations

in cells and determine if co-localization of GFP and mCherry is observed during hyperosmotic stress. If we do not observe co-localization it may mean we cannot visualize transient PrLD interactions microscopically. There is precedence in the literature that transient interactions are not microscopically visible even though they do interact (44, 45). On the other hand, if we observed co-localization, that does not necessarily mean two proteins are interacting directly; therefore, a yeast two hybrid or coimmunoprecipitation experiment would be necessary to show direct interactions; however, such experiments may not detect transient protein interactions. Together, these results show the potential for a prion-like mechanism for the proper recruitment of protein components to the vacuole during hyperosmotic stress.

Second, we showed the overexpression of the PrLDs from the Fab1 complex results in altered vacuole morphology. Overexpressing the full-length proteins Vac7 and Vac14 have been shown to increase PtdIns(3,5)P_2 levels, which result in hyper-fragmented vacuoles (28), while overexpressing Fab1 does not because it requires its positive regulators (5). When we overexpressed Vac14 PrLD or Fab1 PrLD we observed hyper-fragmented vacuoles suggesting we are increasing the number of interactions, via PrLDs, that transduces the Fab1 activation signal. On the other hand, we observed no vacuole fragmentation when Vac7, the non-aggregation prone PrLD, is overexpressed. Consistent with our previous observations that Vac7 PrLD does not aggregate or have an effect in this system ((20), Figure 5.3). Overall, these data support the mechanism that the Vac14 and Fab1 PrLDs' play a role in inducing the signal required for fragmentation of the vacuole, most likely through the interactions of aggregation prone PrLDs in the Fab1 complex proteins.

Lastly, we showed aggregation propensity of Fab1 is required for efficient vacuole fragmentation during hyperosmotic stress. During hyperosmotic stress, Fab1 and its known complex proteins, Vac7, Vac14, Fig4 and Fab1, are required for the increased production of PtdIns(3,5)P_2. Any defects in these proteins result in low to no PtdIns(3,5)P_2 levels and grossly enlarged vacuoles (5, 10, 30). Intriguingly, during hyperosmotic stress, we showed vacuoles are defective in fragmentation when non-aggregation-prone domains are present. On the contrary, when aggregation-prone domains are present, we observed fragmentation of the vacuole during hyperosmotic stress, suggesting we have regained normal function. Therefore, we showed aggregation propensity to affect a function of Fab1 but we did not measure the PtdIns(3,5)P_2 levels, so there is a possibility that we are affecting the vacuole morphology but not Fab1 kinase activity. Thus, measuring the PtdIns(3,5)P_2 levels during hyperosmotic stress for the Fab1 aggregation mutants is required to confirm that aggregation propensity affects Fab1's function.

Collectively, we have proposed when cells encounter osmotic stress, Fab1 and its complex partners utilize protein aggregation for sufficient recruitment to the vacuole, activation of Fab1, and proper signal transduction. The lipid kinase, Fab1/PIKfyve and its effectors Vac14/ArPIKfyve and Fig4/Sac3, interact to form a complex on the vacuole/endolysosome, and this process is conserved between yeast and mammalian cells. In fact, the regulation of PtdIns(3,5)P_2 production is an integral function in mammalian cells, and dysregulation has been linked to neuropathologies including Charcot-Marie-Tooth disease and amyotrophic lateral sclerosis (ALS) (46, 47). Also, PIKfyve has been linked to melanosome biogenesis (48), and the production of

PtdIns(3,5)P_2 is required for efficient viral entry (49). In total, the activation of Fab1/PIKfyve is critical for normal and stress-induced function, and rapid assembly of the complex via prion-like domain aggregation provides a mechanism for efficient activation.

Materials and Methods:

Yeast Strains and Media

Standard yeast media and methods were used as previously described (50). In all experiments, yeast strains were grown at 30^{o}C. See Table 5.1 for a list of strains used in this study.

A PCR-based homologous recombination protocol based on the methods of Longtine *et al.*1998 (51), to endogenously tag Vph1 with mCherry, Briefly, an mCherry-URA3 cassette was PCR amplified from pER1372 (kind gift from Dr. Steven Markus), adding regions of homology to allow for in-frame fusion of the cherry tag with the target gene. These products were transformed into the yER279 strain, selecting on SC-Ura. Genomic PCR and DNA sequencing were performed to confirm correct insertion.

A “flip in, flip out” scheme was used to generate endogenous Fab1 mutants, adapted from (52). First, a URA3 cassette was inserted into the target site within *FAB1* using homologous recombination. Next, PCR products were generated containing the desired mutations; these PCR products were transformed into the *URA3* strain. Cells were plated on medium containing 5-FOA to select for loss of the URA3 cassette. Next, Fab1 mutants were HA_3 tagged, the HA3-KanMX6 cassette was PCR amplified from pFA6a-3HA-KanMX6 plasmid. This fragment was inserted into Fab1 mutant strains by

homologous recombination. Correct integrations were confirmed by genomic PCR and DNA sequencing.

Plasmid construction

To generate the Fab1 PrLD-GFP fusions, the PrLDs were amplified from pER881 with mutagenic primers (20), adding BamHI and XhoI restriction sites, MS codons at the beginning of the PrLD and a flexible linker at the end of the PrLD (see Table 5.2 plasmid descriptions and Table 5.3 for protein sequences). PCR products digested with BamHI and XhoI and ligated into pER760, a *TRP1* 2µm plasmid containing GFP under control of the *GAL1* promoter (53).

To generate the GFP-PrLD fusions, first GFP was cloned under control of the *SUP35* promoter by replacing the Sup35 open reading frame in pJ526 (54), adding a GSAGGS spacer, and BamHI and BglII sites, to generate plasmid pER843. PrLDs were amplified from plasmids (above), adding BglII and BamHI restriction sites. PCR products were cut with BglII and BamHI and cloned into pER843 to generate GFP-PrLDs fusions expressed from the *SUP35* promoter.

To construct purification plasmids, PrLD were amplified from plasmids (above), adding tails homologous to pER1824 backbone double digested by AgeI and BamHI (constructed in (55), kind gift from Roy Parker). The PCR products were cloned in pER1824 using In-Fusion polymerase creating MBP-TEV-SNAP-PrLD-TEV-Hisx6.

Vac7 and Vac14 fused to GFP and expressed under the *GAL1* promoter were previously constructed (20). Fig4's prion-like domain was predicted by PAPA as previously described (20). To generate the Fig4 PrLD-GFP fusion, the PrLD was amplified from the strain yER632/pJ533 (53), adding BamHI and XhoI restriction sites,

as well as a start codon at the beginning of the PrLD and a flexible linker at the end of the PrLD, PCR products were cloned into pER760. Also, the PrLD amplified was amplified with primers containing tails homologous to pER843 backbone and PCR product was cloned into pER843 (double digested with BglII and BamHI) to generate GFP-PrLD under *Sup35* promoter. All sequences were confirmed by DNA sequencing. Fab1 contains a minor polymorphism that altered the amino acid sequence from the reference strain in the *Saccharomyces* Genome Database; see Table 5.2 and 5.3 for plasmid descriptions and protein sequences, respectively.

Microscopy

Foci formation assays were performed as previously described (39). Briefly, yeast strains yER1919 or yER632/pJ533 were transformed with *TRP1* plasmids expressing each PrLD-GFP from the *GAL1* promoter. Strains were grown in galactose/raffinose dropout medium lacking tryptophan for 24 hours, and then imaged by confocal microscopy. To examine vacuole fragmentation, 11 0.5um z-stacks were obtained and the maximum projection was created. For hyperosmotic stress conditions, cells were treated with 0.9M NaCl for 15 minutes.

Western Blotting

To access protein expression levels, yER632 was transformed with TRP1 plasmids expressing PrLD-GFP fusions from the GAL1 promoter. Strains were grown for 24 hours in galactose/raffinose medium lacking tryptophan. Cells were harvested and lysed as previously described (20). The membrane was probed with an anti-GFP primary antibody (Santa Cruz), and Alexa Fluor IR800 goat anti-mouse secondary antibody (Rockland).

Fab1 strains were grown to mid-log phase in YPD. Cells were harvested and lysed in 2M SUMEB buffer, as previously described (Shattuck et al., 2018, in prep). The membrane was probed with an anti-HA primary antibody (BioLegend), and Alexa Fluor IR800 goat anti-mouse secondary antibody (Rockland).

Semi-Denaturing Detergent-Agarose Gel Electrophoresis (SDD-AGE)

For SDD-AGE, yER632/pJ533 were transformed with *TRP1* plasmids expressing each PrLD-HA from the *GAL1* promoter. Strains were grown for 24 hours in galactose/raffinose dropout medium lacking tryptophan. Cells were harvested and lysed as previously reported (20). The membrane was probed with an anti-GFP primary antibody (Santa Cruz), and Alexa Fluor IR800 goat anti-mouse secondary antibody (Rockland).

Bacterial-expressed purification and amyloid assembly reactions

Fab1 and mutant PrLDs were expressed in E.*Coli* strain BL21(DE3)T1^{R} (Sigma-Aldrich) in Terrific Broth at 37^{o}C and induced at OD_{600} 0.6-1.0 with 1mM IPTG at 37^{o}C for 3 hours. Cells were lysed by sonication and cell debris was cleared by centrifugation. Protein was purified using a Ni-NTA column (GE Healthcare) followed by MBPTrap column (GF Healthcare). Protein was eluted in 150mM NaCl, 20mM Tris-HCl pH 7.4, 40mM maltose, 1mM DTT and dialysis was performed overnight in 150mM NaCl, 20mM Tris-HCl pH 7.4, 1mM DTT. Proteins were concentrated via centrifugal filtration (Amicon Ultra Centrifugal Filter Unit, 10,000 MWCO). Protein concentrations for all the proteins were measured from the absorbance at 280nm on Nanodrop and the extinction coefficients were obtained from SnapGene.

FM4-64 staining of vacuoles

To visualize yeast vacuole morphology under steady-state conditions and during hyperosmotic stress the vacuoles were stained with a lipophilic dye, FM4-64 as previously reported (29). Briefly, yeast cultures (yER1091,1939, 1940, 1941, 1942, 1943, 1944, 2167) were grown overnight in YPD. Cultures were diluted to OD_{600} 0.1 in fresh YPD and grown for 3 hours at 30^{o}C. 1ml of culture was pelleted at OD_{600} 0.3-0.4, resuspended in 600ul YPD, 50ul 1M PIPES, 2ul 2mg/ml FM4-64 cells were incubated for 15 minutes. Cell pellets were washed in YPD twice and chased in fresh YPD for 1.5-2.5 hours. Cells were pelleted and washed in SC media prior to imaging using confocal microscopy, 11 0.5mM z-stacks were obtained and maximum projection images were generated. For hyperosmotic stress conditions, cells were treated with 0.9M NaCl for 5 minutes.

Table 5.1: Yeast Strain Descriptions

Yeast strain name	Genotype
yER1939	α kar1 SUQ5 ade2-1 his3 leu2 trp1 ura3 Fab1::Fab1-HAx3-KanMX
yER1940	α kar1 SUQ5 ade2-1 his3 leu2 trp1 ura3 Fab1::Fab1(dPrLD)-HAx3-KanMX
yER1942	α kar1 SUQ5 ade2-1 his3 leu2 trp1 ura3 Fab1::Fab1(PrLD::Proline)-HAx3-KanMX
yER1943	α kar1 SUQ5 ade2-1 his3 leu2 trp1 ura3 Fab1::Fab1(PrLD::K/R)-HAx3-KanMX
yER1944	α kar1 SUQ5 ade2-1 his3 leu2 trp1 ura3 Fab1::Fab1(PrLD::D/E)-HAx3-KanMX
yER2167	α kar1 SUQ5 ade2-1 his3 leu2 trp1 ura3 Fab1 oPrLD::Supergood PrLD-HAx3-KanMX
yER1941	α kar1 SUQ5 ade2-1 his3 leu2 trp1 ura3 Fab1::Fab1(PrLD::Rnq1)-HAx3-KanMX
yER632	α kar1-1 SUQ5 ade2-1 his3 leu2 trp1 ura3 sup35::KanMx pJ533(URA3)
yER279	α kar1 SUQ5 ade2-1 his3 leu2 trp1 ura3
yER1919	α kar1 SUQ5 ade2-1 his3 leu2 trp1 ura3 VPH1::VPH1-mCherry-URA3

Table 5.2: Plasmid Descriptions

Plasmid Name	Description	Reference
pER881	GAL1-Fab1 oPrLD(aa427-552)-GFP,ADH1 Terminator, TRP1, 2μ	(20)
pER1501	GAL1-Fab1 rPrLD(aa427-606)-GFP,ADH1 Terminator, TRP1, 2μ	This study
pER1042	GAL1-Fab1 Proline PrLD(aa427-552)-GFP,ADH1 Terminator, TRP1, 2μ	This study
pER1043	GAL1-Fab1 K/R PrLD(aa427-552)-GFP,ADH1 Terminator, TRP1, 2μ	This study
pER1044	GAL1-Fab1 D/E PrLD(aa427-552)-GFP,ADH1 Terminator, TRP1, 2μ	This study
pER1046	GAL1-Fab1 AggPos PrLD(aa427-552)-GFP,ADH1 Terminator, TRP1, 2μ	This study
pER1896	MBP-SNAP-Fab1 oPrLD (aa427-552)-Hisx6	This study
pER1917	MBP-SNAP-Proline PrLD (aa427-552)-Hisx6	This study
pER1918	MBP-SNAP-K/R PrLD (aa427-552)-Hisx6	This study
pER1919	MBP-SNAP-D/E PrLD (aa427-552)-Hisx6	This study
pER2031	MBP-SNAP-AggPos PrLD (aa427-552)-Hisx6	This study
pER1549	Sup35 Promoter,GFP-Vac7 PrLD (aa377-541), Sup35 terminator, LEU2, cen	This study
pER1550	Sup35 Promoter,GFP-Vac14 PrLD (aa690-818), Sup35 terminator, LEU2, cen	This study
pER1551	Sup35 Promoter,GFP-Fab1 rPrLD (aa427-606), Sup35 terminator, LEU2, cen	This study
pER979	GAL1-Vac7 PrLD(aa377-541)-GFP,ADH1 Terminator, TRP1, 2μ	(20)
pER1183	GAL1-Vac14 PrLD(aa690-818)-GFP,ADH1 Terminator, TRP1, 2μ	(20)
pER2085	GAL1-Fig4 PrLD(aa528-608)-GFP,ADH1 Terminator, TRP1, 2μ	This study
pER760	GAL1-GFP,ADH1 Terminator, TRP1, 2μ	(53)

Table 5.3: Fab1 mutant prion-like domain sequences

Construct	PAPA Score	Protein Sequence
Fab1 original PrLD (oPrLD)	0.06	DNPGRHHHLDSVPTRYTIRDMDNISHYDTNSNSTLRPHYNT NNSTITINNLNNTTSNNSNYNNTNSNSNINNPAHSLRRSIFHY VSSNSVNKDSNNSSATPASSAQSSSILDPANRIIGNYAHRNY
Fab1 revised PrLD (rPrLD)	0.06	DNPGRHHHLDSVPTRYTIRDMDNISHYDTNSNSTLRPHYNT NNSTITINNLNNTTSNNSNYNNTNSNSNINNPAHSLRRSIFHY VSSNSVNKDSNNSSATPASSAQSSSILEPANRIIGNYAHRNY KFKFNYNSKGPSQQNDTANGNNDNNNNNNNNNNNNNS ASGIADNNNIPSNDN
Fab1 Proline PrLD	-0.05	DNPGRHHHLDSVPTRYTIRDMDNISHYDTNSNSTLRPHYNT NNST**P**T**P**NNLNNTTSNNSN**P**NNTNSNSN**P**NNPAHSLRRSIF HYVSSNSVNKDSNNSSATPASSAQSSSILDPANRIIGNYAHR NY
Fab1 K/R PrLD	-0.04	DNPGRHHHLDSVPTRYTIRDMDNISHYDTNSNSTLRPHYNT NNST**R**T**K**NNLNNTTSNNSN**K**NNTNSNSN**R**NNPAHSLRRSIF HYVSSNSVNKDSNNSSATPASSAQSSSILDPANRIIGNYAHR NY
Fab1 D/E PrLD	-0.04	DNPGRHHHLDSVPTRYTIRDMDNISHYDTNSNSTLRPHYNT NNST**E**T**D**NNLNNTTSNNSN**D**NNTNSNSN**E**NNPAHSLRRSIF HYVSSNSVNKDSNNSSATPASSAQSSSILDPANRIIGNYAHR NY
Fab1 AggPos PrLD	0.12	DNPGRHHHLDSVPTRYTIRDMDNISHY**F**TNSNSTL**QYN**YNTN NSTITINNLNNTTSNNSNYNNTNSNSNINNPAHSLRRSIFHYV SSNSVNKDSNNSSATPASSAQSSSILDPANRIIGNYAHRNY

REFERENCES

1. Bryant NJ, Stevens TH (1998) Vacuole biogenesis in Saccharomyces cerevisiae: protein transport pathways to the yeast vacuole. *Microbiology and molecular biology reviews : MMBR* 62(1):230–47.
2. Weisman LS (2003) Yeast Vacuole Inheritance and Dynamics. *Annual Review of Genetics* 37(1):435–460.
3. Odorizzi G, Babst M, Emr SD (2000) Phosphoinositide signaling and the regulation of membrane trafficking in yeast. *Trends in Biochemical Sciences* 25(5):229–235.
4. Odorizzi G, Babst M, Emr SD (1998) Fab1p PtdIns(3)P 5-kinase function essential for protein sorting in the multivesicular body. *Cell* 95(6):847–58.
5. Gary JD, Wurmser AE, Bonangelino CJ, Weisman LS, Emr SD (1998) Fab1p is essential for PtdIns(3)P 5-kinase activity and the maintenance of vacuolar size and membrane homeostasis. *The Journal of cell biology* 143(1):65–79.
6. Dove SK, et al. (1997) Osmotic stress activates phosphatidylinositol-3,5-bisphosphate synthesis. *Nature* 390(6656):187–92.
7. Schu P V, et al. (1993) Phosphatidylinositol 3-kinase encoded by yeast VPS34 gene essential for protein sorting. *Science (New York, NY)* 260(5104):88–91.
8. Ho CY, Alghamdi TA, Botelho RJ (2012) Phosphatidylinositol-3,5-Bisphosphate: No Longer the Poor PIP2. *Traffic* 13(1):1–8.
9. Malia PC, et al. (2018) Control of vacuole membrane homeostasis by a resident PI-3,5-kinase inhibitor. *Proceedings of the National Academy of Sciences of the United States of America*:201722517.
10. Dove SK, et al. (2002) Vac14 controls PtdIns(3,5)P(2) synthesis and Fab1-dependent protein trafficking to the multivesicular body. *Current biology : CB* 12(11):885–93.
11. Botelho RJ, Efe JA, Teis D, Emr SD (2008) Assembly of a Fab1 phosphoinositide kinase signaling complex requires the Fig4 phosphoinositide phosphatase. *Molecular biology of the cell* 19(10):4273–86.
12. Jin N, et al. (2008) VAC14 nucleates a protein complex essential for the acute interconversion of PI3P and PI(3,5)P(2) in yeast and mouse. *The EMBO journal* 27(24):3221–34.
13. Rudge SA, Anderson DM, Emr SD (2004) Vacuole size control: regulation of PtdIns(3,5)P2 levels by the vacuole-associated Vac14-Fig4 complex, a PtdIns(3,5)P2-specific phosphatase. *Molecular biology of the cell* 15(1):24–36.
14. Alghamdi TA, et al. (2013) Vac14 protein multimerization is a prerequisite step for Fab1 protein complex assembly and function. *The Journal of biological chemistry* 288(13):9363–72.
15. Protter DSW, Parker R (2016) Principles and Properties of Stress Granules. *Trends in Cell Biology* 26(9):668–679.
16. Berchowitz LE, et al. (2015) Regulated Formation of an Amyloid-like Translational Repressor Governs Gametogenesis. *Cell* 163(2):406–18.
17. Caudron F, Barral Y (2013) A super-assembly of Whi3 encodes memory of

deceptive encounters by single cells during yeast courtship. *Cell* 155(6):1244–57.
18. March ZM, King OD, Shorter J (2016) Prion-like domains as epigenetic regulators, scaffolds for subcellular organization, and drivers of neurodegenerative disease. *Brain Research* 1647:9–18.
19. Saarikangas J, Barral Y (2016) Protein aggregation as a mechanism of adaptive cellular responses. *Current Genetics* 62(4):711–724.
20. Shattuck JE, Waechter AC, Ross ED (2017) The effects of glutamine/asparagine content on aggregation and heterologous prion induction by yeast prion-like domains. *Prion* 11(4):249–264.
21. Halfmann R, Lindquist S (2008) Screening for amyloid aggregation by Semi-Denaturing Detergent-Agarose Gel Electrophoresis. *Journal of visualized experiments : JoVE* (17). doi:10.3791/838.
22. LeVine H (1993) Thioflavine T interaction with synthetic Alzheimer's disease beta-amyloid peptides: detection of amyloid aggregation in solution. *Protein science : a publication of the Protein Society* 2(3):404–10.
23. Alberti S, Halfmann R, King O, Kapila A, Lindquist S (2009) A Systematic Survey Identifies Prions and Illuminates Sequence Features of Prionogenic Proteins. *Cell* 137(1):146–158.
24. Hyman AA, Weber CA, Jülicher F (2014) Liquid-liquid phase separation in biology. *Annual review of cell and developmental biology* 30:39–58.
25. Weber SC, Brangwynne CP (2012) Getting RNA and Protein in Phase. *Cell* 149(6):1188–1191.
26. Molliex A, et al. (2015) Phase Separation by Low Complexity Domains Promotes Stress Granule Assembly and Drives Pathological Fibrillization Article Phase Separation by Low Complexity Domains Promotes Stress Granule Assembly and Drives Pathological Fibrillization. *Cell* 163(1):123–133.
27. Patel A, et al. (2015) A Liquid-to-Solid Phase Transition of the ALS Protein FUS Accelerated by Disease Mutation. *Cell* 162(5):1066–1077.
28. Bonangelino CJ, et al. (2002) Osmotic stress-induced increase of phosphatidylinositol 3,5-bisphosphate requires Vac14p, an activator of the lipid kinase Fab1p. *The Journal of cell biology* 156(6):1015–28.
29. Duex JE, Nau JJ, Kauffman EJ, Weisman LS (2006) Phosphoinositide 5-phosphatase Fig 4p is required for both acute rise and subsequent fall in stress-induced phosphatidylinositol 3,5-bisphosphate levels. *Eukaryotic cell* 5(4):723–31.
30. Bonangelino CJ, Catlett NL, Weisman LS (1997) Vac7p, a novel vacuolar protein, is required for normal vacuole inheritance and morphology. *Molecular and cellular biology* 17(12):6847–58.
31. Sondheimer N, Lindquist S (2000) Rnq1: an epigenetic modifier of protein function in yeast. *Molecular cell* 5(1):163–72.
32. Decker CJ, Teixeira D, Parker R (2007) Edc3p and a glutamine/asparagine-rich domain of Lsm4p function in processing body assembly in *Saccharomyces cerevisiae*. *The Journal of Cell Biology* 179(3):437–449.
33. Gilks N, et al. (2004) Stress granule assembly is mediated by prion-like aggregation of TIA-1. *Molecular biology of the cell* 15(12):5383–98.
34. Lancaster AK, Nutter-Upham A, Lindquist S, King OD (2014) PLAAC: a web and command-line application to identify proteins with prion-like amino acid

composition. *Bioinformatics (Oxford, England)* 30(17):2501–2.
35. Nelson R, et al. (2005) Structure of the cross-beta spine of amyloid-like fibrils. *Nature* 435(7043):773–8.
36. Toombs JA, et al. (2012) De novo design of synthetic prion domains. *Proceedings of the National Academy of Sciences of the United States of America* 109(17):6519–24.
37. Toombs JA, McCarty BR, Ross ED (2010) Compositional determinants of prion formation in yeast. *Molecular and cellular biology* 30(1):319–32.
38. Kim HJ, et al. (2013) Mutations in prion-like domains in hnRNPA2B1 and hnRNPA1 cause multisystem proteinopathy and ALS. *Nature* 495(7442):467–73.
39. Paul KR, Hendrich CG, Waechter A, Harman MR, Ross ED (2015) Generating new prions by targeted mutation or segment duplication. *Proceedings of the National Academy of Sciences of the United States of America* 112(28):8584–9.
40. Berson JF, et al. (2003) Proprotein convertase cleavage liberates a fibrillogenic fragment of a resident glycoprotein to initiate melanosome biogenesis. *The Journal of cell biology* 161(3):521–33.
41. Ford AF, Shorter J (2015) Fleeting Amyloid-like Forms of Rim4 Ensure Meiotic Fidelity. *Cell* 163(2):275–6.
42. Gary JD, et al. (2002) Regulation of Fab1 Phosphatidylinositol 3-Phosphate 5-Kinase Pathway by Vac7 Protein and Fig4, a Polyphosphoinositide Phosphatase Family Member. *Molecular Biology of the Cell* 13(4):1238–1251.
43. Duex JE, Tang F, Weisman LS (2006) The Vac14p-Fig4p complex acts independently of Vac7p and couples PI3,5P2 synthesis and turnover. *The Journal of cell biology* 172(5):693–704.
44. Markmiller S, et al. (2018) Context-Dependent and Disease-Specific Diversity in Protein Interactions within Stress Granules. *Cell* 172(3):590–604.e13.
45. Youn J-Y, et al. (2018) High-Density Proximity Mapping Reveals the Subcellular Organization of mRNA-Associated Granules and Bodies. *Molecular Cell* 69(3):517–532.e11.
46. Chow CY, et al. (2007) Mutation of FIG4 causes neurodegeneration in the pale tremor mouse and patients with CMT4J. *Nature* 448(7149):68–72.
47. Zhang Y, et al. (2007) Loss of Vac14, a regulator of the signaling lipid phosphatidylinositol 3,5-bisphosphate, results in neurodegeneration in mice. *Proceedings of the National Academy of Sciences* 104(44):17518–17523.
48. Liggins MC, et al. (2018) PIKfyve regulates melanosome biogenesis. *PLOS Genetics* 14(3):e1007290.
49. Qiu S, et al. (2018) Ebola virus requires phosphatidylinositol (3,5) bisphosphate production for efficient viral entry. *Virology* 513:17–28.
50. Sherman F (1991) Getting started with yeast. *Methods in enzymology* 194:3–21.
51. Longtine MS, et al. (1998) Additional modules for versatile and economical PCR-based gene deletion and modification in Saccharomyces cerevisiae. *Yeast* 14(10):953–961.
52. Riback JA, et al. (2017) Stress-Triggered Phase Separation Is an Adaptive, Evolutionarily Tuned Response. *Cell* 168(6):1028–1040.e19.
53. Gonzalez Nelson AC, et al. (2014) Increasing prion propensity by hydrophobic insertion. *PloS one* 9(2):e89286.

54. Ross ED, Edskes HK, Terry MJ, Wickner RB (2005) Primary sequence independence for prion formation. *Proceedings of the National Academy of Sciences of the United States of America* 102(36):12825–30.
55. Lin Y, Protter DSW, Rosen MK, Parker R (2015) Formation and Maturation of Phase-Separated Liquid Droplets by RNA-Binding Proteins. *Molecular cell* 60(2):208–19.

CHAPTER 6: CONCLUSIONS

The importance of glutamine and asparagine residues in yeast prion-like proteins

In Chapter 2, we set out to better understand prion-like activity in yeast. We used our previously characterized prediction algorithm, PAPA, and identified several predicted aggregation-prone prion-like domains (PrLDs) (1, 2). While almost all of the predicted aggregation-prone domains formed protein aggregates when expressed in cells, the ability to form the detergent-insoluble aggregates was highly correlated with glutamine/asparagine (Q/N) content, suggesting that high Q/N content may specifically promote conversion to the amyloid state *in vivo.* Further characterization of this correlation is one interesting future direction of this project.

We found aggregation-prone PrLDs consisting of at least 23% Q/N residues promoted SDS-insoluble aggregation. However, we did not confirm if there was a threshold of Q/N content for PrLDs to form SDS-insoluble aggregates. Therefore, it would be interesting to adjust the Q/N content of these PrLDs and evaluate their SDS sensitivity. We would hypothesize that increasing the Q/N content of PrLDs that did not form SDS-insoluble aggregates would result in the conversion into SDS-insoluble aggregates and vice versa. Additionally, we may increase our dataset, and test whether more PrLDs that contain the above determined compositional parameters are able to form SDS-insoluble aggregates. Together, these additional experiments would define the importance of Q/N content for stabilizing amyloid/amyloid-like structures and clarify if Q/N content should be considered when predicting proteins with prion-like activity in yeast.

Intriguingly, we observed PrLDs that formed SDS-insoluble aggregates were also sufficient to act as [PIN+] and nucleate Sup35 into its prion form, [PSI+] (3, 4). Therefore, if we discover there is a Q/N content threshold, it will be important to investigate if this threshold holds true for “cross-seeding” capabilities for nucleating Sup35 into [PSI+].

Collectively, these additional investigations would aid in understanding the amino acid sequence features that contribute to prion-like activity. In addition, it will contribute to improving our algorithm’s prediction power. While we have shown PAPA is excellent at predicting prion-like aggregation, we have never utilized PAPA to predict other protein assemblies, which regulate cellular processes. Therefore, extending its use to other reversible protein assemblies will be an exciting avenue for future work.

Predicting amino acid compositional requirements for stress granule formation

Prion-like domains (PrLDs) are defined as protein segments with sequence composition similarity to yeast prion proteins, and have been shown to self-assemble and form protein aggregates in cells (1, 5). Many stress granule proteins contain PrLDs, which may serve to help cells rapidly respond to fluctuations in the environment. Moreover, they provide conformational flexibility and contribute to the dynamic nature of a stress granule. Consequently, mutations within these domains can promote amyloid formation, which reduces the dynamic nature of a stress granule, thereby leading to pathological consequences associated with neurodegenerative diseases (6–10). While there is evidence for PrLDs playing diverse roles in fundamentally distinct protein assemblies, is there is a fundamental difference, i.e. amino acid composition, between the PrLDs that participate in prion formation, and PrLDs that participate in reversible

protein assemblies, i.e. stress granules? This question motivated our study performed in Chapter 4, in which we tested a large dataset of PrLDs for their ability to be recruited to heat-induced stress granules. Surprisingly, the preliminary data revealed Q/N content was significantly associated with PrLDs not being sufficient for stress granule recruitment. Traditionally, PrLDs have been generalized as compositionally restricted and structurally flexible domains capable of self-assembly, regardless of the type protein assembly they are involved in. However, our preliminary study suggests a fundamental distinction; prion formation utilizes PrLDs propensity to form stable amyloid structures, while stress granules utilize PrLDs propensity to form reversible protein assemblies. With support from previous findings (1), it appears Q/N content promotes amyloid-like formation and not stress granule recruitment. Refining these requirements will be necessary to confirm fundamental differences between recruitment biases for two different types of protein assemblies. Therefore, we will use mutational analysis. For example, we will decrease the percentage of Q/N residues in PrLDs not recruited to stress granule to determine if we can drive PrLDs to stress granules, and vice versa.

In parallel, we will investigate stress granule recruitment requirements by randomly mutating stress granule PrLDs, Ded1 and Sky1. We hope to shed light on two things. First, it would be interesting to determine what amino acids favor stress granule formation, and what amino acids completely disrupt the recruitment to stress granules. Next, it will be necessary to determine if there are differences between these two stress granule PrLDs. It is possible we will see differences because full-length Ded1 is a “core” stress granule protein, predicted to form stronger solid-like interactions, while full-length Sky1 transiently associates with stress granules. Therefore, if we observe different

amino acid biases, this would provide insights into the underlying mechanisms that promote solid-like interactions versus dynamic transient interactions within a stress granule, a concept that has never been investigated.

Overall from these large screens and library experiments, we intend to uncover amino acid compositional biases, thereby supporting PrLDs associated with prion formation and stress granule formation are two fundamentally distinct categories of PrLDs.

Resolving prion-like protein's, Sky1, kinase activity in stress granule regulation

When cells are faced with fluctuating environments, stress granules form as a mechanism to spatiotemporally reorganize cellular processes for cellular adaptation and survival. Importantly, once the cellular stress is relieved, stress granules rapidly dissolve, and the cell regains normal cellular functions. The dysregulation of stress granules has detrimental consequences to the cell and can lead to neurodegenerative diseases (11). While we have just begun to unravel the intricate mechanisms underlying the regulation of stress granules, in Chapter 3 we contributed to this understanding by identifying and characterizing a novel yeast prion-like protein kinase that regulates stress granules. We demonstrated the presence of functional Sky1 is required for efficient disassembly by regulating the phosphorylation of a RNA-binding protein, Npl3. We proposed that Sky1-mediated regulation is a novel regulation pathway that compensates for defects in other disassembly pathways, suggesting possible therapeutic implications in higher eukaryotic systems.

We identified Npl3 as one target of Sky1-mediated regulation, but as we alluded to in Chapter 3, there are likely more targets of Sky1, which will be important to

investigate in the future. One likely candidate is Gbp2, another confirmed target of Sky1. However, Gbp2 has been previously shown to be a component of heat-induced nuclear stress granules (12). How the phosphorylation state of Gbp2 modulates cytoplasmic granules is conceptually perplexing. However, it is possible Gbp2 may indirectly modulate cytoplasmic granules by regulating mRNA export during stress granule formation (13). In addition, non-phosphorylatable Gbp2 mutants have been shown to relocalize to the cytoplasm (13); therefore, investigating if the mislocalization of Gbp2 by mutation or inactivation of Sky1 alters stress granules will contribute to understanding the Sky1-mediated regulation.

In addition, a study found Sky1 possibly phosphorylates up to 40 other proteins in yeast (14). Notably, this study was performed *in vitro*; therefore, investigating these targets *in vivo*, and confirming these are targets during stress conditions will uncover other possible protein targets that affect efficient dissolution of stress granules. While Sky1 has only two confirmed targets, I speculate that Sky1 may gain promiscuous interactions and phosphorylation functions during stress granule recovery, which would suggest Sky1 as global kinase regulator of stress granules. Identifying stress-specific targets of Sky1 regulation as a targeted study may be cumbersome; therefore, developing alternative methods to identify stress-induced Sky1 targets is critical for future studies.

One alternative method to identify Sky1 targets during stress is to investigate changes in the phospho-proteome between $Sky1^{WT}$ and $Sky1^{K187M}$ strains. These experiments appear to be conceptually straight-forward, but technically difficult for several reasons including assay development (proteomics never performed in our lab)

and deciphering direct targets of Sky1 rather than indirect targets that would arise from the inactivation of Sky1. A more sophisticated method is utilizing proximity-dependent biotin labeling, which biotinylates proteins in “close proximity” to the protein of interest (15). This method provides many advantages when studying transient protein assemblies. For example, because stress granules are highly dynamic and reversible protein assemblies, it is difficult to identify proteins transiently associated with stress granules, as illustrated by Sky1 never being identified in proteomic studies of isolated yeast stress granules (12, 16, 17). However, using proximity labeling in mammalian cells, Sky1’s human homolog, SRPK1 was identified as a stress granule protein, suggesting this method is more sensitive to identifying transient protein interactors (18, 19). Overall, identifying more Sky1 interactions within stress granules will aid in the understanding the intricate mechanisms underlying stress granule regulation.

What are the biophysical properties of Sky1 in stress granules, and are they altered in the presence of Sky1 mutants? These questions were unaddressed in Chapter 3; however, the are important for understanding the mechanism of Sky1-mediated regulation. While not discussed in Chapter 3, we visualized a difference in stress granule morphology between $Sky1^{WT}$ and $Sky1^{K187M}$; “tighter” stress granules with less background for the latter (data not shown). In fact, we found $Sky1^{K187M}$ stress granules contained a significantly higher percentage of protein compared to $Sky1^{WT}$ (data not shown). One possible explanation is $Sky1^{K187M}$ stress granules are less dynamic; therefore, less protein is being exchanged in these granules leading to more protein “stuck” in stress granules. To address this hypothesis, it would be interesting to investigate the dynamics of Sky1-mediated interactions using a photoconvertible

fluorophore, Dendra2 (20, 21). If we determine *Sky1*^{K187M} is forming more static granules, this will suggest Sky1 is actively phosphorylating and regulating the solubility of stress granule proteins during stress. Traditionally, stress granules have been characterized as sites of repression for the cell to conserve energy during stress conditions. However, I am speculating stress granules are active sites of exchange and rearrangement, mediated by Sky1's kinase activity. If we can show Sky1 is actively regulating stress granules during stress, this will revolutionize the way we think and study these dynamic and reversible protein assemblies.

While it is known that stress granules are highly dynamic and reversible, the mechanisms of regulation of granule dissolution are not fully understood. Stress granules can be either dissolved or degraded by several different suggested mechanisms: degradation by autophagy (22); disassembly by the protein quality control system (23, 24); disassembly by RNA/DNA helicases that utilize ATP hydrolysis to disrupt RNA-protein interactions (25, 26); and post-translational modifications that alter protein-protein interactions (27–30). These mechanisms are not mutually exclusive, and since different stresses result in granules with different protein compositions (31, 32), it is possible that the mechanisms of dissolution vary depending on the type of stress. While it's clear different stress conditions induce different pools of proteins to be recruited to different types of stress granules, it remains to be investigated if the disassembly mechanisms are common among all the different types of stress granules. Therefore, investigating whether Sky1 is a universal stress granule regulator is an interesting future direction. Intriguingly, this is a concept not well understood and rarely investigated.

We will use similar techniques performed in Chapter 3, except in we will induce stress granules using different types of stress. Based on preliminary studies, Sky1 is recruited to several different types of stress (Sodium azide, glucose deprivation and stationary phase stress, data not shown). In support of Chapter 3, we have observed Sky1 recruitment to different types of stress granules was dependent on the prion-like domain. Interestingly, during stationary phase *Sky1*^{WT} stress granules form, but are resolubilized once diluted into fresh media; however, in the presence of *Sky1*^{K187M} the recovery to a soluble state was defective (data not shown). These preliminary studies are intriguing and suggest a universal Sky1-mediated regulation for efficient disassembly of several different types of stress granules.

Collectively, the discovery of Sky1-mediated regulation of stress granules has laid the foundation to continue to unravel the complexity of stress granules in eukaryotic cells. Refining the targets of Sky1-mediated regulation, and clarifying the biophysical properties of Sky1 interactions are important avenues for future studies. The list of neurodegenerative diseases associated with aberrant stress granules continues to grow. Therefore, better understanding of the regulation of stress granules in yeast will provide potential therapeutic targets to combat these diseases in mammalian systems (33).

<u>The role PrLDs play in regulating a vacuolar-signaling complex</u>

Phosphoinositide lipids play a central role in a wide-range of cellular functions including regulating organelle-specific functions. Specifically, phosphotidylinositol 3,5-bisphosphate (PtdIns(3,5)P_2) regulates vacuole-specific functions (34). Together, the lipid kinase, Fab1 and its positive effectors, Vac7 and Vac14, assemble on the vacuolar

membrane to regulate PtdIns(3,5)P_2 levels in yeast (35). Interestingly, PtdIns(3,5)P_2 levels are low during steady-state conditions, but during hyperosmotic conditions, levels dramatically increase 20-fold within seconds (36). This rapid and dramatic change triggers the vacuole to remodel in response to osmotic stress. However, the mechanism of how Fab1 and its complex partners are quickly activated is not fully understood. Previously, we identified Fab1 and its complex partners contain prion-like domains that are aggregation-prone. Therefore, in Chapter 5 we set out to investigate whether an aggregation-mediated mechanism plays a role in the assembly of the vacuolar-signaling complex for proper activation of Fab1, during stress conditions. We observed that aggregation-altering mutations affected Fab1's activation during hyperosmotic stress. Altogether, these results uncover a possible mode of action underlying the previously unclear mechanism of Fab1's rapid activation during hyperosmotic stress. Therefore, refining the mechanism is an important avenue for future studies.

In the presence of non-aggregation prone Fab1 mutants, we observed vacuole defects. These defects are indicative of reduced Fab1 kinase activity; therefore, linking reduction in aggregation propensity to a reduction in Fab1 function is critical for understanding the mechanism. Thus, we will measure PtdIns(3,5)P_2 levels. We would predict mutations in Fab1 aggregation propensity would be correlated with lower PtdIns(3,5)P_2 levels.

Defects in Fab1 activity leads to decreased cell viability during stress conditions (37–39). Therefore, we will investigate cellular viability in the presence of elevated ions levels (zinc and calcium) to elucidate the role Fab1's aggregation propensity plays in this process.

Overall, the activation of Fab1 is critical for normal and stress-induced function. Based on our preliminary study we propose that rapid assembly of the complex via prion-like domain aggregation allows for efficient assembly and activation of the vacuolar-signaling complex.

Concluding Remarks

Prion-like domains are prevalent in distinct and fundamentally different types of protein assemblies. The studies described above provided insights into the diverse roles PrLDs play in cellular processes. First, we investigated the yeast proteome, and found several new PrLDs that were aggregation-prone (Chapter 2). We performed follow-up studies on two of the aggregation-prone PrLDs found in Chapter 2. We found one prion-like protein kinase, Sky1, had a novel role in regulating stress granules (Chapter 3). Additionally, we demonstrated that vacuole-signaling complex proteins utilize their PrLDs to mediate aggregation as a mechanism to properly activate a cellular response to stress (Chapter 5). Overall, we established that PrLDs play an important role in the regulation of distinct cellular processes. In closing, I am hopeful that the work illustrated here will lay the foundation for several exciting future projects to come in the Ross lab.

REFERENCES

1. Shattuck JE, Waechter AC, Ross ED (2017) The effects of glutamine/asparagine content on aggregation and heterologous prion induction by yeast prion-like domains. *Prion* 11(4):249–264.
2. Toombs JA, et al. (2012) De novo design of synthetic prion domains. *Proceedings of the National Academy of Sciences of the United States of America* 109(17):6519–24.
3. Sondheimer N, Lindquist S (2000) Rnq1: an epigenetic modifier of protein function in yeast. *Molecular cell* 5(1):163–72.
4. Derkatch IL, Bradley ME, Hong JY, Liebman SW (2001) Prions affect the appearance of other prions: the story of [PIN(+)]. *Cell* 106(2):171–82.
5. Alberti S, Halfmann R, King O, Kapila A, Lindquist S (2009) A Systematic Survey Identifies Prions and Illuminates Sequence Features of Prionogenic Proteins. *Cell* 137(1):146–158.
6. Kim HJ, et al. (2013) Mutations in prion-like domains in hnRNPA2B1 and hnRNPA1 cause multisystem proteinopathy and ALS. *Nature* 495(7442):467–73.
7. King OD, Gitler AD, Shorter J (2012) The tip of the iceberg: RNA-binding proteins with prion-like domains in neurodegenerative disease. *Brain Research* 1462:61–80.
8. Molliex A, et al. (2015) Phase Separation by Low Complexity Domains Promotes Stress Granule Assembly and Drives Pathological Fibrillization Article Phase Separation by Low Complexity Domains Promotes Stress Granule Assembly and Drives Pathological Fibrillization. *Cell* 163(1):123–133.
9. Murakami T, et al. (2015) ALS/FTD Mutation-Induced Phase Transition of FUS Liquid Droplets and Reversible Hydrogels into Irreversible Hydrogels Impairs RNP Granule Function. *Neuron* 88(4):678–90.
10. Mackenzie IR, et al. (2017) TIA1 Mutations in Amyotrophic Lateral Sclerosis and Frontotemporal Dementia Promote Phase Separation and Alter Stress Granule Dynamics. *Neuron* 95(4):808–816.e9.
11. Ramaswami M, Taylor JP, Parker R (2013) Altered ribostasis: RNA-protein granules in degenerative disorders. *Cell* 154(4):727–36.
12. Wallace EWJ, et al. (2015) Reversible, Specific, Active Aggregates of Endogenous Proteins Assemble upon Heat Stress. *Cell* 162(6):1286–1298.
13. Windgassen M, Krebber H (2003) Identification of Gbp2 as a novel poly(A)+ RNA-binding protein involved in the cytoplasmic delivery of messenger RNAs in yeast. *EMBO Reports* 4(3):278–283.
14. Ptacek J, et al. (2005) Global analysis of protein phosphorylation in yeast. *Nature* 438(7068):679–684.
15. Hwang J, Espenshade PJ (2016) Proximity-dependent biotin labelling in yeast using the engineered ascorbate peroxidase APEX2. *Biochemical Journal* 473(16):2463–2469.
16. Cary GA, Vinh DBN, May P, Kuestner R, Dudley AM (2015) Proteomic Analysis of Dhh1 Complexes Reveals a Role for Hsp40 Chaperone Ydj1 in Yeast P-Body

Assembly. *G3: Genes|Genomes|Genetics* 5(11):2497–2511.
17. Jain S, et al. (2016) ATPase-Modulated Stress Granules Contain a Diverse Proteome and Substructure. *Cell* 164(3):487–98.
18. Markmiller S, et al. (2018) Context-Dependent and Disease-Specific Diversity in Protein Interactions within Stress Granules. *Cell* 172(3):590–604.e13.
19. Youn J-Y, et al. (2018) High-Density Proximity Mapping Reveals the Subcellular Organization of mRNA-Associated Granules and Bodies. *Molecular Cell* 69(3):517–532.e11.
20. Brielle S, Gura R, Kaganovich D (2015) Imaging stress. *Cell Stress and Chaperones* 20(6):867–874.
21. Kroschwald S, et al. (2015) Promiscuous interactions and protein disaggregases determine the material state of stress-inducible RNP granules. *eLife* 4:e06807.
22. Buchan JR, Kolaitis R-M, Taylor JP, Parker R (2013) Eukaryotic Stress Granules Are Cleared by Autophagy and Cdc48/VCP Function. *Cell* 153(7):1461–1474.
23. Cherkasov V, et al. (2013) Coordination of Translational Control and Protein Homeostasis during Severe Heat Stress. *Current Biology* 23(24):2452–2462.
24. Walters RW, Muhlrad D, Garcia J, Parker R (2015) Differential effects of Ydj1 and Sis1 on Hsp70-mediated clearance of stress granules in Saccharomyces cerevisiae. *RNA (New York, NY)* 21(9):1660–71.
25. Hilliker A, Gao Z, Jankowsky E, Parker R (2011) The DEAD-Box Protein Ded1 Modulates Translation by the Formation and Resolution of an eIF4F-mRNA Complex. *Molecular Cell* 43(6):962–972.
26. Chalupníková K, et al. (2008) Recruitment of the RNA helicase RHAU to stress granules via a unique RNA-binding domain. *The Journal of biological chemistry* 283(50):35186–98.
27. Poornima G, Shah S, Vignesh V, Parker R, Rajyaguru PI (2016) Arginine methylation promotes translation repression activity of eIF4G-binding protein, Scd6. *Nucleic Acids Research* 44(19):9358–9368.
28. Tsai W-C, et al. (2016) Arginine Demethylation of G3BP1 Promotes Stress Granule Assembly. *Journal of Biological Chemistry* 291(43):22671–22685.
29. Kedersha N, et al. (2002) Evidence That Ternary Complex (eIF2-GTP-tRNAiMet)-Deficient Preinitiation Complexes Are Core Constituents of Mammalian Stress Granules. *Molecular Biology of the Cell* 13(1):195–210.
30. Yoon J-H, Choi E-J, Parker R (2010) Dcp2 phosphorylation by Ste20 modulates stress granule assembly and mRNA decay in Saccharomyces cerevisiae. *The Journal of cell biology* 189(5):813–27.
31. Buchan JR, Parker R (2009) Eukaryotic stress granules: the ins and outs of translation. *Molecular cell* 36(6):932–41.
32. Buchan JR, Yoon J-H, Parker R (2011) Stress-specific composition, assembly and kinetics of stress granules in Saccharomyces cerevisiae. *Journal of cell science* 124(Pt 2):228–39.
33. Maziuk B, Ballance HI, Wolozin B (2017) Dysregulation of RNA Binding Protein Aggregation in Neurodegenerative Disorders. *Frontiers in Molecular Neuroscience* 10:89.
34. Weisman LS (2003) Yeast Vacuole Inheritance and Dynamics. *Annual Review of Genetics* 37(1):435–460.

35. Ho CY, Alghamdi TA, Botelho RJ (2012) Phosphatidylinositol-3,5-Bisphosphate: No Longer the Poor PIP2. *Traffic* 13(1):1–8.
36. Dove SK, et al. (1997) Osmotic stress activates phosphatidylinositol-3,5-bisphosphate synthesis. *Nature* 390(6656):187–92.
37. Denis V, Cyert MS (2002) Internal Ca $^{2+}$ release in yeast is triggered by hypertonic shock and mediated by a TRP channel homologue. *The Journal of Cell Biology* 156(1):29–34.
38. Dong X, et al. (2010) PI(3,5)P(2) controls membrane trafficking by direct activation of mucolipin Ca(2+) release channels in the endolysosome. *Nature communications* 1:38.
39. Malia PC, et al. (2018) Control of vacuole membrane homeostasis by a resident PI-3,5-kinase inhibitor. *Proceedings of the National Academy of Sciences of the United States of America*:201722517.

APPENDIX ONE: DISTINCT AMINO ACID COMPOSITIONAL REQUIREMENTS FOR FORMATION AND MAINTENANCE OF THE *[PSI+]* PRION IN YEAST[5]

Introduction

Misfolding of a wide range of proteins leads to formation of amyloid fibrils, which are ordered, β-sheet-rich protein aggregates. Many human diseases are associated with the formation of amyloid fibrils, including Alzheimer's disease, Type II diabetes, and the transmissible spongiform encephalopathies (TSEs) (1). However, only a small subset of amyloids are infectious (called prions), including the causative agents of TSEs in mammals (2–4) and [URE3], [*PSI*$^+$], [*PIN*$^+$], and others in *Saccharomyces cerevisiae* (5–9).

Most of the known yeast prion proteins contain glutamine/asparagine (Q/N) rich domains that drive amyloid formation. Q/N-rich domains are found in 1-4% of the proteins in most eukaryotic proteomes (10), but very few of these proteins have been shown to undergo amyloid structural conversion. Bioinformatics screens for prions in yeast have had some notable successes (reviewed in (11)); however, despite advances in predicting which Q/N-rich domains may turn out to be *bona fide* prions (12, 13), predictions remain imperfect.

A well-studied model prion from yeast is [*PSI*$^+$], the prion form of the translational terminator protein Sup35 (5). Like other yeast prion proteins, Sup35 is modular,

[5]This chapter has been reformatted from the following publication: MacLea, K.S., Paul, K.R., Ben-Musa, Z., Waechter, A., Shattuck, J.E., Gruca, M., and Ross, E.D. (2015). Distinct amino acid compositional requirements for formation and maintenance of the [PSI$^+$] prion in yeast. Molecular and Cellular Biology *35*, 899–911. My contribution consisted of performing the "decoration assay" to determine if newly formed aggregates can be added to preexisting prion fibers in vivo (Figure 7.6B).

containing a distinct prion-forming domain (PFD), middle domain (M), and C-terminal domain (C; Figure A.1A) (14–17). The PFD (amino acids 1-114) drives the conversion of Sup35 into its amyloid form (15), the charged M domain has no known function other than its ability to stabilize [*PSI*$^{+}$] fibers, and the C domain is an essential component responsible for translational termination (14, 17).

Prion formation by Sup35 is driven primarily by the amino acid composition of the PFD (18). We previously used a quantitative mutagenesis method to determine the prion propensity of each amino acid in the context of Q/N-rich PFDs (13). Briefly, an eight amino-acid segment in the middle of a scrambled version of the Sup35 PFD was replaced with a random sequence to generate a library of mutants. This library was then screened for the subset of mutants that maintained the ability to form and propagate prions. We then derived prion-propensity scores for each amino acid by comparing the frequency of occurrence of each amino acid among the prion-forming sequences to their frequency of occurrence in the starting library. These prion propensity values were used to develop PAPA (Prion Aggregation Prediction Algorithm), a prediction algorithm capable of accurately distinguishing between Q/N-rich domains with and without prion activity (13, 19, 20).

Although PAPA represents a significant advance in prion prediction, it is far from perfect. One likely problem is that there are multiple distinct steps required for prion activity. Specifically, prion formation requires that a protein be able to both form prion aggregates and add onto these aggregates; additionally, prion propagation to daughter cells during multiple rounds of cell division (also referred to as prion maintenance) requires that the aggregates must be fragmented to create new independently

segregating prion seeds to offset dilution by cell division (21). Each of these steps may have distinct amino acid sequence requirements, yet PAPA uses only a single prion propensity score for each amino acid. Making better predictions of prion propensity requires a better understanding of how amino acid composition separately affects prion formation and maintenance.

Sup35 is an ideal substrate for examining these compositional requirements. Unlike the scrambled version of Sup35 used for the initial library experiments, the wild-type Sup35 PFD has two distinct sub-domains with overlapping but separate functions (Figure A.1A). The N-terminal nucleation domain (ND; amino acids 1-39) is highly Q/N-rich, and is primarily responsible for nucleation and growth of prion fibers (16, 22). The remaining portion of the PFD (amino acids 40-114) has been implicated in prion maintenance and contains an oligopeptide repeat domain (ORD) consisting of five and a half imperfect repeats with the consensus sequence (P/Q)QGGYQ(Q/S)YN (16, 23–25). This separation of prion formation from prion maintenance potentially allows for dissection of how amino acid composition separately affects each activity. Importantly, the ND and the ORD have distinct compositional requirements for their respective functions (26).

The functional separation between the ND and ORD is not absolute (13, 22, 27). For example, both the ND and the first two repeats of the ORD are required for efficient *de novo* aggregation (22), and tyrosines in the ORD have been implicated in the early steps of prion nucleation (27). Nevertheless, significant evidence to supports a role for the ORD in prion maintenance (22, 26). Removal of all or part of the ORD (14, 22, 23, 25) or replacement of the ORD with a random sequence (28) destabilizes [*PSI*$^{+}$]. Such

mutations appear to reduce prion aggregate fragmentation, resulting in larger aggregates that are frequently lost as a result of imperfect segregation of aggregates into daughter cells (29). The chaperone protein Hsp104 is essential for [*PSI*$^{+}$] maintenance (30); Hsp104 cleaves prion fibers into smaller fragments better suited to segregate into daughter cells (21, 31, 32). The ORD repeats have been hypothesized to facilitate Hsp104-dependent aggregate cleavage; the repeats could act as Hsp104 binding-sites (although recent evidence suggests that a binding site exists in the M domain (33)), conformationally modify the amyloid core to allow chaperone access, or modulate fiber fragility (24, 34). Interestingly, the mammalian protein PrP also contains an ORD, and PrP repeat expansion is associated with dominantly inherited prion disease (35, 36). This observation, combined with the presence of repeat elements in the PFDs of Rnq1 and New1 (22, 37), suggest a role for repeats in prion maintenance; however, other yeast PFDs, such as in Ure2, do not contain repeats, so repeats cannot be an absolutely necessary feature for prion maintenance. Furthermore, scrambling the Sup35 ORD does not prevent prion formation or maintenance (26), indicating that the activity of the repeats is largely primary-sequence independent.

The amino acid compositional requirements for ORD function have only been explored to a limited degree, mostly through targeted mutations. However, several studies have used artificial polyglutamine-fragments to explore the sequence requirements for aggregate fragmentation. Targeted replacement of Gln with Tyr residues (38) or other aromatic residues (34) reduced average aggregate size, suggesting an increase in fiber fragmentation. The elevated number and regular spacing of Tyr residues in both the Sup35 ORD and in the repeats of prion-like protein

New1 likewise suggest that aromatic residues may act as recognition sites for chaperones such as Hsp104. Indeed, some chaperones are known to use exposed aromatic or hydrophobic residues as binding sites (39, 40).

To perform a more comprehensive analysis of the compositional determinants for prion formation and maintenance, we quantitatively measured how amino acid composition affects the respective activities of the Sup35 ND and ORD. We observed distinct compositional biases in these two domains. To confirm that these differences were due to distinct compositional requirements for prion formation and maintenance, we developed a new method to specifically isolate the effects of amino acid composition on prion maintenance. These studies confirm that nucleation and maintenance of prions have overlapping but non-identical compositional requirements, and highlight a divergent role for aliphatic residues in promoting prion formation while inhibiting prion maintenance.

Materials and Methods

Yeast strains and media

Standard yeast media and methods were as previously described (41), except that yeast extract-peptone-dextrose (YPD) media contained 0.5% yeast extract in place of the standard amount (1%). In all experiments, yeast were grown at 30°C.

A complete strain list can be found in Table A.1. To build YER709/pER589, the *HIS3* gene was amplified from pRS313 using primers EDR1314 and EDR1315. The resulting product was transformed into YER632/pJ533 (42); pJ533 expresses *SUP35* from a *URA3* plasmid as the sole copy of *SUP35* in the cell ((43). Successful knockout of *ppq1* was confirmed by PCR and sequencing. Two rounds of plasmid shuffling were

Table A.1: Yeast strains.

Name	Genotype	Reference
YER709/pER589	*α kar1-1 SUQ5 ade2-1 his3 leu2 trp1 ura3 ppq1*::*HIS3* *sup35*::KanMx [*psi*$^-$] [*PIN*$^+$] pER589 (*URA3, SUP35MC)*	This study
YER632/pJ533	α *kar1-1 SUQ5 ade2-1 his3 leu2 trp1 ura3* *sup35*::KanMx [*psi*$^-$] [*PIN*$^+$] pJ533 (*URA3, SUP35)*	(42)
YER282/ pER1112	a *kar1-1 SWQ5 ade2-1 his3 leu2 trp1 ura3 arg1*::*HIS3* *sup35*::KanMx [*psi*$^-$] [*PIN*$^+$] pER1112 (*URA3, SUP35-27)*	(18)
780-1D/pJ533	α *kar1-1 SUQ5 ade2-1 his3 leu2 trp1 ura3* *sup35*::KanMx [*PSI*$^+$] [*PIN*$^+$] pJ533 (*URA3, SUP35)*	(43)

then used to replace pJ533 with pER589 (a *URA3* plasmid expressing Sup35MC from the *SUP35* promoter).

Building the libraries

To randomly mutate regions of the SUP35 PFD, first the C-terminal portion of Sup35 was amplified with EDR304 paired with either EDR1388 or EDR1384 for the ND and ORD libraries, respectively. These products were then reamplified with EDR304 paired with either EDR1380 [GCAAAACTACCAGCAATACAGCCAGAACGGT$(NNB)_8$TACCAAGGCTACCAGGCTTACAATGC] or EDR1377 [CTGGGTACCAACAAGGTGGCTATCAACAGTACAAT$(NNB)_{10}$CCTCAAGGAGGCTACCAGCAATACAAC]. These oligonucleotides, made by Invitrogen, contain degenerate segments encoding for a 25% mix of each nucleotide at positions 1 and 2 of each mutated codon and a 33.3% mix of C, G and T at the third position. In a second PCR reaction, a primer complementary to the non-degenerate 5' region of EDR1380 or EDR1377 (EDR1389 or EDR1385, respectively) was paired with EDR302 to amplify the N-terminal portion of Sup35. The N- and C-terminal PCR reactions were combined and reamplified with EDR301 and EDR262. The final PCR products were co-transformed with BamHI/HindIII-cut pJ526 [cen *LEU2*; from Dan Masison, National Institutes of Health; (18)] into yeast strain YER709/pER589 for the prion formation experiments and YER282/pER1112 for the prion maintenance experiments. Transformants were selected on SC-Leu.

Prion formation library experiments

Transformants were spotted onto 5-FOA-containing medium to select for loss of pER589. Library mutants that grew on 5-FOA were stamped onto SC-Ade, YPD and YPAD and grown for 3-5 days at 30°C. Isolates that grew red on YPD and did not grow on SC-Ade were pooled into mini-libraries containing ~80 clones. Random isolates were sequenced to generate the naïve data set. Mini-libraries were plated onto SC-Ade at concentrations of 10^6 and 10^5 cells per plate and grown for 5 days at 30°C. To test curability, Ade^+ colonies were grown on YPD and on YPD plus 4mM GdHCl, and then restreaked on YPD to test for loss of the Ade^+ phenotype. Clones in which the Ade^+ phenotype was stable and curable were sequenced. The odds ratio (OR) for each amino acid or group of amino acids was calculated as

$$OR = [f_p/(1-f_p)]/ [f_{np}/(1-f_{np})] \quad (1)$$

where f_p is the per-residue frequency of the amino acid in the mutated region of prion-forming isolates, and f_{np} is the per-residue frequency of the amino acid in the mutated region of the naïve library (44, 45). Prion propensity scores for each amino acid (PP_{aa}) are then calculated as

$$PP_{aa} = \ln(OR) \quad (2)$$

Prion maintenance library experiments

Transformants were replica plated onto 5-FOA-containing medium to select for loss of pER1112. Cells were pooled and mated with 780-1D/pJ533 for 24 h on YPAD. Diploids were selected by replica plating on SD+Ade+Trp+Ura, then replica plated onto 5-FOA-containing medium to select for loss of pJ533. Cells were then plated for single colonies on YPD media to allow color selection. Ade^+ colonies were streaked on YPD

and YPD plus 4 mM GdHCl to test for curability. Clones in which the Ade^+ phenotype was stable and curable were defined as propagators and sequenced. Clones with a strong Ade^- phenotype were defined as non-propagators and sequenced.

The prion maintenance odds ratio (OR_m) for each amino acid or group of amino acids was calculated as

$$OR_m = [f_p/(1-f_p)]/ [f_{np}/(1-f_{np})] \quad (3)$$

where f_p is the per-residue frequency of the amino acid in the mutated region of prion-positive clones, and f_{np} is the per-residue frequency of the amino acid in the mutated region of non-prion clones. Prion maintenance propensity scores for each amino acid (PMP_{aa}) were then calculated as

$$PMP_{aa} = \ln(OR_m) \quad (4)$$

To test whether library mutants that failed to maintain [*PSI*$^+$] could add on to wild-type aggregates when co-expressed with wild-type Sup35, plasmids expressing non-propagating mutants were isolated and transformed into 780-1D/pJ533. Cells were then spread on SD+Trp+Ura supplemented with limiting adenine (10 µg/ml) to allow color selection. To confirm an inability to propagate [*PSI*$^+$], cells were spotted on 5-FOA-containing medium to select for loss of pJ533, and then spread on YPD to test for prion loss.

Prion maintenance library experiments, preselecting for the ability to add on to existing aggregates

To pre-select against any mutants that were unable to add onto wild-type Sup35 aggregates, the library experiments were performed as above, except that selection for diploids was performed on medium lacking adenine (SD+Trp+Ura).

Leave-one-out analysis

To calculate the predicted prion maintenance propensity (PMP) for each isolate in the prion maintenance library dataset, PMP_{aa} scores were first calculated based on the other 151 isolates in the dataset (i.e., “leaving out” the one sequence to be scored), as in Equation 4. The PMP score for the left out isolate was then calculated as the sum of the PMP_{aa} scores for the ten amino acids in the mutagenized region (the third repeat). This process was iteratively repeated for all 152 isolates in the dataset. Four isolates were excluded from the analysis because they contained amino acids for which PMP_{aa} scores could not be calculated. The three lysine-containing red sequences were excluded because the absence of lysine among the propagating clones made lysine’s PMP_{aa} score indeterminate; likewise, the only methionine-containing prion-propagating clone could not be scored, because when it was left out of the PMP_{aa} calculation, the methionine PMP_{aa} score became indeterminate. The accuracy of the leave-one-out PMP scores were assessed using a receiver operator characteristic (ROC) plot.

Creation of de novo mutants in the ORD

A random proteome of 65386 residues was generated using the random number function of the Microsoft Excel software program, with an equal chance of selecting any of the 20 natural amino acids at each position. Windows of 10 amino acid were scored using the calculated PMP values (from the full library dataset). 3628 sequences did not contain any of the low-abundance residues (E, K, M, Q, and W) and were chosen for further evaluation. Sequences with PMP scores at the 95^{th} and 5^{th} percentile were chosen. Sequences were constructed using the same protocol as that used to build the ORD library, except that EDR1471-1473 and 1490-1492 were used in place of

EDR1377 for the 95th percentile mutants, and EDR1480-1482 and 1493-1495 were used for the 5th percentile mutants.

Tyrosine substitutions in the ORD

To make the tyrosine substitution mutations, first the C-terminal portion of *SUP35* was PCR amplified with EDR304 and EDR1890. This product was reamplified with EDR304 paired with EDR1892-1895 or 2156-2158. In a separate reaction, the N-terminal portion of *SUP35* was amplified with EDR302 and EDR1891. The N- and C-terminal reactions were then combined and reamplified with EDR301 and EDR262. The final PCR products were co-transformed with *Bam*HI/*Hin*dIII-cut pJ526 into YER632/pJ533. 5'FOA was used to select for loss of pJ526. Plasmids to transiently overexpress each PFD from the *GAL1* promoter were constructed and prion formation assays performed as previously described (42).

Plasmids expressing PFD-GFP fusions were constructed as previously described (42). To test for foci formation, these plasmids were transformed into 780-1D/pJ533 and YER632/pJ533. Cells were grown for 2 h in galactose/raffinose dropout medium and visualize by fluorescence microscopy.

In silico reanalysis of Alberti et al. data set

Amino acid compositions were compared by calculating the percentage of each amino acid out of the total number of amino acids in each predicted PFD (12). The 18 proteins that passed all four tests in the assays of Alberti *et al.* (12) were as follows: Ure2, Sup35, Rnq1, New1, Puf2, Nrp1, Swi1, Ybr016w, Cbk1, Lsm1, Ybl081w, Pub1, Ksp1, Asm4, Nsp1, Gln3, Ypr022c, and Rlm1. The 12 proteins that failed only in the

Sup35 fusion protein expression assay were as follows: Snf5, Gts1, Scd5, Sgf73, Sok2, Mot3, Ngr1, Jsn1, Pdr1, Cyc8, Pan1, and Ybr108w.

Statistics

Both the two-sided Student's *t*-tests and Fisher's exact tests were performed using the GraphPad QuickCalcs website (http://www.graphpad.com/quickcalcs/). Standard errors (SE) for log odds ratios are estimated as

$$SE = [1/n_p + 1/(t_p - n_p) + 1/n_{np} + 1/(t_{np} - n_{np})]^{0.5} \quad (5)$$

where n_p and n_{np} are the number of times that the amino acid is found in the prion and naïve (or non-prion for the prion maintenance experiments) libraries, respectively, and t_p and t_{np} are the total number of amino acids in the prion and naïve (or non-prion) libraries, respectively (44). To determine if the difference between two log odds ratios is statistically significant, *z* scores were calculated, using a two-sample *z*-test, as

$$z = [\ln(OR_1) - \ln(OR_2)]/[(SE_1)^2 + (SE_2)^2]^{0.5} \quad (6)$$

where OR_1 and OR_2 are the two odds ratios, and SE_1 and SE_2 are the standard errors for the respective log odds ratios.

Results

Prion formation library experiments with the SUP35 ND and ORD

To define the distinct compositional requirements of the Sup35 ND and ORD, libraries of Sup35 mutants were created in which segments of the ND or ORD were replaced with a segment of random amino acids (bold italics in Figure A.1B). The ND segment (amino acids 21-28) was selected because it overlaps the portion of the ND that was previously shown to be critical for aggregate growth (16), and because it contains a mixture of predicted prion-promoting and -inhibiting residues. In the ORD, the

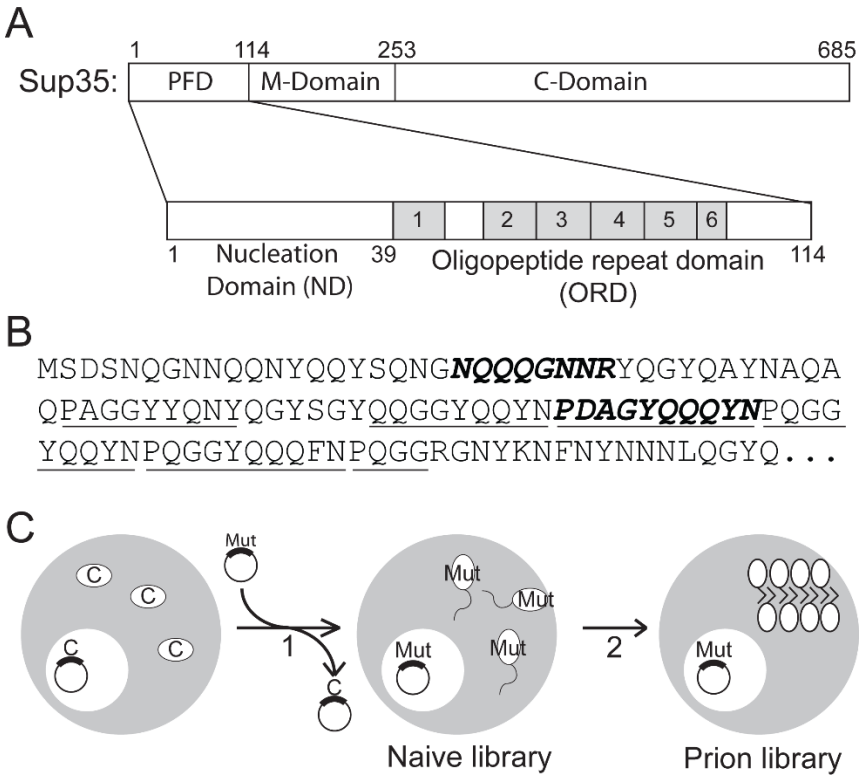

Figure A.1: Prion formation library experiment.
(A) Schematic of Sup35. The PFD is enlarged below, showing the nucleation domain (ND) and ORD. (B) Sequence of Sup35. The oligopeptide repeats are underlined. The region of the ND and ORD targeted for mutagenesis are in bold italics. (C) Experimental scheme for prion formation library experiments. [psi–] cells in which Sup35C was expressed from a URA3 plasmid as the sole copy of Sup35 were transformed with randomly mutated version of Sup35 and then selected for loss of the wild-type plasmid (Step 1). Cells were screened to remove clones in which the mutant Sup35 had compromised activity and randomly selected clones were sequenced to generate the naïve library. The library was then screened for clones that could form and propagate prions (Step 2).

third repeat (amino acids 65-74) was targeted because this repeat is important for efficient prion maintenance, but dispensable for prion nucleation or fiber growth (22).

We utilized an oligonucleotide-based mutagenesis method to build each library (13). Oligonucleotides were designed to anneal to the regions flanking the site of mutagenesis, but with the target codons replaced with the sequence $(NNB)_n$, where N is any of the four nucleotides, B is any of the nucleotides except adenine, and *n* is number of targeted codons (8 for the ND library and 10 for the ORD library). Disallowing adenine at the final position eliminates two of the three stop codons, while still allowing all 20 amino acids to be incorporated in the mutated region. PCR with these oligonucleotides was used to create libraries of randomly mutated versions of *SUP35,* which were then transformed into yeast cells in which *SUP35C* was expressed from a plasmid as the sole copy of *SUP35* in the cell. Through plasmid shuffling, the *SUP35C* expressing plasmid was replaced with the random library (Figure A.1C). Prion formation by Sup35 is extremely rare without PFD overexpression, and only a small fraction of library mutants were expected to form prions. Therefore, to enhance prion detection, a *ppq1* strain was used; this mutation enhances [*PSI*$^+$] formation by approximately 10-fold (46).

The prion-forming libraries were screened as previously described (13). Briefly, to remove any clones that might have compromised Sup35 activity, each clone was first screened for Sup35 activity by monitoring nonsense suppression of the *ade2-1* allele (47). *ade2-1* mutants are unable to grow in the absence of adenine and turn red in the presence of limiting adenine. [*PSI*$^+$] causes stop-codon read-through, allowing for growth without adenine and white or pink colony formation in the presence of limiting

adenine. Colonies that grew red on limiting adenine and did not grow without adenine were pooled into mini-libraries consisting of ~80 mutants. Sup35 was sequenced from randomly selected clones to generate a naïve library data set.

The mini-libraries were plated onto SC-ade to select for prion formation. Ade^+ colonies can result from either DNA mutation or prion formation. To distinguish between these, Ade^+ cells were grown on YPD with and without guanidine HCl, and then restreaked onto YPD to test for loss of the Ade^+ phenotype. Guanidine HCl cures [*PSI*$^+$] (48) by inhibiting Hsp104 activity (49, 50). Cells that lost the Ade^+ phenotype after growth on guanidine HCl, but maintained the Ade^+ phenotype after growth on YPD were considered prion-positive, and were sequenced.

Compositional biases among the ND and ORD prion-forming isolates

For each amino acid, an odds ratio was determined, which represents the degree of over- or underrepresentation of that amino acid among the [*PSI*$^+$] isolates ((13); Table A.2). In many cases, the odds ratios for individual amino acids carry large confidence intervals due to limitation of the library sample sizes. This is particularly true for Met, Trp, Lys, Gln and Glu; because adenine was excluded at the third position of each codon, each was only encoded for by a single codon, and thus each was quite rare among the libraries (Table A.2). Nevertheless, there was a strong correlation (P=0.016 by Spearman rank analysis) between the odds ratios for the ND library and our previously determined odds ratios based on mutagenesis of Sup35-27 (13), a version of Sup35 with a scrambled PFD (Table A.3). Excluding the five single-codon amino acids further strengthened this correlation (P=0.0064).

Table A.2: Amino acid representation within the libraries.

Amino Acid(s)	ND prion formation library [a]			ORD prion formation library [b]			Prion maintenance library [c]		
	Frequency		Odds ratio [d]	Frequency		Odds ratio [a]	Frequency		Odds ratio [e]
	Selected [*PSI*$^+$] library	Unselected naïve library		Selected [*PSI*$^+$] library	Unselected naïve library		White [*PSI*$^+$] colonies	Red [*psi*$^-$] colonies	
Alanine	0.053	0.055	0.96	0.095	0.068	1.40	0.089	0.069	1.32
Arginine	0.024	0.095	0.26***	0.044	0.107	0.41**	0.054	0.121	0.41****
Asparagine	0.061	0.031	1.95	0.047	0.021	2.24	0.038	0.032	1.20
Aspartic Acid	0.028	0.046	0.60	0.033	0.058	0.57	0.054	0.064	0.83
Cysteine	0.065	0.071	0.91	0.084	0.062	1.35	0.072	0.047	1.58*
Glutamic Acid	0.003	0.008	0.42	0.006	0.012	0.53	0.015	0.006	2.70
Glutamine	0.007	0.016	0.41	0.003	0.003	0.94	0.008	0.007	1.12
Glycine	0.13	0.213	0.61*	0.144	0.151	0.95	0.114	0.109	1.05
Histidine	0.031	0.029	1.08	0.047	0.038	1.26	0.04	0.043	0.94
Isoleucine	0.088	0.055	1.60	0.04	0.058	0.69	0.025	0.043	0.57
Leucine	0.065	0.071	0.91	0.058	0.06	0.96	0.04	0.063	0.62*
Lysine	0	0	N/A	0.016	0.009	0.31	0	0.003	0.00
Methionine	0.014	0.014	0.96	0.088	0.06	1.89	0.002	0.009	0.17
Phenylalanine	0.121	0.042	2.88***	0.037	0.053	1.45	0.068	0.049	1.40
Proline	0.017	0.035	0.48	0.123	0.113	0.70	0.048	0.045	1.07
Serine	0.109	0.125	0.87	0.04	0.038	1.09	0.12	0.102	1.20
Threonine	0.061	0.042	1.45	0.016	0.016	1.07	0.037	0.039	0.94
Tryptophan	0.014	0.021	0.67	0.076	0.055	1.04	0.018	0.005	4.07*
Tyrosine	0.069	0.042	1.63	0.076	0.086	1.40	0.074	0.028	2.81***
Valine	0.125	0.078	1.60	0.095	0.068	0.89	0.085	0.116	0.70*
Groups									
Charged (DEKR)	0.054	0.139	0.35***	0.129	0.210	0.43***	0.123	0.194	0.58***
Non-aromatic hydrophobic (ILMV)	0.267	0.206	1.41	0.181	0.200	0.88	0.151	0.231	0.59****
Prion-promoting non-aromatic hydrophobic (IMV)	0.206	0.139	1.61*	0.126	0.143	0.86	0.111	0.168	0.62**
Aromatic (FWY)	0.186	0.101	2.04**	0.168	0.124	1.42	0.160	0.082	2.14***
Polar (NQST)	0.220	0.198	1.14	0.197	0.162	1.27	0.203	0.180	1.16

[a] The ND library consists of 37 selected [*PSI*$^+$] sequences (296 amino acids) and 62 unselected sequences (496 amino acids).
[b] The ORD prion formation library consists of 31 selected [*PSI*$^+$] sequences (310 amino acids) and 58 unselected sequences (580 amino acids).
[c] The prion maintenance library consists of 65 white [*PSI*$^+$] sequences (650 amino acids) and 87 red [*psi*$^-$] sequences (870 amino acids).

[d] Odds ratios reflect the degree of over-representation or under-representation of each amino acid among the prion-forming isolates, as calculated in Equation 1. Values above 1 indicate over-representation among prion-forming isolates. Statistical significance of the over/under-representation is indicated (*, $P < 0.05$; **, $P < 0.01$; ***, $P < 0.001$; ****, $P < 0.0001$).
[e] Odds ratios reflect the degree of over-representation or under-representation of each amino acid among the white (prion-propagating) isolates, as calculated in Equation 3.

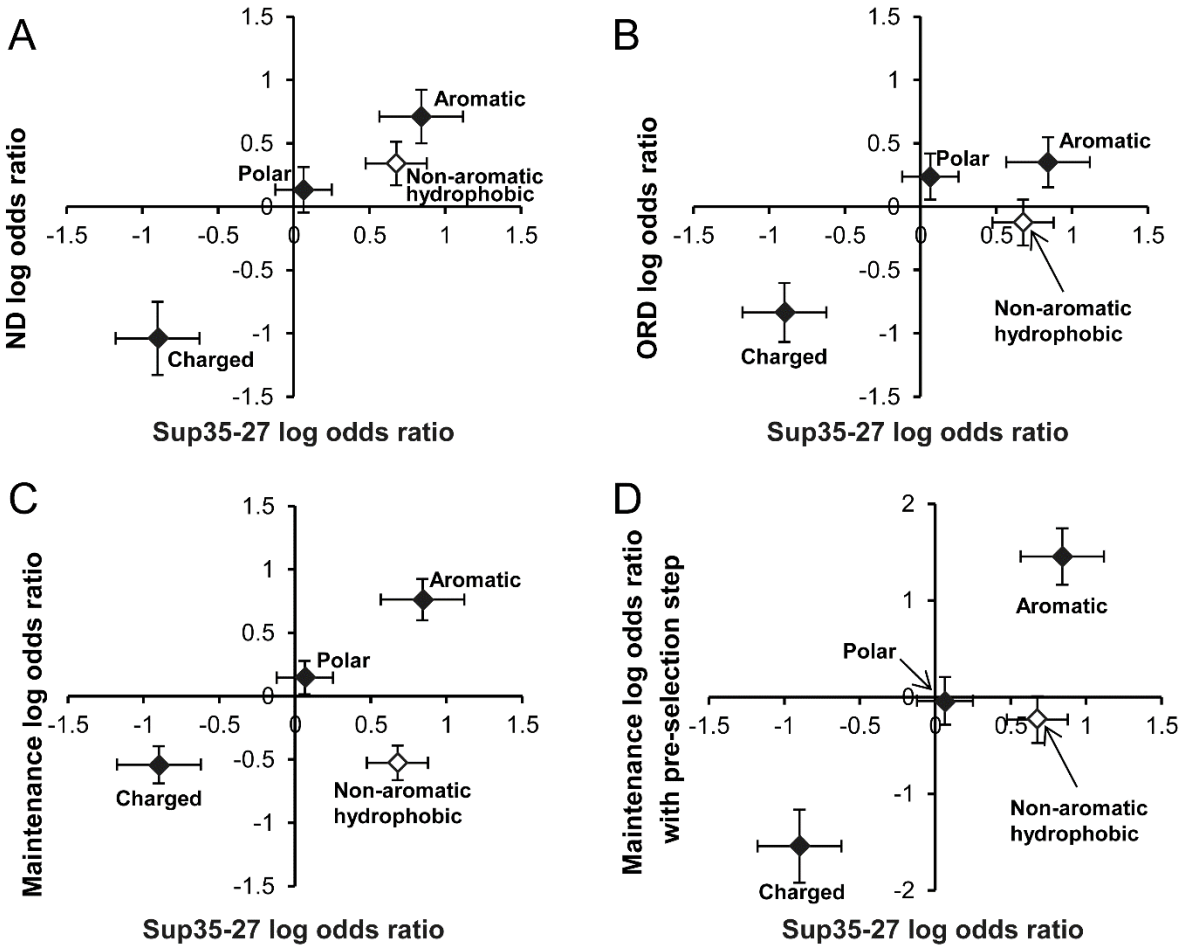

Figure A.2: Non-aromatic hydrophobic residues show different prion formation and maintenance propensities.
Comparison of the previously-determined log odds ratios based on mutagenesis of Sup35-27 (13) was undertaken to the log odds ratios from the ND (A) or ORD (B) prion formation library experiments, the ORD prion maintenance library experiment (C), or the prion propagation library experiment in which an additional step was added to remove mutants that were not efficiently recruited into wild-type prion aggregates (D). While the odds ratios for charged, aromatic and polar residues (filled diamonds) show similar trends in each library, non-aromatic hydrophobic residues (open diamonds) score substantially worse in the ORD prion formation and maintenance libraries. Charged residues are Asp, Glu, Lys, and Arg. Polar residues are Ser, Thr, Asn, and Gln. Aromatic residues are Trp, Tyr, and Phe. Non-aromatic hydrophobic residues are Leu, Ile, Val and Met. Error bars indicate standard errors, calculated as in Equation 5.

Table A.3: Comparison of prion propensity and prion maintenance propensity scores from each library.

Amino acid(s)[a]	Prion propensity scores for each prion formation library[b]			Prion maintenance propensity scores[c]
	Sup35-27[d]	Sup35 ND	Sup35 ORD	
Phenylalanine	0.84	1.06	0.37	0.33
Isoleucine	0.81	0.47	-0.37*	-0.57*
Valine	0.81	0.47	-0.12*	-0.35*
Tyrosine	0.78	0.49	0.34	1.03
Methionine	0.67	-0.04	0.63	-1.80*
Tryptophan	0.67	-0.41	0.039	1.40
Cysteine	0.42	-0.10	0.30	0.45
Serine	0.13	-0.14	0.084	0.18
Asparagine	0.08	0.67	0.81	0.18
Glutamine	0.069	-0.88	-0.067	0.11
Glycine	-0.039	-0.49	-0.047	0.047
Leucine	-0.04	-0.10	-0.039	-0.48
Threonine	-0.12	0.37	0.069	-0.059
Histidine	-0.28	0.077	0.23	-0.064
Alanine	-0.40	-0.036	0.34	0.28
Arginine	-0.41	-1.37	-0.89	-0.88
Glutamic Acid	-0.61	-0.87	-0.63	0.99
Proline	-1.20	-0.73	-0.36	0.065*
Aspartic Acid	-1.28	-0.51	-0.56	-0.19
Lysine	-1.58	N/A[e]	-1.17	N/A[e]
Groups				
Charged (DEKR)	-0.90	-1.04	-0.83	-0.54
Hydrophobic (ILMV)	0.68	0.34	-0.13**	-0.53****
Prion-promoting non-aromatic hydrophobic (IMV)	0.88	0.47	-0.15***	-0.48****
Aromatic (FWY)	0.84	0.71	0.35	0.76
Polar (NQST)	0.064	0.13	0.24	0.15

[a] Amino acids are listed in the order of their prion propensities according to PAPA.
[b] Prion formation libraries were performed as in Figure A.1C. Prion propensity scores are calculated as the natural log of the odds ratios from Equation 2. Statistically significant differences relative to the Sup35-27 library (13) are indicated (*, $P < 0.05$; **, $P < 0.01$; ***, $P < 0.001$; ****, $P < 0.0001$).
[c] The prion maintenance library experiment was performed as in Figure A.1D. Prion maintenance propensity scores are calculated as in Equation 4. Statistically significant differences relative to the Sup35-27 library (13) are indicated (*, $P < 0.05$; **, $P < 0.01$; ***, $P < 0.001$; ****, $P < 0.0001$).
[d] From Toombs *et al.* (13)
[e] Lysine was not found in any of the prion-forming sequences in the ND library or in any of the white colonies in the prion propagation library.

Grouping similar amino acids can effectively increase sample sizes, thereby improving statistical significance. Doing so confirmed that the same broad trends observed for Sup35-27 were seen in the ND library, with both aromatic and non-aromatic hydrophobic residues promoting prion activity, and charged residues strongly inhibiting prion activity (Figure A.2A).

There was also a statistically significant correlation between our previous Sup35-27 odds ratios and those for the ORD library (P=0.017). As in the ND and Sup35-27 libraries, there was a statistically significant bias against charged residues among prion-forming sequences in the ORD library (P=0.0002; Table A.2) and an over-representation of aromatic residues, albeit below the threshold for statistical significance (P=0.084;Table A.2). However, there was one striking difference. With the exception of leucine (which is known to have a low β-sheet propensity; (51), the non-aromatic hydrophobic residues (Ile, Val and Met) were highly enriched among prion-forming sequences in both the Sup35-27 library (P=0.0001) and the ND library (P=0.017), yet they were actually modestly under-represented among prion-forming sequences in the ORD library (Table A.3). The differences between the ORD library and both the Sup35-27 and ND libraries were both statistically significant (Table A.3; P=0.0031 and 0.029, respectively), demonstrating that these residues have significantly different effects in these locations.

Prion maintenance library experiments with the SUP35 ORD

The simplest explanation for the different biases observed in the ND versus ORD is that these differences reflect the distinct functions of the two regions (16, 23–25), and thus that non-aromatic hydrophobic residues promote prion formation, but not prion

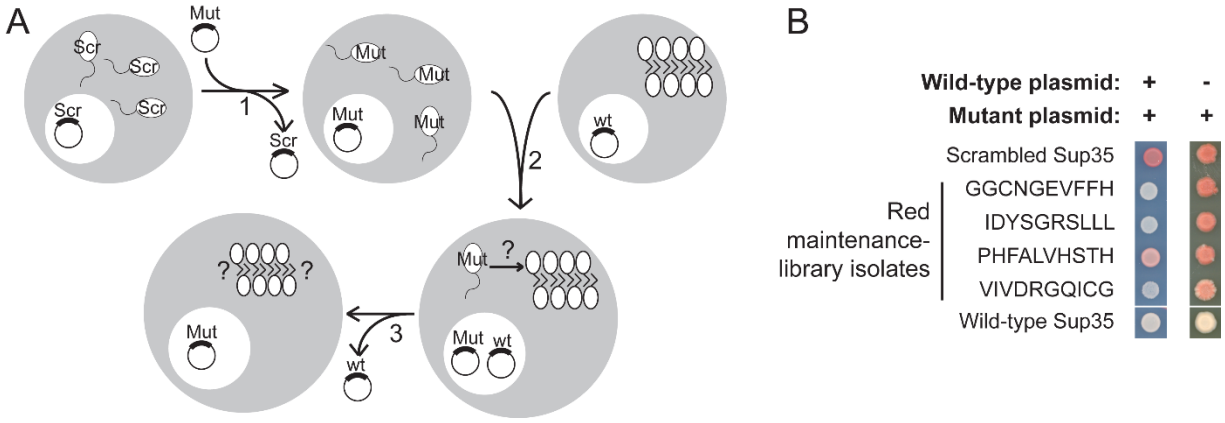

Figure A.3: Prion maintenance library experiments.
(A) Experimental scheme. [psi–] cells in which Sup35C was expressed from a URA3 plasmid as the sole copy of Sup35 were transformed with randomly mutated version of Sup35 and then selected for loss of the wild-type plasmid (Step 1). These cells were mated with wild-type [PSI+] cells in which the sole copy of Sup35 was expressed from a URA3 plasmid (Step 2). After selection for loss of the URA3 plasmid (Step 3), red and white clones were sequenced. In the modified protocol to select against mutants with a defect in adding onto wild-type aggregates, selection for diploid cells in Step 2 was done in the absence of adenine. (B) Plasmids expressing mutant Sup35s from individual red prion maintenance library isolates were transformed into [PSI+] cells in which the sole copy of Sup35 was expressed from a URA3 plasmid. To test whether the mutant Sup35s are inactivated in the presence of wild-type [PSI+], cells were plated on limiting adenine medium selecting for both the wild-type and mutant Sup35-expressing plasmids (left). Cells were then retested on YPD after selection for loss of the wild-type plasmid (right). Representative examples are shown, with the sequences of the mutagenized regions indicated. Sup35-27, a scrambled version of Sup35 that is not incorporated into wild-type [PSI+] aggregates, and wild-type Sup35, are shown as controls.

maintenance. However, the functional separation between the two regions is not absolute, so it is possible that some of the ORD biases that we observed were due to effects on prion formation.

Therefore, we adapted our library screening method to specifically isolate the effects of composition on prion maintenance (Figure A.3A). We constructed a second ORD library as above, but this time assessed the ability of mutants to maintain an existing prion. To accomplish this, we utilized a two-step process. Because our plasmid libraries were constructed directly in yeast using homologous recombination (by co-transforming a mutagenized PCR product and a linearized vector), the libraries were inevitably contaminated with products of recombination between the initial Sup35 maintenance plasmid that was present in the cell and the linearized vector. Thus, when the libraries were built directly in a [*PSI*$^{+}$] cell, because prion-propagating mutants are relatively rare, a large fraction of the prion-propagating clones turned out to contain wild-type Sup35 (data not shown). To avoid this problem, the libraries were constructed in a [*psi*$^{-}$] strain expressing scrambled Sup35 (Sup35-27) from a *URA3* plasmid as the sole copy of Sup35 in the cell. After transformation, we selected for loss of the *URA3* plasmid, so that the library mutants were the sole copy of Sup35. These cells were then mated with wild-type [*PSI*$^{+}$] cells in which the sole copy of Sup35 was again expressed from a *URA3* plasmid. After selection for diploids and for loss of the *URA3* plasmid, clones were plated for single colonies and screened for Sup35 activity using the *ade2-1* allele. Because Sup35-27 is unable to propagate wild-type [*PSI*$^{+}$], any spurious recombination events between the Sup35-27 maintenance plasmid and the linearized

vector during the cloning step would result in [*psi*$^-$] cells. These Sup35-27 clones were excluded from our analysis.

Red colonies were deemed to have lost [*PSI*$^+$]. By contrast, colonies were considered capable of efficiently maintaining [*PSI*$^+$] if they were white on YPD, and stably maintained this white phenotype upon restreaking on YPD, but grew red on YPD after guanidine treatment. Clones of intermediate phenotype (which were substantially pink or sectored on YPD, or that were initially white on YPD, but showed any loss of the prion upon restreaking on non-selective medium) were excluded from the study. A total of 65 distinct white mutants and 87 red mutants were sequenced.

Compositional biases among the propagating prion isolates

For each of the amino acids, an odds ratio was calculated as in Equation 3. Six amino acids showed statistically significant differences between the prion-maintaining (white) and prion-losing (red) isolates: Trp, Tyr, and Cys were significantly overrepresented among the prion-maintaining isolates, while Val, Leu, and Arg were significantly underrepresented (Table A.2). When chemically-similar amino acids were grouped together, aromatic amino acids were overrepresented among the [*PSI*$^+$] isolates ($P<10^{-4}$) and charged residues were underrepresented (P=0.0002), as in each of the previous libraries; however, non-aromatic hydrophobic residues were substantially underrepresented ($P=10^{-4}$). Thus, focusing specifically on prion maintenance amplified the previously observed differences seen between the ND and ORD libraries for non-aromatic hydrophobic residues (Figure A.2B,C). The differences observed for non-aromatic hydrophobic residues between the ORD prion-propagating library experiments and both Sup35-27 and the ND were highly statistically significant

($P<10^{-4}$). Interestingly, even the difference between the ORD prion-propagating experiments and the original ORD library experiments approached statistical significance (P=0.077), suggesting that in the original ORD experiments, non-aromatic hydrophobics may have had partially offsetting effects, promoting prion formation while inhibiting prion maintenance.

ORD mutants that failed to maintain [PSI$^+$] were not due to failure to add on to existing wild-type aggregates

In the prion-maintenance library experiments, a protein could fail to maintain [*PSI*$^+$] for one of two reasons: a mutant could fail to add onto the pre-existing wild-type aggregates (Figure A.3A, after Step 2), or the mutant could successfully add onto pre-existing aggregates, but have a defect in the subsequent prion-maintenance steps (Figure A.3A, after Step 3). To distinguish between these two possibilities, plasmids expressing mutant *SUP35* from individual non-propagating clones were isolated and re-transformed into wild-type [*PSI*$^+$] cells. The phenotype of transformants was examined before and after selection for the loss of wild-type plasmid (analogous to before and after Step 3 in Figure A.3A). If a mutant is unable to add onto the preexisting wild-type aggregates, then it should remain soluble (active) even in the presence of wild-type [*PSI*$^+$], resulting in a red phenotype (Figure A.3B). Of the 14 clones examined, none were fully red when the wild-type and mutant proteins were co-expressed, although three (FYSVSILDRR, GCPRVVIHVD, PHFALVHSTH) showed a mild pink phenotype, suggesting a slightly reduced efficiency of adding on to wild-type aggregates or a partially dominant defect in prion aggregate fragmentation; by contrast, all 14 were red or highly sectored after loss of the wild-type plasmid (Figure A.3B and data not shown).

These results indicate that the majority of library sequences that failed to maintain [*PSI*$^{+}$] were competent for adding onto the pre-existing wild-type aggregates, but had a defect in the subsequent maintenance steps. However, it remained possible that rare mutants with a defect in addition to pre-existing aggregates could skew the results of the library screen. To more comprehensively examine this issue, the library experiment was repeated with an additional selection step to remove such mutants. After mating the mutant library strains with wild-type [*PSI*$^{+}$]-containing cells (Figure A.3A, Step 2), the selection step to select for diploid cells was undertaken in the absence of adenine; this selects against mutants that remain functional in the presence of wild-type [*PSI*$^{+}$] (i.e., that are not efficiently incorporated into [*PSI*$^{+}$] aggregates). Then, after selecting for loss of the wild-type plasmid, each clone was examined as before for its ability to propagate [*PSI*$^{+}$] when expressed as the sole copy in the cell. This method has the substantial downside that it adds an additional prion selection step; nevertheless, it allowed us to confirm that selecting against mutants with a defect in adding to pre-existing aggregates did not substantially change the outcome. With a smaller set of 19 prion-maintaining mutants and 26 non-propagators, the broad trends from the original maintenance library held in this altered experimental system (Figure A.2 C,D).

Predicting propagating versus non-propagating sequences

To assess whether the biases seen in the prion-maintenance library experiments were sufficient to predict the behavior of individual library isolates, we used the standard leave-one-out method of cross-validation. Briefly, there were 152 sequences in the prion maintenance library dataset (65 white and 87 red). To calculate the prion maintenance

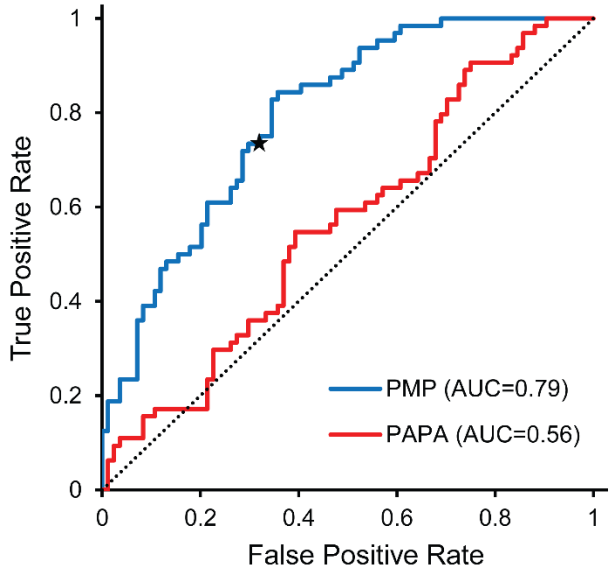

Figure A.4: ROC (receiver operator characteristic) plot (52) assessing the ability of prion maintenance propensity (PMP) scores and PAPA to predict the prion-propagating library mutants.
A leave-one-out method of cross was used to assess whether PMP scores from the prion maintenance library experiment are sufficient to predict which library members will successfully propagate [PSI+]. PMP scores showed reasonable prediction accuracy (AUC=0.79); the star indicates the point on the ROC plot for a PMP score of zero. PAPA showed virtually no ability to distinguish between red and white isolates (AUC=0.56), with prediction accuracy barely above what would be expected by random chance (dotted line). False positive rate = (Number of red isolates scored as prion-propagating)/(total number of red isolates). True positive rate = (Number of white isolates scored as prion-propagating)/(total number of red isolates)

propensity (PMP) score for each sequence, the sequence was excluded (i.e., “left out”) from the dataset, and the remaining 151 sequences were used to calculate prion maintenance propensity scores for each amino (PMP_{aa}) acid using Equation 4. The PMP score for the excluded sequence was then calculated as the sum of the PMP_{aa} values for each of the ten amino acids in the mutated region. This process was iteratively repeated for all 152 sequences. White clones had significantly higher PMP scores ($P<0.0001$ by two-sided t test) than red clones, although there was significant overlap between the two sets (Figure A.4). For example, 73.4% of the white clones had positive PMP scores, while only 32% of the red clones did, and the 26 lowest-scoring sequences were all red. By contrast, PAPA showed almost no ability to distinguish between the red and white clones (Figure A.4), consistent with the idea that PAPA is better correlated with prion formation propensity than prion maintenance propensity (Figure A.2). We then tested whether the observed PMP_{aa} values from the full library dataset (Table A.3) were sufficient to rationally design sequences that could substitute for the third repeat of the ORD (the region mutagenized in the ORD library experiments) in supporting prion propagation. We constructed a random library of 10-amino-acid segments *in silico*, and then used the PMP scores to identify segments with predicted high or low prion maintenance propensity. Six of the randomly-designed sequences that were predicted to be very good at maintaining [*PSI*$^+$] (in the 95th percentile among the *in silico* library) and six versions predicted to maintain [*PSI*$^+$] poorly (5th percentile) were inserted in the place of the third repeat. Plasmids expressing these mutants were transformed into wild-type [*PSI*$^+$] cells in which the sole copy of Sup35 was expressed from a plasmid. After selection for loss of wild-type plasmid, cells were examined for

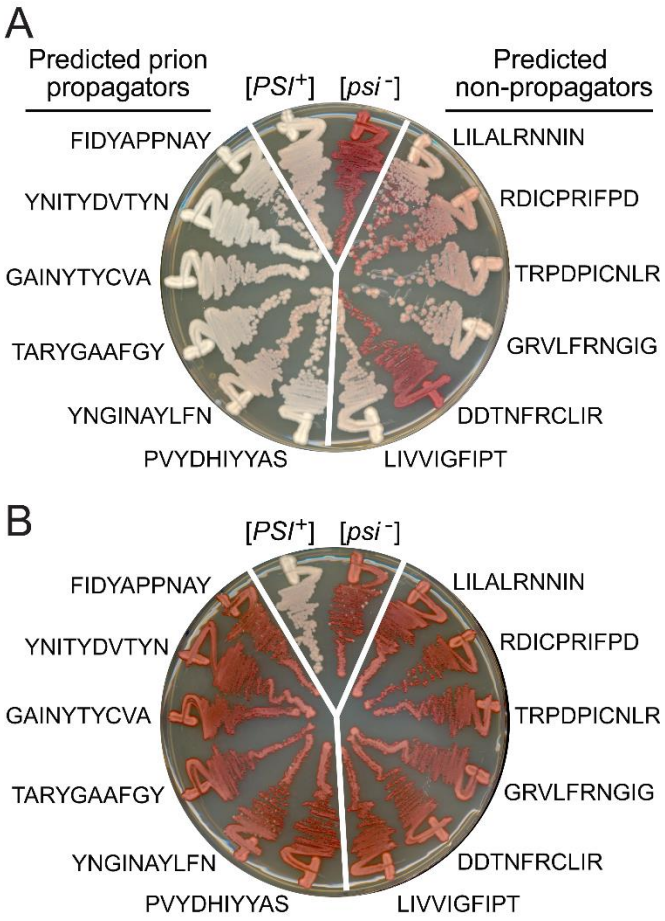

Figure A.5: Successful design of prion-propagating sequences.
A library of random 10-amino-acid sequences was built in silico. The library was screened using the PMP scores from the ORD prion propagation library experiment. Six high-scoring sequences (left side of each panel) and six low-scoring sequences (right side) were selected and inserted into Sup35 in the place of the third repeat of the ORD. Mutants were introduced to wild-type [PSI+] cells. Transformants were spotted onto 5-FOA to select for loss of the plasmid expressing wild-type Sup35, and either: (A) streaked onto YPD medium to test for loss of [PSI+]; or (B) streaked onto SC medium plus 4 mM guanidine HCl, and then streaked onto YPD medium to test for loss of [PSI+]. Untreated wild-type [PSI+] and [psi-] cells are shown as a control.

[*PSI*$^{+}$] loss (Figure A.5A). While all six predicted prion maintaining mutants were uniformly white when plated on YPD (Figure A.5A, left side), the predicted non-propagators were more variable. Three clones showed a mixture of red and white colonies, reflecting a high degree of prion loss, while the others showed only very modest pink phenotypes (Figure A.5A, right side). All 12 mutants were red after treatment with guanidine HCl (Figure A.5B). Collectively, these results suggest that our PMP values are sufficient to identify broad trends, but not sufficient to predict whether a given sequence will support prion maintenance.

Essential role for aromatic residues in prion maintenance

We designed targeted mutations to further examine the differences between the effects of aromatic and non-aromatic residues on [*PSI*$^{+}$] maintenance. The Sup35 PFD contains 20 Tyr residues, one Phe, and no Trp, Ile or Val. Five of the Tyr residues are located in the ND, and non-aromatic hydrophobic residues can substitute for these ND tyrosines in supporting prion activity (42). Here, we examined the effects of substituting different residues for Tyr in the ORD.

We replaced the five tyrosine residues in the third, fourth and fifth repeat of the ORD with Ala, Val, Ile, Leu, Met, Phe, or Trp. Each mutant was transformed into a wild type [*PSI*$^{+}$] cell in which the sole copy of Sup35 was expressed from a plasmid. After selection for loss of the wild-type plasmid, only the two constructs with aromatic substitutions were able to stably maintain [*PSI*$^{+}$] (Figure A.6A). Prion loss was not due to inability to be recruited to pre-existing Sup35 aggregates. When GFP fusions of each mutant PFD were transiently expressed for 2 h in wild-type [*psi*$^{-}$] cells, each remained diffuse (Figure A.6B); however, when the GFP fusions were transiently expressed in

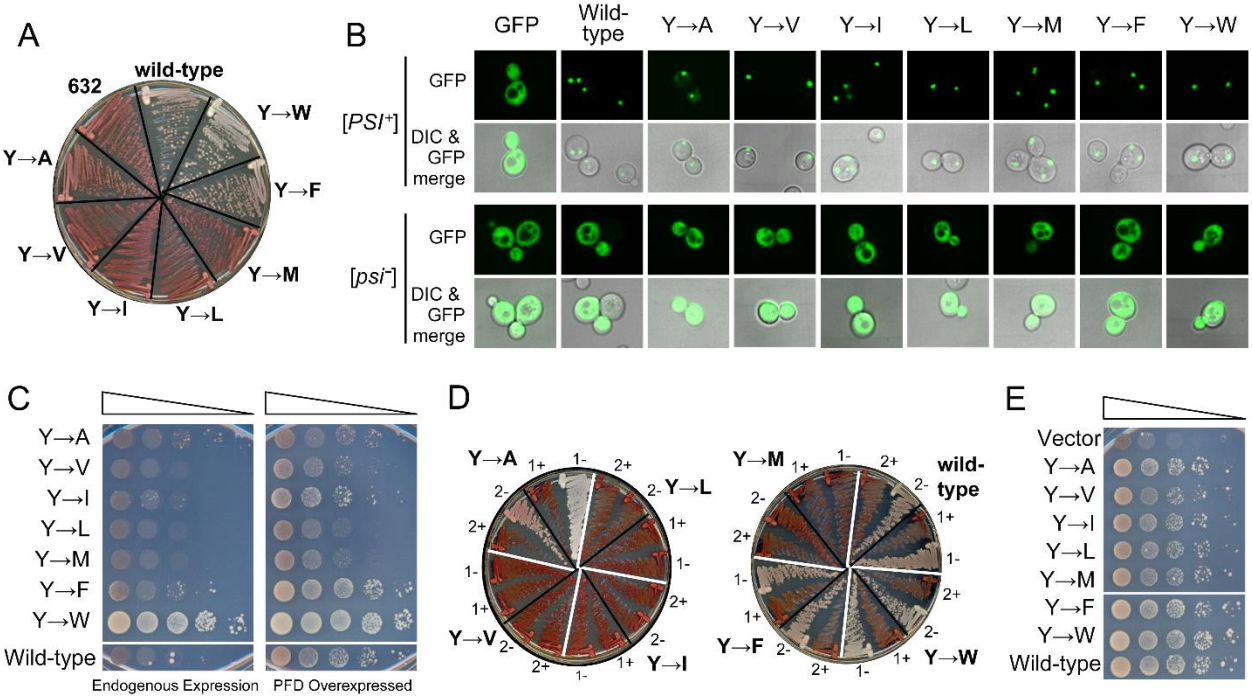

Figure A.6: Aromatic residues in the ORD are critical for prion propagation. (A) Prion maintenance by tyrosine substitution mutants. The five tyrosines in repeats 3-5 of the Sup35 ORD were replaced with Ala, Val, Ile, Leu, Met, Phe or Trp. These mutants were introduced into wild-type [PSI+] cells expressing wild-type Sup35 from a plasmid. After selection for loss of the wild-type plasmid, cells were streaked onto YPD medium to test for the ability to maintain [PSI+]. (B) Tyrosine substitution mutants are efficiently incorporated into wild-type [PSI+] aggregates. Plasmids expressing GFP fusions of each tyrosine substitution mutant PFD under control of the GAL1 promoter were transformed into wild-type [PSI+] and [psi-] strains. Cells were grown in galactose/raffinose dropout medium for two hours and visualized by confocal microscopy. Foci were observed for each fusion in [PSI+] cells, but not [psi-] cells. (C) Prion formation by tyrosine substitution mutants. [psi-] strains expressing each mutant as the sole copy of Sup35 were transformed either with an empty vector (left) or with a plasmid expressing the matching Sup35 mutant under control of the GAL1 promoter (right). All strains were cultured for three days in galactose/raffinose dropout medium, and then 10-fold serial dilutions were plated onto medium lacking adenine to select for [PSI+]. (D) Tryptophan, alanine and phenylalanine substitution mutants form stable, curable prions. Ade+ isolates from panel B were streaked onto either SC medium (-) or SC plus 3 mM guanidine HCl (+) and then restreaked onto YPD to test for prion loss. Two representative Ade+ isolates are shown for each mutant. (E) Overexpression of the tyrosine substitution mutants induces wild-type [PSI+] formation. Yeast expressing wild-type Sup35 were transformed with either an empty vector (vector), or the vector modified to express either the wild-type Sup35 NM domain (wild-type) or the NM domain of the ORD tyrosine substitution mutants under control of the GAL1 promoter. Cells were then tested for [PSI+] formation.

[*PSI*$^+$] cells, each rapidly coalesced into foci (Figure A.6B), indicating that the mutants were efficiently recruited into wild-type [*PSI*$^+$] aggregates.

Although these results suggest that substitution of ORD tyrosines with non-aromatic hydrophobic residues results in a defect in [*PSI*$^+$] maintenance, it remained possible that these constructs are able to maintain some variant of [*PSI*$^+$], but just not the specific [*PSI*$^+$] variant present in these cells. Therefore, each of the mutants was tested for the ability to form [*PSI*$^+$] *de novo* when expressed as the sole copy of Sup35 in the cell. Cells were grown either with or without overexpression of the matching PFD, and then plated onto SC-ade medium to test for prion formation. PFD overexpression increases prion formation by increasing the probability of the initial prion-forming nucleation events (5). All of the constructs were able to form Ade$^+$ colonies upon PFD overexpression (Figure A.6C), albeit with varying frequencies; in fact, the Trp substitutions actually substantially increased prion formation. However, the Ade$^+$ colonies formed by the Phe and Trp substitution constructs, and to a lesser extent by the Ile construct, were substantially bigger than those formed by the Ala, Val, Leu or Met constructs. Furthermore, as in the plasmid shuffling experiments (Figure A.6A), Phe and Trp constructs were able to consistently maintain a white [*PSI*$^+$] phenotype when passage on YPD medium, while the Val, Ile, Leu and Met Ade$^+$ isolates all reverted to a red phenotype after growth on non-selective medium (Figure A.6D). The only mutant that behaved differently from the shuffling experiment was the Ala substitution mutant, which was able to form rare stable, curable prions (Figure A.6D).

The low frequency of Ade$^+$ colonies seen for some of the mutants (Figure A.6C) could be due to either a defect in prion nucleation, or in maintenance of prion

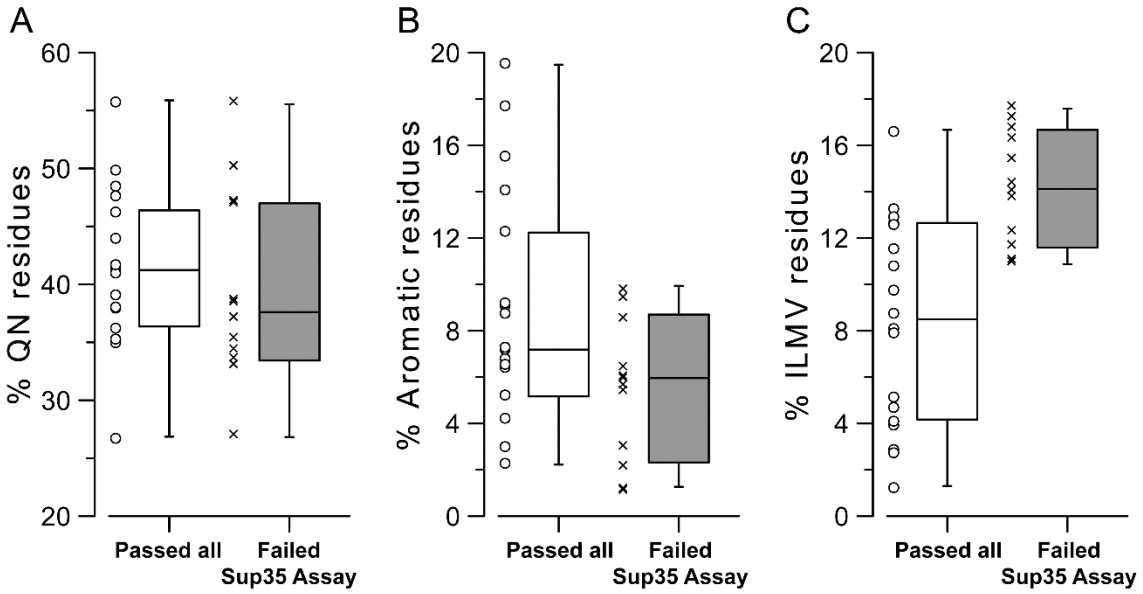

Figure A.7: Aromatic residues are overrepresented and non-aromatic hydrophobics underrepresented among domains with prion activity.
Alberti *et al*. (12) tested 100 prion-like domains in four assays for prion-like activity. Three of the assays tested aggregation activity, while a fourth tested the ability of the domains to support prion activity when inserted in the place of the Sup35 PFD. Box and whiskers plots show the frequency of Q/N residues (A), aromatic residues (B), and non-aromatic hydrophobic residues (C; Ile, Leu, Met, and Val) among each of the Alberti proteins that passed all tests (white bars) or that passed all tests except the Sup35-fusion protein assay (gray bars).

aggregates. However, overexpression of each of the mutants efficiently stimulated wild-type Sup35 to form prions, suggesting that these mutants do not have a nucleation defect (Figure A.6E). Collectively, these results indicate that the mutants containing non-aromatic hydrophobic replacements for tyrosine are able to efficiently aggregate, but are unable to stably propagate these aggregates as prions.

Yeast PFDs that successfully propagate show similar compositional biases

Alberti *et al.* previously generated a large data set in which the 100 yeast protein fragments (averaging about 160 amino acids in length) with the greatest compositionally similarity to the Sup35, Ure2, Rnq1, and New1 PFDs were tested in four distinct assays of prion-like activity (12). The four assays used in this study included three measures of aggregation (formation of fluorescent foci when expressed as an EYFP fusion; formation of SDS-resistant aggregates in an SDD-AGE assay; and *in vitro* aggregation of purified recombinant proteins, as monitored by thioflavin-T fluorescence) and one assay (replacement of the PFD of Sup35 with a portion of each ORF) that tested for the ability to support true prion activity (12).

Eighteen of the fragments in the dataset passed all four assays (12). Another 12 of the passed all three of the aggregation assays, but failed the Sup35 fusion assay; this indicates that these domains have an ability to form aggregates, but may have a defect in prion maintenance, although it is important to note that proteins can fail the Sup35 fusion assay for a variety of reasons, and that even some known PFDs fail in this assay (see Discussion). These two sets had very similar Q/N content (Figure A.7A) and predicted aggregation propensity according to PAPA (data not shown). However, consistent with the results of our library screens, aromatic residues (Figure A.7B) were

overrepresented and non-aromatic hydrophobic residues under-represented (Figure A.7C) among the proteins that passed all four assays. Strikingly, each of the most hydrophobic non-aromatic residues (Ile, Met, Val, and Leu) were more common among the proteins that passed the three aggregation assays but failed the Sup35 assay, although this bias was only statistically significant for Leu and Val (P=0.008 and 0.0002, respectively). While neither the over-representation of aromatics nor the underrepresentation of non-aromatic hydrophobics was absolute, both were statistically significant (P = 0.0003 for non-aromatic hydrophobics and P = 0.05 for aromatics), suggesting that the trends identified in our library experiments may extend to other prion-like domains.

Discussion

We previously showed that the ND and ORD have distinct compositional requirements (26). Here, we make first steps towards quantitatively defining these requirements. Most significantly, we show that aliphatic residues promote prion activity in the ND while inhibiting prion activity in the ORD. It appears that this difference is due to the distinct functions of the two regions in supporting prion activity. Consistent with earlier work suggesting that the ORD is largely dispensable for prion formation (22), replacement of aromatic residues in the ORD with aliphatic residues does not significantly affect the ability of the PFD to nucleate prion formation, but does disrupt maintenance of prion aggregates.

These experiments nicely complement previous work using poly-glutamine to study the effects of amino acid composition on fiber fragmentation (34, 38). Alexandrov *et al.* inserted different residues into polyglutamine stretches and found that aromatic

residues reduce average aggregate size (34). However, there are challenges in interpreting these experiments. While poly-Q forms aggregates, it does not form prions *per se*, and it is not clear how similar the structure of poly-Q aggregates is to prion aggregates; the authors suggest that the uniform sequence of poly-Q likely results in "staggered" aggregates, rather than the ordered, in-register parallel β-sheet aggregates formed by Sup35 (34). Additionally, while smaller aggregate size is consistent with an increase in fiber fragmentation, average aggregate size would also be expected to be a function of the frequency of spontaneous aggregate nucleation and the rate of fiber growth rates. For example, spontaneous nucleation, like fragmentation, creates new independently segregating aggregates; so, if nucleation rates are exceptionally high, such that many nucleation events happen per cell division, this would increase the number of independent aggregates, and thus decrease average aggregate size. The current experiments expand on this previous work by beginning to parse out the specific steps in prion activity affected by each amino acid.

The observation that specific amino acids can have different effects at different positions is itself not surprising or unprecedented. For example, Bondarev *et al.* recently showed that insertion of lysine residues into the first or second repeat of the Sup35 ORD resulted in [*PSI*$^{+}$] loss, but similar insertions in the other repeats did not (53). This result makes sense; the ND and first two repeats of the ORD are required for efficient nucleation of prion formation and for addition to pre-existing [*PSI*$^{+}$] aggregates (22), suggesting that this region forms critical contacts that mediate fiber growth. By contrast, the third through fifth repeats are dispensable for these activities. Therefore, it is not surprising that mutations in the first two repeats might have stronger effects. Indeed, we

saw what may be a similar effect; proline and glycine, both of which have low β-sheet propensities, were better tolerated in the ORD than the ND. However, our results also show something more unexpected – that amino acids that promote prion activity at one region in a PFD can actually inhibit prion activity in other regions.

Although the differences between the amino acid compositions of red and white clones in our prion maintenance library experiments were highly statistically significant, they were not sufficient to predict with 100% accuracy whether a given mutant could propagate prions (Figs. 7.4 and 7.5). Part of this could be due to the large confidence intervals associated with each amino acid's PMP score. Also, factors other than just simple amino acid composition may affect prion maintenance. For example, there may be certain positions where specific amino acids are favored or disfavored. We did not observe any strong positional biases in any of our libraries, but this in part could be due to limitations of our sample sizes. We also examined whether a number of other factors might, in conjunction with PMP score, improve discrimination between the sets. These include presence/absence of groups of amino acids, total number of charges, net charges of each 10-mer, distribution of charges within each 10-mer, hydrophobicity, predicted β-sheet propensity, and disorder propensity. However, none of these improved the discrimination between the propagating and non-propagating sequences compared to PMP scores alone (data not shown).

Similarly, the biases for aromatic residues and against aliphatic residues among domains that can substitute for the Sup35 PFD in supporting prion activity were also not absolute. The prion protein Ure2 is a good example of this. The Ure2 PFD has only two aromatic residues (both F) and 12 non-aromatic hydrophobic residues (I, L, V, and M)

(54). It is possible that other residues that modestly promote prion maintenance can substitute for aromatic residues when present at high enough density; for example, Ure2 has very high Ser and Asn content, both of which scored as modestly promoting prion maintenance in our assays. Alternatively, different prions have different chaperone requirements (55), so the trends that we observed might be specific for the constellation of chaperones that propagate [*PSI*$^{+}$]. Consistent with this, Crist *et al.* (28) identified repeat sequences lacking aromatic residues that could substitute for the Sup35 ORD in supporting prion activity, but the resulting prions were Hsp104-independent. Thus, more detailed comparison of the amino acid compositions and chaperone requirements of different PFDs many provide insight into the mechanism by which specific compositional features promote prion maintenance.

Because of the distinct chaperone requirements for different prions, it may prove difficult to develop a simple method to predict whether a given sequence will be able support prion maintenance. The prion prediction algorithm PAPA is able to effectively discriminate between Q/N-rich proteins that have high versus low aggregation propensity (19), but for proteins that show high aggregation propensity, it is ineffective at predicting which will be able to support full-fledged prion activity. The current experiments explain why; the prion propensity scores that make up PAPA match the ND library scores more closely than the ORD library scores (Figure A.2), suggesting that PAPA predominantly scores aggregation propensity.

There are some important caveats to consider when analyzing constructs in the Sup35 fusion assay (as in Figure A.7). First, Sup35 is an essential gene, so any [*PSI*$^{+}$] prion that too effectively sequesters and inactivates Sup35 will be lethal; indeed, many

spontaneously-formed [*PSI*$^{+}$] variants are lethal (56). Thus, a fragment could fail the Sup35 assay because it forms too strong of a prion variant. Additionally, context does affect prion activity. Some known PFDs fail to support prion activity when fused to Sup35, and conversely, many of the fragments that support prion activity when fused to Sup35 have not yet been shown to form prions in their native context. Therefore, while our analysis may help explain why some prion-like fragments fail in the Sup35 fusion assay, additional experiments will be needed to determine whether similar effects would be seen in other sequence contexts.

Finally, it should be noted that the prion maintenance library experiments were done with a single strong [*PSI*$^{+}$] strain. We chose to use a strong [*PSI*$^{+}$] variant for two reasons. First, it increased the chances that any red clones were due to a prion maintenance defect, as opposed to the spontaneous prion loss that would be common with a weak strain. Second, various evidence suggests that the amyloid core extends further into the ORD in weak prion variants (24, 57), increasing the chances that red isolates could be due to an inability to add onto pre-existing aggregates rather than a defect in the subsequent maintenance steps. The difference in prion maintenance ability between aromatic and aliphatic residues appears to be prion variant independent, as the ORD mutants in which tyrosines were replaced with aliphatic residues not only failed to propagate an existing strong prion variant (Figure A.6A), but were also unable to form their own stable prion variants (Figure A.6D). Nevertheless, it remains possible that some of the other observed biases might be prion variant-dependent.

REFERENCES

1. Chiti F, Dobson CM (2006) Protein misfolding, functional amyloid, and human disease. *Annual review of biochemistry* 75:333–66.
2. Prusiner SB (1982) Novel proteinaceous infectious particles cause scrapie. *Science (New York, NY)* 216(4542):136–44.
3. Prusiner SB (1991) Molecular biology of prion diseases. *Science (New York, NY)* 252(5012):1515–22.
4. Weissmann C (1991) Spongiform encephalopathies. The prion's progress. *Nature* 349(6310):569–71.
5. Wickner RB (1994) [URE3] as an altered URE2 protein: evidence for a prion analog in Saccharomyces cerevisiae. *Science (New York, NY)* 264(5158):566–9.
6. Wickner RB, Masison DC, Edskes HK (1995) [PSI] and [URE3] as yeast prions. *Yeast (Chichester, England)* 11(16):1671–85.
7. Lindquist S (1997) Mad cows meet psi-chotic yeast: the expansion of the prion hypothesis. *Cell* 89(4):495–8.
8. Sondheimer N, Lindquist S (2000) Rnq1: an epigenetic modifier of protein function in yeast. *Molecular cell* 5(1):163–72.
9. Derkatch IL, Bradley ME, Hong JY, Liebman SW (2001) Prions affect the appearance of other prions: the story of [PIN(+)]. *Cell* 106(2):171–82.
10. Michelitsch MD, Weissman JS (2000) A census of glutamine/asparagine-rich regions: implications for their conserved function and the prediction of novel prions. *Proceedings of the National Academy of Sciences of the United States of America* 97(22):11910–5.
11. MacLea KS, Ross ED (2011) Strategies for identifying new prions in yeast. *Prion* 5(4):1–6.
12. Alberti S, Halfmann R, King O, Kapila A, Lindquist S (2009) A Systematic Survey Identifies Prions and Illuminates Sequence Features of Prionogenic Proteins. *Cell* 137(1):146–158.
13. Toombs JA, McCarty BR, Ross ED (2010) Compositional determinants of prion formation in yeast. *Molecular and cellular biology* 30(1):319–32.
14. Ter-Avanesyan MD, et al. (1993) Deletion analysis of the SUP35 gene of the yeast Saccharomyces cerevisiae reveals two non-overlapping functional regions in the encoded protein. *Molecular microbiology* 7(5):683–92.
15. Ter-Avanesyan MD, Dagkesamanskaya AR, Kushnirov V V, Smirnov VN (1994) The SUP35 omnipotent suppressor gene is involved in the maintenance of the non-Mendelian determinant [psi+] in the yeast Saccharomyces cerevisiae. *Genetics* 137(3):671–6.
16. DePace AH, Santoso A, Hillner P, Weissman JS (1998) A critical role for amino-terminal glutamine/asparagine repeats in the formation and propagation of a yeast prion. *Cell* 93(7):1241–52.
17. Liu J-J, Sondheimer N, Lindquist SL (2002) Changes in the middle region of Sup35 profoundly alter the nature of epigenetic inheritance for the yeast prion [PSI+]. *Proceedings of the National Academy of Sciences of the United States of*

America 99 Suppl 4:16446–53.
18. Ross ED, Edskes HK, Terry MJ, Wickner RB (2005) Primary sequence independence for prion formation. *Proceedings of the National Academy of Sciences of the United States of America* 102(36):12825–30.
19. Toombs JA, et al. (2012) De novo design of synthetic prion domains. *Proceedings of the National Academy of Sciences of the United States of America* 109(17):6519–24.
20. Ross ED, Maclea KS, Anderson C, Ben-Hur A (2013) A bioinformatics method for identifying Q/N-rich prion-like domains in proteins. *Methods in molecular biology (Clifton, NJ)* 1017:219–28.
21. Paushkin S V, Kushnirov V V, Smirnov VN, Ter-Avanesyan MD (1996) Propagation of the yeast prion-like [psi+] determinant is mediated by oligomerization of the SUP35-encoded polypeptide chain release factor. *The EMBO journal* 15(12):3127–34.
22. Osherovich LZ, Cox BS, Tuite MF, Weissman JS (2004) Dissection and design of yeast prions. *PLoS biology* 2(4):E86.
23. Liu JJ, Lindquist S (1999) Oligopeptide-repeat expansions modulate “protein-only” inheritance in yeast. *Nature* 400(6744):573–6.
24. Shkundina IS, Kushnirov V V, Tuite MF, Ter-Avanesyan MD (2006) The role of the N-terminal oligopeptide repeats of the yeast Sup35 prion protein in propagation and transmission of prion variants. *Genetics* 172(2):827–35.
25. Parham SN, Resende CG, Tuite MF (2001) Oligopeptide repeats in the yeast protein Sup35p stabilize intermolecular prion interactions. *The EMBO journal* 20(9):2111–9.
26. Toombs JA, Liss NM, Cobble KR, Ben-Musa Z, Ross ED (2011) [PSI+] maintenance is dependent on the composition, not primary sequence, of the oligopeptide repeat domain. *PLoS ONE* 6(7):e21953.
27. Ohhashi Y, Ito K, Toyama BH, Weissman JS, Tanaka M (2010) Differences in prion strain conformations result from non-native interactions in a nucleus. *Nature chemical biology* 6(3):225–230.
28. Crist CG, Nakayashiki T, Kurahashi H, Nakamura Y (2003) [PHI+], a novel Sup35-prion variant propagated with non-Gln/Asn oligopeptide repeats in the absence of the chaperone protein Hsp104. *Genes to cells : devoted to molecular & cellular mechanisms* 8(7):603–18.
29. Derdowski A, Sindi SS, Klaips CL, DiSalvo S, Serio TR (2010) A size threshold limits prion transmission and establishes phenotypic diversity. *Science (New York, NY)* 330(6004):680–3.
30. Chernoff YO, Lindquist SL, Ono B, Inge-Vechtomov SG, Liebman SW (1995) Role of the chaperone protein Hsp104 in propagation of the yeast prion-like factor [psi+]. *Science (New York, NY)* 268(5212):880–4.
31. Wegrzyn RD, Bapat K, Newnam GP, Zink AD, Chernoff YO (2001) Mechanism of prion loss after Hsp104 inactivation in yeast. *Molecular and cellular biology* 21(14):4656–69.
32. Ness F, Ferreira P, Cox BS, Tuite MF (2002) Guanidine hydrochloride inhibits the generation of prion “seeds” but not prion protein aggregation in yeast. *Molecular and cellular biology* 22(15):5593–605.

33. Helsen CW, Glover JR (2012) Insight into molecular basis of curing of [PSI+] prion by overexpression of 104-kDa heat shock protein (Hsp104). *The Journal of biological chemistry* 287(1):542–56.
34. Alexandrov AI, Polyanskaya AB, Serpionov G V., Ter-Avanesyan MD, Kushnirov V V. (2012) The Effects of Amino Acid Composition of Glutamine-Rich Domains on Amyloid Formation and Fragmentation. *PLoS ONE* 7(10):e46458.
35. Wadsworth JDF, Hill AF, Beck JA, Collinge J (2003) Molecular and clinical classification of human prion disease. *British medical bulletin* 66:241–54.
36. Prusiner SB, Scott MR, DeArmond SJ, Cohen FE (1998) Prion protein biology. *Cell* 93(3):337–48.
37. Vitrenko YA, Pavon ME, Stone SI, Liebman SW (2007) Propagation of the [PIN+] prion by fragments of Rnq1 fused to GFP. *Current genetics* 51(5):309–19.
38. Alexandrov IM, Vishnevskaya AB, Ter-Avanesyan MD, Kushnirov V V (2008) Appearance and propagation of polyglutamine-based amyloids in yeast: tyrosine residues enable polymer fragmentation. *The Journal of biological chemistry* 283(22):15185–92.
39. Rüdiger S, Germeroth L, Schneider-Mergener J, Bukau B (1997) Substrate specificity of the DnaK chaperone determined by screening cellulose-bound peptide libraries. *The EMBO journal* 16(7):1501–7.
40. Rüdiger S, Schneider-Mergener J, Bukau B (2001) Its substrate specificity characterizes the DnaJ co-chaperone as a scanning factor for the DnaK chaperone. *The EMBO journal* 20(5):1042–50.
41. Sherman F (1991) Getting started with yeast. *Methods in enzymology* 194:3–21.
42. Gonzalez Nelson AC, et al. (2014) Increasing prion propensity by hydrophobic insertion. *PloS one* 9(2):e89286.
43. Song Y, et al. (2005) Role for Hsp70 chaperone in Saccharomyces cerevisiae prion seed replication. *Eukaryotic cell* 4(2):289–97.
44. Morris JA, Gardner MJ (1988) Statistics in Medicine: Calculating confidence intervals for relative risks (odds ratios) and standardised ratios and rates. *BMJ* 296(6632):1313–1316.
45. Agresti A (2007) *An Introduction to Categorical Data Analysis, 2nd Edition - Alan Agresti* (Wiley, Hoboken, New Jersey).
46. Tyedmers J, Madariaga ML, Lindquist S (2008) Prion switching in response to environmental stress. *PLoS biology* 6(11):e294.
47. Cox BS (1965) Ψ, A cytoplasmic suppressor of super-suppressor in yeast. *Heredity* 20(4):505–521.
48. Tuite MF, Mundy CR, Cox BS (1981) Agents that cause a high frequency of genetic change from [psi+] to [psi-] in Saccharomyces cerevisiae. *Genetics* 98(4):691–711.
49. Jung G, Masison DC (2001) Guanidine hydrochloride inhibits Hsp104 activity in vivo: a possible explanation for its effect in curing yeast prions. *Current microbiology* 43(1):7–10.
50. Ferreira PC, Ness F, Edwards SR, Cox BS, Tuite MF (2001) The elimination of the yeast [PSI+] prion by guanidine hydrochloride is the result of Hsp104 inactivation. *Molecular microbiology* 40(6):1357–69.
51. Street AG, Mayo SL (1999) Intrinsic beta-sheet propensities result from van der

Waals interactions between side chains and the local backbone. *Proceedings of the National Academy of Sciences of the United States of America* 96(16):9074–6.
52. Fawcett T (2006) An introduction to ROC analysis. *Pattern Recognition Letters* 27(8):861–874.
53. Bondarev SA, Shchepachev V V, Kajava A V, Zhouravleva GA (2013) Effect of charged residues in the N-domain of Sup35 protein on prion [PSI+] stability and propagation. *The Journal of biological chemistry* 288(40):28503–13.
54. Du Z (2011) The complexity and implications of yeast prion domains. *Prion* 5(4):311–316.
55. Reidy M, Masison DC (2011) Modulation and elimination of yeast prions by protein chaperones and co-chaperones. *Prion* 5(4):245–249.
56. McGlinchey RP, Kryndushkin D, Wickner RB (2011) Suicidal [PSI+] is a lethal yeast prion. *Proceedings of the National Academy of Sciences of the United States of America* 108(13):5337–5341.
57. Toyama BH, Kelly MJS, Gross JD, Weissman JS (2007) The structural basis of yeast prion strain variants. *Nature* 449(7159):233–7.